# JOURNAL OF APPLIED PHYSICS

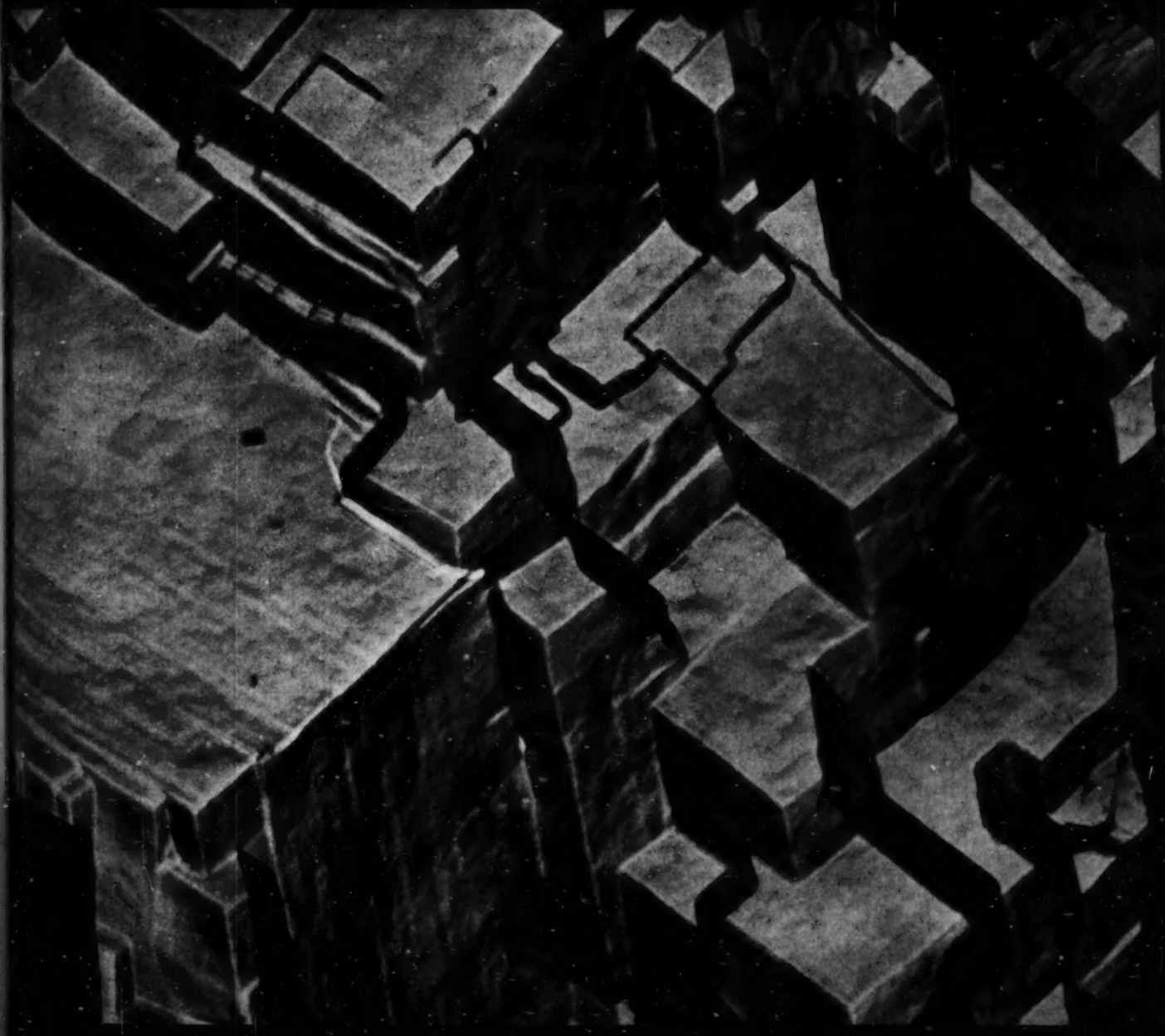

JOURNAL
OF
# APPLIED PHYSICS

Vol. 15, No. 2 FEBRUARY, 1944

## *In This Issue*

*Page*

**Physics in 1943** THOMAS H. OSGOOD 89

**Creep of Metals**
SAUL DUSHMAN, L. W. DUNBAR, AND H. HUTHSTEINER 108

**Gaseous Diffusion as a Tool for Locating Critical Points in Metals and Alloys**
HOWARD S. COLEMAN AND HENRY L. YEAGLEY 125

**The Cyclotron. II** M. STANLEY LIVINGSTON 128

*Contributed Original Research*

**Electromagnetic Velometry. I. A Method for the Determination of Fluid Velocity Distribution in Space and Time** ALEXANDER KOLIN 150

**Twinning in Zinc Oxide** M. L. FULLER 164

**Impedance of Short, Long, and Capacitively Loaded Antennas with a Critical Discussion of the Antenna Problem** RONOLD KING AND CHARLES W. HARRISON, JR. 170

**Terminal Functions for Antennas**
D. D. KING AND RONOLD KING 186

**Bonding and Structural Variations of Commercial Electroplatings 2–55×10⁻⁶ Inch Thick**
GEORGE L. CLARK, GEORGE PISH, AND LEONARD E. WEEG 193

**Letter to the Editor:**

**Mounting of Pigments for Electron Microscopy**
M. L. FULLER, D. G. BRUBAKER, AND R. W. BERGER 201

*In Every Issue*

**Calendar of Meetings** 147
**New Books** 148
**Here and There** 148
**New Booklets** 149
**Recent Applications of Physics** 202
**Index to Advertisers** xx

**BOARD OF EDITORS**

ELMER HUTCHISSON, *Editor*

*Associate Editors*

R. B. BARNES
OTTO BEECK
W. F. BUSSE
CLARK GOODMAN
SELIG HECHT
W. J. LYONS
MORRIS MUSKAT
THOMAS H. OSGOOD
PAUL E. SABINE
FREDERICK SEITZ
J. R. TOWNSEND

**Publication of the American Institute of Physics**

**ADMINISTRATIVE STAFF**

HENRY A. BARTON, *Director*

MADELINE M. MITCHELL, *Publications Manager*

JOHN T. TATE, *Adviser on Publications*

**GOVERNING BOARD**

PAUL E. KLOPSTEG, *Chairman*

GEORGE B. PEGRAM, *Secretary*

T. D. COPE
R. B. DOW
L. A. DUBRIDGE
FLOYD A. FIRESTONE
HARVEY FLETCHER
R. C. GIBBS
K. S. GIBSON
ARTHUR C. HARDY
HERMANN MARK
A. G. WORTHING
JOHN T. TATE
N. W. TAYLOR
WALLACE WATERFALL

The JOURNAL OF APPLIED PHYSICS, published monthly at Prince and Lemon Sts., Lancaster, Pa., is devoted to physics in its role as the science basic to other natural sciences and to the arts and industries. Previous to 1937 this publication was known as PHYSICS. The JOURNAL OF APPLIED PHYSICS publishes editorials, news of physicists, and reviews, as well as technical papers of applied physics.

**Manuscripts** should be submitted to Elmer Hutchisson, Editor, 50th floor, 350 Fifth Avenue, New York 1, New York.

**Subscriptions** and orders for back numbers should be addressed to Prince and Lemon Streets, Lancaster, Pa. or to the American Institute of Physics, 57 East 55 Street, New York 22, N. Y.

**Subscription Price**

| | U. S. AND CANADA | ELSEWHERE |
|---|---|---|
| To members of scientific societies | $5.00 | $5.70 |
| To all others | 7.00 | 7.70 |

**Back Number Prices**

Complete set: Vol. 1, July, 1931–Vol. 14, 1943—$87.50
Yearly back number rate: $7.70
Single copies: $0.70 each.

**Changes of address** and proofs should be addressed to the Publications Manager.

**Advertising rates** supplied on request. Orders, advertising copy, and cuts should be sent to the American Institute of Physics.

Entered as second class matter January 22, 1937, at the Post Office at Lancaster, Pennsylvania, under the Act of March 3, 1879. Accepted for mailing at the special rate of postage provided for in the Act of February 28, 1925, authorized May 2, 1932.

Copyright 1944, by the American Institute of Physics.

Journal
of
Applied Physics

Volume 15, Number 2 February, 1944

# Physics in 1943

BY THOMAS H. OSGOOD
*Michigan State College, East Lansing, Michigan*

IN 1899, during the Boer war, *Nature* remarked that "The scientific lessons of the war are crowding upon us. We have already referred to the blunder made by our military authorities, in not sending Marconi apparatus to South Africa among the first equipments. We now learn indeed, after the investment of Ladysmith is drawing to a close, that Marconi apparatus is being sent out. . . . We have been informed on good authority that some time ago the importance of a locomotive search-light in operations of war was strongly represented to the military authorities; but they would have none of it. Fortunately, however, the naval force in Natal has now provided the army with one. It is certain to do good service.

"There can be little doubt that the presence of another scientific instrument, the balloon at Ladysmith, has saved the situation. A moment's consideration of what this touch of science can do for us will indicate that the above expression is well grounded. . . . The telephone of the balloon will inform the gunners how the shell has been dropped, and any directions regarding range can be given. It will therefore be impossible for the rebels, thanks to the balloon, to form in daylight in any large numbers for an attack on the camp, without rendering themselves liable to the searching fire of the guns. . . . Seeing then how important scientific instruments are in the struggle, in which millions are freely spent, we return to our question, how is it that there is no scientific committee to advise the Government in such matters, even if only to anticipate scientific applications? and how is it that from the Grand Council of the nation, the Privy Council, men of science are rigorously excluded?"

Forty-four years later we find every resource of science mobilized to help the fighting forces of our own country and of our allies. Physics has an importance it never possessed before. But whatever his part in the present conflict, it is the duty of every physicist to see that his profession also plays its full part in the stabilization of the postwar peace.

## I. NEUTRONS

The lack of the electric charge which encumbers most of the other fundamental particles enables slow neutrons to penetrate with peculiar ease through the network of electric fields which hold the particles of a solid together. Nevertheless, the neutrons' considerable magnetic moment, $-1.9$ nuclear magnetons each, makes their transmission through matter susceptible to control by magnetization in a way that has no counterpart in the case of other particles. Not that this control extends over a wide range—it does not, for the difference between the transmission of neutrons through magnetized and through unmagnetized iron amounts to only a few percent. Yet the phenomenon offers a new method of

exploring the interior of a solid on an atomic scale.

Consider the transmission of slow unpolarized (i.e., randomly orientated) neutrons through a thickness $d$ of material. The intensity of the emerging beam, if the substance be magnetized, is slightly greater than if it be unmagnetized. According to recent theories, for most practical conditions of experiment,

$$\Delta I/I = \tfrac{1}{2}n^2p^2d^2, \qquad (1)$$

where $I$ is the intensity of the beam, $n$ is the number of atoms per unit volume, $d$ is the thickness of the material, and $p$ is a quantity related to the scattering cross section of the material for neutrons in the following way.

One can imagine a beam of unpolarized neutrons, one cm² in cross section, passing through unmagnetized iron. The chance that a particular neutron will be deflected from the beam by one of the obstructing iron atoms is $\sigma_0$, the scattering cross section. If now the iron be magnetized, not necessarily in the direction of motion of the neutrons, and the neutrons traverse it with their spins either parallel or antiparallel to the magnetic field, then the scattering cross sections will be slightly different, *viz.*, $\sigma_0+p$ or $\sigma_0-p$. The precise evaluation of $p$ by theoretical means is still an unsolved problem, since it rests on certain factors which are themselves not yet exactly known, or which can be handled only in approximate form. The equation above, however, offers an experimental opportunity of evaluating $p$, if only the other quantities involved can be measured with reasonable accuracy.

Such an experiment has been carried out by Bloch, Hamermesh, and Staub[1] at Stanford University. Unpolarized thermal neutrons were passed through a piece of hot rolled iron into a frequently used detecting device, an ionization chamber filled with boron trifluoride. The iron was mounted between the poles of an electromagnet of moderate dimensions so that the neutron count could be made conveniently with the field either off or on. The procedure appears to be straightforward. It happens, however, that the ratio $\Delta I/I$ is extremely sensitive to the degree of saturation of the iron, especially in the last few tenths of a percent before ideally complete saturation is reached. Such a state cannot be attained until all the microcrystals of the iron have been orientated in the proper direction, a condition which demands a theoretically infinite magnetizing force, just as a stiff door requires an infinite force, parallel to the wall, to close it completely.

Since Eq. (1) applies only to a completely magnetized substance, any single measurement of $\Delta I/I$ made under conditions of incomplete saturation must necessarily fail to lead to a correct value of $p$, though any series of measurements of $\Delta I/I$ with different thicknesses of material ought to provide a check on the proportionality of the ratio to $d^2$. Since both points were among the objectives of the experiments of Bloch, Hamermesh, and Staub, their procedure involved also a measurement of the degree of saturation of the iron. The departure from complete saturation possesses a peculiar interest of its own, from the point of view discussed in 1941 by Halpern and Holstein,[2] that a neutron, like a spinning top in a gravitational field, precesses around the lines of magnetic induction $B$ as it penetrates the iron. Such a point of view, indeed, leads to a plausible reason why the ratio $\Delta I/I$ should be so acutely sensitive to incomplete saturation. Owing to the slight variation in the direction of the magnetic induction from one microcrystal to the next, under conditions of incomplete saturation, a neutron which is precessing will spend much of its time with its magnetic axis farther displaced from the mean direction of the magnetic induction than would be the case for a non-precessing neutron. The net result, then, is that the beam of neutrons behaves as though it were less completely polarized than if there were no precession. In short, a depolarizing effect is introduced by the joint effects of the precession and the variation in the direction of magnetic induction.

The three investigators therefore measured $\Delta I/I$ for two iron specimens of different thicknesses for various values of the magnetic field in which the iron was placed. At the same time they measured the departure from complete saturation. If the magnetic saturation were complete, then $M$ in the familiar equation $B=H+4\pi M$ would be constant, so that $\Delta B$ would be equal to $\Delta H$. The difference between $\Delta B$ and $\Delta H$ could

therefore be used as a basis for calculating the departure from complete saturation.

From the series of values of $\Delta I/I$ at various degrees of saturation, a limiting value of the ratio was deduced, both graphically and analytically, which was appropriate for use in Eq. (1). Thence the value of $p$ was readily found as $2.0\pm0.1\times10^{-24}$ cm$^2$. This is to be compared with the admittedly approximate value $1.1\times10^{-24}$ cm$^2$ derived by Hamermesh[3] on theoretical grounds. The agreement is good enough to encourage and bad enough to warrant further experiments along the same lines. Furthermore, the dependence of the ratio $\Delta I/I$ on the square of $d$, as predicted by Halpern and Holstein in Eq. (1), is well verified; but in some other details their theory lacks confirmation to such an extent that its fundamental assumptions may well be re-examined.

## II. MESOTRONS

A second report containing an analysis of further data obtained during their world-wide cosmic-ray survey has been published by Millikan, Neher, and Pickering.[4] Using the magnetic field of the earth as a giant analyzer of cosmic-ray particles, they show first that their experimental results are consistent with the hypothesis that the rays are created by atomic annihilation in interstellar space; and second, that the energy spectrum of cosmic rays, as deduced from the variation in intensity with geomagnetic latitude, is consistent with the relative abundances of known atoms in space, on the basis that individual primary rays possess energies proportional to the masses of the atoms of whose destruction they are the only observable relics. Apart from this general study of the origin and energy spectrum of the primary rays, most work on the subject has been of narrower scope, dealing with details of the processes by which the rays are absorbed in the atmosphere and the earth. In particular, much attention has been paid to the penetrating component which is currently believed to consist of fast-moving mesotrons, and which is also responsible for initiating that remarkable sequence of events in which the energy of a cosmic ray is tossed backwards and forwards from particles to photons and then from photons to particles, and is, at the same time, gradually frittered away in trivial secondary processes.

These latter studies fall naturally into two groups, those designed to study the production of electron showers by mesotrons and those designed to study the disintegration of the mesotrons themselves. In both types of investigation counter tubes and Wilson cloud chambers play complementary roles. Some investigators rely on electrical counting methods. Others prefer to study the photographic cloud-chamber records. It will be appropriate, then, as an example of the first type of such studies to direct attention to a few points in a report by Wilson and Hughes[5] which was based upon both techniques.

Their apparatus, arranged practically in one vertical plane, consisted of the following units, named in order, reading down. First a few counter tubes; then a space, not always filled, for a block of lead; next, a counter tube immediately above a cloud chamber; below this, a space, not always filled, for another block of lead, and finally a few more counters, one under the other. An enormous variety of combinations of these units is, of course, possible. Three combinations were selected as likely to give the most significant information. (a) The tube immediately above the chamber, and all those below it were connected in such a way as to register a count only if an ionizing particle passed through them all, and to set off the cloud-chamber mechanism simultaneously. This ionizing particle might be a penetrating one or a soft electron. (b) The necessary distinction between these two particles could be made by making a run either without or with a block of lead immediately below the chamber. (c) With lead above the chamber and trigger tube, but none below, coincidences recorded the passage of an ionizing particle, or the creation of a shower in the lead by such an ionizing primary ray, whether or not it traversed all the counters itself. At the same time, the topmost tubes were used to discriminate between ionizing and non-ionizing primary rays. If they discharged in coincidence, a ray was an ionizing primary; if they failed to count, the shower produced in the lead and recorded by the lower counters must have been due to a non-ionizing primary.

Wilson and Hughes transported their apparatus, including a 600-pound Alnico permanent magnet (to provide a magnetic field for the cloud

chamber), to the Isle Royale copper mine in northern Michigan, where it was used at various distances below the surface of the earth, to a depth as great as that equivalent to 645 meters of water. The purpose of the experiments was to help clear up the "diversity of fact and interpretation" which beclouded current knowledge of the passage of cosmic rays through matter after they had already penetrated to great depths. In their appraisal of information available at the time of their experiments (1940–41) the authors said that "some observers think the penetrating rays are ionizing, and others believe that below 250 m the energy is carried down by a non-ionizing ray that produces softer ionizing secondaries. The cloud chamber work shows that at 71 m most of the rays are penetrating and ionizing. There might be, however, a small fraction of secondaries created by non-ionizing primaries. If, as the rays pass to greater depths, the ionizing rays are absorbed, the majority of the remaining rays observed might be secondaries from these non-ionizing primaries. If this is the case, the absorption of rays present at great depths would be greater with material between the counters than with material above the counters. Material between the counters would give the absorption curve for the secondaries produced in the rock, and material above would give the absorption of the primaries."

To this particular point the experiments of Wilson and Hughes offer a definite answer. Within the limits of error, the absorption curves at 71 m and at 657 m are the same, so that there can be no large fraction of non-ionizing primaries in cosmic rays at such depths. Over all, their results show that the behavior of the penetrating rays underground is similar to that of ionizing mesotrons, which produce showers of electrons of such energies that they are readily absorbed by a few cm of lead. With increasing depth, it should be observed, the average shower size grows larger, since cosmic rays which attain such depths must be more energetic than those which disappear by absorption on the way.

The experiments of Wilson and Hughes deal only with cosmic rays which have penetrated far below sea level. At high altitudes a different story must now be told. There has just come to hand a report by Regener[6] which demonstrates that at an altitude of about 10,000 feet, nine-tenths of the recorded showers are produced by non-ionizing primary rays, and only one-tenth by ionizing particles. Earlier work by Jánossy and Rochester indicates that at sea level, some non-ionizing primaries produce showers. Therefore, as the penetrating rays pass through more and more matter, the proportion of those non-ionizing primaries which produce showers decreases very fast.

Mesotrons disintegrate spontaneously, and in this process follow the laws of radioactive decay. The products are probably an electron and neutrino, between which most of the mass energy of the disappearing mesotron is shared. Cloud-chamber photographs of the process are not yet numerous enough to make this interpretation absolutely certain. Nevertheless, it forms a good working hypothesis in the absence of a better one. Any series of measurements of the decay of mesotrons can be used to find a value for their decay constant and average life, as in the case of any commoner radioactive substance, but such measurements throw little light on the nature of the decay products.

The lifetime of mesotrons is an important quantity, however, since it controls to some extent the absorption coefficient of the particles in tenuous media. New experiments to determine this time have been described by Rossi and Nereson,[7] and by Auger, Maze and, Chaminade,[8] all of whose methods, though not identical, utilize the following general principle. A beam of mesotrons is counted by coincidences between two Geiger-Müller tubes, one above, one below a screen of lead thick enough to absorb any particles of secondary origin. About 10 cm of lead is enough for this. Below the lower counter is a block of metal a few cm in its horizontal dimensions, and of arbitrary length in the vertical dimension. Some of the mesotrons, after causing a coincidence, are absorbed in this block. Not immediately, but after a short and variable interval, the individual mesotrons, having been absorbed and being now at rest, will disintegrate emitting disintegration electrons. Some of these will be caught and recorded by counters placed appropriately close to the absorber. In general,

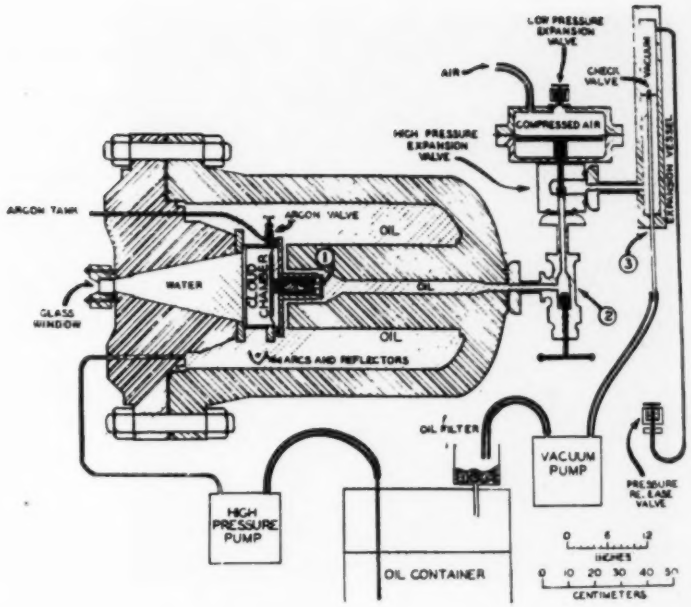


FIG. 1. High pressure cloud chamber of the Bartol Research Foundation.

then, the discharge of the mesotron counters and the discharge of the disintegration electron counters will not occur simultaneously. The disintegration electron counter can, however, be arranged to be sensitive for a brief interval, at a predetermined time after the mesotron counters have fired. This predetermined time is variable over a range of some microseconds. Therefore, if counts are made of the numbers of disintegration electrons at a series of values of the delay time, a radioactive decay curve can be plotted for the mesotrons, and from this the half-life can be found as in any commoner case of radioactive decay. The experiments of Rossi and Nereson* give a value $2.3\pm0.2\times10^{-6}$ sec., and those of Auger, Maze, and Chaminade, $1.3\times10^{-6}$ sec. The latter value is estimated to be correct only within 50 percent, so there is a possibility that the two results are not contradictory. This possibility is, however, rather slight. For the moment, Rossi and Nereson's value, having the smaller statistical error, is to be preferred, but there is room for a careful inquiry into the bearing of different geometrical and electrical details upon the numerical results.

The most important new cosmic-ray instrument is undoubtedly the high pressure cloud chamber constructed by Johnson, DeBenedetti, and Shutt[9] at the Bartol Research Foundation. The absorbing power of the gas of a cloud chamber operated near atmospheric pressure is so small that the chance of photographing certain interesting cosmic-ray events by random operation of the chamber is prohibitively remote within, let us say, the time normally allotted to the acquisition of a Ph.D. degree. Hence most low pressure chambers are usually counter-controlled. Some events like the disintegration of a mesotron are, however, so rare that even with this refinement the accumulation of experimental data is a wearisome undertaking.

High pressure cloud chambers have been used for some ten years, but they have been of conventional design, with walls and windows of extra strength. They have had to be rather small to make their operation a reasonably safe undertaking. In the new chamber of the Bartol Research Foundation these limitations have been avoided by immersing the chamber and some of the accessory equipment in a tank filled with transparent oil under high pressure, so that the difference in hydrostatic pressure inside and outside the chamber walls is negligible. Figure 1 is given with no attempt at a complete explanation which can be found in another paper.[6] The outer tank weighs about 5 tons. Immersed in the

* In a late report, the value is given as $2.15\pm0.07\times10^{-6}$ sec.

FIG. 2. Cosmic rays in a cloud chamber at 110 atmospheres. Most of the straight tracks are due to mesotrons. At the upper left is seen a pair of electrons produced by collision of a mesotron with a gas atom in the chamber. The prominent track on the right is that of a slow mesotron which ends its life and its run in the chamber (courtesy of T. H. Johnson, S. DeBenedetti, and R. P. Shutt).

oil and designed to withstand high pressures are the light sources and the trigger counters for controlled expansions. Space is provided round the central horizontal post for a copper winding to provide a magnetic field of 10,000 oersteds if required. The chamber is designed to operate with argon up to pressures of 200 or 300 atmospheres, when the absorption along a diameter of the chamber is equivalent to two or three hundred feet of standard air. The gain over low pressure chambers represented by these figures is further enhanced by the fact that at high pressures an expansion chamber is sensitive over a longer interval of time than at low pressures. A photograph taken at 110 atmospheres with this chamber is reproduced in Fig. 2. Several interesting events are discernible there. The number of tracks is very large. Indeed, the tracks in the picture may be considered as showing all that happens in the atmosphere within a vertical circle of area about ten thousand square feet. Standing out clearly on the right is a slow mesotron which ends its run in the gas of the chamber. In the upper left center is a pair of electrons, distinguished by their tortuous tracks, liberated from the gas by a mesotron collision.

### III. DISINTEGRATION BY PROTONS

Programs of research which, in times of peace, are undertaken by teams of research men, have been among the first to be discontinued or seriously disrupted by the present world-wide hostilities. A key man is called away to carry out an urgent assignment in the applied research which is constantly demanded by ever-changing military or naval strategy, and the team is crippled. Nor can it be built up again to its full efficiency before it suffers a second or third loss, and the work comes to a standstill. Investigations centering around the operation of high voltage generators offer perhaps the best example of this enforced postponement of interesting problems in academic research. We are able to report, however, the publication of an article upon the proton-fluorine reactions by Becker, Fowler, and Lauritsen,[10] though it deals with work practically completed in 1941.

When fast protons fall upon fluorine (contained

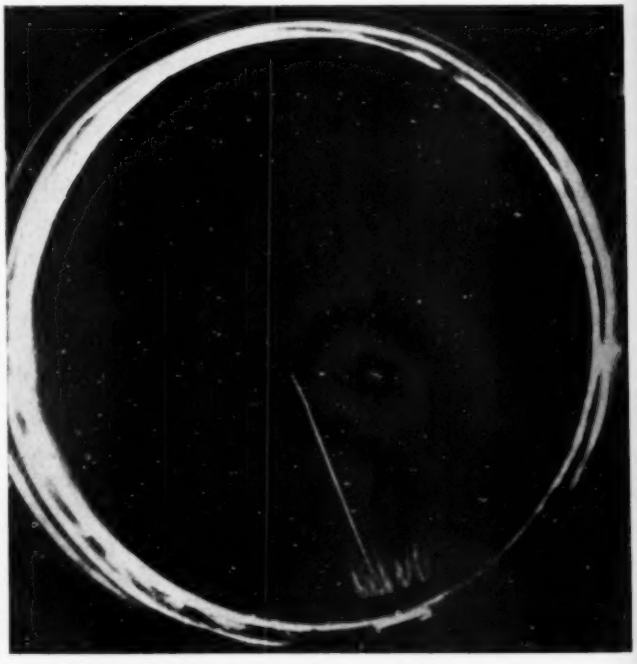

FIG. 3. Short range alpha-particle track produced in a cloud chamber by bombardment with high voltage protons of a target containing fluorine. Protons scattered from the target produce the numerous tracks of very short length close to the rim of the chamber (courtesy of C. C. Lauritsen).

in one of its chemical compounds) a number of parallel and interrelated reactions occur, which, it is now almost certain, can be summarized in the following equations.

$$F^{19}+H^1\rightarrow{}^*Ne^{20}\longrightarrow O^{16}+He^4+Q_0, \quad (2)$$

$$F^{19}+H^1\rightarrow{}^*Ne^{20}\rightarrow{}^*O^{16}+He^4+Q_1\rightarrow O^{16}+\gamma+He^4+Q_1, \quad (3)$$

$$F^{19}+H^1\rightarrow{}^*Ne^{20}\rightarrow{}^*O^{16}+He^4+Q_2\rightarrow O^{16}+e^+ +e^- +He^4+Q_2. \quad (4)$$

It should be pointed out that the confidence with which it can be stated that these three equations represent the facts is to some extent based upon the experiments about to be discussed. Each equation really represents a group of reactions, identical as far as the nature of the products is concerned, but differing in the energies involved. For example, the first process, described by (2), has several resonances, or in less precise language, goes particularly well for certain energies of the incident protons. To every resonance there corresponds a particular alpha-particle range, such that $Q_0$, which measures the energy liberated in the reaction, is always the same. The other equations are to be interpreted in a similar fashion, except that the gamma-ray in (3) or the pair of electrons in (4) carries away the balance of energy. Thus it is not surprising to find that the ranges of the alpha-particles in (2) are long, while those in (3) and (4) are short. $^*Ne^{20}$ does not, of course, represent the normal neon nucleus, but rather neon in one of a set of possible excited states—one set for each equation. Since it is found that resonances for one equation may coincide with resonances for another, some of the energy levels of one set may also belong to another set. Great importance is attached to the accurate determination of the energies of the particles involved, for this information leads directly back to the location of the energy levels of the excited parent nucleus. In the same notation, the star attached to the symbol $^*O^{16}$ implies that the oxygen nucleus is in a higher-than-normal state of energy.

The purpose of the experiments of Becker, Fowler, and Lauritsen, which were concerned mainly with the processes described by Eqs. (3) and (4), was to make a precise determination of the energy of the short range alpha-particles whose emission causes $^*Ne^{20}$ to degenerate to $^*O^{16}$ before the expulsion of a gamma-ray brings the reaction to an end. They hoped also to measure the short range alpha-particles which play a corresponding part in the reaction in which an electron pair is created.

Since protons scattered by the target at the end of the accelerating tube mingled with the alpha-particles which were created by the target's gradual disintegration, it was sometimes necessary to arrange for a partial separation of the two types of particle before they entered a cloud chamber to be photographed; otherwise a proton track might be mistaken for an alpha-trail, if they happened to have about the same length. This was accomplished by a magnetic field which deflected the particles some twenty or thirty degrees from their original direction, before they entered the cloud chamber. Figures 3 and 4 show solitary alpha-trails in the chamber, emerging from a "brush" of protons, which, in this case, have short tracks. One of the alpha-particles has collided with a helium nucleus in the chamber, giving a characteristic right-angled fork.

Turning now to the results, without pausing for any cataloging of the details of measurement, the three authors found that a single value of $Q_1$, 1.81 Mev, fitted the observations at the 334-, 867-, 927-, and 1363-kev resonances, indicating that they all belonged to the group of events described by (3); but that a $Q_2$ value of 1.93 Mev was required to fit the process (4) at 1220 kev. These $Q$'s differ by just enough to demonstrate that it is very probable that the $^*O^{16}$ in each of the Eqs. (3) and (4) represents a different energy state, separated by 0.12 Mev; and that the electron pairs of Eq. (4) are emitted by $^*O^{16}$ and not directly by $^*Ne^2$. The argument runs somewhat as follows.

In (3) the resonances have been fairly well surveyed, and the gamma-rays are known to be

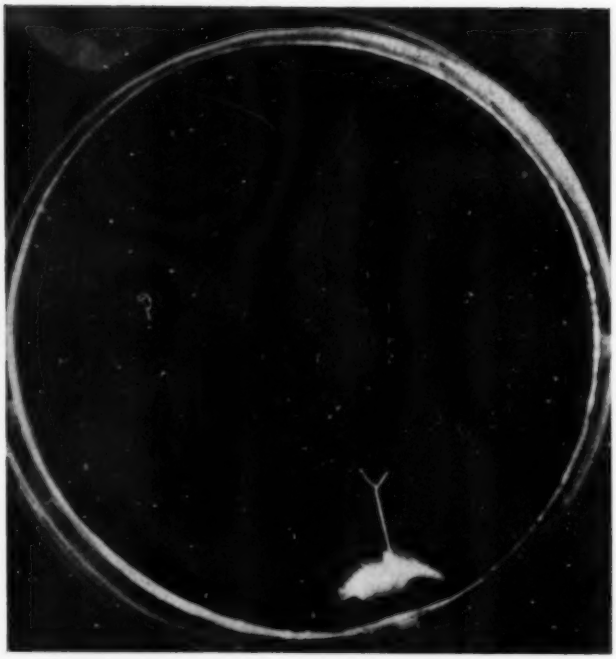

FIG. 4. A variation of Fig. 3. Here the alpha-particle has collided with a helium nucleus in the gas of the cloud chamber. Having identical masses the particles produce a characteristic fork with the branches at right angles (courtesy of C. C. Lauritsen).

monochromatic with 6.2-Mev energy. For (2) and (4) there is certainly a coincidence of resonance at 1350 kev and perhaps at 850 kev. The process (4) shows a resonance of its own at 1220 kev, which is not detected in (2). It has been assumed, thus far without contradiction, that for coincident resonances, $^{*}Ne^{20}$ is the same in (2) as in (4), the reasons for the subsequent divergent behavior being hidden, for want of definite knowledge, under the cloak of "selection rules." Now in (4), Becker, Fowler, and Lauritsen found a group of alpha-particles at the 1220-kev resonance which possessed energies greater than those in (3); therefore $^{*}O^{16}$ in (4) must be lower than $^{*}O^{16}$ in (3). Were this not so, $^{*}O^{16}$ in (4) would be expected first to give off a weak gamma-ray, thereby descending to the level of $^{*}O^{16}$ in (3) and then decaying by the emission of a 6.2-Mev gamma-ray according to Eqs. (3). The pair-emitting level of $^{*}O^{16}$ is thus 0.12 Mev lower than the level responsible for the emission of the monochromatic gamma-rays. Confirmatory evidence, though not as precise as might be desired, is available from a contemporary measurement[11] of the pair energy, which has the value $6.0\pm0.2$ Mev. If the interpretation is correct, this ought to be 0.12 Mev lower than the energy of the monochromatic gamma-rays of Eq. (3). Thus there is no numerical contradiction in the acceptance of the three equations, but more refined experiments are needed to prove the case beyond all shadow of doubt.

## IV. ČERENKOV RADIATION

In 1934 the Russian physicist Čerenkov discovered a new faint radiation associated with the passage of high speed electrons through matter. The portion of the radiation which falls in the visible region of the spectrum can therefore be observed only in the case of transparent media. That the radiation represents a new phenomenon is evident from its remarkable directional properties. With a homogeneous beam of electrons and a thin film of material, it is emitted only along the generators of a cone whose axis coincides with the beam. Since the first announcement perhaps half a dozen reports have been published, dealing with its production, and the dependence of its properties upon electron velocity and upon the refractive index of the medium.

Čerenkov radiation cannot be produced unless electrons move with velocities greater than that of light in the transparent medium. Figure 5, which is copied from a paper by Wyckoff and Henderson,[12] shows that if coherent radiation is produced along the path of the electron $AB$, then it will be emitted only in a direction which makes an angle $\theta$ with the direction of the electron beam. Certain assumptions are tacitly involved. The loss of energy of the electron between $A$ and $B$ must be small, and at the same time it is presumed that the distance to the position of the observer is very large compared to $AB$. These conditions are fulfilled if, as in some recent experiments, electrons with energies of the order of 0.5 Mev are allowed to fall on a film of mica or Cellophane. Then $\cos\theta=1/\beta n$, where $n$ is the refractive index of the substance, $c$ is the velocity of light in vacuum, and $\beta c$ is the velocity of the electrons.

The usual experimental arrangement is to have

the thin film inside a small conical mirror, on its axis, and to photograph the radiation at a distance which allows for protection from the penetrating x-rays which are formed when the electron beam is stopped by the mirror. It is clear that according to the simple theory, there are only two matters which require checking—the dependence of $\theta$ on $\beta$ and the dependence of $\theta$ on $n$. Both these things have been done, the first by Wyckoff and Henderson, over the range 0.240 to 0.815 Mev, and the second by Collins and Reiling[13] for three materials of different refractive indices. In no case is there any certain departure from the predictions of the simple theory. This must not be taken to mean, however, that Čerenkov radiation ceases to be interesting. Numerous questions can be asked but are not yet answerable concerning its spectrum and its distribution in angle from specimens which are not extremely thin; and on the theoretical side it will be interesting to find the reason for the coherence of the radiation and its relation to the incoherent bremstrahlung.

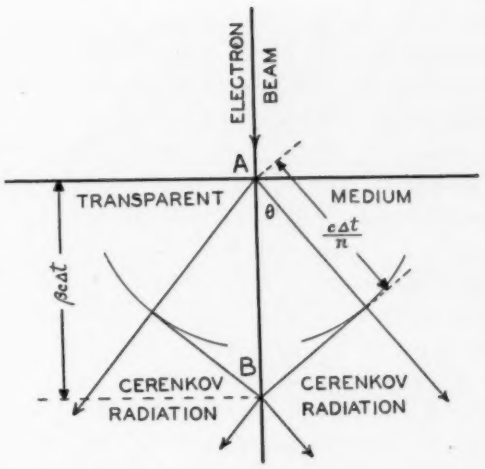


FIG. 5. Illustrating the production of Čerenkov radiation. While electrons move along $AB$ in a transparent medium with a velocity greater than that of light in the medium, they give rise to coherent radiation which can be observed only in a direction $\theta$ with respect to the electron beam.

## V. IONS

Great strides have been made in understanding the process of ion formation since the time when a mass spectrograph was first coupled to an ionization tube. Most of this work in the United States is traceable to Tate and his school at the University of Minnesota. Developments in technique have brought mass spectrometers and electron guns to such perfection that they exhibit a nicety of control undreamed of by earlier investigators. It is possible now not only to investigate the products of ionization, but to choose neatly from among a great variety of simple and complex ions just one type for examination.

In all but the simplest of monatomic vapors, the process of ionization is likely to proceed by stages. When a beam of electrons whose energy can be increased gradually is allowed to strike the gas to be ionized, different types of ions first appear at different values of electron energy. Such events are termed appearance potentials of the ions in question. When a particular ion can be formed by alternative sequences of events, it may have more than one appearance potential. In general, the appearance potential of an ion may be represented as the sum of three quantities, a dissociation energy, an ionization energy, and an energy equivalent to the kinetic energy and energy of excitation of the products at the instant of ionization. In symbolic form, this can be written as

$$A(R^+)=D(R)+I(R)+E.$$

The direct measurement of $E$ is difficult, but it is usually small, and therefore the ionization potential of $R$, or at least an upper limiting value, can be taken as equal to $A(R^+)-D(R)$. The necessary dissociation energy can frequently be calculated from the data of physical chemistry. Another way of allowing for the dissociation energy is to hold the ionization tube at a temperature high enough to ensure that dissociation occurs. Then the appearance potential of $R^+$ gives its ionization potential directly.

In any modern apparatus for determining ionization potentials, it is necessary to pump the gas to be investigated continuously through the ionization tube, in order that the appropriate high vacuum may be maintained in the adjoining spectrograph. Hipple and Stevenson[14] of the Westinghouse Research Laboratories have made use of this circumstance to design an ionization apparatus and spectrometer in which the sub-

stance to be investigated is allowed to enter the ionization region only through a tiny furnace, whose temperature can be regulated to fix the required degree of dissociation of the entering molecules. The interest of these men has centered of late on the methyl and ethyl radicals, derived from the breakdown of lead tetramethyl and lead tetraethyl. Figure 6 shows their apparatus in process of assembly, after which it is centered between two large hemispherical windings whose current provides the magnetic field to bend the moving ions along a semicircular path into a collector. A picture of the spherical magnet appeared as a cover illustration of this Journal in April, 1940. The furnace consisted of a quartz capillary, 1-mm inside diameter, wrapped with a spiral heating element. A stream of particles, in the proper state of dissociation, emerging from the end of this capillary was crossed a few mm farther on by a well-defined electron beam of controlled energy. The products of ionization were drawn out sideways by small auxiliary electrostatic fields, which sped them on their way through the mass spectrograph.

First, it was necessary to discover at what furnace currents different free radicals appeared. With an electron beam of moderate energy, the relative abundances of ions were determined for various values of the heating current. In the case of $Pb(CH_3)_4$, for example, the number of $PbCH_3^+$ ions, though large at room temperature, dropped rapidly with increasing furnace current, while $CH_3^+$ ions increased rapidly to a sharp maximum and then decreased. It may be noted, in passing, that up to a certain temperature, as the $PbCH_3^+$ ions decreased in number, the supply of $CH_3^+$ and $CH_4^+$ ions continued to increase steadily until the heavy ions had almost disappeared. From this observation, and a corresponding one for $Pb(C_2H_5)_4$, it can be deduced that the lead alkyls decompose on a hot quartz or tungsten surface to give the stable hydrocarbons methane, ethane, and acetylene at all temperatures up to a red heat. On the strength of this preliminary information, furnace temperatures could be chosen at which one particular ion was present in great abundance, offering good conditions for studying appearance potentials. A detailed enumeration of the results would be out of place here. Let it suffice to say that the technique of Hipple and Stevenson made it possible to distinguish clearly between the different products of thermal decomposition, so that appearance potentials could be ascribed unambiguously to ions resulting from specific dissociation processes. In addition the improved accuracy of their measurements, coupled with a certainty of interpretation, has gone far towards removing certain inconsistencies in values of ionization and dissociation energies related to the ethyl and methyl radicals.

### VI. THERMAL DIFFUSION

The simple experimental facts concerning thermal diffusion are now widely known. In general, it may be said, a steady temperature gradient in a mixture of two gases will gradually lead to an equilibrium state in which the concentrations of the components are different in regions of different temperature. The apparatus may be designed in the form of a pair of reservoirs connected by a long tube so that a remixing of the constituents by convection currents is effectively prevented. Such a scheme can be used to separate isotopes on an easily measurable scale. But the theory is not in such a happy state. In the words of Jones,[15] the theory of thermal diffusion appears as a by-product of any sufficiently complete and rigorous kinetic theory of the phenomena of thermal conductivity, viscosity, and diffusion in gases. The catch lies in the phrase "sufficiently complete and rigorous." To most readers, the words kinetic theory conjure up a picture of small, perfectly elastic, spherical molecules simple enough for pictorial animation in scientific motion pictures, and yet adequate to explain the simple laws of gases. A "sufficiently complete and rigorous" theory for the subject of thermal diffusion involves also precise knowledge of the forces between molecules and of the symmetry or lack of symmetry of those forces. The collisions of impenetrable, undeformable elastic spheres are merely a special case of the elusive complete theory, and can represent only a rough approximation to the truth. Molecules are not impenetrable spheres nor do they possess spherical fields of force, if we are to believe our eyes when we look at a variety of natural crystals.

The law of force between two similar molecules cannot be written down in exact mathematical

FIG. 6. Assembling the Westinghouse mass spectrometer. The tube is being fitted into the spherical coil providing the uniform magnetic field for the deflection of the ions. This tube is of the 180° deflection type and has been used in the study of the ionization and dissociation of various molecules by electron impact (courtesy of J. A. Hipple).

form. The chances are that if it could, it would be too elaborate to be handled in the theory of thermal diffusion with the analytical techniques now available. Certain facts are, nevertheless, obvious. The magnitude of the force diminishes with increasing separation of the particles, provided they are more than a certain distance apart. In a gas, the molecules are always more than this critical distance apart. In the case of some molecules, the force may increase gradually from a negligible value at infinity, and then suddenly, at a certain distance, become very large. In other cases the force may increase smoothly all the way in, corresponding to what are sometimes called soft molecules. It is therefore necessary to have recourse to plausible mathematical approximations to the laws of force between molecules, approximations which are simple enough to be tractable.

In recent mathematical work on thermal diffusion the calculations have been made particularly for four types of molecular models. The first is the solid elastic sphere, or perfectly hard molecule. The others can be understood by considering the equation $F=k/r^{\nu}-k'/r^{\nu'}$, where $F$ is the force between two molecules, $r$ the distance apart of their centers, and $k$, $k'$, $\nu$, and $\nu'$ are constants. In addition $\nu$ and $\nu'$ are integers. The second model is obtained by putting $\nu'=\infty$, giving a force which follows a simple inverse power law. This can be handled mathematically, and leads to the interesting result that if $\nu=5$, then no separation of molecules by thermal diffusion is possible.

The third is the particular case in which $\nu=\infty$, giving an attractive force $-k'/r^{\nu'}$ between molecules. To keep them from coalescing when in the gaseous form it is necessary that the molecules be impenetrable spheres of a specified diameter, whose boundaries set a lower limit to the range of the attractive forces. This is the Sutherland model. The behavior of such molecules in thermal diffusion has been worked out approximately for several values of $\nu'$.

The fourth type of intermolecular force is given by setting $\nu'=3$ and letting $\nu$ take any one of a series of values. This is the model of Lennard-Jones who first used it twenty years ago in calcu-

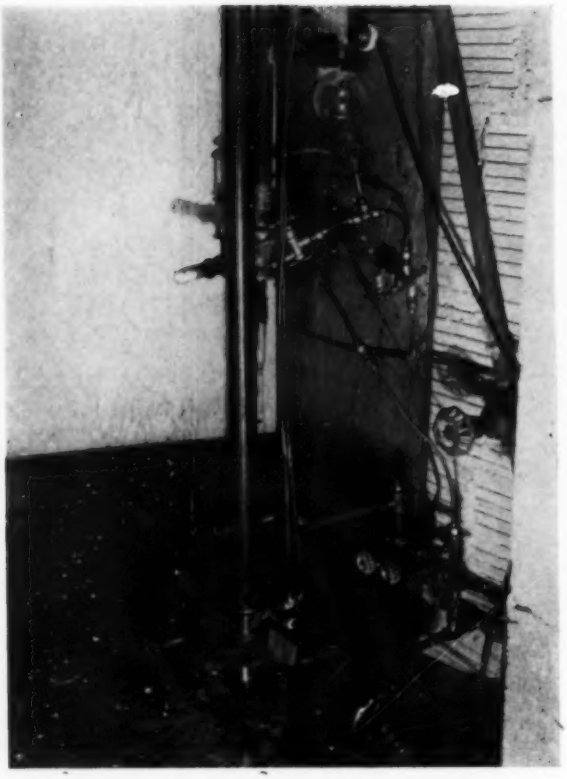

FIG. 7. The foot of the thermal diffusion column at the University of Minnesota. Near the top of the picture is the bulb in which the heavy methane is collected for removal to a mass spectrograph for analysis. The column is 24 ft. long with an external diameter of 2.5 in. A temperature difference of about 300°C is maintained by electrical heating across the annular space between the inner and outer cylinders (courtesy of J. W. Buchta).

lations relating to equations of state. The choice $\nu'=3$ is purely arbitrary, without simple physical basis but justified by mathematical convenience. As might be predicted, the behavior of this model has been worked out only approximately. The treatment has been extended, however, to include cases other than that described by $\nu'=3$. Again, the mathematical difficulties limit very severely the choice of values of $\nu$ and $\nu'$. Only values which are connected by the relation $\nu=2\nu'-1$ can be handled. In the interests of brevity, a special type of Lennard-Jones model is referred to by its $\nu$, $\nu'$ numbers. It may be said, for example, that the 9, 5 model has received the major share of attention to date in matters dealing with thermal diffusion, and that the 13, 7 model has been used extensively in treating problems of solids and fluids by the methods of statistical mechanics.

A few years ago most experiments were made with long thermal diffusion columns in an effort to separate isotopes on a worth-while scale and to check the salient features of the theory. At the University of Minnesota, for example, Nier[16] found that in a Clusius-Dickel column 24 ft. long, the bottom of which is shown in Fig. 7, a fourfold decrease in the concentration of $C^{13}$ methane occurred in a period of three days at the bottom of the column with a corresponding increase at the top. This separation was accomplished by maintaining a difference of temperature of some 300°C between the inner and outer walls of the annular column. In this picture the dimensions of the parts may be inferred roughly from the size of the fractional horsepower pump motor. The outside diameter of the column is 2.5 inches.

Since the beginning of 1942, however, many experimenters have had a different objective. They have assumed the essential correctness of the theory of thermal diffusion and have used it to deduce new information concerning intermolecular forces, or at least to find out what type of simple intermolecular force most accurately describes the behavior of certain molecules. To do this it is not necessary to achieve a sharp separation of isotopes because simple mass spectrographs can be used to analyze the enriched gaseous mixtures with more than sufficient precision. Therefore simple apparatus consisting of two glass bulbs joined by a narrow tube has been used in place of long columns. For example, Watson and Woernley,[17] using such a method, have investigated the behavior of ammonia containing about 15 percent of $N^{15}$. Perhaps the most interesting of their observations is that the direction of the process of thermal diffusion reverses at about room temperature, in qualitative agreement with earlier results of Grew upon neon-ammonia mixtures. This effect has good theoretical backing, though the temperature at which such a reversal occurs cannot be predicted with any accuracy. Watson and Woernley also found that the value of the thermal diffusion constant was proportional to the logarithm of the absolute temperature, with a rate of change about eight times that which has been reported for the symmetrical molecules neon and argon. They present a qualitative argument in explanation of these effects which is based upon the

known dipole behavior of the ammonia molecule. Further experiments with molecules of related types will undoubtedly throw new light on long range intermolecular forces.

### VII. ELECTRON MICROSCOPY

In the course of a few years the electron microscope has emerged from being a novelty, a stage in which its possibilities were explored by examination of the most spectacular and readily accessible objects, into a powerful accessory instrument of research with which practical problems can be solved. In the standard type of instrument, only objects suitable for forming into, or being mounted upon, very thin transparent films can be investigated, for the electron beam has to penetrate this film on its way to a fluorescent screen or photographic plate without appreciable loss of energy of the majority of electrons. Hence the thin parts of the film appear in the final picture brightly illuminated, the thicker portions being darker, since their extra mass gives them more opportunity to deflect electrons from the working beam. The surface of a metal cannot therefore be investigated directly, nor can the result be achieved by using instead a metallic film of sufficient transparency, for the properties of thin metallic films are vastly different from those of the same metal in mass. Some means of reproducing the detail of a metal surface on an amorphous stable film is therefore required. Several techniques have been tried with moderate success. A new method which appears to have great promise has been developed in the last two years by Heidenreich and Peck[18] of The Dow Chemical Company's Physical Research Laboratory.

The process is a two-stage one. First, the surface to be examined is prepared upon a small piece of the metal, perhaps one or two cm in each dimension. Without delay, plastic polystyrene is molded on to it, and squeezed into intimate contact with the surface by a pressure of a few thousand pounds per square inch at 160°C. After cooling, most of the metal is sawed off, leaving a piece as thick as a small coin im-

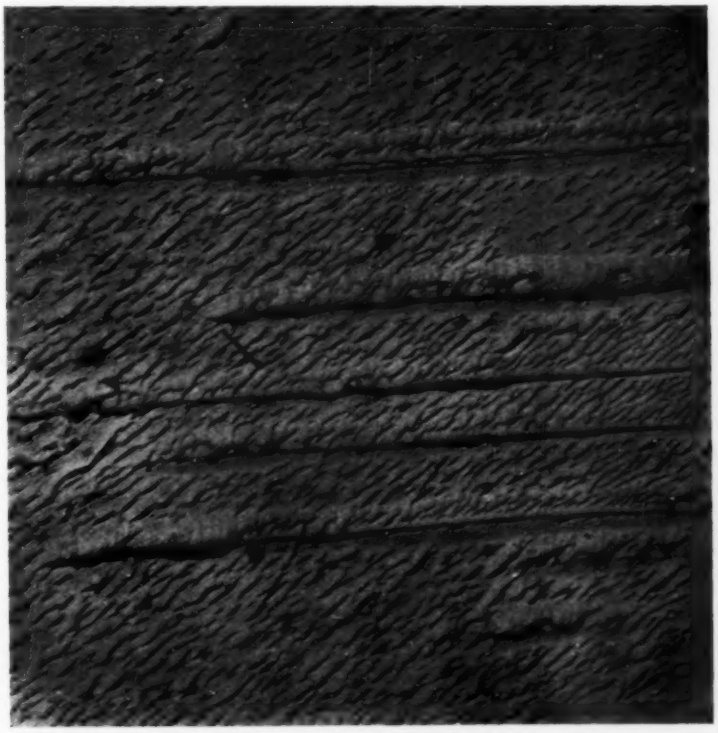

FIG. 8. Carbides in stainless steel with twin bands which are presumably Neumann bands. Polystyrene-silica replica, ×9000 (courtesy of R. D. Heidenreich).

FIG. 9. Rolled Dow metal. Polystyrene-silica replica, ×4500 (courtesy of R. D. Heidenreich).

bedded in the polystyrene. The usual procedure is then to dissolve away the remaining metal with dilute acid. A negative imprint of the original metal surface is thus left on the plastic.

The plastic is now mounted in a vacuum above a conical filament holding small particles of pure quartz. Upon heating to the right temperature, silica is evaporated on to the polystyrene. This operation must be performed quickly lest the temperature of the plastic block rise so high as to cause deformation of the surface details. It happens that freshly deposited silica molecules are extraordinarily mobile on a polystyrene surface. Were it not for this effect, the silica would probably condense in an uneven layer. As it is, the remarkable mobility carries silica molecules even into little crannies, and once the surface is covered the outer side of the silica film builds up rather smoothly. The plastic with its surface layer of silica is then cut up into small pieces; the polystyrene is dissolved away in a dish of ethyl bromide, leaving tiny areas of silica film floating on the surface. These pieces are mounted on frames and are then ready for the electron microscope. A typical silica film has one liquid-smooth surface, and one which is a replica of the original metallic surface. The electron microscope picture of such a film will show heavily exposed parts which correspond to hollows in the original metal surface. Three pictures made by this polystyrene replica process in a Type B RCA electron microscope are reproduced in Figs. 8–10. The following photograph, Fig. 11, from the same instrument, but made by a slightly different process of reproduction, is remarkable in demonstrating the great depth of focus of the microscope, and in producing a striking three-dimensional illusion. The reader should bear in mind that in these prints the contrast is reversed, the dark portions corresponding to raised parts of the original metal surface.

The limit of resolution obtainable with such replicas is between 150A and 200A, poorer by a factor of three or four than the best performance of the electron microscope under ideal conditions,

but surpassing that of the optical microscope twenty-fold. So many problems of film and surface structure await solution in this range that a new type of electron microscope has been developed in the laboratories of the General Electric Company expressly for the work. In this new microscope high resolving power has been consciously sacrificed for simplicity, compactness, and mobility. Designed by Bachman and Ramo,[19] it operates entirely on electrostatic principles, without the precise current regulation which is so necessary in other types of microscope. The lenses are entirely electrostatic. An image of intermediate magnification but of high resolution is formed by them upon a fluorescent screen of which a microphotograph is then made with an optical microscope. Four of the important parts, removed from the main vacuum case, are shown in Fig. 12. They are, reading from left to right, the fluorescent screen, the electron gun, the lens cylinder, and the object manipulator. In the next photograph, Fig. 13, the lens cylinder, with the object manipulator attached, has been removed from the vacuum chamber for adjustment. Within the limits of its design, the instrument possesses many advantages, mainly of simplicity and electronic stability, over the magnetic lens type of electron microscope. It must be remembered, however, that the one is not intended to supplant, but rather to supplement the other, in the same way as a prism spectrograph may perform as useful work as a grating spectrograph.

## VIII. X-RAYS

From the time of their discovery, x-rays have been one of the most powerful tools at the command of the scientist in problems of atomic and crystal structure. Following this pattern, publications during the last two years have been concerned with such matters as the determination of Planck's constant from the short wave-length limit of the continuous spectrum, and the interpretation of faint lines in x-ray spectra under various conditions of excitation. At the same time there has been a continued rapid expansion in the use of x-rays in the industrial testing of metals. For large masses of metal penetrating

FIG. 10. Lamellar pearlite and fine carbides in steel. Polystyrene-silica replica ×7500 (courtesy of R. D. Heidenreich).

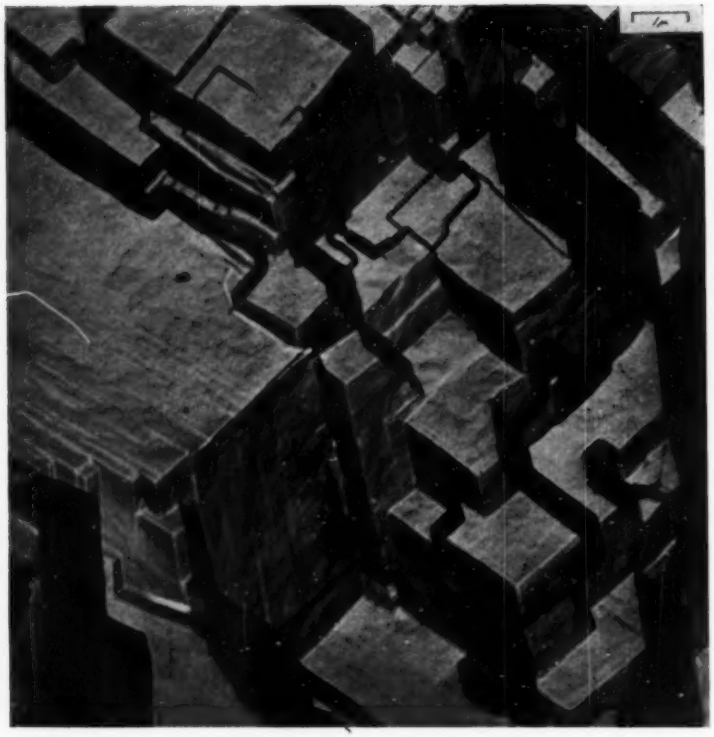

FIG. 11. Crystallographic etch figures in pure aluminum. Anodic oxide replica; ×7500 (courtesy of R. D. Heidenreich).

x-rays are needed. The voltages at which commercial tubes are designed to operate are continually increasing, and information is therefore needed, derived from experimental installations, about such obvious matters as the production and absorption of high voltage x-rays. Measurements of this type have been made in the years since 1939 by Petrauskas, Van Atta, Myers, and Northrup, with the high voltage equipment available at the Massachusetts Institute of Technology. Their researches have covered the range 0.7 Mev to 2.5 Mev, corresponding to limiting wave-lengths between 0.017 and 0.005A.

A description of the high voltage plant has already appeared in the literature,[20] but we give here three new views showing some of the details which will be of interest to physicists. Figure 14 shows the assembling of the high voltage terminal which is formed of the two large spheres originally belonging to the outfit at Round Hill. They are supported on two hollow insulating cylinders which the picture shows still surrounded by

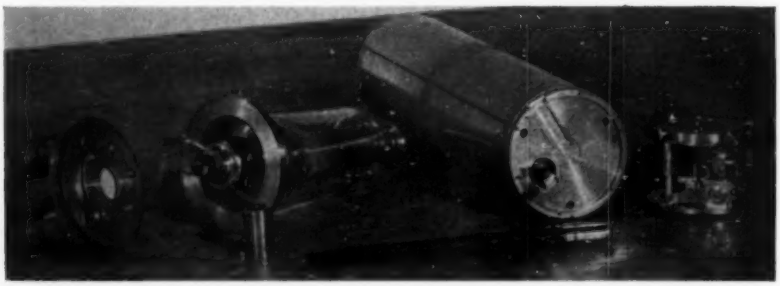

FIG. 12. The essential electron-optical elements of the General Electric electrostatic electron microscope. From left to right the parts are the fluorescent screen, the electron gun, the lens cylinder, and the object manipulator (courtesy of C. H. Bachman).

FIG. 13. A technician has removed the lens cylinder from the electrostatic electron microscope for adjustment (courtesy of C. H. Bachman).

scaffolding. The necessary electric charge is hoisted up inside one of these cylinders on charging belts made of insulating material, and descends again to ground potential down an accelerating tube fixed inside the other hollow pillar. These charging belts, which are several feet wide, are shown in the background of Fig. 15, which gives a view, underground, below one of the pillars. In the top left of the picture is an arc marking the bottom of the hollow pillar through which the charging belts run. The motor on the ceiling of this laboratory is coupled by a long insulating belt to a generator in an auxiliary laboratory inside the high voltage terminal, so that electric power may be available there even when it is at one or two million volts above ground potential. The lower end of the accelerating tube, arranged for the production of penetrating x-rays, is shown in the next photograph, Fig. 16. The outline of the circular base of one of the supporting pillars is clearly seen, and, through a port in the ceiling, part of the accelerating tube itself is visible. Right in the center of this picture is a diffusion pump with its cooling jacket well covered with thermally insulating material. The water-cooled target where x-rays are produced is at the bottom end of the projecting cylinder in the lower right of Fig. 16. The x-rays emerge through the target.

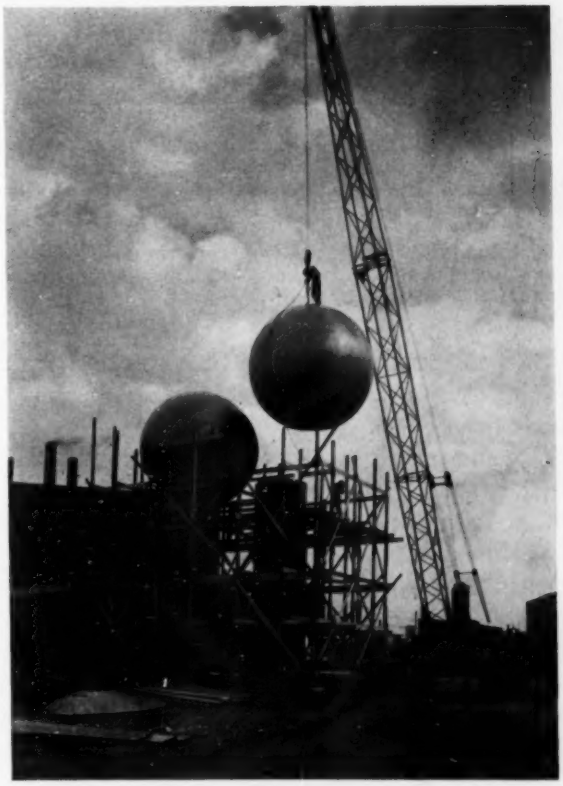

FIG. 14. Assemblying the high voltage terminal of the high voltage generator of the Massachusetts Institute of Technology. The cylindrical pillars inside the scaffolding are hollow insulators (courtesy of L. C. Van Atta).

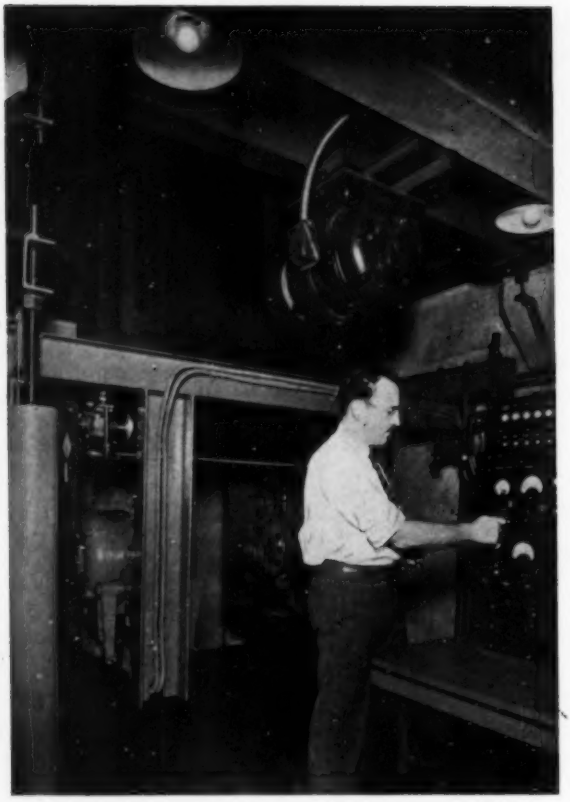

FIG. 15. The Massachusetts Institute of Technology high voltage generator. Looking up from the underground laboratory at the bottom of the hollow insulating pillar through which the charging belts run. The wide belts on their rollers, with driving motors and charging combs, are seen behind the T-frame. The motor on the ceiling drives a generator in the laboratory inside the high voltage terminal (courtesy of L. C. Van Atta).

When the photograph was taken, the apparatus for measuring x-ray intensities near the target was not in place.

Radiation from an x-ray tube is not emitted with equal intensity in all directions. In the case of these penetrating x-rays the asymmetry is very marked. At 2.35 Mev, for example, the measurements of Petrauskas, Van Atta, and Myers[21] show that the intensity at 90° from the direction of the electron beam is less than 20 percent of that in the forward direction which would be straight downwards in Fig. 16. An interesting trend which is in reasonable agreement with theory is found in the efficiency of production of the rays. In a tube operating at 100,000 volts, the fraction of the electrical energy which reappears as x-radiation is considerably less than 0.01. As the voltage increases, however, this fraction also increases, until at 2.35 Mev the efficiency is about 10 percent.

At 2.2 Mev the observed mass absorption coefficients range from 0.048 per g for tin to 0.059 per g for water, in the order tin, copper, aluminum, carbon, lead, water. The same curious order is preserved,, with values about twice as great, at 1 Mev for all except the heavy elements lead and tin; at the lower voltage these two begin to show the influence of increased absorption due to the production of photoelectrons and of electron pairs, effects which are most noticeable in heavy elements. The extraordinary penetrating power of these rays can perhaps be visualized by noting that these figures imply that at 2.5 Mev, a beam still possesses 5 percent of its original intensity after passing through 4 cm of lead.

## IX. LOOKING AHEAD

Since this review of 1943 is concerned with physics in America and is written mainly for American physicists, it is permissible to look forward to consider developments which may be expected in this country when the war is over. Already the American Institute of Physics has, in acquiring a national headquarters[22] for physicists, expressed in tangible form the increasing respect and dignity which the profession now enjoys. When these words appear in print, it is to be hoped that all physicists will have availed themselves of the privilege of helping to establish this landmark in the history of physics.

The majority of physicists, in normal times, are occupied either in colleges and universities, or in industrial laboratories. A few years hence, a larger percentage than before may be employed in government laboratories. Both in the past and now, technical physicists have known too little about the work, both in research and teaching, in which their academic colleagues are engaged; and an even more lamentable ignorance of the practical problems of the age which are being solved by physicists in industry has been displayed by those who train students in the rudiments of physics in our educational institutions. These statements may be criticized as being too sweeping, for there is a notable group of men, to whom the physics profession owes much of its present eminence, who are well

acquainted with both aspects of the situation. Nevertheless, some new common meeting ground for the two main groups of scientific workers should be found. The need for it is clearly indicated by excerpts from letters[23] of technical physicists published in this Journal. Here the unifying influence of the American Institute of Physics and the stability which its new headquarters confers upon it will make themselves felt. The general body of physicists, both technical and academic, must not expect a new basis for common understanding to develop of itself, or to be developed by a very few of their number. They must do it themselves, even if it involves a somewhat larger allotment of time to matters of organization than they have been accustomed to spare from their urgent scientific tasks. Something may undoubtedly be learned from the sister organizations in chemistry and engineering.

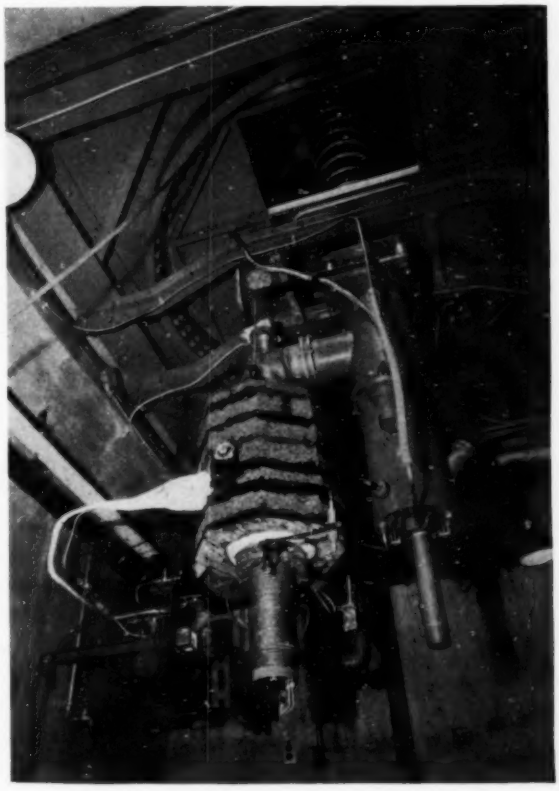

FIG. 16. The Massachusetts Institute of Technology high voltage generator. Looking up at the bottom of the accelerating tube into one of the insulating pillars. Part of the tube is seen through an opening in the ceiling. The x-ray tube target is at the bottom of the small cylinder which projects downwards at the lower right of the picture. The diffusion pump, cooled by a refrigerating unit in the bottom left corner, occupies most of the middle of the photograph. Apparatus for measuring the intensity of the x-rays as they emerge through the target has been removed (courtesy of C. L. Van Atta).

At the same time, colleges and universities must re-examine the curricula according to which they train undergraduate and graduate students in physics. A shift of emphasis may be required in view of Harnwell's statement[24] that the war has demonstrated the need for more intensive cultivation of classical physics, without any sacrifice of attention to modern branches of the subject, and in recognition of the responsibility of the universities in training enough physicists for the type of work which is most in demand. The future looks difficult and stimulating.

The author acknowledges with gratitude the kindness of those men who have provided photographs and captions for the illustration of this article. He is also indebted to his colleagues at Michigan State College, who have read the manuscript and have proferred many helpful suggestions.

## BIBLIOGRAPHY

(1) F. Bloch, M. Hamermesh, and H. Staub, Phys. Rev. **64**, 47 (1943).
(2) O. Halpern and T. Holstein, Phys. Rev. **59**, 960 (1941).
(3) M. Hamermesh, Phys. Rev. **61**, 17 (1942).
(4) R. A. Millikan, H. V. Neher, and W. H. Pickering, Phys. Rev. **63**, 234 (1943).
(5) V. C. Wilson and D. J. Hughes, Phys. Rev. **63**, 161 (1943).
(6) V. H. Regener, Phys. Rev. **64**, 250 (1943).
(7) B. Rossi and N. Nereson, Phys. Rev. **62**, 417 (1942).
(8) P. V. Auger, R. Maze, and R. Chaminade, Phys. Rev. **62**, 307 (1942).
(9) T. H. Johnson, S. DeBenedetti, and R. P. Shutt, Rev. Sci. Inst. **14**, 265 (1943).
(10) R. A. Becker, W. A. Fowler, and C. C. Lauritsen, Phys. Rev. **62**, 186 (1942).
(11) E. P. Tomlinson, Phys. Rev. **60**, 159A (1942).
(12) H. O. Wyckoff and J. E. Henderson, Phys. Rev. **64**, 1 (1943).
(13) G. B. Collins and V. G. Reiling, Phys. Rev. **54**, 499 (1938).
(14) J. A. Hipple and D. P. Stevenson, Phys. Rev. **63**, 121 (1943).
(15) R. C. Jones, Phys. Rev. **58**, 111 (1940).
(16) A. O. Nier, Phys. Rev. **57**, 30 (1940).
(17) W. W. Watson and D. Woernley, Phys. Rev. **63**, 181 (1943).
(18) R. D. Heidenreich and V. G. Peck, J. App. Phys. **14**, 23 (1943).
(19) C. H. Bachman and S. Ramo, J. App. Phys. **14**, 155 (1943).
(20) L. C. Van Atta, D. L. Northrup, R. J. Van de Graaff, and C. M. Van Atta, Rev. Sci. Inst. **12**, 534 (1941).
(21) A. A. Petrauskas, L. C. Van Atta, and F. E. Myers, Phys. Rev. **63**, 389 (1943).
(22) R. V. Hutchisson, J. App. Phys. **14**, 501 (1943).
(23) J. App. Phys. **14**, 438 (1943).
(24) G. P. Harnwell, Rev. Sci. Inst. **14**, 233 (1943).

# Creep of Metals

SAUL DUSHMAN, L. W. DUNBAR, AND H. HUTHSTEINER
*Research Laboratory, General Electric Company, Schenectady, New York*

## 1. INTRODUCTORY REMARKS

THE flow of metals under stress, or creep, is a subject of considerable interest from both the theoretical and practical points of view.[1] The increasing demands for materials that will operate satisfactorily at high temperatures has led to the accumulation of a vast amount of creep data[2] on different types of alloys and to the formulation of empirical relations which might be used for extrapolation. Also, a number of investigators have considered the phenomena from an "atomistic" point of view, and deduced from these considerations certain relations which are more or less in agreement with observations.

Some time ago the first-named author became interested in this subject and started some experimental work with the object of obtaining creep data on pure metals and alloys, which should form a basis for more theoretical considerations. In order to obtain data in a relatively short period of time, it was obviously necessary to carry on the observations under such conditions of temperature and stress as would yield much more rapid rates of creep than those dealt with in engineering tests. In the case of the more refractory metals and alloys, such rapid rates are obtainable, with moderate stresses, only at temperatures which range from 1000°K to 1400°K, and this led to the choice, in these cases, of an experimental technique in which the material under investigation is used in the form of a wire or filament and heated to the desired temperature by the passage of current. This technique is described in detail in a subsequent section.

Moreover, the choice of experimental conditions was largely influenced by certain theoretical considerations which were based upon the views developed by H. Eyring and his associates, for the interpretation of rate processes in chemical and physical reactions. Upon this basis the first-named author derived a relation for rate of creep as a function of temperature and stress which is discussed in the following section.

Before, however, presenting the derivation of this relation, it is necessary to discuss more fully the conditions under which the observations on creep recorded in this paper have been made.

A plot of elongations *versus* time, at constant temperature and constant total stress, has, in general, the form shown in curve $A$, Fig. 1. Initially there is a rather rapid rate of creep, which then decreases gradually to a *constant* value. This period of constant rate is maintained for a certain period, after which the rate increases rapidly and rupture occurs.

In a number of cases, the rate never attains a constant value but decreases continuously, as shown in $B$. This is ascribed to "work hardening," and obviously such behavior cannot lend itself to the same interpretation as the occurrence of constant creep rate. Consequently, the attempt has been made in the experiments discussed in this paper to limit the observations only to such cases as are represented by curve $A$ in Fig. 1, that is, to cases in which the rate of creep is constant over a certain period, since it is only under these conditions that the theory developed in a subsequent section should be applicable.

## 2. EXPERIMENTAL PROCEDURE

In the present investigation, the rates of creep measured varied from about $10^{-7}$ sec.$^{-1}$ to $10^{-5}$ sec.$^{-1}$. For a 10-cm length of wire, these would correspond to rates of elongation of $6\times10^{-5}$ cm min.$^{-1}$ to $6\times10^{-3}$ cm min.$^{-1}$, respectively. During the first period of the work, this elongation was measured by means of a cathetometer reading to 0.01 cm. Subsequently, an arrangement was developed which made it possible to record the elongation automatically, as a function of time. This equipment is described in the following section.

For observations on creep in the range of temperatures at or below 500°C, a Nichrome-wound tubular furnace was used and the wire, fastened between two chucks, was suspended along the axis of the furnace. The length used corresponded in all cases to that of the zone in the furnace at

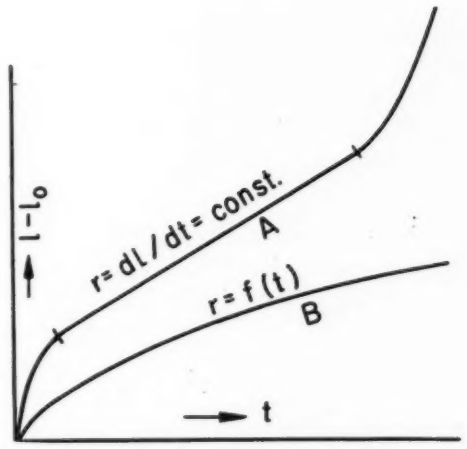


FIG. 1. Plot of elongation *versus* time. Curve *A*, rate of creep is constant; curve *B*, rate of creep decreases continuously.

uniform temperatures. This was 10 cm in at least two sets of measurements, and 5 cm in the case of the other measurements.

In the case of the more refractory metals, such as platinum, and alloys of iron, for which the temperatures had to be raised to 1000°K and higher, the arrangement illustrated diagrammatically in Fig. 2 was used.

The wire, in the form of a V-shaped filament (*FF*), was raised to the desired temperature by current from a regulated power supply, and the *brightness temperature* was determined by viewing the filament against the tungsten ribbon in a projection lamp *P*, which was calibrated against a standard tungsten filament lamp by Mr. F. Benford of our laboratory.

Since nearly all alloys and metals, with the exception of platinum, become oxidized when raised to such temperatures in air, the filaments were operated in an atmosphere of highly purified nitrogen. The latter was obtained by passing the nitrogen obtained from our supply line through sulphuric acid bottles and then, in succession, over $CaCl_2$ and $P_2O_5$ to remove water vapor. After this, the gas was passed through a tubular furnace containing copper filings and operating at 500°C, to remove oxygen. In spite of this purification procedure, the nitrogen still contained an extremely small trace of oxygen, which was indicated by the observation that at temperatures of 1100°K to 1300°K the surface of some of the more readily oxidizable alloys became oxidized during the test. Attempts to remove this residual oxygen and water vapor, by passing the gas through a liquid trap and over a tungsten filament operating at 2600–2800°K, proved unsatisfactory, and consequently tests on some of the iron alloys could not be carried out. It should also be stated that diffusion of air into the bottle through the very fine opening at the bottom was kept at a minimum by having the opening only slightly larger than the wire used to suspend the weight *W* and keeping it covered with stopcock grease. In this connection it should also be mentioned that, while pure iron does not react with nitrogen to form a nitride, the formation of this compound may occur in the presence of nitrogen in the case of iron-chromium alloys. Furthermore, as has been shown by Dr. H. H. Uhlig of this laboratory, phase changes are induced in iron alloys by the presence of nitrogen, which would not occur in air. For these reasons results on the rates of creep of iron alloys were found to be extremely erratic.

### 3. AUTOMATIC RECORDING OF ELONGATION

During the first period of this investigation, the elongation was observed directly by means of an ordinary cathetometer by means of which elongations of the order of $10^{-2}$ cm could be read

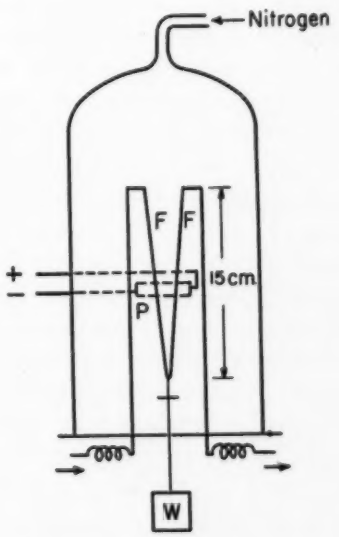


FIG. 2. Diagrammatic sketch of apparatus for determination of creep rates at incandescent temperatures. *FF*—filament 0.010″ diam.; *P*—ribbon filament lamp; 1 g wt. = 14 lb./in.²; $1 \times 10^{-4}$ cm/min. = 0.04 percent per hour.

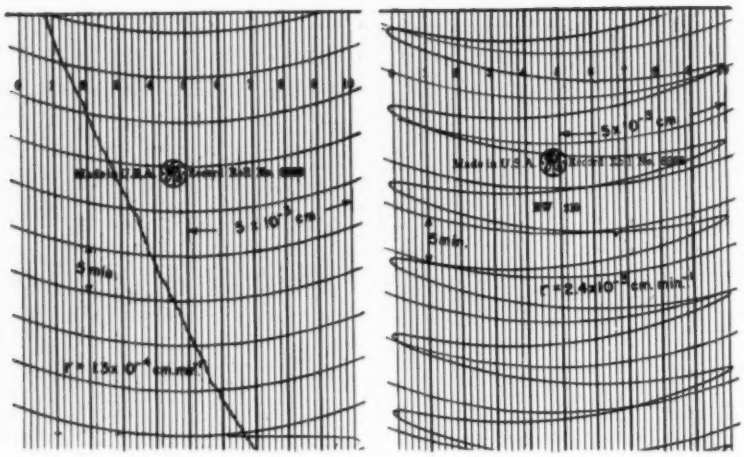

(a) (b)

FIG. 3. Illustrating type of record of elongation *versus* time obtained by use of photo-cell and photo-recorder.

accurately. Later on, an arrangement for automatic recording of elongation as a function of time was designed for us by Mr. J. Malpica of the General Engineering Laboratory and constructed under the supervision of Mr. Eric T. Asp of the Research Laboratory, to both of whom the authors wish to express their appreciation.[3]

In principle, the method involves a determination of the rate at which one set of alternate dark and light bands, spaced uniformly, passes in front of a similar set of black and light bands, thus varying the intensity of the light passing through the latter from zero to a maximum value. Actually, two glass plates are used which have parallel dark bands 0.004 inch wide and 0.004 inch apart. One of the plates is stationary, while the other is mounted in a frame which is attached between the wire under test and the pan containing the weights.

The plates are illuminated by a 50-cp, 6–8-volt lamp and condenser lens, as in the projection of slides. An objective forms a magnified image of the plates on an adjustable opening which is placed in front of a blocking-layer cell, and the latter is connected directly to a photo-recorder.[4]

To obtain best results, the lamp should be operated at 6 volts from a voltage stabilizer.

The window in front of the photoelectric cell is adjusted to give full-scale deflection on the recorder when the clear bands on the glass plates coincide. Since a vertical motion of 0.004 inch of the plate corresponds to a full-scale deflection which is 3.75 inches, the linear magnification obtained in this manner is 937.5 to 1.

Figure 3 shows a reproduction of two sample records obtained by this equipment. Figure 3(a) shows a relatively slow rate of elongation ($r=1.3\times10^{-4}$ cm min.$^{-1}$) observed on a 5-cm length of Mg-Al alloy wire at 360°C, with $W=185$ g. In such a case, the rate was derived from the average slope of the line measured between the abscissae marked 2 and 8. Owing to diffraction effects, the deflections near the sides (in the regions 0 to 2 and 8 to 10) are not strictly proportional to the elongation.

With the rate of motion of the paper as indicated, which was that used throughout the investigation, it is thus possible to observe rates of elongation as low as one division in 10 minutes, corresponding to $r=2\times10^{-5}$ cm min.$^{-1}$. Assuming $l=10$ cm, this yields the result $\nu=(dl/l)/dt=6.7\times10^{-8}$ sec.$^{-1}$.

In the case of relatively high rates of creep, such as illustrated in Fig. 3(b), in which one or more loops are obtained during the period of observation, the rate is derived by measuring the average time interval between the zero points on successive loops. This interval corresponds to a total elongation of 0.008 inch (=0.02 cm). The record shown was obtained with a 10-cm length of constantan wire at 500°C, with $W=105$ g, and yields the result, $r=2.4\times10^{-3}$ cm min.$^{-1}$, corresponding to $\nu=4\times10^{-6}$ sec.$^{-1}$.

## 4. THEORETICAL CONSIDERATIONS

About the same time as the first-named author had deduced, on the basis of simple kinetic theory considerations, an equation for rate of creep as a function of temperature and stress, W. Kauzmann[5] published a very stimulating discussion of this subject in which he deduced a relation of substantially the same form. However, since Kauzmann's derivation is based on a much more rigorous consideration of the mechanism involved in creep, we have summarized it in the following section.

The point of view adopted by Kauzmann is based on Eyring's general theory of shear rates which he has applied to viscous flow of liquids and which involves the concept of *units of flow*. "These are the structures in a body whose motions past one another make up the unit shear process. In a liquid such as water, the units of flow are believed to be single molecules, and the unit process is the passage of single molecules past one another in some such manner as is illustrated in Fig. 4. Here the motion of the molecules through the stages a, b, c has resulted in a shear strain of $\lambda/L$ in the direction indicated by the solid arrows, while the rate of shear is equal to the shear resulting from each jump times the number of jumps occurring in unit time. Clearly we can in general say that

$$\text{shear rate} = s = (\lambda/L)\omega, \tag{1}$$

where $\lambda$ is the average distance in the shear direction moved by units of flow past one another in one jump, $L$ is the average distance between layers of units of flow, and $\omega$ is the net number of jumps per second made by the unit of flow in the shear direction."

As is well known, the rate of creep at constant stress varies rapidly with temperature, and from the kinetic point of view, this means that an

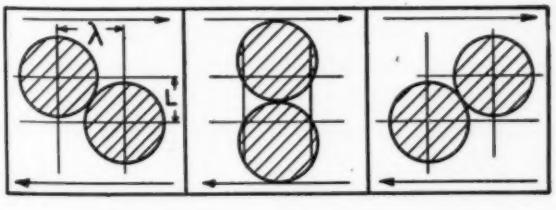


FIG. 4. Postulated mechanism of molecular shear process in ordinary liquids.

*activation energy* $Q$ is involved, which corresponds to the height of the "potential hill" between two successive "valleys." Hence, we should write

$$\omega \sim \epsilon^{-Q/RT}, \tag{2}$$

where $Q$ refers to the *activation energy per g atom*,

$R$ = gas constant per mole
$= 1.968$ cal. deg.$^{-1}$, mole$^{-1}$
$= 8.315 \times 10^7$ erg deg.$^{-1}$ mole$^{-1}$

and $T$ = absolute temperature.

At equilibrium, that is, in absence of stress, the frequency of jumps in one direction must be equal to that in the opposite direction and will be given, in accordance with Eyring's theory, by the relation

$$\omega = (kT/h)\epsilon^{\Delta\eta/R}\epsilon^{-Q/RT}, \tag{3}$$

where

$k$ = Boltzmann's constant $= 1.3805 \times 10^{-16}$ erg deg.$^{-1}$,

$h$ = Planck's constant $= 6.624 \times 10^{-27}$ erg sec.,

and $\Delta\eta$ = increase in entropy.

This can be written in the form

$$\omega = (kT/h)\epsilon^{-\Delta F/RT}, \tag{4}$$

where

$$\Delta F = \text{change in free energy} = Q - T\Delta\eta. \tag{5}$$

When a shearing stress of magnitude $\sigma$ is applied, the frequency of jumps in the direction of creep is increased, and that in the opposite direction decreased, because the activation energy in the direction of creep is $Q - j\alpha\sigma$, while that in the opposite direction is $Q + j\alpha\sigma$. The magnitude $\alpha$ corresponds to the volume of the unit of flow *per g atom*,[6] and $j$ denotes the conversion factor from ergs to calories ($= 2.39 \times 10^{-8}$ cal. erg$^{-1}$).

Hence, Eq. (4) assumes the form,

$$\omega = (kT/h)\epsilon^{-\Delta F/RT}(\epsilon^{x} - \epsilon^{-x}), \tag{6}$$

$$= (2kT/h)\epsilon^{-\Delta F/RT} \sinh x, \tag{7}$$

where

$$x = j\alpha\sigma/RT = j\alpha S/2RT, \tag{8}$$

since, as pointed out by Kauzmann, $\sigma = S/2$, where $S$ denotes the *applied tensile stress* (expressed in dyne cm$^{-2}$). Furthermore, the *rate of*

*elongation* is given by

$$\nu=(1/l)(dl/dt)=\tfrac{2}{3}s,$$

where $s$ is defined by Eq. (1).

Consequently, Eq. (7) assumes the form,

$$\nu=\frac{4}{3}\frac{\lambda}{L}\cdot\frac{kT}{h}\epsilon^{-\Delta F/RT}\sinh x. \tag{9}$$

Since both $\lambda$ and $L$ are of the same order of magnitude as interatomic distances, we introduce the assumption,

$$\tfrac{2}{3}(\lambda/L)\approx 1.$$

In terms of ordinary logarithms, Eq. (9) assumes the form,

$$\log\left(\frac{\nu}{T}\right)=\log\left(\frac{k}{h}\right)+\frac{\Delta\eta}{4.577}-\frac{Q}{4.577T}+\log(2\sinh x), \tag{10}$$

where $4.577=2.303R$.

Now for $x\geqslant 1.60$, the difference between $\log(2\sinh x)$ and $\log(e^x)$ is equal to or less than 0.02, corresponding to a difference in the values of $\nu$ of less than 5 percent. Since this condition held for the observations described subsequently, we can replace Eq. (10) by the more convenient form,

$$\log(\nu/T)=10.319+\Delta\eta/4.577-Q/4.577T+\gamma S, \tag{11}$$

where, as follows from Eq. (8),

$$\gamma=j\alpha/9.154T.$$

Hence

$$\alpha=3.830\times10^8\gamma T \tag{12}$$

and

$$n=3.830\times10^8\gamma T/V_0, \tag{13}$$

where $n$ denotes the number of atoms per unit of flow, and $V_0$=atomic volume.

At constant temperature, Eq. (11) assumes the form,

$$\log\nu=\log\nu_S+\gamma S, \tag{14}$$

where

$$\log\nu_S/T=10.319+\Delta\eta/4.577-Q/4.577T. \tag{15}$$

Equation (14) has been deduced empirically by previous investigators and is known as *Ludwig's law*.

Obviously, $\gamma$ and $\log\nu_S$ may be determined from a plot of $\log\nu$ *versus* $S$, and $Q$ and $\Delta\eta$ are then derived from a plot of $\log(\nu_S/T)$ *versus* $1/T$.

On the basis of Eq. (5), Eq. (15) can be written in the form,

$$\log(\nu_S/T)=10.319-\Delta F/4.577T, \tag{16}$$

from which $\Delta F$ may be calculated as a function of $T$. Since both $Q$ and $\Delta\eta$ are constants, it follows that $\Delta F$ must be a *linear* function of $T$, and that

$$\partial(\Delta F)/\partial T=-\Delta\eta, \tag{17}$$

while

$$(\Delta F)_{T=0}=Q. \tag{18}$$

The last relation is, of course, valid independently of the value of the constant on the right-hand side of (16).[7] Thus $\Delta\eta$ may be derived either directly, by application of Eq. (15), after $Q$ has been determined from a plot of $\log(\nu_S/T)$ *versus* $1/T$, or by means of the relation

$$\Delta\eta=-\Delta F-Q/T. \tag{19}$$

In the latter case, $\Delta F$ is first calculated for each value of $\nu_S$ and from these values an average value of $\Delta\eta$ is obtained.

Since the observations yield $\log\nu_S$ directly, it is more convenient to plot $\log\nu_S$ *versus* $1/T$. Denoting the value of the activation energy thus derived, by $Q_1$, it is evident that

$$Q=Q_1-2T_a,$$

where $T_a$ is the average temperature for the series of observations. The value of $Q$ thus deduced does not differ from that deduced by means of Eq. (15) by an amount which is as much as that due to actual experimental errors.

The relations deduced above involve the assumption of the validity of Eyring's theory of absolute rates, applied to the interpretation of creep. As shown in the following discussion, this theory, which involves the validity of Eq. (6), leads to the very interesting conclusion that in all the cases investigated by us, $\Delta\eta$ is found to have a large *negative* value. The physical interpretation of this result obviously presents certain difficulties.

A decrease in entropy indicates that the elongation is accompanied by a certain amount of orientation of atoms or units of flow. It would seem that some sort of cooperation is required

among the atoms within the unit of flow before elongation can occur. This led to the suggestion that $\Delta\eta$ might be proportional to log $n$, but while, in general, the entropy increases with the size of the unit of flow in accordance with some such relation, the evidence for its validity is not very satisfactory. In the present state of our knowledge of the actual mechanism of creep, it does not, however, seem that we have sufficient information from which any definite conclusions may be drawn.[8]

Apart from any theoretical considerations, it is evident that the experimental data lead to the following conclusions:

Under conditions such that the rate of creep is *constant* over a considerable period, at a given temperature and stress, the rate can be represented as a function of $T$ and $S$ by an *empirical* relation of the form

$$\log \nu = \log \nu_0 - Q_1/4.577T + \log (2 \sinh x)$$
$$= \log \nu_S + \log (2 \sinh x), \qquad (20)$$

where $x = 2.303\gamma S$.

For values of $x \geqslant 1.60$, that is, $\gamma S \geqslant 0.70$, the difference between log $(2 \sinh x)$ and $\gamma S$ is less than 5 percent. Consequently Eq. (20) can be written in the form

$$\log \nu = \log \nu_S + \gamma S. \qquad (14)$$

For values of $x \leqslant 0.50$, that is, $\gamma S \leqslant 0.217$ and $(\log \nu - \log \nu_S) \leqslant 0.02$, the equation for creep assumes the simpler form

$$\nu = 4.606\gamma\nu_S S, \qquad (21)$$

that is, $\nu$ *varies linearly with* $S$ at constant temperature. Obviously, this relation is applicable when $\nu$ is equal to or less than $\nu_S$ for the given value of $T$. The error involved in calculating $\nu$ by means of Eq. (21) instead of (20) is only 4 percent for $x = 0.50$ and decreases for smaller values of $x$.

As an illustration of the application of these equations for calculating rates of creep, Fig. 5 shows plots of log $\nu$ *versus* $S$ for a case in which $\nu_S = 1.6 \times 10^{-8}$, and $\gamma = 6.75 \times 10^{-9}$.

For $\gamma S \geqslant 0.70$, i.e., $S \geqslant 1.037 \times 10^8$, Eq. (14) is applicable. This is shown by the linear plot, I. In the range $1.037 \times 10^8 \geqslant S \geqslant 3 \times 10^7$, Eq. (20) has been used, corresponding to section Ia of the plot. For smaller values of $S$, Eq. (21) leads to

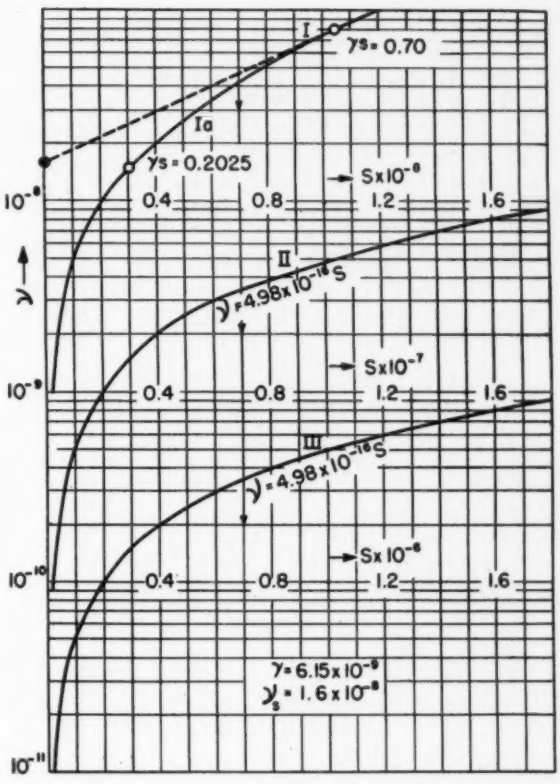


FIG. 5. Plots of log $\nu$ ($\nu$ = creep rate in sec.$^{-1}$ *versus* $S$ stress in dynes cm$^{-2}$) for the case $\nu_S = 1.6 \times 10^{-8}$ and $\gamma = 6.15 \times 10^{-9}$.

the relation,

$$\nu = 4.98 \times 10^{-16} S,$$

and the corresponding plots are shown in curves II and III. The scale of values of $S$ is indicated under each curve.

## 5. EXPERIMENTAL RESULTS

### (1) Constantan

This alloy has the composition 55 Cu, 45 Ni, with traces of Mn and Fe. A 10-mil diameter wire was used, and observations on rates of creep were made with the cathetometer. Before taking creep data, the wire was aged ten minutes at 500°C, with just sufficient tension to straighten it. After this, the temperature was lowered rapidly to the desired point and measurements taken on the rate of elongation as a function of stress, at constant temperature. Since the length of wire used was 10 cm,

$$\nu = r/600,$$

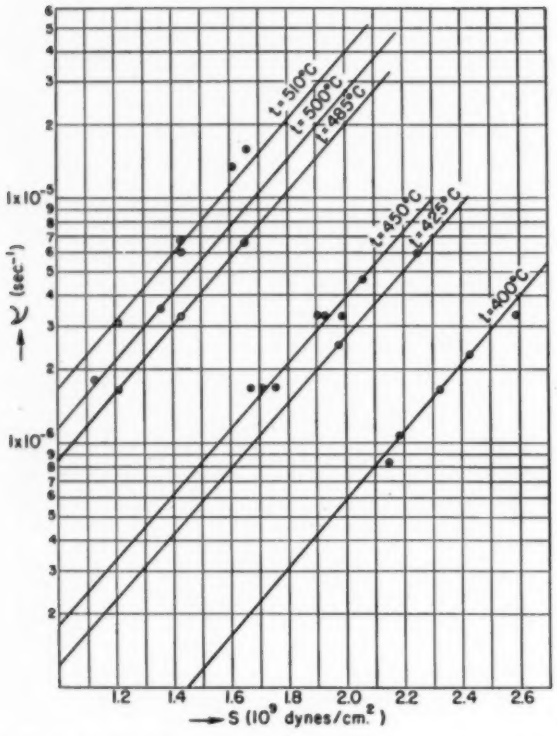


FIG. 6. Plots of log $\nu$ *versus* $S$ for different values of temperature, for constantan wire.

where $r$ = observed rate of creep in cm min.$^{-1}$.

From the plots of log $\nu$ *versus* $S^9$ (see Fig. 6) and of log $\nu_S$ *versus* $1/T$ (see Fig. 7), the following values of the characteristic constants are deduced:

$$\gamma = 1.433 \times 10^{-9},$$
$$Q_1 = 41{,}800; \quad Q_1/4.577 = 9{,}133,$$
$$\log \nu_0 = 4.54,$$
$$T_a = 720,$$
$$Q = 40{,}360,$$
$$\Delta\eta = -41.4,$$
$$\Delta F = 40{,}360 + 41.4T,$$
$$\alpha = 0.548T,$$
$$n = \alpha/7.30 = 0.075T.$$

### (2) Pure Aluminum

A rod of extremely pure metal (99.99 percent Al) was drawn down to 20 mils and observations of creep rates were made in the same furnace as used for constantan. In this case, also, $l = 10$ cm, and $\nu = r/600$.

As is well known, the crystal structure of a metal is affected by annealing treatment. In the case of the aluminum wires, three different temperature treatments were tried out. In the first of these, the wires were annealed in the furnace for fifteen minutes at 500°C. The furnace temperature was then lowered rapidly to the testing temperature and creep data taken. In the second method, the wires were maintained at 500°C for two hours before lowering the furnace temperature. In both of these cases, large crystals were developed having a length considerably greater than the wire diameter, and on the whole it may be stated that the creep rates were about the same, irrespective of length of anneal at 500°C.

At the suggestion of Dr. R. Smoluchowski, observations were also made on some "single-crystal" wires prepared by him, from the 20-mil wire, by a special heating schedule. In the range 300°C to 400°C the creep rates observed for these wires were not materially different from those observed for the wires annealed at 500°C, but at lower temperatures, especially below 250°C, the single-crystal wires exhibited much more rapid rates of elongation, and the actual observations varied over a wide range. This was

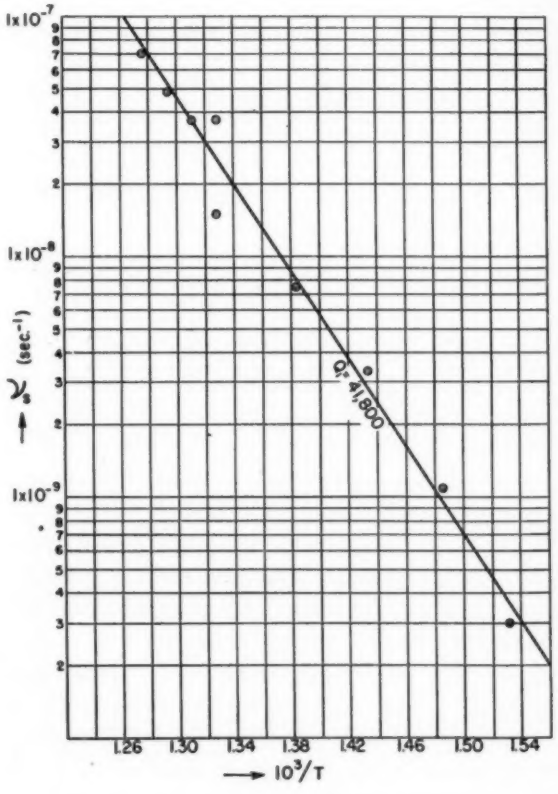


FIG. 7. Plot of log $\nu_S$ *versus* $1/T$ for constantan.

due to the gradual formation, during elongation, of constrictions at more than one point along the wire, whereas in the case of the wires annealed at 500°C, only one constriction would form when the elongation approached the rupture point.

In the case of constantan and many of the other materials investigated, it was possible to observe rates of elongation on any one sample at constant temperature for a series of weights. But in the case of the aluminum wires, the best results were obtained by observing elongation *versus* time for an interval of several hours with the weight constant. Thus for each point on the plot of creep rate *versus* stress, a different sample of the wire was used.

The creep rates observed for temperatures ranging from 250°C to 400°C are shown in Fig. 8. The most striking feature of the data is the fact that $\gamma$ varies rapidly with temperature. Owing to the scattering of the points for any one temperature, it was difficult to determine $\nu_S$ with any degree of accuracy. Furthermore, it is quite possible to draw the straight-line plots in such a manner that the order of values of $\nu_S$ is contrary to that expected from the corresponding temperatures. After several trials it was found possible to obtain a set of self-consistent plots for which the characteristic constants are given in Table I.

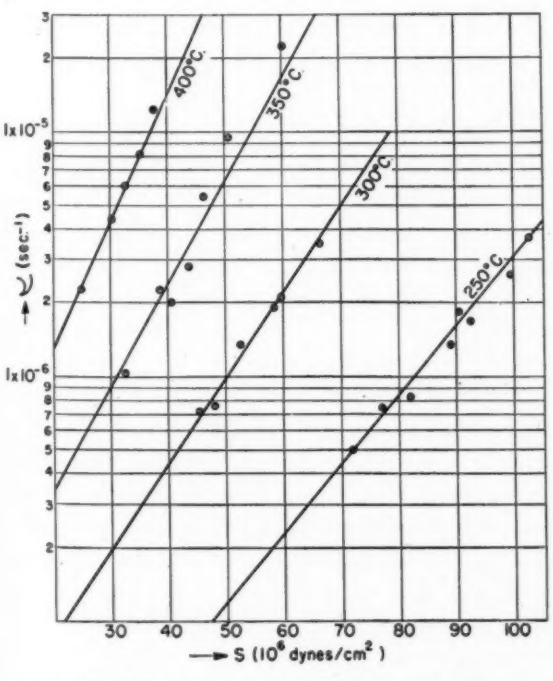


FIG. 8. Plots of log $\nu$ *versus* $S$ for pure aluminum.

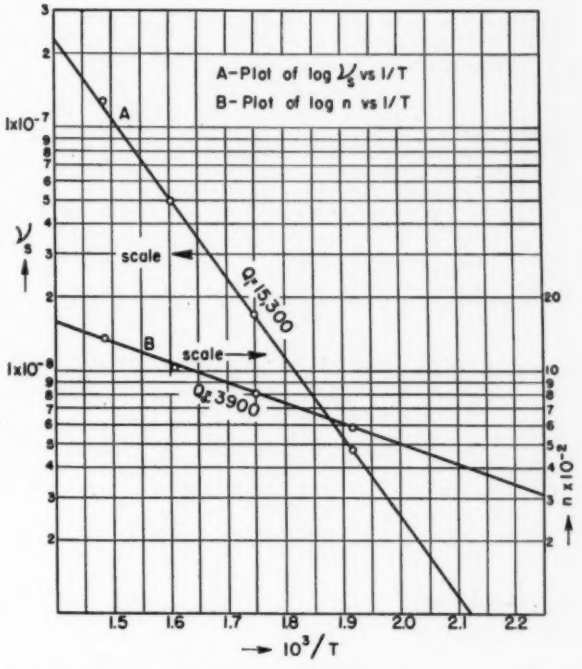


FIG. 9. Plots of log $\nu_S$ *versus* $1/T$ and of log $n$ *versus* $1/T$ for pure aluminum.

TABLE I.

| $T$ | $\gamma \times 10^8$ | $n$ | $\nu_S$ | $\Delta F$ | $-\Delta\eta$ |
|---|---|---|---|---|---|
| 673 | 5.43 | 1400 | $1.27\times10^{-7}$ | 61,730 | 70.2 |
| 623 | 4.42 | 1054 | $5.0\times10^{-8}$ | 58,080 | 70.6 |
| 573 | 3.78 | 830 | 1.67 | 54,710 | 70.8 |
| 523 | 2.99 | 598 | $4.7\times10^{-9}$ | 51,140 | 70.6 |
| | | | | Average = | 70.6 |

From the plots shown in Fig. 9, we obtain the following results:

$$Q_1 = 15{,}300; \quad Q_1/4.577 = 3{,}343,$$
$$\log \nu_0 = -1.936,$$
$$Q = 14{,}100,$$
$$\Delta\eta = -70.6,$$
$$\log \gamma = -(3.191 + \log T + 852/T),$$
$$\log n = 4.392 - 852/T.$$

For Al, $V_0 = 10$.

### (3) Aluminum-Magnesium Alloy

An alloy was made up containing 98 percent Al and 2 percent, by weight, Mg. According to the phase diagram, this alloy exists as a solid solution over the whole range of temperatures.

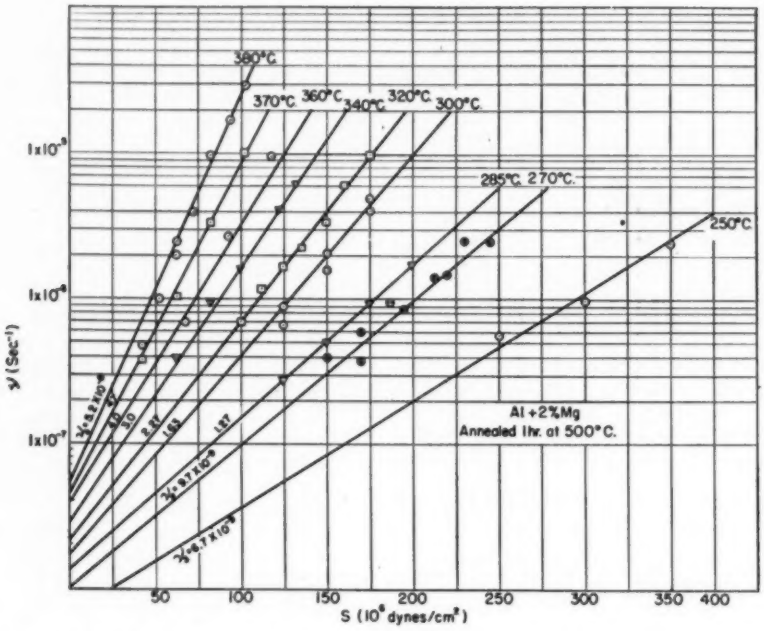


FIG. 10. Plots of log $\nu$ *versus* $S$ for aluminum-magnesium alloy (2 percent Mg).

The alloy was drawn down to 20 mils, and observations made with the recording arrangement described previously. Since the length of the hot zone in the furnace used was 5 cm, this corresponds to the value of $l$. After suspending the wire with a weight of 20 g (the weight of the lower chuck) in the hot zone of the furnace, the temperature of the latter was raised to 500°C and maintained at this value for one hour. Then the temperature was lowered to that desired for the creep test and observations taken on the recording paper for a series of gradually increasing stresses.

Figure 10 shows plots of log $\nu$ *versus* $S$ for the temperature range 250°C to 380°C. Table II gives values of $\nu_S$, $\gamma$, and $n$ for the series of temperatures. This series corresponds to $T_a=600$.

The values of $\nu_S$ were obtained from a plot of approximate values of log $\nu_S$ *versus* $1/T$ corresponding to

$$Q_1=10{,}770; \quad Q_1/R=2{,}354,$$
$$\log \nu_0=-3.685,$$
$$\log \gamma=-(2.293+\log T+1622/T),$$
$$\log n=5.29-1622/T \text{ (see Fig. 11).}$$

A plot of log $(\nu_S/T)$ *versus* $1/T$, shown in Fig. 11, yields the values

$$Q=9540, \quad \Delta\eta=-78.8.$$

TABLE II.

| $T$ | $\nu_S\times10^8$ | $\gamma\times10^8$ | $n$ |
|---|---|---|---|
| 653 | 5.2 | 2.79 | 696 |
| 643 | 4.7 | 2.35 | 578 |
| 633 | 4.0 | 1.99 | 482 |
| 613 | 3.0 | 1.82 | 438 |
| 593 | 2.27 | 1.57 | 356 |
| 573 | 1.63 | 1.42 | 312 |
| 558 | 1.27 | 1.13 | 240 |
| 543 | 0.97 | 1.06 | 220 |
| 523 | 0.67 | 0.78 | 156 |

### (4) Commercial Aluminum

Observations were also made on a sample of commercial aluminum wire drawn down to 20 mils. This material contains as impurities traces of Fe, Si, and Mn and is considerably harder than the pure metal. The tests were made by means of a cathetometer in the same furnace as used for tests on pure aluminum, with $l=10$ cm. Before starting a series of observations at any temperature, the wire was annealed for thirty minutes at 450°C and the temperature of the furnace was then lowered to the desired value. As in the case of the creep tests on the pure metal, the rate of elongation was observed at constant stress until the sample broke.

The observed rates of elongation varied at any one temperature and stress over a much greater

range than in any of the other samples tested. However, by taking a large number of observations, it was found possible to deduce average values for any one combination of values of $S$ and $T$, which lead to the results given in Table III.

TABLE III.

| $T$ | $\nu_S$ |
|---|---|
| 673 | $3.0\times10^{-8}$ |
| 623 | $6.0\times10^{-9}$ |
| 573 | $3.7\times10^{-10}$ |
| 523 | $1.7\times10^{-11}$ |

The plots of log $\nu$ *versus* $S$ indicated the same value of the slope at all values of $T$, corresponding to

$$\gamma=2.79\times10^{-8} \quad \text{and} \quad n=1.068T.$$

From the plot of log $\nu_S$ *versus* $1/T$, we obtain the values,

$$Q_1=34{,}340; \quad Q_1/4.577=7{,}494,$$
$$\log \nu_0=3.66,$$
$$Q=33{,}140,$$
$$\Delta\eta=-32.5.$$

In view of the spread of the original observations, these values must be regarded as rough approximations involving errors which may be as much as 10 percent in the case of $Q_1$ and $Q$.

### (5) Platinum

For this investigation, a sample of "pure" wire, 10-mil diameter, was used in the form of a V-shaped filament, each leg having a length of

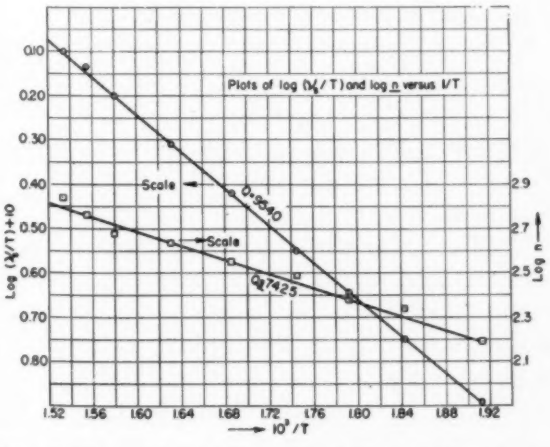


FIG. 11. Plots of log ($\nu_S/T$) *versus* $1/T$ and of log $n$ *versus* $1/T$ for aluminum-magnesium alloy.

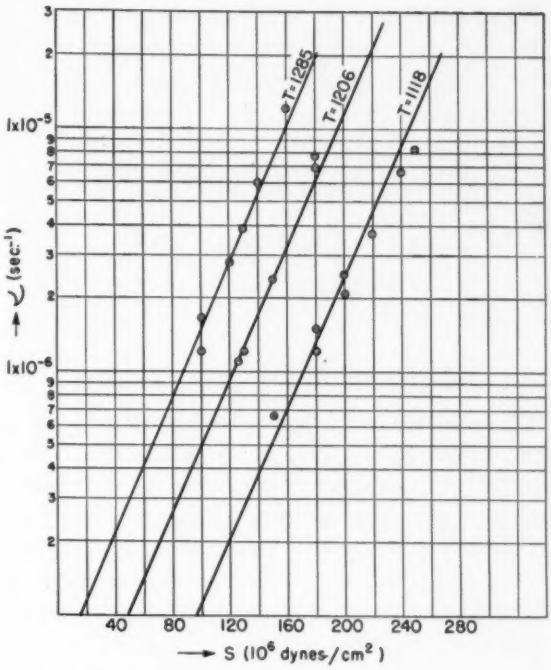


FIG. 12. Plots of log $\nu$ *versus* $S$ for pure platinum.

15 cm. Hence $\nu=r/900$. The arrangement shown in Fig. 2 was used and the wire raised to the desired brightness temperature (as obtained by comparing with the tungsten ribbon lamp) by passing current through it. Rates of elongation were observed by means of a cathetometer.

For a given brightness temperature $T_B$, the true temperature ($T$) of the filament is given by the relation,

$$\frac{1}{T}-\frac{1}{T_B}=\frac{2.303\times0.665}{1.438}\log e_\lambda,$$

where $e_\lambda$ = emissivity at $\lambda=0.665\mu$.

This value of $e_\lambda$ was used since the color, at the temperatures used, corresponds approximately to this wave-length. It was actually observed that the same values of $T_B$ were obtained with and with and without a red filter.

For tungsten at $T=1000$, $e_\lambda=0.456$, while for platinum $e_\lambda=0.30$. Inserting these values in the above equation, the following results are obtained:

| $T$ | $T_B$ for tungsten | $T_B$ for platinum |
|---|---|---|
| 1000°K | 966 | 947 |
| 1100 | 1058 | 1037 |
| 1200 | 1149 | 1125. |

Figure 12 shows plots of log $v$ *versus* $S$ for three temperatures. Observations were also made at other temperatures. From these data the following results were deduced:

$\gamma = 1.413 \times 10^{-8}$ for all values of $T$,
$n = 0.593T$ (corresponding to $V_0 = 9.12$),
$\log \nu_0 = 0.235$,
$Q_1 = 44{,}500$; $Q_1/R = 9{,}723$,
$Q = 42{,}100$ (corresponding to $T_a = 1200$),
$\Delta\eta = -61.5$.

### (6) Nickel-Molybdenum Alloy

A sample of a special alloy for high temperature work, prepared by Mr. R. Thielemann of this laboratory, was drawn down to 10 mils, and tested in the form of a V-shaped filament, in nitrogen. The alloy had the composition 56 Ni, 20 Mo, 12 Co, and 12 Cr. Observations of elongation were made by means of a cathetometer at different brightness temperatures. While the emissivity was not determined, the appearance of the surface indicated that the temperatures measured by pyrometering against the tungsten ribbon filament were not very different from the true temperatures. Table IV gives values of $\log \nu_S$ and $\gamma$ for different values of $T$.

TABLE IV.

| $T$ | $\log \nu_S$ | $\gamma \times 10^9$ |
|---|---|---|
| 1095 | $\bar{8}.461$ | 1.61 |
| 1110 | .590 | 1.66 |
| 1125 | .709 | 1.90 |
| 1155 | .950 | 2.35 |
| 1183 | $\bar{7}.176$ | 2.68 |
| 1210 | .368 | 3.32 |
| 1239 | .564 | 4.18 |

From these data we deduce the following values:

$Q_1 = 47{,}670$; $Q_1/R = 10{,}420$,
$\log \nu_0 = 1.977$.

Since $T_a = 1150$, $Q = 45{,}370$ and $\Delta\eta = -52.7$,
$\log \gamma = -(5.331 + 3810/T)$,
$\log n = 2.392 + \log T - 3810/T$ (corresponding to $V_0 = 7.24$).
For $T = 1000$, $n = 38$ and for $T = 1300$, $n = 376$.

Values of $v$ calculated by means of these constants differ from those observed by 15 percent or less in the majority of cases, although larger differences have also been obtained.

Table V gives values of $T$ and $S$ calculated for two creep rates.

TABLE V.

| $T$ | $\log \nu_S$ | $\log \gamma$ | $S \times 10^{-8}$ calculated For $v = 5 \times 10^{-7}$ | For $v = 5 \times 10^{-8}$ |
|---|---|---|---|---|
| 1000 | $\bar{9}.557$ | $\bar{10}.859$ | 29.7 | 15.8 |
| 1100 | $\bar{8}.484$ | $\bar{9}.206$ | 7.6 | 2.0* |
| 1200 | $\bar{7}.295$ | $\bar{9}.495$ | 1.5* | 0.74* |

* The values marked with an asterisk were derived by means of Eq. (20a).

### (7) Silver

A sample of pure metal (99.99 percent, Ag) was drawn down to 30-, 20-, 15-, and 10-mil sizes. In the cases discussed previously, only one diameter of wire had been used. While it seems obvious that the rate of creep should depend only on the stress and temperature, it seemed of interest to determine whether the same stress applied to different sizes would result in the same creep rate at any given temperature.

The wires were tested in the furnace used for testing the aluminum-magnesium alloy, so that $l = 5$ cm; the rate of elongation was determined by means of the photoelectric recorder arrangement.

Three different annealing treatments were used as follows: (A) annealed 2 hours in air at 500°C, (B) annealed 2 hours in vacuum at 525°C, (C) annealed 1 hour in hydrogen at 525°C followed by 1 hour in vacuum at 525°C.

The object of treatments (B) and (C) was the elimination of oxygen in the wire, as demonstrated by the metallographic observations on samples annealed by schedule (A).

Table VI presents a summary of the whole series of observations. Some of the conclusions from these data are as follows:

(1) The nature of the annealing schedule exerts a profound effect on the values of the creep constants.

(2) The value of $\gamma$, which expresses the variation in rate of creep with stress at constant temperature, varies to some extent with the diameter of the wire. Theoretically, this should be independent of the diameter and the fact that this is not always confirmed by observation is due, as microphotographs show (see discussion in next section), to a difference between the

TABLE VI.

| Anneal schedule | $d$ in mils | $\nu g$ for $T=$ 523 | 573 | 623 | 673 | 723 | $\gamma\times10^{-9}$ | $n$ | $Q_1$ | $\log \nu_0$ | $Q$ | $\Delta\eta$ |
|---|---|---|---|---|---|---|---|---|---|---|---|---|
| A | 10 | $1.8\times10^{-9}$ | $8.0\times10^{-9}$ | $3.3\times10^{-8}$ | | | 5.23 | $0.195T$ | 20,340 | −0.246 | 19,100 | −63.5 |
| | 15 | | $1.2\times10^{-8}$ | $5.8\times10^{-8}$ | | | 5.23 | $0.195T$ | 20,340 | −0.105 | 19,100 | −62.7 |
| | 20 | $7.7\times10^{-10}$ | $3.5\times10^{-9}$ | $1.6\times10^{-8}$ | $6.0\times10^{-8}$ | $1.75\times10^{-7}$ | 6.75 | $.251T$ | 20,340 | −0.702 | 19,100 | −65.1 |
| | 30 | | $4.3\times10^{-9}$ | $2.0\times10^{-8}$ | | $2.3\times10^{-7}$ | 6.72 | $.250T$ | 20,340 | −0.613 | 19,100 | −64.7 |
| B | 10 | $7.3\times10^{-9}$ | $2.0\times10^{-8}$ | $4.3\times10^{-8}$ | $1.17\times10^{-7}$ | | 4.75 | $.177T$ | 12,700 | −2.857 | 11,500 | −75.0 |
| | 20 | | $1.2\times10^{-8}$ | $2.6\times10^{-8}$ | $5.0\times10^{-8}$ | $1.33\times10^{-7}$ | 4.65 | $.173T$ | 14,080 | −2.554 | 12,800 | −73.7 |
| | 30 | | $5.7\times10^{-9}$ | $1.7\times10^{-8}$ | $4.0\times10^{-8}$ | | 5.88 | $.219T$ | 15,260 | −2.427 | 14,000 | −72.8 |
| C | 20 | $1.7\times10^{-10}$ | $2.0\times10^{-9}$ | $9.3\times10^{-9}$ | $4.1\times10^{-8}$ | | 8.04 | $.300T$ | 26,000 | 2.527 | 24,800 | −56.9 |
| | 30 | | $3.7\times10^{-10}$ | $3.3\times10^{-9}$ | $1.8\times10^{-8}$ | | 10.46 | $.390T$ | 29,900 | 0.481 | 28,700 | −52.8 |

For $T=500$, $n=0.2T=100$
$=0.18T=90$
$=0.25T=125$
$=0.4T=200$.

grain structure of the outer layers of the wire and that of the inner ones.

(3) Theoretically, $\log \nu_0$ should also be independent of wire size. In the case of wires annealed according to schedule A, the variation in values of $\log \nu_0$ corresponds to a fourfold variation in value of $\nu_0$; in the case of wires annealed according to schedule B, there is observed an approximately threefold variation in value of $\nu_0$.

Of course, it should be noted that because of the exponential form of the equation for creep, even a small variation in value of $Q_1$ affects the value of $\nu_0$ to a much greater extent.

## 6. CREEP DATA ON METALS, IN LITERATURE

### (1) Polycrystalline Tin

Observations have been published by L. C. Tyte.[10] A plot of $\log_e \nu$ *versus* $P$, the load, expressed in kg cm$^{-2}$, is observed to consist of two straight lines, of which the first one, that at lower loads, is flatter than the second. The observations are represented by relations of the form

$$\log \nu = 0.4343(\log A + BP),$$

where $P$ is expressed in kg cm$^{-2}$. It follows that $\alpha = 169.5BT$ (cm$^3$ g atom$^{-1}$).

From the values of $A$ and $B$ given for the first portion of each of the plots for constant $P$, it is found that

$$Q = 5290, \quad \Delta\eta = -78.6,$$

and using the value $V_0 = 16.3$, the values for $B$ lead to the relation

$$\log n = 3.90 - 2300/4.577T.$$

### (2) Polycrystalline Lead

From the observations published by L. C. Tyte,[11] for the range 148°C to 296°C, and omitting the data obtained for 178°C (which seem to be inconsistent with the data at other temperatures), the following results are deduced:

$$Q = 11{,}500,$$
$$\Delta\eta = -92,$$
$$\log n = 4.50 - 4080/4.577T,$$

where $n = 99\beta T$ (in terms of Tyte's constant).

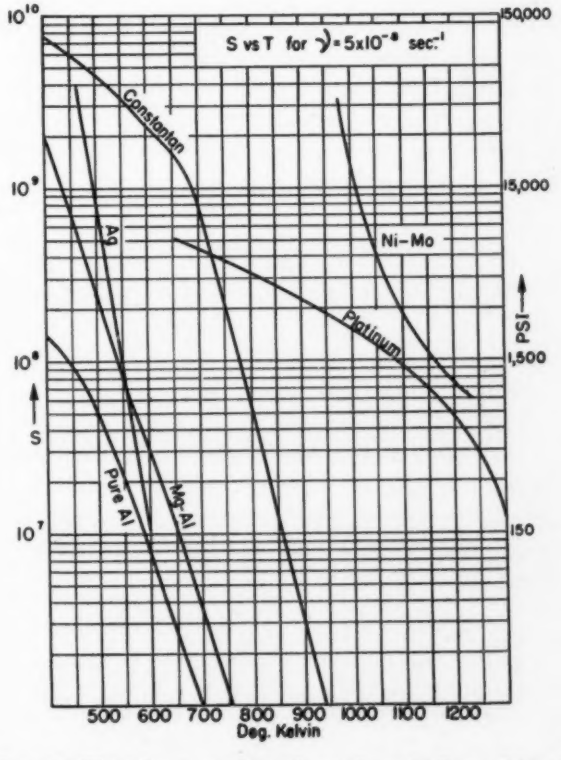


FIG. 13. Plots for a number of metals and alloys of log $S$ *versus* $T$ for constant creep rate, $\nu = 5\times10^{-8}$ sec.$^{-1}$.

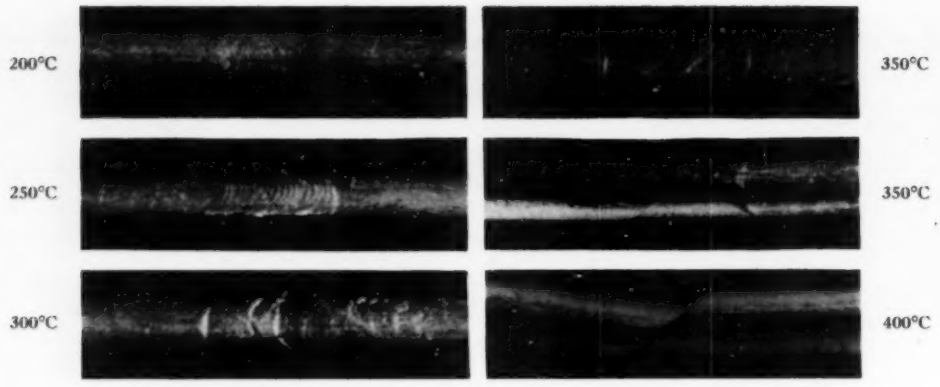


FIG. 14. Pure aluminum. Not etched. ×15. Sample elongated at different temperatures by application of stress.

Creep data on "virgin lead in the form of extruded rod" have been published by J. McKeown[12] for 17°C to 80°C. The plot of log $\nu$ *versus* $S$ for the lower temperature leads to the values $\nu_S = 4.63 \times 10^{-12}$ and $n = 441$. From the two points available for 80°C, we obtain the values $\nu_S = 1.45 \times 10^{-11}$ and $n = 1070$. Hence $Q_1 \approx 3050$ and $\Delta\eta \approx -89$.

The differences between the results obtained in the two series of investigations are probably due to the presence of impurities in the lead used by McKeown and to a difference in annealing treatment. The latter observed that the creep rate at room temperature increases considerably with decrease in grain size.

### (3) Single Crystals

For tin, Kauzmann has deduced from available data the value $n = 2270$ (temperature not given) which is much larger than the value obtained above for polycrystalline metal.

E. N. da C. Audrade, in his very interesting lecture on "The flow of metals," [13] has given data on single crystals of cadmium. The total periods required to obtain an elongation of 1 percent at room temperature for a series of stresses are stated to be as follows:

| Stress in g mm$^{-2}$ | Time in hours |
|---|---|
| 17 | 0.067 |
| 15 | 0.25 |
| 13 | 1.0 |
| 10 | 7.0 |
| 5 | 300.0. |

A plot of log(time) *versus* stress yields a good straight line for which,

$$\nu_S = 2.92 \times 10^{-10}, \quad \alpha = 3.47 \times 10^{5},$$

and

$$n = 26{,}700.$$

From these results for single crystals, it would appear that in these cases the values of $n$ are much greater than for polycrystalline material, which is consistent with the observations that rate of creep increases with stress much more rapidly for single crystals than for polycrystalline materials.[14]

### 7. GENERAL REMARKS ON CREEP DATA

Creep observations on high conductivity copper at 200°C have been made in this laboratory by Mr. E. R. Parker. The tests were carried out on various-sized cylindrical rods ranging from 0.160 to 0.505 inch in diameter, which were annealed according to different schedules in order to vary the grain size. It was observed that, in all cases, Eq. (14) could be applied and that the value of $\gamma$ was constant, independent of grain size. While earlier observations led to the conclusion that log $\nu_S$ passes through a maximum with decrease in grain size, this was not found to be the case when the smaller diameter rods were electroplated with cadmium or the tests were carried out on 0.5-inch diameter rods. In these cases (where presumably the effects of surface oxidation were minimized) it was observed that log $\nu_S$ increased with decrease in grain size, to a constant value.[15]

From the observed value, $\gamma = 3.3 \times 10^{-9}$ cm$^2$

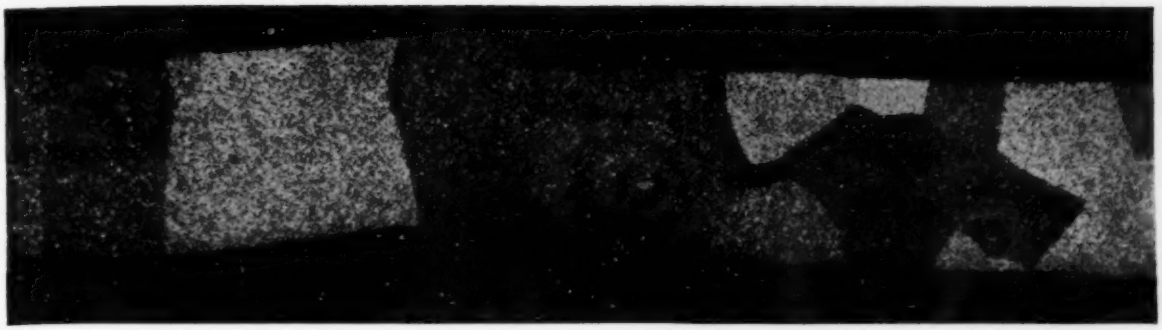

FIG. 15. Pure aluminum. Etched with 0.5 percent hydrofluoric acid. ×50. Photomicrograph of constricted part of wire tested at 400°C, showing initiation of trans-crystalline fracture.

dyne$^{-1}$, it follows that $\alpha = 597$ cm$^3$, and $n = 84$ (since $V_0 = 7.12$ for Cu). This value is to be compared with the value $n = 90$ at $T = 500$, observed for Ag (as shown in Table VI, for schedule B).

Creep data published in the literature on a number of iron alloys have been used by Kauzmann[16] to calculate values of $Q$ and $\eta$. In general, these alloys exhibit values of $Q$ ranging from 5000 to 102,000 and large negative values of $\eta$, ranging from $-55$ to $-108$. The preliminary experiments which the first-named writer of this paper carried out with filaments of such alloys in nitrogen gave extremely erratic results in most cases. This was ascribed to the quite frequent occurrence of phase transformations such as are characteristic of iron alloys.

The most creep-resistant alloys for high temperatures are those containing nickel, molybdenum, chromium, and tungsten. Data for one such alloy (nickel-molybdenum) have been given in a previous section. A number of other alloys were also tested, and while they exhibited creep rates of the same order of magnitude as the Ni-Mo alloy, the observations were too widely scattered for use in calculating creep constants.

It has seemed to the writers that the most satisfactory method of comparing creep resistance of different materials is that of plotting curves, for each, of values of $S$ *versus* those of $T$ for a given value of $\nu$.

Figure 13 shows such plots for the value $\nu = 5 \times 10^{-8}$ sec.$^{-1}$ (corresponding to 0.018 percent per hour) for the different materials on which data were obtained in the present investigation. The values of $S$ are given in dynes per cm$^2$ on the left-hand side, and in pounds per square inch on the right. It should, of course, be pointed out that these plots represent an extrapolation from actual observations made in the range $10^{-5} > \nu > 5 \times 10^{-7}$, that is, under conditions in which the creep rate was at least ten times that used in calculating the plots of Fig. 13. Furthermore, in actual practice, the engineer is interested in rates of creep which are 100 to 1000 times *less*. Whether the creep constants obtained from short-period tests, such as those carried out in the present investigation, can be used for extrapolation to long-period tests is extremely questionable. On the other hand, it is much more likely that such plots as these given in Fig. 13, which are based on short-period tests, may be used to give *relative* creep-resistance values for materials, even under very long-period tests.

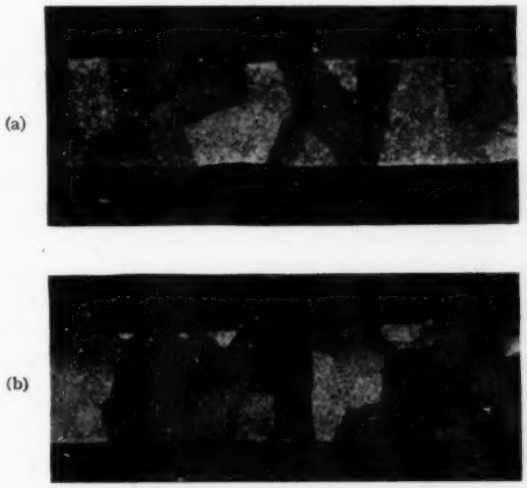


FIG. 16. Pure aluminum. Etched with 0.5 percent hydrofluoric acid. ×30. Photomicrographs of wire tested at 200°C. (a) Of constricted, central region, (b) of the cold end.

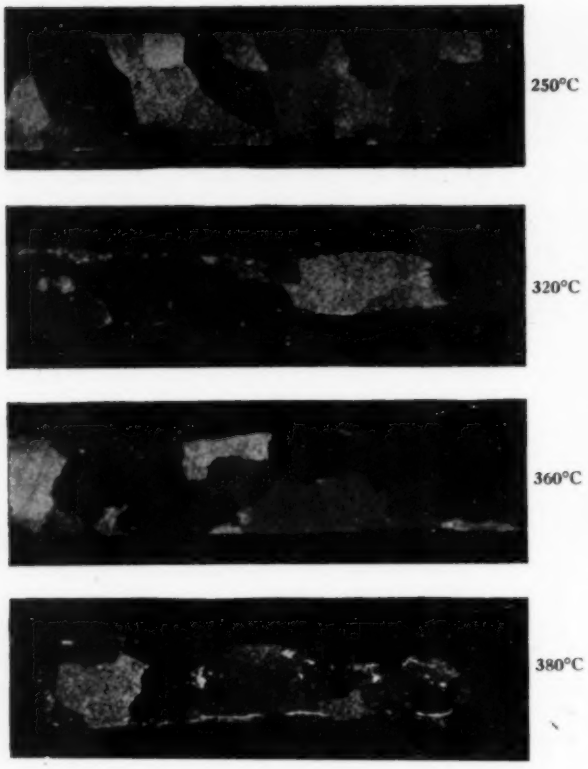


FIG. 17. Aluminum 98 percent, magnesium 2 percent. Etched with 0.5 percent hydrofluoric acid. ×30.

Furthermore, as pointed out in the introduction, the results described in this paper were obtained only under conditions of *constant creep rate*, that is, where the elongation-*versus*-time plot was linear for an appreciable period. In many cases we found it impossible to reach such a condition, since the rate of creep at constant stress decreased continually without exhibiting any tendency towards reading a constant value. For instance, in the case of gold wires, we were unable to attain a condition of constant creep rate in spite of many attempts at varying annealing schedule as well as combinations of temperature and stress. In the case of aluminum and aluminum-magnesium alloy wires, each point on the rate-of-creep *versus* stress plot had to be determined from an elongation *versus* time plot which was taken over a period of several hours until fracture occurred.

That metals underoing deformation under stress gradually "harden" is well known, and this effect is much more pronounced at low rates of creep. For this reason, as well as on account of other practical difficulties, we were unable to obtain data on creep rates much below that corresponding to $\nu \approx 5 \times 10^{-7}$ sec.$^{-1}$. It follows that an extrapolation from the rates observed to lower values is likely to be erroneous because of failure to take into account these hardening effects.

## 8. METALLOGRAPHIC INVESTIGATION OF ELONGATED WIRES

During the course of the investigation, a considerable number of photomicrographs were taken of longitudinal sections of the elongated wires. For these photographs, we are greatly indebted to Mrs. C. B. Brodie, who is in charge of the Metallographic Section of the Research Laboratory. Some of the more interesting observations are discussed in the following sections.

### Pure Aluminum

Photographs of the elongated wires at 15-fold magnifications are shown in Fig. 14. The temperature at which the creep test was carried out is indicated beside each photograph. It will be observed that elongation is accompanied by the formation of slip planes and that fracture ultimately occurs by gliding along one such plane. It is of interest to observe that the distance between successive slip planes increases with increase in temperature.

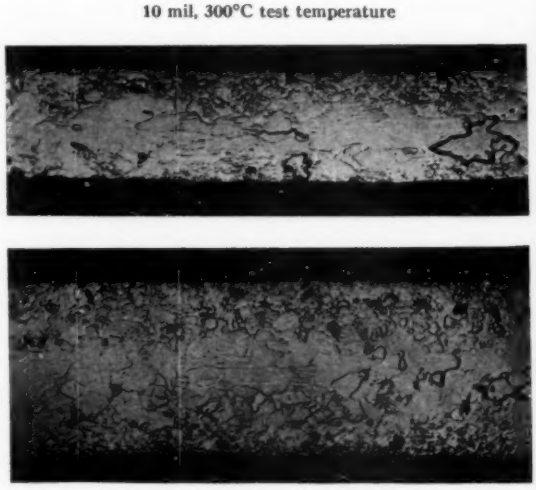


FIG. 18. Silver. Etched with chromic acid—sulphuric acid reagent. ×60. Wires annealed 2 hours at 500°C in air (schedule A).

That these slip planes are formed *within* the grains is shown by the photomicrographs of longitudinal sections taken through the necked portions of the wires.

Figures 15 and 16(a) show the grain structure at the narrowest portions of the wires tested at 400°C and 200°C, respectively. These were taken at 50-fold and 30-fold magnification, respectively. Figure 16 (b) shows the structure at the cold end of the wire which was tested at 200°C. As mentioned previously, the original samples of wire were annealed at 500°C to produce large grain structure.

### Aluminum-Magnesium Alloy

(2 percent Mg)

Figure 17 shows a series of photomicrographs (at 30-fold magnification) of four samples of this alloy tested at temperatures ranging from 250°C to 380°C. In these cases, as in that of pure aluminum, large grains were developed by the annealing treatment and the fracture occurred by necking *within* a grain.

20 mil, 450°C test temperature

30 mil, 350°C test temperature

FIG. 19. Silver. Etched with chromic acid—sulphuric acid reagent. ×60. Wires annealed as per schedule A.

10 mil, 250°C test temperature

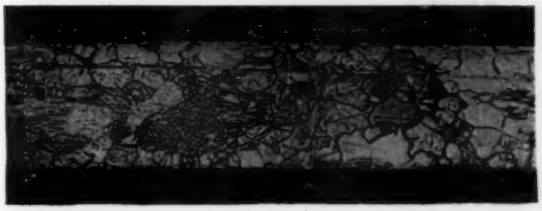

20 mil, 350°C test temperature

FIG. 20. Silver. Etched with chromic acid—sulphuric acid reagent. ×77. Wires annealed 2 hours in vacuum at 525°C (schedule B).

### Silver

As mentioned in the previous section, three different anneal schedules were used, designated A, B, and C. Figure 18 shows the structures of 10- and 15-mil wires, annealed according to schedule A and tested for creep at 300°C and 350°C, respectively. Figure 19 shows photomicrographs of 20- and 30-mil wires annealed according to schedule A and tested at 450°C and 350°C, respectively. It will be observed that the proportion of large-grain material tends to decrease as we pass from 10- to 30-mil size, which undoubtedly accounts for the observed differences in rates of creep.

The wire annealed according to schedule B has the structure shown in Fig. 20, which represents a photomicrograph of a 10-mil wire tested at 250°C and a 20-mil wire tested at 350°C.

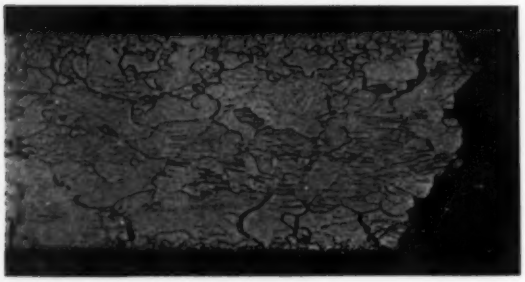

20 mil

FIG. 21. Silver etched with chromic acid—sulphuric acid reagent. ×60. Wire annealed 1 hour at 525°C in $H_2$ followed by 1 hour at 525°C in vacuum (schedule C). Test temperature 350°C.

Large-grain structure was developed by annealing schedule C, as shown in Fig. 21, which also shows the *intercrystalline* type of fracture. This seemed to be specially characteristic of this type of structure.

On the whole, these photomicrographs, as well as a large number of similar photographs taken for some of the other wires, emphasize the intimate relation between grain structure and rate of creep. The change in structure may affect not only the magnitude of the unit of flow (that is, the factor $\gamma$ which gives the variation of rate of creep with stress) but also the magnitudes of the activation energy and of the entropy constant. In order to determine the nature of the relations between the creep constants and the crystal structure more work will be required of a much more precise nature than that attempted in the investigation, the results of which have been presented in this paper. It may be possible to carry out such an extensive program in the future, when conditions permit.

In conclusion the authors wish to express their appreciation of the interest taken in this work by a number of their associates in the Research Laboratory, especially Drs. R. P. Johnson, R. Smoluchowski, and H. H. Uhlig; and Mr. E. R. Parker.

## REFERENCES

(1) This subject has recently been treated very comprehensively in *Physics of Metals* by F. Seitz (McGraw-Hill Book Company, Inc., New York, 1943), which also contains references to the extensive literature from both the practical and the theoretical points of view.

(2) Creep data, *Compilation of Available High-Temperature Creep Characteristics of Metals and Alloys* (A.S.M.E. and A.S.T.M., 1938).

(3) After the equipment had been constructed, a description was found of a similar arrangement by C. W. Gadd and T. C. Van Degrift in a paper entitled "A short gage-length extensometer and its applications to the study of crankshaft stresses" which was presented at the Annual Meeting of the American Society of Mechanical Engineers, December 1–5, 1941.

(4) The cell used is of a type developed by Dr. Hewlett of this laboratory, and the photo-recorder was built by the General Engineering Laboratory at Schenectady.

(5) W. Kauzmann, Metals Tech. **8** (June, 1941). The paper was delivered before a meeting of the American Institute of Mining and Metallurgical Engineers, New York, February, 1941.

(6) In terms of Kauzmann's unit volume of flow, $\alpha = 6.023 \times 10^{23}\, qAl.$

(7) This is, of course, a consequence of the third law.

(8) In this connection the reader will find it of interest to read the discussion in Kauzmann's paper.

(9) The correct values of $S$ are 97 percent of those shown in this and in subsequent plots of $\log \nu$ *versus* $S$.

(10) L. C. Tyte, Proc. Phys. Soc. **50**, 153 (1938).

(11) L. C. Tyte, Proc. Phys. Soc. **51**, 203 (1939).

(12) J. McKeown, J. Inst. Metals **60**, 201 (1937).

(13) E. N. da C. Audrade, J. Inst. Metals **60**, 427 (1937).

(14) Also see discussion by F. Seitz, reference 1, Chapter VI.

(15) Complete data will be published shortly in a paper in Trans. A.I.M.E.

(16) See W. Kauzmann, reference 5.

# Gaseous Diffusion as a Tool for Locating Critical Points in Metals and Alloys

BY HOWARD S. COLEMAN AND HENRY L. YEAGLEY

*The Pennsylvania State College, State College, Pennsylvania*

METALLURGISTS, physicists, and chemists investigating the properties of metals and alloys frequently are concerned with what they call a "critical point." A number of different interpretations have been made of this phrase. A critical point as used here refers to the temperature at which some discontinuity or irregularity occurs in the physical properties of a system involving metals. In this sense, the temperature at which a change occurs in, crystal structure, magnetic state, electronic state, elasticity, expansion, or in state, is a "critical point." Because of great commercial importance, new methods are constantly being sought to determine these points with greater precision.

It is the purpose of this paper to call attention to a method that is little used and often erroneously regarded as too complicated, requiring great skill and long preparation before it can be mastered. This method will be referred to here as "the gaseous diffusion method." We wish to present the method in general and to emphasize that anyone who can read a temperature measuring instrument and a pressure gauge can use gaseous diffusion as a tool.

The field of the diffusion of gases into metals might well be divided into two parts, namely, "gaseous diffusion as a phenomenon," and "gaseous diffusion as a practical tool." As a phenomenon, one deals with the actual physical and chemical mechanisms that occur from an experimental and a theoretical point of view. Gaseous diffusion as a tool, on the other hand, deals only with the actual taking of data to be used by the experimental physicist and metallurgist to correlate and check results obtained by other methods. The present progress in the former part of the field has been reviewed in considerable detail in text by McBain,[1] Smithells,[2] and Barrer.[3] In the following, we shall confine our attention almost entirely to discussion of the diffusion of gases into metals as a tool.

In general, the diffusion of gases through metals is observed by noting the rate at which some gas passes through a thin diaphragm of metal as a result of having a difference of pressure on the two sides of the diaphragm. Figure 1 is a schematic diagram of a common type of apparatus used in measuring diffusion rates. Such apparatus is described in detail by Ham[4] and co-workers.

The specimen to be studied is mounted in a heavy-walled metal tube and placed in a furnace to permit observation of the diffusion rates at various temperatures. The pressure is measured by a McLeod gauge and the temperature by a thermocouple as indicated in the sketch.

It is found by experiment that the rate at which a diatomic gas diffuses through the metal disk into a vacuous space depends upon the pressure and the temperature as indicated by the following equation:

$$dp_0/dt = AP^{\frac{1}{2}}T^{\frac{1}{2}}e^{-b/T}, \qquad (1)$$

where $dp_0/dt$ is the rate of increase in pressure on the outgoing side of the diaphragm, $A$ is a constant determined largely by the units, dimensions of the apparatus, the gas, and the metal in question. $P$ is the pressure on the ingoing side, and $T$ is the absolute temperature; $b$ is a constant related to the energy of activation $Q$, as indicated

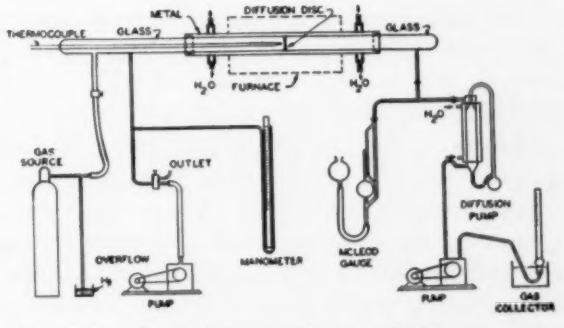


FIG. 1. Apparatus for measuring gas diffusion through metals.

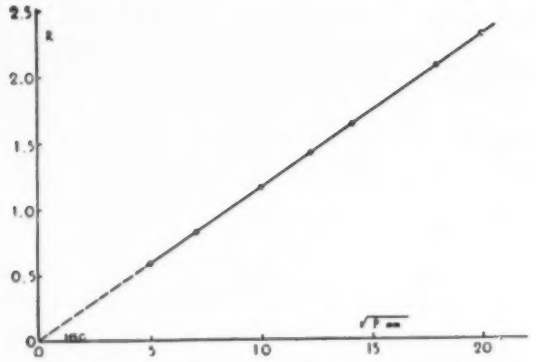


FIG. 2. Diffusion isotherm. Rate of hydrogen diffusion *vs.* $\sqrt{}$ pressure at 725°C.

by Eqs. (2) and (3) in which $R$ is the gas constant. The activation energy is a measure of the ease with which the lattice of the metal may be permeated by the diffusing gas.

$$dp_0/dt = P^{\frac{1}{2}}T^{\frac{1}{2}}e^{-Q/RT}, \tag{2}$$

$$Q = 2.3Rb. \tag{3}$$

Equation (1) is used as the basis for handling gaseous diffusion data. It is common practice to make plots of diffusion rate against square root of the pressure at some particular temperature. An example of such a plot is shown by Fig. 2 for hydrogen diffusing through iron at 725°C. Such plots are referred to as isotherms. It is also convenient to rectify a plot of the rate *vs.* the absolute temperature. This is done by plotting for some particular pressure, $\log_{10}$ (rate) *vs.* $1/T$, which yields a very nearly linear graph since the $T^{\frac{1}{2}}$ term becomes insignificant except at very high temperatures (above 1200°C) in comparison with the exponential term. An example of such a plot, known as an isobar, is shown in Fig. 3 for the diffusion of hydrogen through copper.

The diffusion of a gas through a metal is very similar to an electric current through a metal. In fact, it is a current in that positively charged particles (the gaseous ion) are the moving constituents in the current rather than the usual negative charges (electrons). Just as an ordinary electric current is modified when a metal undergoes a change in energy state (or passes through a critical point), so is the diffusion rate. This is of particular importance if we are to consider gaseous diffusion as a tool. Since the gaseous ion passes from lattice point to lattice in the metal forming temporary compounds, it might be expected that the rate of travel would be "temperature" and "structure" sensitive. That is, if at some particular temperature a transition or transformation were to occur in the metal lattice, the binding forces (which are associated with the outer electrons) would be altered and hence the length of time at which the gaseous ion resides at a particular lattice point would be changed. This of course would effect the diffusion rate. If at some temperature the system were to pass through a critical point, the change in diffusion rate would also change abruptly. This fact makes it possible to use the diffusion rate to locate critical points.

As indicated above, the variables usually measured to determine transformations, or more generally critical points, are the rate and temperature. After one obtains the diffusion rate at various temperatures, a graph is usually made in which the data are plotted using the reciprocal of the absolute temperature as abscissa and the logarithm of the rate as ordinates. According to Eq. (1), such a graph should be very nearly a straight line, as long as the metal does not pass through a critical point, and the pressure is held constant. If some sort of a transformation does occur, it gives rise to an irregularity in the logarithmic plot. We shall refer to such irregularities as "breaks." Breaks often are accompanied by a change in slope of the line which makes it possible to locate the temperature of the transition with great precision. An example of a break may be found in the isobar graph (Fig. 4) of the diffusion of hydrogen through nickel. It

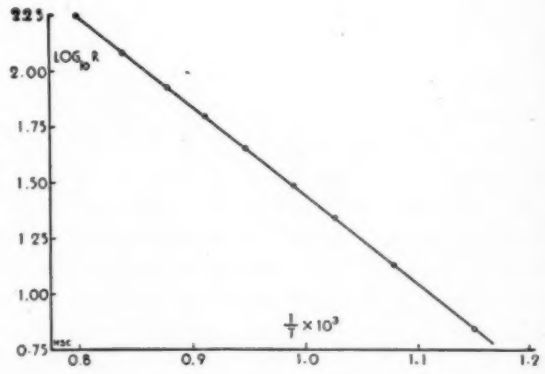


FIG. 3. Diffusion isobar. $\text{Log}_{10}$ (diffusion rate) *vs.* $1/T$. The diffusion of hydrogen through copper at constant pressure.

will be noted that at 360°C on the temperature scale there is an irregularity of diffusion rate. This temperature is the common "Curie" temperature above which nickel is non-magnetic. In the case of hydrogen diffusion through iron, breaks are found corresponding to the critical points $A_2$ (magnetic) at about 770°C, $A_3$ (crystal structure) at about 900°C, and $A_0$ at about 315°C. These breaks found by gaseous diffusion are in excellent agreement with the specific transformations detected by other means; however, the advantage in the diffusion technique is the great precision and the ease with which one may study a metal over a great range of temperatures (50°C–1300°C for iron, for example), and the fact that it is possible to maintain constant temperature over great lengths of time with relatively simple apparatus.

The practical problem of determining segregation in alloys is very easily handled by gaseous diffusion. Another example of the use of the gaseous diffusion method is in the case of the diffusion of air through an alloy, in which one may have either order-disorder or some solid solution of oxide in the occurring alloy. Coleman and Yeagley[5] have found a critical point at 925°C for the diffusion of air through monel metal. This was confirmed later by careful dilatometer measurements. To emphasize further the great sensitivity of gaseous diffusion technique, a case might be cited in the work of Ham and Bennett[6] on hydrogen diffusion through carefully homogenized ferromagnetic alloys. In this case the experimenters found that not only did they find breaks in the diffusion curves at the Curie temperature for the alloys, but also at the Curie temperatures for the constituents. This at first was thought to be simply an indication of ordinary segregation, but subsequent study shows that if it were a result of segregation, it was a very unusual type since during the diffusion study the specimens received very drastic heat treatment and had hydrogen flowing through them for long periods of time. The hydrogen would have a

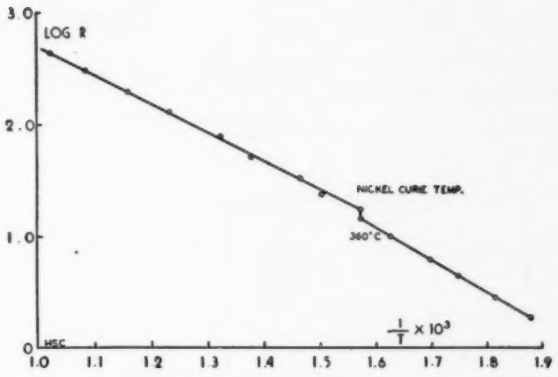


FIG. 4. Diffusion isobar. Log (diffusion rate) *vs.* $1/T$; pressure = 1 atmos.

tendency to reduce the usual impurities which promote segregation. Segregation could not be found by careful microscopic examination or by x-ray diffraction. These same samples in which apparent segregation was found by hydrogen diffusion were later investigated magnetically and the position of the breaks confirmed. Many other specific cases can be found in the literature illustrating the use of the diffusion methods.

It is hoped that this report will help to bring gaseous diffusion technique a little nearer to research laboratories as a general tool and that it may be used when appropriate, as frequently as the established techniques of chemical analysis, electron diffraction, and x-ray diffraction in the study of metallic systems.

## REFERENCES


(1) J. W. McBain, *The Sorption of Gases by Solids* (George Routledge & Sons, London, 1932).

(2) C. J. Smithells, *Gases and Metals* (John Wiley & Sons, Inc., New York, 1937).

(3) R. M. Barrer, *Diffusion in Through Solids* (Macmillan Company, New York, 1941).

(4) W. R. Ham, Trans. A. S. M. E. **25**, 536 (June, 1937).

(5) H. S. Coleman and H. L. Yeagley, J. Chem. Phys. **11**, 135 (1943).

(6) A dissertation by F. D. Bennett, submitted in partial fulfillment for the requirements for the degree of Doctor of Philosophy at The Pennsylvania State College, May, 1941.

# The Cyclotron. II*

BY M. STANLEY LIVINGSTON

*Massachusetts Institute of Technology, Cambridge, Massachusetts*

## 11. TARGET ARRANGEMENTS

THE several purposes of the cyclotron necessitate many different targets, the type being largely determined by the physical properties of the target material. The arrangement in most general use is the external target, in which the deflected beam passes through a thin foil vacuum window over the exit port and against a target located in a closed housing or chamber which can be readily opened for target changing. See Fig. 13. The target chamber can be evacuated by an auxiliary rough vacuum pump or filled with an inert gas.[22] Inert, as used in this sense, means a gas which, in addition to being chemically inactive, produces no objectionable radioactivities which would be driven onto the target surface. Helium is most satisfactory for this purpose since no activities are produced and it also serves as a cooling agent for the target. The emergent beam is spread out horizontally by the fringing magnetic field and also has a small vertical spread. The foil window of the M. I. T. cyclotron is located on the end of a divergent spout about 24 inches from the diametral line of the chamber. At this distance the beam has dimensions of approximately $6\times\frac{3}{4}$ inches. The copper target plates, of $6\times5\frac{1}{2}$ inches, can be tilted to spread the $\frac{3}{4}$-inch beam over any desired width up to $5\frac{1}{2}$ inches. This large surface makes cooling problems relatively simple; water-cooling tubes are soldered to the back of the target plates. Low melting materials and soft metals such as sodium are spread thinly over the surface of a plate which is scored with narrow, undercut grooves similar to a coarse file. Powders can be exposed in a similar manner with the target tilted to an almost horizontal position. Some substances can be melted onto the surface of a smooth plate; others adhere better if the surface is scored or knurled. To standardize this technique small plates ($1\times1\frac{1}{2}\times\frac{1}{16}$ inches) are stamped on one face with a diamond knurl on which the targets are prepared. The plates are then soft-soldered to the backing plate in a pattern to fill the area determined by the angle of tilt. Any material which by melting, sputtering, or evaporation would be harmful to the chamber vacuum or lower the photoelectric threshold of the electrode surfaces must be bombarded behind a foil window. The limitation on this type of target is the low specific activity (activity per gram of target material) resulting from the diffuse beam and large area, and the limited intensity of the deflected beam which is seldom more than 25 percent of the resonant ion current.

The material which has been found most suitable for the foil window is Dural 17 SH microphone diaphragm stock obtained as $6\times6$ inch squares of 0.0010- or 0.0015-inch thickness. The energy loss in the foil is equivalent to about 4.0 cm of air at N.P.T. per mil, or about 0.5 Mev for 10- to 15-Mev deuterons. The foil is clamped between water-cooled Dural plates with rubber gasket vacuum seals, located at the end of the divergent spout. In this location the foil melts at beam currents of about 100 microamperes; if located at the base of the spout where the beam is about $3\times\frac{1}{2}$ inches the limit is 50 microamperes. To raise these limits a double-foil window with intermediate air jet cooling of the foil surfaces is used. This is accomplished by separating the two clamping plates and inserting a third plate which has a row of small air jets and an exhaust manifold. The compressed air line is equipped with a filter and refrigerating condenser to

---

* This is the second of two parts of a comprehensive paper on the cyclotron. The first appeared in January [J. App. Phys. **15**, 2 (1944)]. An outline of the topics treated in the entire paper is given below. Part I included Sections 1 to 10.

1. Introduction
2. Physical Principles
3. Electric and Magnetic Focusing
4. Maximum Energy
5. Oscillator Circuit
6. Magnet
7. Resonant Circuit and Chamber
8. Ion Source
9. Shimming
10. Deflector
11. Target Arrangements
12. Vacuum Pumps
13. Vacuum Seals and Techniques
14. Controls
15. Laboratory Design
16. Shielding
17. Cyclotron Costs
18. Yields of Nuclear Reactions
19. Optimum Size
20. Conclusions and Results

eliminate oil and water vapor. The air used for cooling becomes strongly radioactive and is led outside the building by a conduit. Other laboratories have used similar air-cooled foil windows and have reported transmission of beams of over 200 microamperes. A vacuum valve in the emergent beam port ahead of the foil window which can be closed automatically by a vacuum interlock protects the chamber vacuum when foil windows burn out and facilitates their replacement. For targets which can be bombarded safely in chamber vacuum, the foil holder is removed and the beam is not limited by the transmission of the window. The vacuum valve serves here to change targets without destroying the chamber vacuum. Emergent beam intensities up to 350 microamperes at a nominal 12 Mev have been reported with such an arrangement.[19]

An alternate target location having many advantages is on a probe between the dee tips so as to intercept the resonant ions before they reach the radius of the deflector septum. On such a probe the full resonant beam current is available and the beam is strongly focused by the fringing field. The effective size of the beam in the M.I.T. cyclotron is about $\frac{1}{4}$ inch high by $\frac{1}{8}$ inch wide, the latter being the $\Delta R$ between successive ion paths. Beam currents of up to 1.0 milliampere of resonant ions of 12-Mev energy have been obtained at this laboratory. This represents 12 kilowatts of power to be dissipated in the target, or about 380 kilowatts per square inch of beam cross section. No known method of heat transfer can dissipate this power density and any stationary target would be melted through immediately. We have made several successive steps in the direction of improving heat transfer and enlarging target surfaces. The first was to tilt the target face at a sharp angle to the beam, spreading the $\frac{1}{8}$-inch width over a $\frac{1}{2}$-inch target face. The probe target head was formed in one piece from copper tubing by flattening and bending to give a thin channel (0.012 inch) for water flow. A booster water pump was installed to give pressures up to 90 lb. per square inch, with which the flow was about 1 gallon per minute. The high velocity flow improved heat transfer by a large factor. Next a mechanical shaking device was devised to move the target head up and down at 10 oscillations per second and spread the $\frac{1}{4}$-inch height of beam over the full 1-inch height of the target face. With this arrangement beam currents of up to 500 microamperes have been used successfully for a few metallic targets silver-soldered to the copper target face. Most targets have lower heat conductivities and the intensity is restricted to 100 to 300 microamperes to prevent melting or evaporation. The oscillating probe target stem consists of two copper tubes spaced $1\frac{1}{2}$ inches apart mounted through sliding seals and a vacuum lock so that the targets can be withdrawn and changed without losing chamber vacuum. The emergent beam can pass between the tubes so that external and probe targets can be used together if desired by adjusting the probe location so as to intercept only a small percentage of the emergent beam. In this location the probe is still bombarded by a considerable fraction of the resonant beam which does not have the proper center of curvature to traverse the deflector channel.

The high beam density results in high specific activities for such targets as can be placed in the cyclotron chamber without harm. The limit has always been melting or evaporation of the target surface by the beam. A 1.0-milliampere beam was obtained on a chromium plated copper target head, and the beam melted through the copper and caused a water leak in the head just at the edge of the constricting channel with the high velocity flow. This indicates an average heat transfer limit of about 25 kilowatts per square inch with this target design. Beam currents cannot be measured directly on the probe target, due to secondary emission from the target, electrical discharges, and radiofrequency pick-up. So beam currents are determined from the observed heating of the cooling water and an estimate of the average ion energy. Thermocouples in the inlet and outlet water circuits register the temperature difference and the flow is continuously metered by a rotameter flow meter.

A rotating probe target has been designed to increase still further the surface area of the target and raise the beam limits. See Fig. 13. The target heads are cylindrical cups 2 inches in diameter and 1 inch deep with $\frac{1}{16}$-inch wall thickness. Metallic targets which can be machined are made into this shape; other target

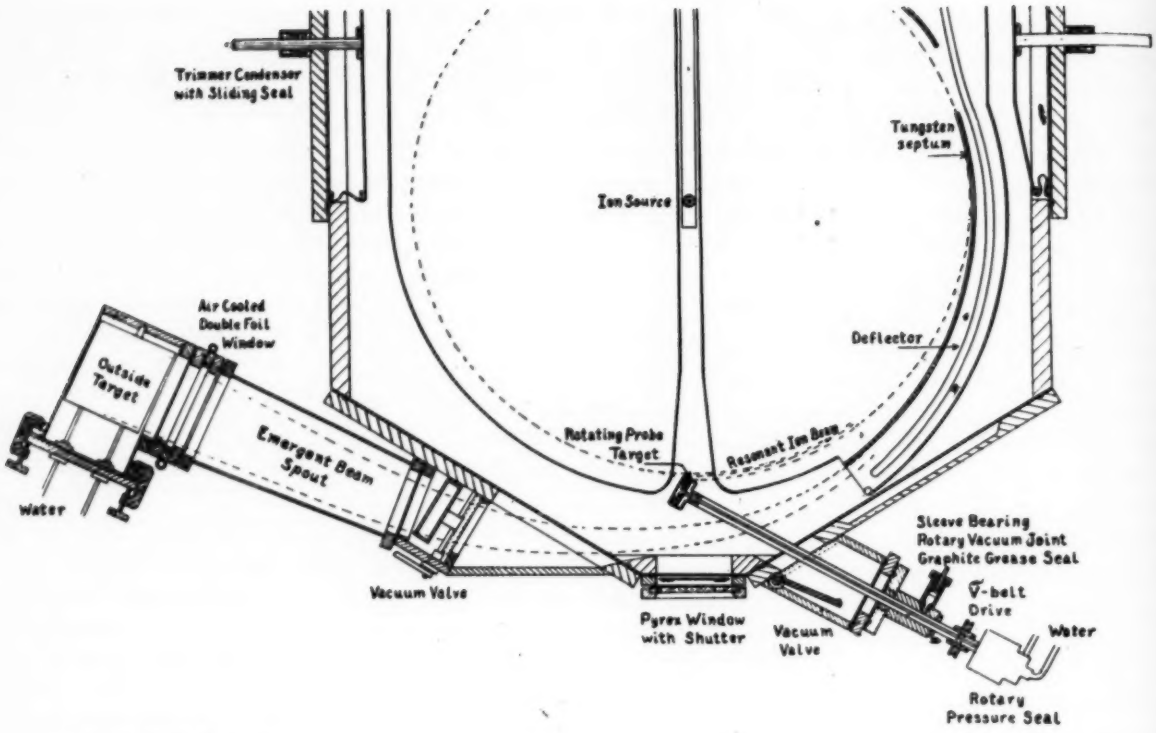


FIG. 13. Target arrangements for the emergent beam and the resonant ion beam in the M.I.T. cyclotron.

materials are electroplated, soldered, or melted onto the cylindrical surface of copper cups. A 0.003-inch channel between the inside cylindrical surface and a central core provides the constriction for high velocity water flow. The target heads are mounted on a stem which rotates about its axis so that the beam is spread over the 2-inch diameter cylindrical surface. A vacuum tight bearing allowing high speed rotation consists of a long, carefully machined sleeve bearing packed with Apiezon grease and graphite under pressure. The water inlet and outlet is a Johnson rotary pressure seal. Exhaustive tests of this unit have not yet been made and further development may be needed to adapt it to the large variety of probe targets desired. It has resulted in increasing the beam current limits for most targets used to date to above 500 microamperes.

For short bombardments where intensity is not a factor and rapid target changing is imperative, a target chamber at the end of the deflector channel has been used. In this arrangement a 3-inch diameter re-entrant tube is inserted through the probe target port and vacuum lock, interchangeable with the probe targets. A $\frac{3}{4}$-inch diameter side port covered with a thin foil vacuum window admits the beam through the side of the tube and allows it to strike a small target inside the tube. At this location, just outside the deflector channel, the deflected beam is small, about $\frac{1}{4}$ inch high and $\frac{1}{2}$ inch wide. Beam intensity is limited by the foil to about 25 microamperes; no attempt at air jet cooling has been attempted. Helium is used inside the re-entrant tube to protect targets if required as in the larger outside target chamber. This arrangement is of historical interest as the first type of external target to be used with the cyclotron.

Care must be used in design to protect operators against beta- and gamma-radiation from targets during removal. Speedy changing techniques are the best protection, and methods of handling targets from a distance and with suitable lead shielding still further reduce the risk. A skin erythema due to the beta-rays is the first indication of overexposure to such mixed radiation. Such beta-ray burns are slow healing but apparently do not cause permanent damage. If

beta-ray exposure is adequately controlled the accompanying gamma-ray dosage is negligible.

Targets for neutron bombardment are located outside the cyclotron as close to the beam target as practical. Samples for fast neutron bombardment are placed closest to the target; when samples are small they have been occasionally mounted on the rear face of the probe target head. Slow neutron bombardments use materials in water solution or between paraffin blocks, and are often of large volume. To obtain the most compact arrangement of such materials around the target spout and between magnet coils, and yet to allow reasonable accessibility for target changing and repairs, we have standardized on square glass jars of 1-gallon capacity. They are located on three layers—one on the surface of the lower coil, one on a removable shelf hanging from brackets below the upper coil, and a central layer on a shelf supported by the lower layer. Normally only a few bottles of the central layer have to be removed for target changing or other manipulations, and the whole assembly can be dismounted in reasonable time if necessary. It is possible to install about 200 gallons between coils. When a larger volume is desired containers on wheeled carts are rolled up as close to the target as possible.

Beryllium targets give maximum neutron intensities and can stand quite high beam intensities if silver-soldered to the cooled target backing. On the outside port a $6\times1$ inch beryllum target is mounted against the end of the spout with the foil holder removed and will stand any outside beam obtained to date. A $1\times\frac{1}{2}$ inch beryllium plate on the oscillating probe target will stand up to 400 microamperes. A beryllium cup for the rotating probe is planned and will probably handle maximum probe currents.

The energy of ions incident upon a target is seldom as large as the nominal value computed from the frequency setting and cyclotron dimensions. Ions entering the deflector channel are usually of lower energy due to a migration of ion paths in the magnetic field produced by shimming to obtain maximum intensities. In our case the measured energy of the deflected emergent beam (see Section 20) is about 1 Mev less than the nominal energy. This is still further reduced by absorption in the foil window and the He gas in the target chamber. So the effective external beam energy is about 0.7 Mev less than the measured value for most bombardments. The probe target is set at about $\frac{1}{2}$ inch smaller radius than the deflector septum in order to intercept the total resonant ion beam. This results in a probe ion beam energy of about 0.5 Mev less than the deflected emergent beam. We strongly urge that the distinction be made in future reports from cyclotron laboratories between nominal energy and effective energy.

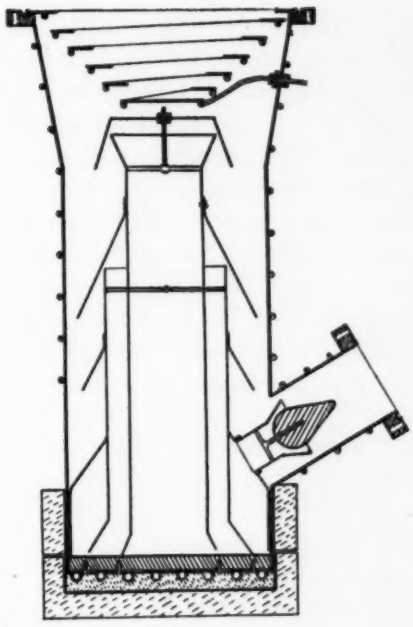

FIG. 14. Diagram of the 12-inch, 3-stage, fractionating oil diffusion pump. The measured pumping speed through the baffle is 1200 liters/sec. at $10^{-5}$ mm of Hg.

### 12. VACUUM PUMPS

The large vacuum chambers resulting from the coaxial dee line design require high speed pumps. A good rule-of-thumb is a pumping speed of 1 liter/sec. at $10^{-5}$ mm Hg per liter of volume. Oil diffusion pumps of large diameter which have 2 or 3 pumping stages and automatic fractionation of the oil are best suited to this purpose. The 3-stage, fractionating, oil diffusion pump used in this installation (see Fig. 14) is a composite design having features taken from pump designs of several other laboratories. Two pumps are used, one on each dee line. The first stage is a 2-inch gap of 12-inch O.D., the second stage is a

¾-inch gap of 12-inch O.D., and the third stage a ½-inch gap of 4½-inch O.D. mounted in the manifold leading to the mechanical pump. Oil condensed on the water-cooled surfaces returns to the boiler at the outer edge and is constrained to flow inward through the third-, second-, and first-stage boilers in succession, with a resulting fractionation. High vapor pressure fractions in the third stage which do not condense are eliminated through the mechanical pump. Narrow apertures between boiler chimney and umbrellas in all three stages are adjustable and are used to vary the relative vapor flow in the stages as well as to increase the jet velocities. A setting of ⅛ inch in first and second and ¼ inch in the third stage gave the best over-all pumping speed and an adequate backing pressure of $5\times10^{-2}$ mm Hg. Lytton Molecular Lubricant "C" is the oil used, although several other oils are available which are probably equivalent, and the fractionating feature can be used to separate an adequate pump oil out of a variety of crude materials if desired.

The 12-inch diameter steel shell of the pump is enlarged at the top by a conical section to 15-inch diameter in order to accommodate a baffle. The baffle is a "one hit" type designed to intercept back-streaming oil vapor yet give maximum transmission for gas in the forward direction. It consists of a conical spiral of narrow, overlapping half-rings of thin copper with water-cooling tubing soldered along one edge of the rings. It provides one hit on a cooled surface for all oil vapors from the first stage of the pump, yet the apertures between layers in the spiral have a total area for gas flow greater than the 15-inch diameter opening. Above the baffles coarse copper wire screens (4×4 mesh) clamped inside the 15-inch ports in the dee lines shield the baffles from electrical fields in the lines and prevent discharges from the oily surfaces. Electrical heating units were constructed of three 1-kilowatt Calrod elements, one under each boiler stage, separately adjusted with external resistors to give maximum pumping speed. In operation the power requirement is 1.8 kilowatts for each pump.

In test runs with a calibrated air leak the diffusion pumps developed a speed through the baffle of 1200 liters/sec. each at $10^{-6}$ mm Hg. This compares favorably with the theoretical speed of the 2-inch gap of the first stage of 3000 liters/sec., considering the baffle as reducing pump speed by about 50 percent. The total effective speed for the two pumps of 2400 liters of air/sec. is adequate for the 2000-liter volume. With no gas flow, chamber pressures of better than $1\times10^{-6}$ mm of Hg are obtained; with the deuterium gas flow from the ion source the operating pressure is about $1\times10^{-5}$ mm of Hg and pumping speed is materially increased by substitution of deuterium for air. Packless valves made from 2-inch steam valves are located in the manifold between diffusion pumps and the mechanical pump. No high vacuum valves are used, being considered unnecessary in view of the infrequent need for letting the chamber down to atmospheric pressure. Diffusion pumps are allowed to cool for at least ½ hr. before admitting air.

The mechanical pump is a Kinney CVD 5×5 two-stage unit with a maximum displacement of 7 liters/sec. It will pump down the 2000-liter volume to the backing pressure limit of the diffusion pumps in about ½ hour. In service it develops a backing pressure of $1\times10^{-3}$ mm Hg in blank runs, a value of $2\times10^{-3}$ mm Hg under normal high vacuum conditions in the chamber, and about $5\times10^{-3}$ mm Hg with the cyclotron in operation and a deuterium gas flow from the ion source.

### 13. VACUUM SEALS AND TECHNIQUES

Probably as many variations of vacuum techniques can be found as there are experimental laboratories. The description to follow claims neither completeness nor uniqueness but reports techniques which have been found adequate for maintaining large metal chambers within the vacuum range required for cyclotron operation. The problem of adsorbed gases and vapors in metal chambers of large volume has been brought under control by the development of high speed pumps using low vapor pressure oil, so that refrigerants are not needed. The remaining problems are in the design of seals and the location and sealing of leaks. A wide variety of rubber gasket seals has been designed and successfully used; all that is required is sufficient pressure to compress the gasket properly.

A basic design for a seal between parallel surfaces or flanges consists of a groove machined in one surface to hold the gasket in position, having a depth of about half the uncompressed thickness of the gasket. For large apertures we use a groove $\frac{1}{4}$ inch wide by $\frac{1}{8}$ inch deep and a strip gasket $\frac{1}{4}$ by $\frac{1}{4}$ inch. The strip stock is cut to length allowing for a 1- to $1\frac{1}{2}$-inch overlap with the ends beveled on an abrasive wheel and joined with rubber cement. On smaller apertures the gasket is $\frac{1}{4}$ by $\frac{1}{8}$ inch with a $\frac{1}{16}$-inch deep groove and can be cut from flat stock with a gasket cutter if desired. Machine practice will indicate the proper size and spacing of bolts to give adequate pressure. This technique is used both for round and for rectangular apertures. In the latter case, the groove is cut in a milling machine with a $\frac{1}{4}$-inch end mill. Under compression the free face of the gasket against the flat surface expands considerably but the metallic surfaces do not come into contact. In cyclotron practice it is often necessary to have good electrical contact across the gasket gap. This is accomplished by inserting a soft copper foil strip $\frac{3}{8}$ inch wide and 0.004 inch thick on edge between gasket and groove on the vacuum side of the $\frac{1}{4}\times\frac{1}{4}$ inch gasket. When folded over the rubber and compressed it covers less than half the surface, leaving adequate rubber surface for the seal yet providing a positive metallic contact. This is illustrated in Fig. 15a. Conversely, such a gasket can be readily adapted as an insulator by fiber tubing liners for bolt holes and fiber washers under bolt heads. This is used primarily for electrically insulated target plates and ports, in which case the resistance is greater than that of the paralleling water-cooling hose-leads.

A variation of the gasket-groove design recommended by other laboratories uses two gaskets in two parallel grooves with the intermediate region tapped by a hole leading to a spout which can be connected to a portable rough vacuum pump for testing. A leak so located can be kept under control by the rough vacuum pump until repairs can be made. The technique provides maximum protection against gasket leaks. In defense of the single-gasket design it can be said that leaks through such seals are rare (only two in a year of operation in this laboratory), even speedier alternative leak testing techniques are available (see below), the necessary width of flanges is reduced, and machining and design problems are considerably simplified.

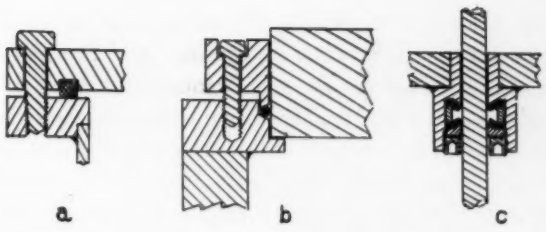


FIG. 15. Rubber gasket vacuum seals for several purposes: (a) Strip gasket in groove with copper foil for metallic contact. (b) Round gasket and packing ring for edge seal on chamber plates. (c) Modified "Wilson" seal for both vacuum and pressure, allowing lateral and rotary motion of the shaft.

The large diameter seals between iron cover plates and the chamber wall require a special design. We use a seal first developed at the University of Rochester. In our modification a $\frac{3}{16}$-inch diameter round rubber extruded strip is pressed against the side of the iron plate by a packing ring. It is illustrated in Fig. 15b. Such a design gives a positive metallic seat for the cover plate and gasket pressure is independent of magnetic forces. The round gasket is bevelled and lapped as previously described.

Rubber gasket seals have largely displaced the copper bellows or sylphons formerly used to obtain motion for mechanical adjustments through the vacuum wall. A shaft can be sealed for both rotation and lateral motion by a gasket with a sharply cut hole somewhat smaller than the shaft diameter, which is toed outward so that the external atmospheric pressure aids the elasticity of the rubber in maintaining close contact.[23] Such seals can be made very large; a 7-inch diameter pipe is sealed by a single gasket, in which a 4-inch hole was cut, to provide for angular adjustment of the pipe. A lubricant is usually helpful. Stopcock grease is not too satisfactory since it becomes gummy with time and stiffens at cooling water temperatures. Graphite or molybdenum sulphide avoids these faults but must be replaced periodically. The most satisfactory lubricant has been found to be castor oil. With two gaskets, both toed outward and a pumping outlet between to test for leaks, this is known as the "Wilson seal." [23] A local modifica-

tion with the outer gasket reversed to toe inward is a seal for both vacuum and pressure, useful in some applications such as target chambers and valves. See Fig. 15c. With the intermediate space tapped by a vertical tube and filled with low vapor pressure oil, such as castor oil, to the top of the tube, it is immune to vacuum leaks because of the positive pressure of the oil and allows low speed rotation of a shaft.

Neoprene, Koroseal, or other plastics can be substituted for rubber if desired. They lack the elasticity of rubber and take a permanent set with time so cannot be reused as often as rubber. Their oil-resistant properties make them valuable for seals adjacent to vacuum pumps; they do not deteriorate with ozone and are free from the sulfur vapors from rubber gaskets which blacken metallic surfaces. We have recently tried a technique recommended by other laboratories of applying a film of castor oil to rubber gasket surfaces. This preserves the rubber and seals small leaks due to rough surfaces; less pressure is needed to obtain a tight seal.

A trustworthy high vacuum gauge is the Western Electric D 79510 manometer tube. When operated according to specifications with 21 milliamperes grid current, the plate current in microamperes reads the gas (air) pressure in $10^{-5}$ mm of Hg units. We use a compensating circuit to limit emission to 10 milliamperes grid current; a 25-microampere plate meter covers the practical operating and leak testing range. The oxide coated filament emission is extremely sensitive to changes of constitution of the gas, particularly to organic vapors such as ether. In testing for vacuum leaks within the working range of the gauge, we use a hypodermic syringe to spray ether over suspected joints, and the increased emission from the filament indicates the leak. For such testing, the 10-milliampere limiter is released and both grid and plate currents show a sharp rise. An air leak raising the background pressure by $1\times10^{-5}$ mm of Hg when sprayed with ether will double the emission current to the grid and increase the plate current by a factor of 10. Leaks raising the pressure by as little as $1\times10^{-6}$ mm of Hg can be readily detected. Once the ether has evaporated, the gauge returns to normal emission in less than a minute. The life of a manometer tube in continuous daily operation and with occasional leak testing has been well over a year. A caution is indicated in location of the gauge; with high speed pumps a leak between gauge and pump shows a much smaller response than when the gauge is between leak and pump.

The rough vacuum gauge is a G. E. 5310620G-1 thermocouple mounted on the manifold between the diffusion pumps and the mechanical pump. The heater current of 50 milliamperes is supplied by a 1.5-volt dry cell; a Weston low resistance (55 ohm) 200-microampere meter is used in the thermocouple output. The range is from 10 microamperes at $2\times10^{-1}$ mm Hg to 180 microamperes at $1\times10^{-3}$ mm of Hg, and operating pressures are in the most sensitive region. It also responds to ether due to the large specific heat relative to air, showing a drop in temperature of the thermocouple. It can be used to locate leaks in the fore-vacuum manifold and in the main chamber for the pressure range above backing pressure of the diffusion pump.

A simple discharge tube with two metallic electrodes in a glass envelope is also mounted on the manifold. The potential supply is adjusted so that the tube discharges and actuates a relay at a pressure of about $5\times10^{-2}$ mm of Hg, the backing pressure of the diffusion pumps. The relay is used as a vacuum interlock to turn off power circuits and pump heaters or close vacuum valves in emergencies such as when a foil window breaks.

The ranges of vacuum leaks giving pressures above the sensitivity limits of the vacuum gauges are often neglected in discussions of vacuum techniques, but can be serious time wasters. We find the most satisfactory method is to use pressures well above atmospheric in the chamber and search for leaks externally with soap solution applied by a camel's-hair brush. Leaks raising background pressure by $2\times10^{-6}$ mm of Hg on the ionization gauge have been located with this method. To make this possible in emergencies all gasket seals are designed to seal for both vacuum and pressure, as described. A serious type of leak unfortunately common to cyclotrons with their array of internal cooling circuits is a small water-vapor leak. It is often recognizable by the sharply decreased life of tungsten filaments and by the increased emission

of the ionization gauge filament. Emptying water circuits and evacuating with a test pump is usually a certain method of identification, followed by a pressure-soap solution test with the chamber opened.

Vacuum-leak trouble is usually traceable to poor design of chamber and seals and experience is the only cure. Generally speaking, castings of non-ferrous metals are subject to porosity and should be avoided. Brazing and welding of non-ferrous metals require unusual skill for vacuum tight joints, and such joints often show leaks if the surface is removed by machining. Free flowing hard solders such as Easy-Flo silver solder require less manipulative skill. To reduce the number of joints in the copper dee lines all openings and ports were drawn and shaped around steel flanges by alternate annealing and cold hammering, so that the rubber gaskets seal directly to the copper face of the flanges. Vacuum tight design of the cyclotron chamber wall is a serious problem. Successful castings have been obtained with special alloys but the large majority have been porous to some extent. We chose to use rolled brass and silver-soldered joints but technical errors resulted in a few leaks. The best designs to date use non-magnetic alloys such as Herculoy or Everdur which can be welded with good chance of success. A standard procedure to seal small leaks in metallic joints is to paint with Glyptal, a thick, elastic, slow drying paint of low vapor pressure. The prevalence of red Glyptal patches on essentially all cyclotron chambers is an indication of the seriousness of the vacuum-leak problem.

### 14. CONTROLS[24]

The operators must be protected from the cyclotron radiations, so control benches are placed behind shielding walls at some distance from the cyclotron. We chose to have all switches, meters, and control circuits located on a rack and panel assembly at the control bench with individual circuits localized to single panels wherever possible. Each panel is equipped with a terminal block and the safety interlocks between circuits are cross-wired behind the rack. The advantage of easy removal for repair or testing of individual circuits has been greatly appreciated. The circuits will be discussed here in a qualitative way only, without attempting to give full details or circuit diagrams.

The magnet is powered by a 90-kva motor-generator on 2300 volts 3 phase with the d. c. generator terminals permanently connected to the magnet coils. An exciter unit on the same shaft supplies the generator field and is itself controlled by the electronic regulator panel at the control bench. The 2300-volt oil-immersed contactor in the motor circuit is operated by a master switch on the panel, interlocked with the magnet water-cooling circuit. With the motor-generator running, a second switch applies the output of the exciter unit to the generator in series with a manually operated rheostat at the panel for rough adjustment, normally left at the correct setting for resonance. A third switch turns on a power supply for the electronic regulator device which has controls and meters on the panel. The regulator output of 0 to 300 milliamperes d. c. at potentials up to 220 volts is applied to the field coils of the exciter in parallel with a considerably larger current available from the exciter output. The regulator is a modification of a circuit developed by the University of Rochester cyclotron group and the principal feature is a double control to prevent overcorrections or hunting. One control is based on current in the magnet coils. The potential across a calibrated series shunt is bucked by a precision potentiometer calibrated against a standard cell and the differential current is applied to a galvanometer. A lamp and translucent scale (mounted flush with the panel) show the magnitude of hunting fluctuations and are used to balance the potentiometer. The potentiometer setting for balance gives a precision measurement of the current in the magnet coils. Another galvanometer lamp throws a spot between two photo-cells which control the 0–300-milliampere output of the regulator tubes. The second control uses the voltage across magnet coils (opposed by an adjustable bucking potential) to bias the cathodes of the photo-cells, thereby also controlling the regulator output. Since the voltage fluctuations across the magnet coils lead the corresponding current fluctuations in phase due to the large inductance of the coils, the double control prevents overcorrections and provides

an effective anti-hunting feature. The regulation of the magnet current is ±0.01 percent, and in steady operation after a short warm-up period the resonant beam is maintained for hours.

The oscillator power supply uses a 150-kva, 3-phase, 2300–13,800-volt power transformer connected delta-delta to give 19,500-peak voltage between terminals. Lower voltage taps and connections are available. The rectifier unit is a standard 3-phase, full-wave circuit with six W. E. 255B mercury vapor tubes which have filaments heated in quadrature from a low voltage 3-phase supply and insulation transformers. Quadrature connection increases the available maximum d. c. output from 5 to 10 amp. A 2-henry choke and ¼-microfarad condenser form the output filter. Rectifier filaments are turned on by a relay operated from the control bench and the same switch starts air blowers on rectifier and oscillator tubes. A master push-button switch activates a relay which closes the 3-phase, 2300-volt contactor in the power transformer circuit and a prominent long-handled trip switch opens it. Safety interlocks in the relay circuit operating through time-delays prevent closing unless rectifier and oscillator filaments have been on for 2 minutes and 1 minute, respectively. Suitable pilot lights in green, yellow, and red indicate the status of the interlock circuits and show when they are cleared for operation.

Two RCA 899A tubes are used as oscillators in a push-pull neutralized circuit, described in detail in Section 5. Filaments are turned on and brought up to operating temperatures slowly as recommended by the manufacturers by means of a hand-operated tapped resistance. An interlock requires that all pertinent water-cooling circuits be operating before filaments can be turned on. Reversible motors controlled by two-way switches on the panel operate a variable water column resistor in the plate circuit, a tuning condenser in the oscillator grid circuit, and trimmer condensers in the dee circuits. Meters for plate current, plate voltage, and grid current are on the control panel and are used to adjust the oscillator to optimum conditions in operation under load. An overload relay protects the tubes from excessive currents by opening the power contactor. No other current limiting circuits or devices are used since the basic problem of chamber sparks and discharges is taken care of by the radiofrequency power limiting feature inherent in the feed-back oscillator circuit. Two small pick-up electrodes mounted on spark plug insulators through the chamber wall actuate vacuum-tube voltmeter circuits with d. c. meters on the panel and are calibrated to read dee voltages in kilovolts.

A vacuum pump panel has switches, current meters, and pilot lights for the mechanical and oil diffusion pumps. The discharge tube vacuum interlock previously described is powered by the switch for the mechanical pump and allows the diffusion pump heaters to be on only for adequate backing pressure. Mu-switches on the hand-operated valves in the manifold between pumps, requiring that the valves be open, and an interlock on the cooling water, protect the diffusion pumps against accidental damage due to human error.

An ionization gauge panel with all appropriate controls, meters, and pilots is interlocked with the diffusion pump power relay so the gauge filament cannot be heated unless pumps are on. A 10-mil emission limiting circuit protects the meters but can be cut out for vacuum-leak testing. The thermocouple gauge requires no protection except a pilot light to indicate on and off conditions.

The ion source filament is heated by a 2-kw oscillator-amplifier at 150 kilocycles which is mounted in a shielded rack and panel cabinet in the cyclotron room.[25] In circuit design and construction it is equivalent to a low frequency radio transmitter and has all necessary controls for adjustment and testing. The basic controls for operation and adjustment of power output are extended to the ion source panel at the control bench. A transmission line couples to a matching unit at the ion source filament terminals between dee lines to provide the proper impedance for the low voltage, high current power. The water for filament stem cooling flows in series through the high current coil in this matching unit. The whole filament stem and matching unit are insulated and maintained at a negative d. c. potential relative to ground by an auxiliary 300-volt motor generator set controlled at the panel. The ion source anode is the grounded jacket and cone. A voltmeter registers

the potential drop across the arc, and an ammeter the total current. The symmetrical construction of the ion source includes a second jacket and cone identical with the filament housing. An auxiliary "test anode" located in this housing is connected through a meter on the panel to read the fraction of the discharge current which traverses the gap between the cone tips. Interlocks protect against operation of filament or discharge unless all water-cooling circuits are properly adjusted and the diffusion pump is operating.

Deuterium for the ion source is obtained as compressed gas in dental style cylinders. It is reduced to about 5 lb./in.$^2$ above atmospheric pressure by a Hoke Ouncer reducing valve and then valved through an adjustable leak to a tube leading to the filament housing of the ion source. The leak consists of a long shaft inserted to a variable depth into a reamed hole. The external adjusting screw has a vacuum-pressure seal and a needle point tip on the shaft provides a cut-off valve. With the adjustable leak set for correct flow with the Hoke at 5 lb., variation of the Hoke output between 0 and 10 lb. gives $\pm 25$ percent control of gas flow, with a regulation of better than 1 percent. A packless valve between the Hoke and the leak is used to turn gas off or on, and outlet valves in both high and low pressure leads are used to pump out air following tank changes. The unit is mounted behind a panel with valve handles and gauges showing.

Deflector voltage is obtained from an x-ray transformer and kenotron rated for 100 kilovolts mounted on a platform hung from the ceiling in the cyclotron room. A 1-megohm wire wound resistor in the output protects the kenotron and a 0.002-microfarad condenser stack is the filter. An insulated high tension cable enters a screened cage surrounding the deflector terminal and hose reel at the end of the dee line. The gate on the cage is protected with a mu-switch interlocked with the transformer power. On the control panel the kenotron filament switch activates a 1-minute time-delay relay which indicates with a pilot light when the transformer power circuit is cleared. An auto-transformer in the primary gives 100 percent variation of output voltage. Sparks or discharges in the chamber are observable on the primary current meter; an overload current relay is a protection against short circuits. The water hose reel is formed of two 60-ft. lengths of $\frac{1}{4}$-inch plastic tubing wound around a large fiber tube and has a d. c. resistance of about 75 megohms. Suitable corona shields protect the terminals of the tube, the protective resistance, and other exposed parts.

Each water-cooling circuit has a pressure gauge into which is built an electrical contact. A stub of silver wire soldered to the pointer rides in a cut-out sector of a brass disk mounted through and inside the face glass with an external electrical connection and a knob for setting. The gauge is located between the flow adjustment valve and the circuit. Water pressure failure or a clogged valve lowers gauge pressure and makes the electrical contact; a stoppage in cooling circuit or drain makes contact on the high pressure side of the sector. Separate 110-volt circuits for each bank of gauges with a common ground return light appropriate pilot lights on the water circuits panel at the control bench and ring a bell to call the attention of the operator. Relays in the more important gauge circuits act as safety interlocks in the respective power circuits as described. The gauges used are of the cheapest type, $2\frac{1}{2}$-inch dial, with plastic face glasses for ease in mounting the contacts. They are mounted with their individual valves on a manifold having a master valve from the water supply line. One master valve and manifold supplies all cooling circuits for the chamber (ion source, targets, etc.). Similar master valves supply the magnet, the dees and dee lines, the oscillator unit, and the pumps. Only the master valves are used to turn water off or on so that individual valve adjustments are not disturbed.

The ion beam current to the target operates a multi-range microammeter which can be switched to any one of the several target locations. A small correction factor must be applied to account for the loss in the paralleling resistance of the water-cooling circuits. The same current operates a beam current integrator consisting of a thyratron-condenser circuit operating a message register. Several ranges are available, giving the integrated intensity in microampere hours. Difficulties in separating true ion beam current from discharge or secondary emission currents and radiofrequency pick-up on the probe target

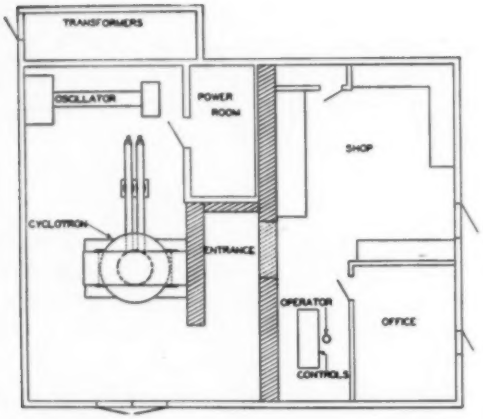


FIG. 16. Floor plan of the M.I.T. cyclotron laboratory, showing built-in water tank walls for neutron shielding.

have led to the use of a thermometric method. The high velocity water-cooled target head has a sufficiently large flow resistance to produce up to 50 deg. C temperature rise in the water. Flow is continuously metered by a rotameter flow meter at the control bench, and a 5-junction thermocouple registers the temperature difference between inlet and outlet water on a second galvanometer behind the control panel with the light spot on a translucent scale on the panel. No method has been found as yet to apply the thermocouple output to the integrator so probe current readings are visual.

A two-way intercommunication system at the control bench can be switched to several stations around the cyclotron or to other laboratories and offices in the Institute.

### 15. LABORATORY DESIGN

The building to house the M.I.T. cyclotron was designed to provide only the minimum accommodations for operation and maintenance of the instrument. Laboratory facilities for the manifold other purposes of the M.I.T. Radioactivity Center were arranged in other existing buildings. This has the advantage of separating sensitive detection instruments from the high radiation background near the cyclotron. We lacked the fortunate circumstances of other laboratories of a hillside location to reduce the problem of shielding, and built on filled land at ground level. The location was chosen as far from other inhabited buildings as possible so that the primary shielding problem was for operators and staff of the cyclotron building itself.

The floor plan of the building is shown in Fig. 16, with the two built-in water tank shielding walls indicated and the baffle-type entry between the cyclotron room and the shop, control room, and office. Because of the small shop and light machines much of the cyclotron chamber construction had to be done elsewhere, but the shop has proved adequate for maintenance work and normal developments. On one side of the shop a chemical bench and hood serve the needs for target preparation and handling. A lead box under the hood is used for temporary storage of radioactive materials. Radioactive materials for shipment are packed in lead cyclinders and enclosed in wooden shipping containers; for transfer to the other laboratories long-handled lead carrying cases are available. Another bench in the shop is for electrical work on control circuits. The remainder of the shop space is occupied by machine tools, work benches, and stock bins.

The cyclotron is mounted on caisson foundations slightly below floor level to have the chamber at a proper working height. A chain hoist on an overhead trolley crosses over the cyclotron for handling chamber and line assembly and to the door for unloading heavy equipment. The oscillator unit is installed in the rear of the cyclotron room, connected to the dee circuits by transmission lines. One corner of the room is enclosed as a power vault for the rectifier unit and magnet motor generator. An external transformer vault houses the 2300-volt 3-phase power transformers and switching equipment. Due to excessive humidity in summer months which causes condensation on water-cooled surfaces and consequent danger to electrical insulation, a compact 3-ton air conditioning unit is installed in the cyclotron room. Services for water, electrical power, gas, and compressed air are spotted at convenient points in the building. Number 14 lead covered pair pulled through large metal under-floor conduits forms the bulk of the wiring and provides double shielding against interference and radiofrequency pick-up.

The cyclotron crew consists of two operator-technicians and one machinist, with half-time supervision by the author and a physics graduate

student. This staff has been adequate for 72 hours per week operation and the usual maintenance and development work of the laboratory. It was enlarged temporarily by additional mechanical technicians during the installation period and a third operator has recently been added to increase operating time. Aside from time spent on developmental improvements, experience shows an operational efficiency of better than 80 percent of working hours.

### 16. SHIELDING

The necessity for protection of cyclotron workers from the harmful effects of the radiations has been appreciated from the start. Methods of shielding from neutrons were developed before the increasing size of cyclotrons gave biologically dangerous intensities and have prevented a repetition of the unhappy experiences in the early days of x-rays. Knowledge of the large elastic scattering cross sections for neutrons in substances of low atomic weight has made it possible to shield with water tanks or with equivalent thicknesses of other materials. Charged particles from disintegration reactions in the target are completely absorbed in the walls of the target chamber; the neutron and gamma-radiations are much more penetrating. Without shielding, the neutrons or their secondary products can be shown to be more dangerous, so the primary problem of shielding is for neutrons.

We shall discuss the shielding requirements for a cyclotron of 16-Mev nominal deuteron energy with resonant ion currents of the order of 0.5 to 1.0 milliampere of which the emergent beam on a Be target would be approximately 200 microamperes. This represents a practical operating limit for existing larger installations, and is an estimate of the probable maximum of the M.I.T. cyclotron. The total neutron yield of the University of California 60-inch cyclotron, operating with a nominal[26] 16-Mev deuteron beam on a Be target has been reported[27] to be 1 neutron per 200 deuterons, which is $6.3\times10^{12}$ neutrons/sec. for a beam of 200 microamperes. The value per unit solid angle of $5.0\times10^{11}$ neutrons/sec. is an average including a maximum value in the forward direction of the deuteron beam and a minimum in the backward direction. A calculation of the angular distribution expected from this Be$(d, n)$ reaction shows an intensity in the forward direction of 1.28 times the average value and of 0.75 $I_N$ at 180° to the beam. The laboratory was designed to take advantage of this asymmetry by locating the control bench at the 180° position. So the basic shielding for operators is for $3.8\times10^{11}$ neutrons/sec. per unit solid angle. The additional attenuation due to the inverse square reduction of intensity at greater distances for other angles should result in adequate shielding in all directions. The M.I.T. control bench is 20 feet from the target; from the inverse square law this predicts maximum fast neutron intensities of $1.0\times10^{6}$/cm²/sec. without shielding.

The biological unit of radiation dosage is the roentgen unit, and radiation intensity is expressed in roentgens per unit time. One roentgen, 1 r, produces an ionization of 1 e.s.u. of charge per cm³ in air in equilibrium with secondary electrons. It is commonly measured in the Victoreen r-meter, a thimble type ionization chamber with a Bakelite wall which duplicates air in its scattering and absorption of x-rays and secondary electrons. The accepted continuous tolerance dose for humans is 0.1 r/day for x-rays and gamma-rays.[28] To emphasize the cumulative effects of ionization and the significance of shock doses, it is probably better expressed as 3.0 r/month. The Victoreen chamber has also been adapted to the measurement of neutron intensities;[29] the unit observed is called the "neutron roentgen," the n unit. Fast neutrons produce ionization in the chamber largely through the columnar ionization of the air by recoil protons from the Bakelite wall. The amount of ionization observed in a fast neutron beam will depend on wall thickness and constitution and on the size and geometry of the chamber. Although there are valid criticisms of the significance of this method of measuring neutron intensities, it can serve as a relative method as long as identical chambers are used in all measurements. Considerations of the relative ionization efficiencies of x-rays and neutrons in the Victoreen chamber and the human body have led to the general acceptance of the figure of 0.01 n/day (or 0.30 n/month) as a tolerance

rate for continuous exposure to fast neutrons.[29] This figure is not yet verified by biological tests and must be considered as tentative. The fast neutron ionization in a Victoreen chamber has been observed[30] to be 0.005 n unit/min. at 5 cm from a Li($d$, $n$) neutron source of the same intensity as 1 g equivalent of Rn-Be, or:

*1 g. equivalent of Rn-Be* $= 2.1 \times 10^{-3}$ *n unit/sec. at 1 cm.* The total number of neutrons from a Rn-Be source[31] has been redetermined by Fermi[32] at $1.0 \times 10^7$/sec. per g equivalent Rn-Be. So:

*1 n unit* $= 3.8 \times 10^8$ *fast neutrons/cm*$^2$. If the *tolerance rate* is computed for an 8-hour daily exposure, it can be expressed as $3.5 \times 10^{-7}$ n unit/sec. or

*Tolerance rate* $= 130$ *neutrons/cm*$^2$*/sec.* The shielding problem is to reduce the $1.0 \times 10^6$ neutrons/cm$^2$/sec. estimated intensity at the control bench to the tolerance rate, requiring a shielding factor of approximately $10^{-4}$.

No unique value for the absorption coefficient of fast neutrons in water or other materials can be given, since this is a function of neutron energy. The neutrons from the Be($d$, $n$) reaction in the cyclotron have a broad energy distribution with only a relatively small percentage having maximum energy. Furthermore, neutrons are slowed down by nuclear collisions so that even an originally homogeneous beam would degrade into a distribution after traversing the first layers of absorber. For such inhomogeneous radiation, the shielding factor can best be obtained by experimental measurements with absorbers of thickness equivalent to that required for shielding.

The attenuation of neutrons in water has been studied in this laboratory[33] by observing the induced radioactivity produced in gold foils placed at various distances up to 2 feet inside the surface of a 4×4×4 foot water tank. The radiation was the neutrons from the Be($d$, $n$) reaction with 12-Mev deuterons, observed at 90° to the beam. The results are shown in Fig. 17. An initial rise in the first 5 cm of water is due to production of slow neutrons. The relative fast neutron intensity in this region can be estimated by extrapolating the curve back to zero thickness, to an estimated intercept of 10 times the slow neutron reading. Although the reaction observed is a slow neutron reaction, they are to a good approximation in equilibrium with the fast neutrons considering the large thicknesses of water used in the experiment and the thorough shielding by the remainder of the water tank. The curvature of the logarithmic plot indicates a continuous decrease in absorption coefficient with thickness of absorber, varying from 0.18 cm$^{-1}$ at 10 cm to 0.11 cm$^{-1}$ at 55 cm. This is interpreted as a "hardening" of the radiation due to relatively smaller absorption of the high energy part of the neutron energy distribution. The results show a shielding factor of $2 \times 10^{-4}$ in 2 ft. of water and a long extrapolation of the curve indicates that 4 ft. would give a factor of approximately $10^{-6}$.

The result obtained above justifies the 4 feet of water shielding for the shop and control room which was installed in the cyclotron building in its construction, although much less direct evidence was available at that time. This is arranged in two 2-foot tanks, both shadowing the whole of the shop and control room regions, with a baffle entrance covered by an overhead tank. The larger 2-foot wall extends to the ceiling and across the width of the building, and the entry through it is also shadowed by the iron upright of the magnet frame, giving approximately the same shielding. Additional shielding was obtained by boxes of crude paraffin and borax closely fitted between the magnet coils, but not continuous due to the necessity of leaving space for dee lines and adjustments. When installed they further reduced control bench intensities by a factor of 3. This shielding has been found satisfactory for operation at 12 Mev for two years of operation. Monthly blood analyses for each member of the crew have shown no fluctuations which could be attributed to overexposure to radiation, and ionization chamber measurements have always been below tolerance levels.

The calculations of fast neutron intensities given above are only the first step in the shielding problem. Many other factors must be considered, such as neutron scattering around the walls, secondary gamma-radiation produced by neutrons in the water tanks, and primary gamma-radiation from the cyclotron. Each of these should be analyzed to determine its relative im-

portance in raising the ionization level behind the water walls. Scattered neutrons can be of major importance under certain conditions, especially when large amounts of heavy scattering material are present such as in roofs and ceilings. For this reason, the M.I.T. laboratory was designed with a flat roof and with the large water wall extending to the ceiling. With roof scattering eliminated the neutrons scattered from the air above the buildings are of next importance. The mean free path of fast neutrons in air can be estimated from the elastic scattering coefficients in $N_2$ and $O_2$ to be about 145 meters or a half-value distance of 100 meters. To visualize the scattering process and simplify calculations we can consider all impacts to occur in a thin hemispherical dome of about 100 meters or 300-ft. radius, bounded by the water tank shields. Only that angular area of the dome visible from the control bench would be important. Intensity would be decreased by any shielding over the cyclotron and by the attenuation in the roof, counted twice. The inverse square law attenuation in the mean scattering distance of 145 meters would give intensities of $1.8\times10^{-3}$ the unshielded value at the control bench. A large fraction of the scattering dome is shielded by the magnet yoke and upper coil; the estimated fraction of the total solid angle of sky radiated which can be seen from the control bench is less than 0.1. Since back scattering is less probable than forward scattering by about a factor of 2, only about $\frac{1}{3}$ will be effective, reduced to about 0.1 by roof absorption. The net result is an estimate of approximately $2\times10^{-5}$ of the control bench intensity due to unshielded direct fast neutrons, about 0.2 the fast neutron tolerance rate but still larger than the residual neutron intensity through 4 feet of water shielding. Although this estimate is crude, it agrees with observations when the cyclotron was later boxed in by overhead and side water tanks. The control bench intensity dropped by only about 20 percent when the overhead tanks were filled, eliminating a large fraction of scattered radiation. The significance of this result as compared with the much larger reductions due to overhead tanks at the Berkeley 60-inch cyclotron is in pointing out the importance of heavy roof materials in scattering fast neutrons.

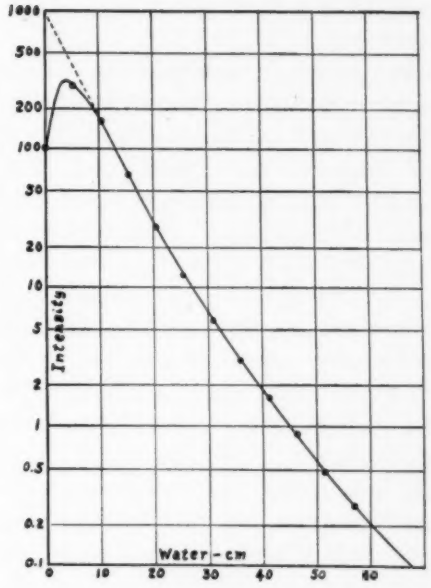


FIG. 17. Attenuation of neutron intensity in water by measurement of the 2.6-day period of the Au($n$, $\gamma$) reaction, corrected for solid angle. A decreasing absorption coefficient with absorber thickness is shown by the curvature of the logarithmic plot. (Courtesy of Mr. Hoyt Whipple.)

The primary gamma-radiation from the target is absorbed by the heavy metals of the chamber walls and by the water tank neutron shields, and attenuated by the inverse square law. Taking the largest estimate of source intensity of "several hundred curies," and the number of Ra gamma-ray quanta per curie, we obtain an estimate of $3.0\times10^{12}$ gammas/sec. per unit solid angle, or about 5 to 10 gamma-ray quanta per neutron. This seems reasonable in view of the number of excitation states available at such high bombarding energy. Applying the inverse square attenuation and absorption in the shielding materials, we can estimate about 50 gamma-ray quanta/sec./cm$^2$ at the control bench. A calculation of the gamma-ray intensity equivalent to the tolerance rate of 0.1 r/day along lines similar to the calculation for neutrons gives a result of $4\times10^3$/cm$^2$/sec. for an 8-hour daily exposure.

*Tolerance rate* $=4\times10^3$ *gamma-ray quanta (of 2.2 Mev) cm*$^2$*/sec.* It does not seem advisable to include the detailed calculations here, since the control bench intensity for primary gamma-radiation is only 1 percent of the tolerance rate, and can be neglected. Furthermore, the gamma-

ray intensities can be readily measured with the Victoreen r-meter.

Fast neutrons are slowed down to thermal energies by elastic impacts in the water shields; in the heavier atoms of the magnet iron and coils inelastic impacts also occur and scattered neutrons have a mean energy of about 1.5 Mev, the "nuclear temperature." [34] Slow neutrons are ultimately absorbed through a disintegration reaction, of which the most probable is the $H(n, \gamma)$, emitting gamma-radiation of 2.2 Mev. The water tanks are thus a source of secondary, hard gamma-radiation; this component is by far the most important in producing ionization at the control bench. The absorption in water, estimated to be 0.046/cm, is considerably smaller than that for fast neutrons, and the proximity of the water walls to the control bench gives no important reduction due to distance. Gamma-radiation also originates from $(n, \gamma)$ reactions in all surrounding material, produced by slow neutrons diffusing over and around the water tanks. Victoreen measurements of ionization at the control bench for 12-Mev operation show from 0.01 to 0.03 r/day, up to one-third of the tolerance rate for gamma-radiation. This is predominantly gamma-radiation, as has been proved at this and other laboratories by observations of identical readings in ionization chambers with and without paraffin linings. A method of reducing this gamma-ray intensity is to absorb most of the slow neutrons by a nuclear reaction producing charged particle products. The reactions $B^{10}(n, \alpha)$, $Li^{6}(n, \alpha)$, and $N^{14}(n, p)$ have positive $Q$ values and extremely large probabilities for slow neutrons, following the $1/v$ law with neutron velocity. The $B^{10}(n, \alpha)$ reaction has the largest probability and is favored economically due to the low cost of borax and its derivatives. We used a mixture of 40 percent borax and 60 percent crude paraffin in the boxes fitted between magnet coils, with good results. We plan to use saturated sodium metaborate solution in the water tanks if this radiation component becomes a limiting factor in the future. The gamma-ray intensity from the tanks should be reduced to less than 5 percent by this procedure.

Shielding requirements for sensitive detection instruments are much more rigorous than for personnel protection. Counter backgrounds in the main laboratory 150 yards away were raised by a factor of 5 to 10 with the cyclotron operating and no shielding. This is interpreted as due to secondary and scattered radiations from the air above the buildings. To reduce this effect, tanks of water were installed over and around the cyclotron. Intensities in the main laboratory were reduced by a factor proportionate to the fraction of sky aperture closed by the tanks. Remaining apertures probably account for most of the residual intensity. In agreement with calculations on the relative importance of air scattering of neutrons and secondary gamma-radiation from the water walls, these overhead tanks did not improve control bench intensities significantly. A more important improvement would probably result by closing all apertures.

From the foregoing discussion, it can be seen that water tanks can be used successfully for cyclotron shielding. It is obvious, however, that better and cheaper methods are possible where space and location allow. A hillside location with thick earth walls and roof and a remote control room such as at Washington University at St. Louis would be much more satisfactory. Such a design should result in shielding from fast neutrons, slow neutrons, and the resulting gamma-radiation simultaneously. Data on the shielding properties of earth and other materials should be available from such laboratories soon.

### 17. CYCLOTRON COSTS

The several fields of usefulness of the cyclotron have already resulted in specializations of design. The optimum size and certain design features will differ for installations specializing in production of induced radioactivities, those intended as high intensity neutron sources, or those emphasizing nuclear research. The size and energy range desirable for research may vary from the cheap, compact 1- to 2-Mev units developed for small laboratories[35, 36] to the giant project being undertaken by Professor Lawrence and the Berkeley group. For commercial applications more attention must be paid to the economics of cost and output. Production costs of radioactive materials have been estimated in several of the academic installations able to supply such materials, and tentative prices have been estab-

lished. More adequate cost analyses are needed and in their absence only rough limits can be placed on the size or energy range for the most economical operation.

The initial investment includes housing, purchase price of materials, and equipment, and cost of installation including technical services. The largest single item of purchase price is the magnet. For a particular design costs are closely proportional to weight or to the cube of a linear dimension such as pole diameter. Size and power ratings of some auxiliary equipment such as exciting coils, motor-generators, etc., are determined by magnet size and costs can be assumed to show the same variation. Many parts of a cyclotron installation exceed the limits of normal commercial availability and surcharges based on excessive dimensions and increased installation costs can be expected for very large sizes. Of more importance is the rapid increase in cost of the radiofrequency power installation (transformers, rectifiers, oscillators, and controls) at high energies. The power requirements increase with $E^{7/2}$ as shown in Section 4, or with $D^7$, where $D$ is the pole face diameter. So power installation costs will increase at a much faster rate than other items, and will become the dominant factor at high energies.

Magnet designs have been based upon two fundamentally different principles. One employs a large amount of the cheapest form of soft steel plates, bolted or welded together, having mediocre magnetic properties. The other uses a minimum of highest quality magnetic iron as castings, with a resultant reduction in size and weight. The price differential between magnetic iron castings and soft steel plate is essentially balanced by the smaller amount needed to give equivalent magnetic fields. This has been confirmed in several recent installations by comparisons of competitive bids. A more important advantage of the higher permeability magnetic iron is the higher ion energies available, proportional to the square of the magnetic field. Comparison of magnet costs should be based upon equivalent ion energy output, not on magnet weight or pole face diameter. The smaller weight and dimensions of a magnet made of high permeability iron result in proportionate savings in foundations, copper for magnet coils, installation costs, and in many other features.

Housing and laboratory facilities are largely determined by interests extending beyond the maintenance and operation of the cyclotron. That fraction which can be referred to cyclotron costs may also be taken as proportional to the cube of pole diameter without serious error. The cyclotron chamber and much of the auxiliary apparatus must be made to order and require the facilities of a well-equipped machine shop with heavy machines. Shop facilities needed for maintenance are considerably smaller. Additional facilities for handling of radioactive materials, chemical procedures, and the detection and measurement of activities are essential but may be housed elsewhere than in the cyclotron laboratory. A large item of housing expense is the shielding. Shielding practice varies widely, from water tank housing to burial beneath earth fills, to location on a remote hill top. Little is known about the relative merits of different absorbers for shielding; it is possible that the most economical design has not yet been visualized.

Operating costs include salaries, electrical and water services, deuterium consumption, and a proper allotment for improvements, maintenance, and repairs. These items are nearly proportional to operating time and can be lumped as an hourly cost. Interest on the investment and amortization charges can be included in a total cost per hour and will obviously be a minimum for 24-hour, continuous operation. Such totals have been estimated for several installations in the 12- to 16-Mev range and are of the order of $25 per hour.[37]

### 18. YIELDS OF NUCLEAR REACTIONS

The variation of yield of nuclear reactions with bombarding energy can be predicted only from an intimate knowledge of nuclear binding energies, potential barriers, competing reactions, and other factors. However, certain generalizations with regard to relative yields of the several type reactions are possible based upon experimental observations and fundamental concepts:

(a) Deuterium reactions generally show higher yields than proton or helium ion reactions for equivalent ion energies. It is also easier to obtain deuteron beams in the cyclotron for technical

reasons. So production cyclotrons are usually operated as deuteron accelerators, except where a desired reaction or radioactivity can be obtained only by other ions. It is customary to describe cyclotron output in terms of deuteron energy.

(b) In the low energy range the yield of reactions with charged bombarding particles increases exponentially with energy, following the probability of penetration of the nuclear potential barrier. This exponential increase far outweighs other factors at low energies but becomes less important for energies greater than the barrier height. Essentially all radioactive materials which have been found useful for applications are in the lower half of the periodic table, with $Z<54$, for which the barrier is about 8 Mev. This sets an extreme lower limit on ion energies for economic efficiency.

(c) For energies above the barrier height it is believed that the total probability of disintegration (including all competing reactions) is essentially constant. The differential or "thin target" yield would flatten off from its exponential rise to a constant value. In this region the increase in yield for a thick target would be proportional to the range penetration into the target, varying approximately as $E^{\frac{1}{2}}$. Total thick target yields would show the exponential persisting with decreasing exponent to energies well above barrier height, becoming an $E^{\frac{1}{2}}$ variation at high energies.

(d) Reactions having charged particle products are usually less probable than those producing neutrons, since charged particles must penetrate a potential barrier to be emitted. This is most evident for targets of high atomic number or for low bombarding energies. The relative yields of competing reactions in the same target are conditioned by this factor. The $(d, \alpha)$ reaction usually has a smaller yield than the $(d, p)$ since the double charge on the $He^{++}$ ion results in a double potential barrier.

(e) Reaction energy $Q$ is positive for most proceses of the $(d, \alpha)$, $(d, p)$, and $(d, n)$ types, i.e., energy is released in the disintegration. Reactions having negative $Q$ values, such as the $(p, n)$ and $(d, 2n)$ types will have zero probability below a threshold energy. Yields will start at this threshold energy, will show a similar exponential rise, and should have the same $E^{\frac{1}{2}}$ relationship for very high energies.

(f) The compound nucleus, temporarily formed by the entry of the bombarding particle into the target nucleus, can disintegrate in various ways. These competing reactions, in which the product particles can be either a $p$, $n$, $\alpha$, $d$, $\gamma$, $2n$, $pn$, $3n$, etc., have relative probabilities determined by the energy available for the disintegration, the potential barriers involved, and other factors. Reactions which are highly probable at low energies, such as the $(d, n)$ type, will in general show a decrease in probability below the $E^{\frac{1}{2}}$ variation at high energies as other reactions become more probable, the $(d, 2n)$, for example. On the other hand, the new reactions entering the competition at high energy may show the exponential type increase persisting to energies many times the barrier height. So each nuclear reaction will have its characteristic yield or excitation function as bombarding energy is increased.

(g) Neutron yields for practically all deuteron energies are greatest from Li and Be targets. $Li(d, n)$ neutrons have the highest known energy (over 17 Mev) and are useful as bombarding particles in secondary reactions requiring high neutron energy such as $(n, \alpha)$, $(n, p)$, and $(n, 2n)$ types. The $Be(d, n)$ reaction is used when maximum neutron intensities are desired, since Be targets can be silver soldered to backing plates for cooling and will stand intense beams. Slow neutron bombardments are arranged with target materials in water solution or between paraffin layers outside and surrounding the target chamber. Maximum yield involves maximum utilization of solid angle around the target, or between the coils of the magnet.

(h) Isotope abundance in target materials modifies yields directly and may set a limit so that an alternate reaction with different target and bombarding particle leading to the same product is more efficient than deuteron bombardment. Similarly, the chemical dilution required to obtain a sufficiently refractory target for beam bombardment may force a change to another type reaction.

(i) Finally, yields are directly proportional to beam intensity and any comparisons of yield must assume equal beam currents. The outside

beam is usually only a fraction of the total resonant ion intensity. Cooling problems increase with energy, but are much simpler for the extended outside target. Refractory materials of good heat conductivity can be mounted on a probe target. With the present cooling techniques only a few targets can handle the maximum resonant ion beams available. Even with the smaller beam and larger dimensions of the outside target our experience is that the beam intensity is often limited by melting or evaporation of the target. For a representative target these limits will result in the yield falling below the $E^{\frac{1}{2}}$ variation with increasing ion energy. Averaged over all targets, this decreasing yield can be estimated to become important below 20 Mev with present available beam intensities and target arrangements.

Radioactive yields are expressed in terms of millicuries or microcuries per microampere-hour of bombardment, usually stated for zero time, the termination of bombardment. By a millicurie of activity we mean $3.7\times10^{7}$ disintegrations per second. To state such a value with precision requires a knowledge of the disintegration scheme and radiation energies, and recording equipment calibrated in absolute number of radiation quanta. In the absence of such information gamma-ray emitters can be defined in terms of their radium gamma-ray equivalent. A milligram radium equivalent is equal in gamma-ray ionization to that from a milligram of radium filtered through 0.1 or 1.0 cm of lead. Even in this case the response of the measuring instrument to radiations of different energy must be considered.

### 19. OPTIMUM SIZE

The original cost of a cyclotron has been shown to be roughly proportional to the cube of magnet pole diameter, or the $\frac{3}{2}$ power of ion energy $E^{\frac{1}{2}}$, up to the limits of commercial availability, and to rise more steeply beyond this limit. Experience in this laboratory has made us believe that such surcharges become evident for sizes representing about 15- to 20-Mev deuterons. The increasing cost of the high frequency generator and power supply will also become important at about this energy range, and will result in even more steeply rising costs. This is indicated in Fig. 18 in which

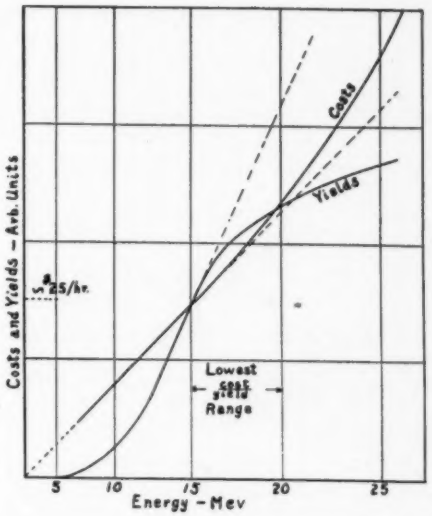


FIG. 18. Diagram illustrative of costs and yields of cyclotrons as a function of the maximum deuteron energy.

the total cost per hour of operation is plotted against the $\frac{3}{2}$ power of deuteron energy.

On the same figure the yield of a typical radioactivity is predicted, having three regions: an exponential rise extending to about 12 Mev, a region proportional to range penetration of the target, and a falling off at high energies where target cooling limitations occur and competing reactions become more important. The lowest cost/yield ratio will occur well above the potential barrier minimum but before the diverging factors of cost and yield become important. Our estimate of the most economical size cyclotron for the production of induced radioactivities of the types now in greatest demand is in the 15- to 20-Mev range. For heavy targets where the exponential increase in yields persists to higher energies, larger sizes would be more efficient. Also a cyclotron specializing in the production of neutrons, using a Be target, would not have as severe cooling limitations and the most efficient size might be for a higher energy range. The estimate above is probably valid, however, for the targets encountered in the large majority of applications of induced radioactivity, and for present cyclotron designs and techniques.

### 20. CONCLUSIONS AND RESULTS

The M.I.T. cyclotron was originally designed for 12-Mev deuterons, but with ample safety

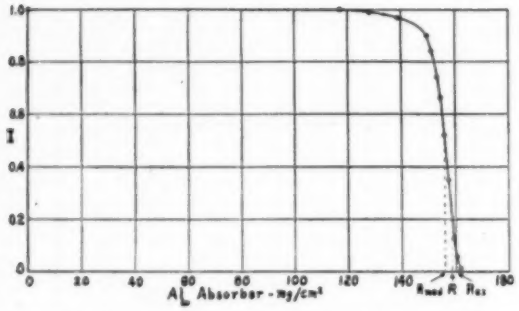


FIG. 19. Range curve of "14-Mev" deuteron beam in aluminum absorbers, showing a half-value range $R_{med}$ of 156 mg/cm² and a mean range $R$ of 158.4 mg/cm² computed from the observed extrapolated range $R_{ex}$. The respective energies are 13.0 and 13.1 Mev. (Courtesy of Mr. E. T. Clarke.)

factors on all essential parts. It has operated at that energy for over two years, maintaining a fairly continuous production schedule of induced radioactivities. Resonant ion beam intensities up to 400 microamperes were obtained on the oscillating probe target, but were restricted to 100 to 300 microamperes for most operations by target cooling limitations. Emergent beam intensities were low in the original chamber design and external targets were used only for a few target materials which could not be mounted on a probe.

A continuous program of development and improvement, slowed down by maintenance of an operating schedule of up to 75 hours per week, has increased the reliability and output. The most recent change was the installation of the chamber and dee line system described in this report. Development is not complete but has already resulted in an increase of deuteron energy to a nominal 15 Mev, resonant ions beams up to 1.0 milliampere, and emergent beam intensities of the order of 100 microamperes. There are justified expectations of a final operating range of 16 Mev, 1.0 milliampere resonant, and 200-microampere emergent beams with further development.

Range measurements of the emergent beam using aluminum absorbers have been made at several energies.[38] The emergent beam through a $\frac{1}{4}$-inch hole shows a very slight inhomogeneity which is only twice the theoretical straggling for a homogeneous beam in the aluminum absorbers. The current-range curve for a deuteron beam of 14-Mev nominal energy is shown in Fig. 19. The energy equivalent of the half-value thickness $R_{med}$ of 156.0 mg/cm² is 13.0 Mev.[39] The mean range $R$ of 158.4 mg/cm² is computed from the extrapolated range $R_{ex}$ of 160.5 mg/cm² and the theoretical straggling for a homogeneous beam, and has an energy equivalent of 13.1 Mev. Assuming the correctness of the range-energy relation used, the measured energy of the beam is 13.0±0.1 Mev.

The power efficiency of the M.I.T. cyclotron can be computed for the maximum beam of 1.0 milliampere obtained with 12-Mev ions. This represents 12 kilowatts in the ion beam. The input power to the oscillator was 50 kilowatts, giving a gross efficiency of 24 percent. Adding 25 kilowatts for magnet power and 15 kilowatts for pumps, ion source, and other auxiliary equipment, the net efficiency is over 13 percent.

Professor Robley D. Evans, organizer and director of the M.I.T. Radioactivity Center, of which the cyclotron is the production unit, has sponsored and supported the cyclotron throughout its development, and has assisted in many difficult decisions with his help and advice. Grants by the John and Mary R. Markle Foundation for the construction and subsequent development have been augmented by the Institute Administration and private donors. Dr. J. H. Buck assisted greatly in the design and installation, and is primarily responsible for the control circuits. Dr. J. H. Cook of the Electrical Engineering Department designed the neutralized oscillator circuit and assisted in the testing and development of the oscillator unit. In the continuing progress of the instrument, Dr. J. R. Downing and Mr. E. T. Clarke have each played a large part. Professor J. W. Irvine, Jr., of the Chemistry Department has developed radiochemical procedures and has collaborated in many problems of target design and technique. To the technical staff, especially Mr. Earle White, Mr. Edwin Pulster, and Mr. Edward Hamacher, go our thanks for their loyal service and many valuable suggestions.

## REFERENCES

(22) Franz N. D. Kurie, Phys. Rev. **55**, 241 (1939).
(23) R. R. Wilson, Rev. Sci. Inst. **12**, 91 (1941).

(24) Control and interlock circuits were designed and developed primarily by Dr. J. H. Buck.
(25) Designed and constructed by Mr. Earle White in accordance with standard radio principles.
(26) We are informed by Dr. J. G. Hamilton that range measurements taken later showed a somewhat inhomogeneous beam of about 14.5-Mev energy, probably due to a migration of ion paths as discussed in Section 8.
(27) R. Cornog and W. F. Libby, Phys. Rev. **59**, 1046 (1941).
(28) Handbook H23, "Radium protection," National Bureau of Standards.
(29) P. C. Aebersold, J. App. Phys. **12**, 344 (1941).
(30) M. A. Tuve and R. E. Roberts, private communication.
(31) E. Amaldi, L. R. Hafstad, and M. A. Tuve, Phys. Rev. **51**, 896 (1937).
(32) Private communication, via H. A. Bethe.
(33) These measurements were made as a graduate student project by Mr. G. Hoyt Whipple.
(34) R. F. Bacher and D. C. Swanson, Phys. Rev. **53**, 676 (1938).
(35) M. S. Livingston, Rev. Sci. Inst. **7**, 55 (1936).
(36) P. G. Kruger and G. K. Green, Phys. Rev. **51**, 699 (1937).
(37) M. S. Livingston, J. App. Phys. **12**, 339 (1941).
(38) Observations by Mr. E. T. Clarke in the course of a Ph.D. thesis investigation.
(39) M. S. Livingston and H. A. Bethe, Rev. Mod. Phys. **9**, 276 (1937).

## Calendar of Meetings

**February**

14–17 Technical Association of the Pulp and Paper Industry, New York, New York
18 American Geophysical Union, Berkeley, California
18–19 American Philosophical Society, Philadelphia, Pennsylvania
21–24 American Institute of Mining and Metallurgical Engineers, New York, New York
25–26 American Physical Society, Metropolitan Section, Brooklyn, New York
26 American Mathematical Society, New York, New York
28–March 3 American Society for Testing Materials, Cincinnati, Ohio

**March**

1 Inter-Society Color Council, New York, New York
2–4 Optical Society of America, New York, New York

**April**

2–5 American Ceramic Society, Pittsburgh, Pennsylvania
5–7 Society of Automotive Engineers, New York, New York
20–21 American Institute of Mining and Metallurgical Engineers, Pittsburgh, Pennsylvania
20–22 American Philosophical Society, Philadelphia, Pennsylvania
24–26 National Academy of Sciences, Washington, D. C.
25–27 Society of Motion Picture Engineers, New York, New York
27–29 American Physical Society, Pittsburgh, Pennsylvania
28–29 American Mathematical Society, New York, New York
28–29 American Mathematical Society, Chicago, Illinois
29 American Mathematical Society, Berkeley, California

**May**

12–13 Acoustical Society of America, New York, New York
14–16 American Institute of Chemical Engineers, Cleveland, Ohio
17–18 Society of Automotive Engineers, New York, New York

**June**

5–7 Society of Automotive Engineers, Detroit, Michigan
26–30 American Institute of Electrical Engineers, St. Louis, Missouri
26–30 American Society for Testing Materials, New York, New York

# New Books

## Die Methoden der Mathematischen Physik. Volumes I and II

By R. Courant and D. Hilbert. Pp. 469+xiv and 549+xiv, 15×23½ cm. Interscience Publishers, Inc., New York, 1931 and 1937. Price $14.00 set, each $8.00.

Through the fortunes of war this well-known work is now available in a photolithoprint reproduction. There are many who would have preferred a translation, but most students of mathematical physics have had enough training in German to read the original.

Although the title of the book is "Mathematical physics," the emphasis is on the mathematics and the unity of the work is a mathematical one. This makes it especially valuable for physicists who already know the physical facts and can appreciate the wide range of phenomena treated by a single mathematical technique. Without any mention of quantum mechanics, the first volume contains the mathematics necessary for a mastery of that field. One is tempted to suspect that many parts of quantum mechanics were developed after, and because, a physicist had studied this work.

The second volume gives special attention to the general theory of partial differential equations, including the Hamiltonian equations of mechanics and the Maxwell equations of electrodynamics. If, as some persons think, the scientific work during the war may bring about a revival of interest in the problems of classical physics, this volume may be of considerable value in future developments.

W. V. Houston
*Columbia University*

## Sub-Atomic Physics

By Herbert Dingle. Pp. 272+vii, Figs. 147, 13½×20 cm. The Ronald Press Company, New York, 1943. Price $2.25.

This book forms half of a course in physics for aeronautical students. The first part of physics is called mechanical physics and embraces those mechanical and thermal phenomena which arise from the behavior of atoms as wholes. The remainder is called sub-atomic physics. The present volume contains little more than an elementary treatment of a few selected topics in electricity, magnetism, and optics.

On page 80 a blunder may be noted. Object and image are interchangeable for lenses just as they are for mirrors; but in both cases it must be remembered that a virtual image becomes a virtual object. Furthermore, there are too many statements which are erroneous or misleading when removed from their immediate context.

The discussion is simple and vivid, and may be read with profit by any student who has not had a college course in physics.

E. H. Kennard
*On leave from Cornell University*

## Symposium on Powder Metallurgy

The seven technical papers and extensive discussion comprising the *Symposium on Powder Metallurgy*, which were presented at the 1943 Spring Meeting of the American Society for Testing Materials, have recently been published.

The Symposium was arranged by the Buffalo Committee headed by B. B. McCarthy. Following the paper on fundamentals necessary to apply powder metallurgy, by Charles Hardy, there is an extensive discussion on effect of pressure on the properties of compacts by C. W. Balke and on effect of particle size by P. R. Kalischer. There is also a discussion on alloy powders, metal powder friction materials, and hot pressing of metal powders. F. N. Rhines and R. A. Meussner cover the influence of homogenization upon the physical properties of copper-nickel powder alloys. An important part of the 60-page symposium is the discussion by other leading authorities in the field. The symposium includes materials on a number of current problems in this rapidly growing industry.

Copies of this publication can be obtained from the American Society for Testing Materials Headquarters, 260 South Broad Street, Philadelphia 2, Pennsylvania, at $1.00 per copy.

# Here and There

### Warning

Subscribers to physics journals are advised to scrutinize carefully any offers they may receive from unknown individuals for the purchase of sets of back numbers. For obvious reasons it is best to deal only with agencies known to be reputable. The publication of this warning is occasioned by the fact that in recent months such offers have been received from an individual who on a previous occasion accepted a shipment of back numbers from a subscriber and then never made the promised remittance in spite of much correspondence and many promises on his part.

### Reports on Progress in Physics

The Physical Society of London has announced a change of price on volumes of *Reports on Progress in Physics*. Each volume is now to be priced at $6.00. Volumes III, V, VI, VII, VIII are obtainable at this rate from the office of the society in London or from the American Institute of Physics, 57 East 55 Street, New York 22, New York.

### News Notes

David T. Siegel, founder and President of the Ohmite Manufacturing Company, Chicago, was elected to the Board of Trustees of Illinois Institute of Technology at the annual meeting. Mr. Siegel was one of five new members named to the Institute's board. The others are: Whipple

Jacobs, President of the Belden Manufacturing Company; Claude A. Knuepfer, President and General Manager of the General Engineering Works; T. Albert Potter, President of the Elgin National Watch Company; and Harold B. Smith, President of the Illinois Tool Works. The Board of Trustees includes in its membership 56 industrial executives and professional men of the Chicago area. Mr. Siegel was elected as an alumni representative to the board, having been nominated by the Illinois Tech Alumni Association.

It has been announced that the next meeting of the Optical Society of America will be held at the Hotel Pennsylvania in New York City, March 2–4, 1944.

### Institute of Radio Engineers

On Friday and Saturday, January 28 and 29, 1944, the Institute of Radio Engineers held its winter technical meeting at the Hotel Commodore, New York City. Under the chairmanship of Dr. L. P. Wheeler, retiring President of the I.R.E., a general conference was held on the morning of January 28, at which technical papers were presented and open discussions held. Dr. W. R. G. Baker, head of the Radio Technical Planning Board, spoke at a meeting at which several chairmen of the panels under the board discussed problems and technical activities upon which the panels will be engaged. E. K. Jett of the Federal Communications Commission headed a discussion by engineers of the F.C.C. covering police, aviation, and maritime service; international point-to-point problems and allocation problems; and matters of general interest to the Commission as of the time of the convention.

A President's luncheon was given, as well as a banquet at which the presentation of Institute awards were made and the inauguration of Professor H. M. Turner of Yale University, President-Elect of the I.R.E. for 1944, took place.

The American Institute of Electrical Engineers held its technical meeting beginning in the early part of the same week. They reserved their communications papers for presentation on Thursday afternoon, January 27. On Thursday evening, Major General Colton spoke on "Enemy communication equipment" at a joint A.I.E.E.-I.R.E. session. Both of these meetings were held at the Engineering Societies Building, 29 West 39 Street, New York City.

### Bulletin of Mathematical Biophysics

The March, 1944 issue of *The Bulletin of Mathematical Biophysics*, Volume 6, Number 1, which is edited by N. Rashevsky, has the following table of contents:

MARCH, 1944

**Studies in the Physicomathematical Theory of Organic Form,** N. RASHEVSKY
**Introduction. Form of Plants**
**Locomotion and Form of Snakes**
**Some General Considerations on the Shape of Quadrupeds**
**General Theory of Quadruped Locomotion**
**Loss of Energy due to Impact of Extremity Against the Ground**
**Suggestions for an Approximation Method for Solving the Equations of Motion of a Chain of Linked Levers**
**Flight of Birds and Insects in Relation to Their Form**
**The Internal Structure of Animals**
**Some Remarks on Unicellular Organisms**

## New Booklets

A 40-page bulletin (GEA-4025) featuring the Thy-motrol, G.E.'s pioneer electronic drive for providing and controlling adjustable-voltage power from a.c. lines, thus making possible the utilization of the inherent advantages of d.c. motors, has recently been issued by the General Electric Company. This bulletin is well illustrated and is divided into two parts. The first part explains the Thy-motrol's drive in detail, its functions, and its applications. The second part is devoted to a complete explanation of the Thy-mo-trol's drive operation.

The RCA Victor Division of Radio Corporation of America, Camden, New Jersey, has just released a 44-page booklet which presents a clear-cut exposition of the practical part electronics are playing in various industrial fields. Illustrated in color and written in non-technical language, this booklet, "Electronics in Industry," is being made available to business executives, manufacturers, and industrialists in whose fields the science of electronics may find applications.

*Interchemical Review*, Volume 2, Number 3 is a quarterly published by the Research Laboratories of Interchemical Corporation, 432 West 45 Street, New York 19, New York. This issue features articles on industrial viscometers and also surface-active agents. Requests for copies should be addressed to the Editor at the above address.

Allied Radio Corporation, Chicago, announces the release of a new slide-rule type rapid calculator, permitting quick and accurate determination of inductance, capacitance, and frequency components of series or parallel-tuned r-f circuits as well as inductance, turns per inch, wire type, wire size, coil diameter, and coil length for single layer-wound solenoid type r-f coils. All values, in either case, are found with a single setting of the slide and are accurate to within approximately 1 percent for coils ranging from ½ inch to 5½ inches in diameter and ¼ inch to 10 inches in length. All possible combinations within these limits are shown. Wire types and sizes include 11- to 35-gauge plain enamel, 11- to 36-gauge s.s.c., d.s.c., and s.c.c., and 12- to 36-gauge d.c.c. The rule is also engineered to indicate: turns per inch from 10 to 160; inductance from 0.1 to 15 microhenrys; capacitance from 3 to 1000 micromicrofarads; frequencies from 400 kilocycles to 150 megacycles with equivalent wave-lengths in meters. The calculator, which is priced at 25 cents, can be obtained from the Allied Radio Corporation, 833 West Jackson Boulevard, Chicago 7, Illinois.

# Contributed Original Research

## Electromagnetic Velometry. I. A Method for the Determination of Fluid Velocity Distribution in Space and Time*

ALEXANDER KOLIN
*Fluid Mechanics Laboratory, Columbia University, New York, New York*
(Received November 4, 1943)

A method is described which permits the determination of the local velocity of flow, as well as of turbulent fluctuations at a given point, or a prescribed series of points in a moving liquid. The method is based on the induction of a potential gradient in the flowing medium as it traverses a magnetic field perpendicularly to its direction. The absence of lag in the process of induction makes the method particularly suitable for the study of rapidly varying velocities and the sharp localization of measurements allows the determination of spatial velocity distributions. In an adaptation of the method for small scale laboratory experiments, the magnetic field is created by a large a.c. magnet in whose gap the conduit is placed, while two minute exploring electrodes pick up the induced e.m.f. at the desired locations. For large scale experiments and field work, a self-contained unit has been designed which comprises a minute electromagnet with attached pick-up electrodes. The applicability of this method is demonstrated by velocity distribution curves taken under different conditions and by records of liquid turbulence and transient velocity changes in different forms of flow. This paper is confined to the presentation of the principle involved, to the description of the apparatus, to the discussion of the experimental technique, and to demonstrations of the applicability of the method. A theoretical analysis of the characteristics and limitations of this method will be dealt with in a separate publication.

### PRINCIPLES OF THE METHOD

THE principle underlying the method herein described[1] is that of electromagnetic induction. When a fluid moves through a constant magnetic field of intensity $H$ a potential gradient $E$ is induced in the fluid which, at a point where the local velocity of flow is $v$, is given by the expression:

$$\mathbf{E}=(\mu/c)[\mathbf{H}, \mathbf{v}]. \quad (1)$$

If the magnetic field is known, the determination of $E$ at any point will enable one to evaluate the instantaneous value of the local velocity $v$. Figure 1 presents a clear idea of the experimental arrangement by showing its stepwise evolution from Faraday's original unipolar induction machine.

Figure 1A shows the original unipolar inductor. The e.m.f. induced in the part of the metal disk that moves between the magnetic poles is picked up and conveyed to the measuring device by the indicated sliding contacts. In Fig. 1B the disk is replaced by a straight metal belt in which an e.m.f. is induced at right angles to its direction of motion and to the lines of force of the homogeneous magnetic field. Since this induced e.m.f. is proportional to the instantaneous velocity of the moving belt we can obtain a picture of the belt velocity and its fluctuations by recording the induced e.m.f.

The next step, shown in Fig. 1C, consists of replacing the metal belt by an electrolytic conductor flowing through a pipe made of electrically non-conducting material. The voltage induced in the moving liquid is picked up by electrodes which are introduced through the wall of the conduit to make contact with the electrolyte. The meter readings prove to be proportional to the average velocity of flow (Fig. 1F)[2] and follow rapid variations of flow without distortion if an appropriate oscilloscope is used as an indicator.

We now imagine the pick-up electrodes of Fig. 1C pushed into the conduit until they are

* Publication assisted by the Ernest Kempton Adams Fund for Physical Research of Columbia University.
[1] A. Kolin, Phys. Rev. **63**, 218 (1943).
[2] A. Kolin, 1937 (unpublished).

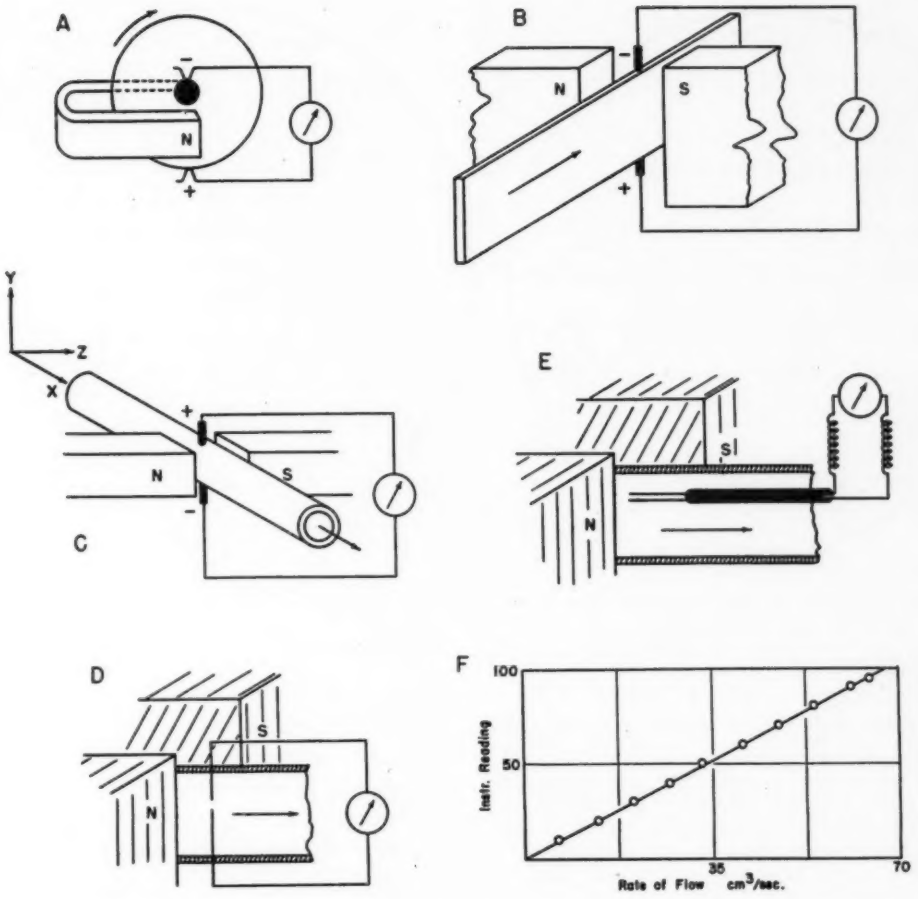


FIG. 1. Evolution of the electromagnetic velometer from Faraday's unipolar inductor. A: Unipolar inductor. B: Induction of an e.m.f. in a straight belt. C: Induction flow-meter. D: Measurement of local velocity. E: Set-up for studies of velocity distributions. F: Calibration of induction flow-meter.

separated by only a small gap as shown in Fig. 1D. We assume the electrodes to be thin enough so as to cause only a negligible disturbance in the local flow and we take them to be insulated except for the tips. Under such conditions, the microvoltmeter reading will be proportional to the axial velocity component of the liquid between the electrodes, thus enabling one to obtain a time record of the variations of the local velocity of flow.

In order to be able to study the velocity distribution in space, we alter the arrangement of electrodes as shown in Fig. 1E. Two parallel fine wires which are insulated except for the tips are mounted on a holder which can be moved up and down by means of a rack and pinion. (Such an arrangement will be subsequently referred to as the "probe" or the "exploring electrodes.") In this manner, the velocity distribution in the vertical plane along a line traced by the wire tips can be obtained.† In the figure the wires (diameter of the bare wire $4.10^{-3}$ in.; with the insulation between $6.10^{-3}$ in. and $8.10^{-3}$ in.) and the holder are shown on a greatly exaggerated scale in comparison to the pipe. The gap between the wires in most of the studies ranged from $4.10^{-3}$ in. to $15.10^{-3}$ in.

So far, we have made the simplifying assumption that the induced potential gradient can be measured directly by the voltmeter without further complications. Actually, however, the

† Provisions for additional motion along the $x$ and $z$ axes would enable one to study velocity distribution along any prescribed path in space.

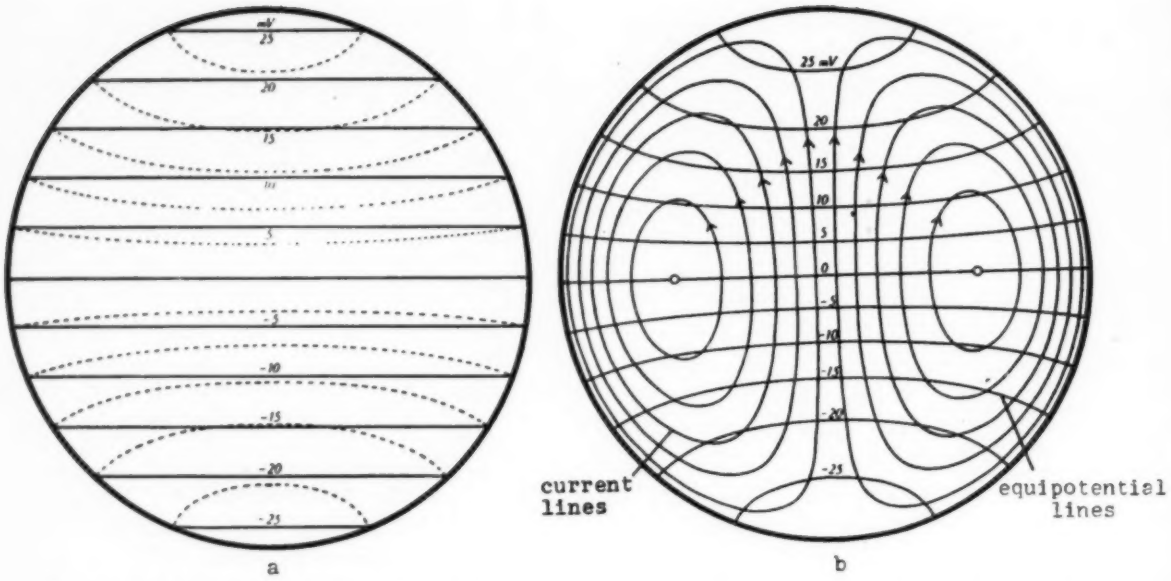


FIG. 2. (a) Solid lines: equipotential lines for the case of a uniform velocity throughout the cross section of the pipe. Broken lines (shown for comparison): equipotential lines in the case of a laminar velocity distribution. (b) Equipotential lines and current lines, in the case of a laminar velocity distribution.

potential difference picked up by the exploring electrodes is determined not only by the induced potential gradient but also by currents set up in the liquid due to the induced e.m.f. The actually observed potential gradient is expressed by the following equation:

$$\text{grad } U=(\mu/c)[\mathbf{H}, \mathbf{v}]-\gamma\mathbf{i} \qquad (2)$$

(where $\gamma$ is the specific resistance and $i$ current density). We now assume an homogeneous, infinitely extended magnetic field $H_z$ in the direction of the $Z$ axis and consider fluid flow through a uniform pipe whose axis coincides with $X$ (Fig. 1C); if the velocity at any point is $v_x$, the induced potential gradient will be in the direction of the $Y$ axis, and Eq. (2) can be resolved into the following component equations:

$$\partial U/\partial y=(\mu/c)v_xH_z-\gamma i_y, \qquad (2a)$$

$$\partial U/\partial z=-\gamma i_z, \qquad (2b)$$

$$\partial U/\partial x=-\gamma i_x=0, \qquad (2c)$$

of which only Eq. (2a) is of immediate interest to us, since we shall confine our study to the velocity distribution along the $Y$ axis, by observing $\partial U/\partial y$. The measured value of the potential difference will consist of the induced e.m.f. and the potential drop due to the flow of current. Since our measurements of the velocity distribution depend on the detection of the induced potential gradient, the effect of these electrical currents will either have to be eliminated by appropriate devices, or calculated and corrected for, unless it proves to be negligible. Observations have shown that, under certain conditions, the potential drop due to currents can be neglected. Moreover, we shall describe an arrangement by which the undesired currents can be suppressed to an extent permitting measurements under the most adverse conditions.

These induced currents are due to the existence of a velocity gradient in the liquid as it moves through a pipe. Only when the conditions $\partial v_x/\partial z=0=\partial v_x/\partial x$ are satisfied for all points in the pipe, the planes $y=$const. will be equipotential surfaces and there will be no circulating currents* (Fig. 2a).[3] The condition $\partial v_x/\partial z=0$ is, however, practically never realized in flow through a pipe. Under the assumption of a parabolic velocity distribution the resulting distribution of currents and equipotential lines, which is shown in Fig. 2b,[3] can be determined for

* This will hold only at a distance from the edges of the magnetic field where $\partial H_z/\partial x=0=\partial H_z/\partial z$.

[3] Thürlemann, Helv. Phys. Acta **14**, 383–419 (1941).

laminary flow by suitable transformation and integration from Eqs. (2).[3] It is interesting to note that whereas the voltage drop due to current flow opposes the induced e.m.f. along the vertical diameter, it increases the value of $\partial U/\partial y$ in the vicinity of the wall at the extreme ends of the horizontal diameter owing to the fact that in that region the current flows in the reverse direction. The lines of current are not perpendicular to the equipotential lines and are seen to diverge from the vertical axis of symmetry in the vicinity of the pipe wall. This indicates clearly the marked diminution of $i_y$ for values of $y$ approaching the tube radius. In the case of turbulent flow in a pipe of uniform cross section, the value of the velocity gradient is comparatively small in the central region but very large in a narrow zone bordering on the pipe wall. The density of the electric currents will consequently be relatively small throughout the central portions of the pipe and quite large in the narrow boundary zone. Since, however, the boundary zone is located near the insulating pipe wall, the lines of current will be deviated tangentially to the wall, similarly to the case shown in Fig. 2b, so that no excessive values for $i_y$ should be expected in the median region. Measurements of the turbulent velocity distribution in a straight pipe neglecting the influence of the induced currents lead to satisfactory results showing a close agreement between electrical and hydraulic measurements (Fig. 6 and Table I).

So far we have been assuming a flow through a constant, homogeneous magnetic field. In such a field, a steady flow will give rise to a constant induced e.m.f. The detection of small constant potential differences induced in an electrolyte is, however, connected with very great experimental difficulties, even when non-polarizable electrodes are used.

The experimental problems (polarization of the electrodes being one of the chief difficulties) are greatly simplified by utilizing an alternating magnetic field. In this case an alternating e.m.f. is induced in the moving liquid. The Maxwell-Lorentz Eq. (3)

$$\text{curl } \mathbf{E} = \text{curl } (\mu/c)[\mathbf{H}, \mathbf{v}] - (\mu/c)(d\mathbf{H}/dt), \quad (3)$$

shows that there will be an induced e.m.f. even while the fluid is at rest with $v=0$. This induced e.m.f. due to the second term of the equation is 90° out of phase with respect to the induced e.m.f. due to the motion of the medium as expressed by the first term. Hence, if we arrange to make our observations of the induced e.m.f. at a moment when $H=H_{\max}$ the second term will vanish since $dH/dt=0$ at that instant and Eq. (3) assumes the form of Eq. (1). The amplitude of the e.m.f. induced due to the motion of the medium is proportional to $H_{\max}$ and to the velocity of flow and a reversal of the direction of flow is indicated by a phase shift of 180° in the induced e.m.f.

## THE APPARATUS

Figure 3 shows the general scheme of the apparatus. By means of a circulating system a constant flow is maintained through a glass pipe which passes between the poles of an electromagnet energized by 60 cycles a.c., providing an homogeneous field of 2000 oersteds peak value across its gap. The exploring electrodes, shown on a greatly exaggerated scale, can be moved in the vertical direction by means of the rack and pinion. The picked-up voltage is conveyed to the amplifying system and cathode-ray oscilloscope.

A variable flow gives rise to a modulated 60-cycle signal which is amplified and conveyed to the cathode-ray oscilloscope whose sweep is synchronized so as to give a standing wave pattern the amplitude of which is observed. The maximum of this standing sine wave rises and falls in linear proportion to the instantaneous velocity of the varying flow (provided a linear amplifier is used) and becomes inverted when the direction of flow is reversed. By screening off† the wave image on the screen of the oscilloscope except for a narrow slit at the location of the maximum (Fig. 3) only a fluorescent point remains visible indicating by its position the rate, as well as the direction, of axial flow. The position of this luminous dot can be readily photographed.

The use of an alternating magnetic field in

† A slotted mask can be equally mounted in front of the photographic film of a moving camera used to record the flow. This procedure has the advantage of leaving the oscilloscope screen unobstructed.

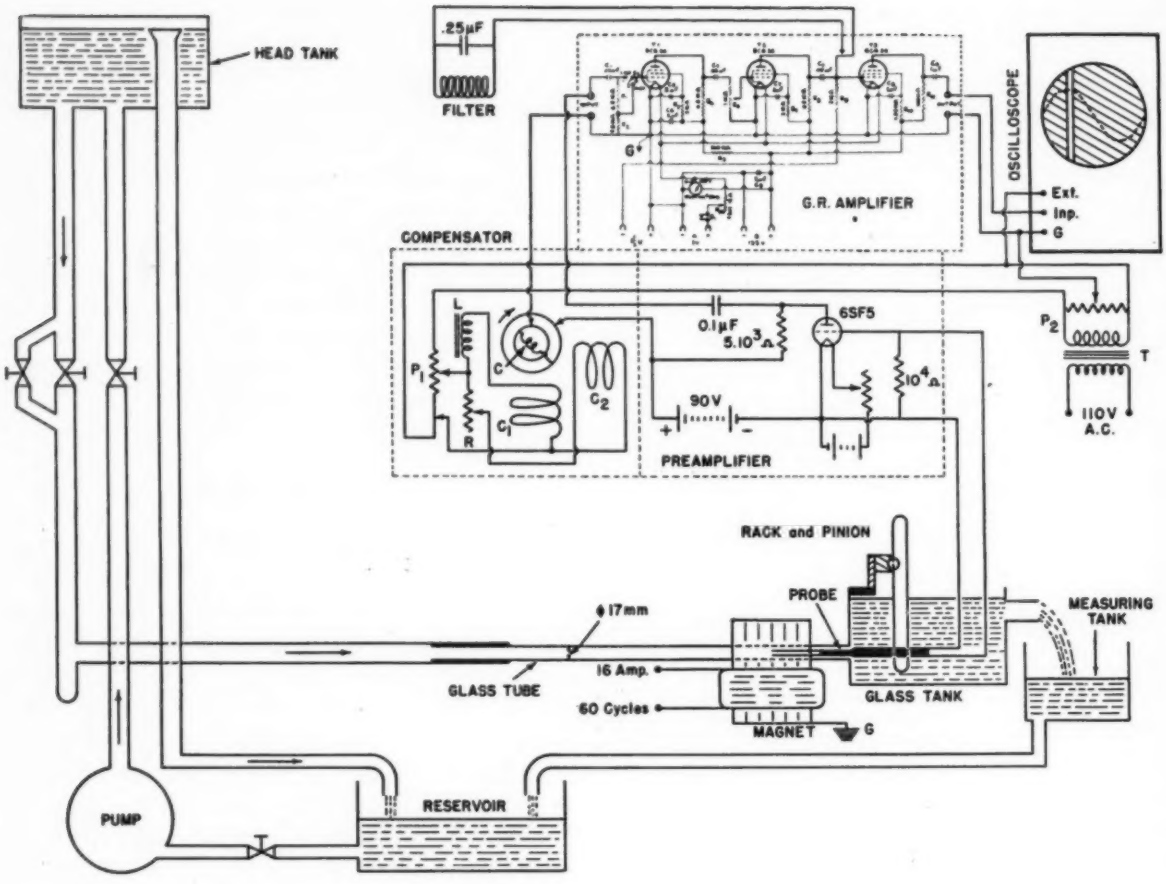


FIG. 3. The hydraulic circuit in conjunction with the exploring probe (greatly exaggerated in size) and the amplifying circuit.

conjunction with an a.c. amplifier eliminates the difficulties arising from the polarization of the electrodes encountered with a d.c. or a permanent magnet, and avoids disturbances developing from undesired galvanic potentials which may under certain circumstances mask the induced voltage in the case of the "constant field method." This improvement introduces, on the other hand, an undesired alternating e.m.f., mostly induced by the alternating magnetic field in the lead wires of the input circuit. The feature of this voltage is that its value does not depend on the motion of the liquid, and that it has the same value, even when the latter is at rest. This e.m.f. is eliminated by means of a special variable phase transformer[4] which in Fig. 3 is designated as "compensator." The primary field of this transformer is a rotating magnetic field obtained by superposing two mutually perpendicular magnetic fields 90° out of phase. These fields are generated by the coils $C_1$ and $C_2$, traversed by currents whose phases have been properly adjusted by means of a series inductance $L$ and a series resistance $R$, respectively. The secondary coil $C$ can be oriented in different directions. This varies the phase of the voltage induced in it by the rotating magnetic field. The amplitude can be varied by adjusting the potentiometer $P_1$ which regulates the intensity of the current in $C_1$ and $C_2$. The phase and amplitude of the output of coil $C$ are altered until the oscilloscope gives a zero reading for zero flow. The amplifying circuit consisted of a 814A General Radio amplifier in conjunction with a preamplifier utilizing a

[4] A. Kolin, Rev. Sci. Inst. **12**, 555 (1941).

6SF5 triode. A G.R. Filter Type 814-P3* passing a narrow band of frequencies in the vicinity of 60 cycles greatly helped in reducing the noise level of the amplifying system.

Figure 4a shows the construction of the exploring probe. Two thin platinum wires Pt ($4.10^{-3}$ in. in diameter) are insulated by means of a glass sleeve *I* or by means of a layer of a waterproof lacquer except at their tip. The wires are cemented on to a thin glass rod *G* which in turn is cemented to the tip of a drawn-out glass tubing. (The distance *d* ranged from $4.10^{-3}$ in. to $15.10^{-3}$ in. and *t* from $6.10^{-3}$ in. with lacquer insulation to $8.10^{-3}$ in. with glass insulation.) At *S* two thin copper wires Cu are soldered to the platinum wires Pt. They convey the voltage picked up at the electrode tips to the amplifier input through a shielded cable *SC*. The bare platinum and copper wires in the region of their junction are protected from contact with the water by a coating of Picein wax.

If such a probe, however, is used for flow measurements without a special treatment of the wire tips, it proves entirely ineffective. Bare metal tips seem to behave in general as though they were surrounded by a thin gas layer which acts as a high series reactance in the input circuit. The partial washing away of this layer by the moving liquid alters the impedance of the input circuit and upsets the conditions under which the instrument was adjusted to read zero at zero flow by means of the compensator. As a result, flow of water gives rise to erratic readings even when the magnetic field is off. These disturbances are completely eliminated by coating the exposed surface at the platinum wire tips (*C* in Fig. 4a) with colloidal graphite (Aquadag). The graphite layer has to be sufficiently thick and dense so as to prevent water from contacting the platinum wire. Heating the graphite deposit for a few seconds to a dim red glow secures a satisfactory adhesion. It is important, moreover, to insure an airtight seal between the glass sleeves and platinum wires at *C* by heating the electrode tip in a flame prior to the application of graphite.

The quality of the insulating lacquer (Duco and Zapon lacquer as well as white baking enamel were used successfully) is also of great importance, since its porosity can easily impair the performance or at least the durability of the electrode. We found glass to be by far the most satisfactory material for the preparation of permanent electrodes whose calibration would not change with time. Very thin glass sleeves (0.008 in. in diameter) can be easily prepared by drawing out soft glass tubing. The insertion of the platinum wire into these sleeves is a rather tedious process but one is rewarded by the durability of electrodes prepared in this manner.

* When interpreting records of fluctuating flow, one should take into account the frequency characteristic of this filter. It would be preferable, however, to use a filter with a constant attenuation over the range of the required side bands so as to avoid excessive distortion.

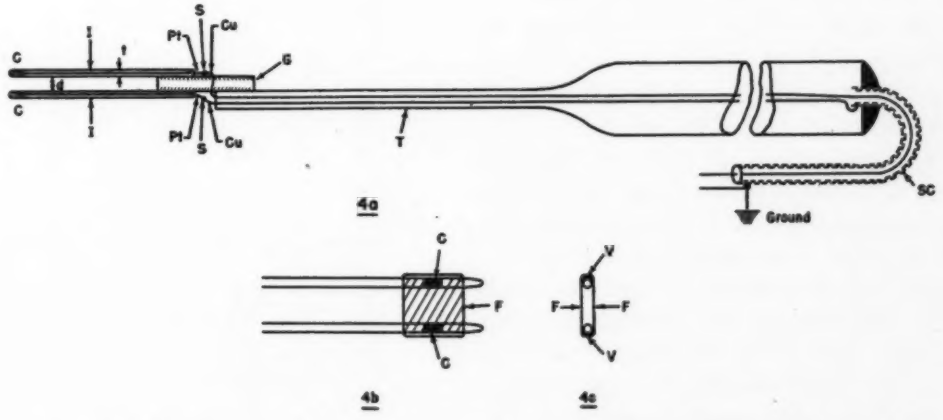


FIG. 4. (a) Construction of the "unprotected" electrodes. *C*, graphite tips; *I*, insulation; Pt, platinum wire; Cu, copper wire; *S*, junction; *G*, glass rod; *T*, stem of probe; *SC*, shielded cable. (b) Side view of "shielded" (or "protected") electrodes. *C*, graphite; *F*, foil. (c) Front view of "shielded" electrodes. *V*, insulating varnish.

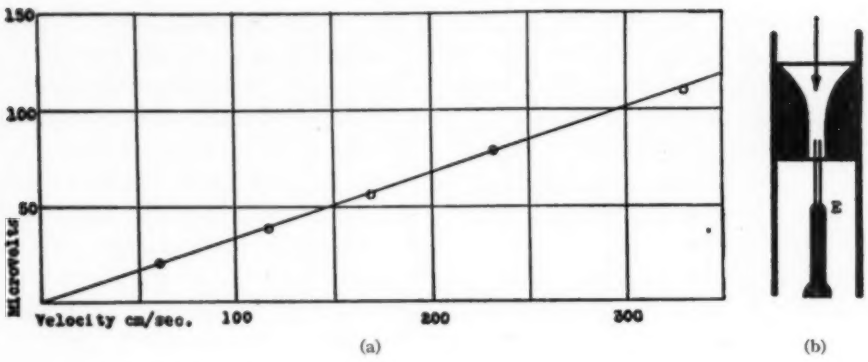


FIG. 5. (a) Calibration of exploring probe. (b) Nozzle used for calibration.

With the unavoidable retarding effect of the electrodes upon the neighboring flow and with the voltage drop caused by the induced currents, an attempt to compute theoretically the local velocity of flow from the recorded microvoltage would be an altogether hopeless task. We therefore adopted the empirical procedure of calibrating the electrodes used, for example, with Pitot tubes. The exploring electrodes $E$ were inserted into the mouth of a nozzle (Fig. 5b), where the velocity could be considered as practically constant throughout the cross section, and the oscilloscope was read at different known rates of discharge, determined by weighing the liquid. Figure 5a shows a calibration record thus obtained. As expected, it is a straight line passing through the origin.

## MEASUREMENTS NEGLECTING CIRCULATING CURRENTS

As stated before, velocity distributions in uniform pipes may be obtained in a satisfactory manner by using the "unprotected" electrodes of Fig. 4a, disregarding the effect of the possible presence of induced electrical currents. Figure 6 shows a set of velocity distribution curves, obtained in a glass pipe of 17-mm diameter at various rates of flow. The calibration of the probe was accomplished by means of the nozzle of Fig. 5b. In each instance the volume of water discharged per second was calculated from the respective curve by computing the volume of the body of revolution obtained by rotating the velocity distribution diagram about its axis of symmetry. The average velocity of flow $\bar{v}$ is then equal to the volume of the body so obtained, divided by $\pi R^2$. In other words:

$$\bar{v}=\frac{\int_0^R v2\pi y\cdot dy}{\pi R^2}=\frac{2}{R^2}\int_0^R vy\cdot dy, \qquad (4)$$

where $v$ is the velocity at the distance $y$ from the center of the pipe and $R$ is the pipe radius. The discharge values obtained by integration of the velocity curves, and the corresponding volumes of flow, measured hydraulically, are listed in Table I.

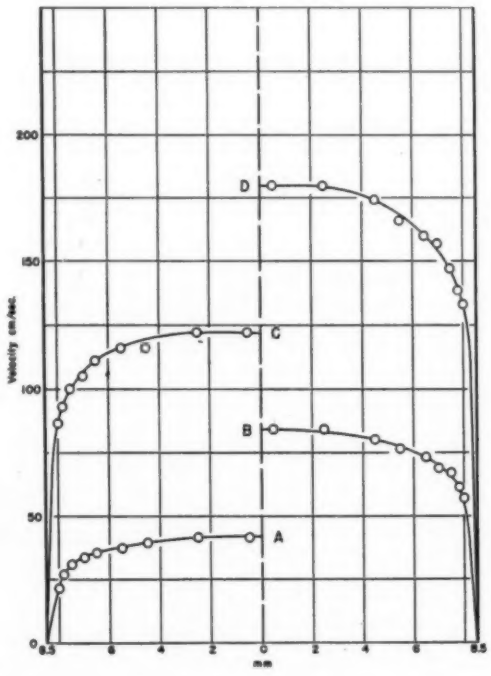


FIG. 6. Velocity distribution in a straight pipe at different rates of discharge.

TABLE I.

| | Average velocity electromagnetic | Average velocity hydraulic |
|---|---|---|
| *A* | 33.2 cm/sec. | 34.0 cm/sec. |
| *B* | 70.4 cm/sec. | 72.4 cm/sec. |
| *C* | 106.0 cm/sec. | 106.0 cm/sec. |
| *D* | 155.0 cm/sec. | 150.0 cm/sec. |

Within the limits of experimental error (of about 3 percent) the agreement is quite satisfactory.

Figure 7 illustrates the use of this method for the study of a rapidly varying velocity of flow in a hydraulic system containing air. The exploring probe was placed at the center of the 17-mm glass pipe, and the valve was rapidly opened and then suddenly closed. Owing to the presence of air pockets, the sudden closure of the valve led to an oscillatory motion, shown in the figure. The dotted appearance of the record is due to the use of a slotted mask in front of the photographic film as previously described. The image of the fluorescent spot of the cathode-ray oscilloscope sweeps past the slot 60 times per second and records the instantaneous value of the velocity of flow in time intervals of 1/60 of a second. In subsequent photographs a continuous curve has been drawn through these recorded points. For studies of more rapid variations of flow, it would be advantageous to use alternating magnetic fields of a higher frequency.

Figure 8 presents records of turbulent velocity fluctuations (a) at the center and (b) at a distance of 0.3 mm from the wall of the 17-mm glass pipe. The high intensity of turbulence in the proximity to the wall is very marked. Whereas the deviations from the average velocity at the center hardly ever reach the value

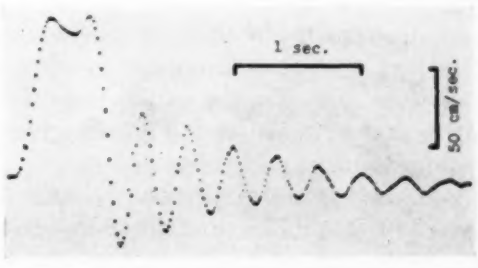


FIG. 7. Variation of local velocity in an oscillating water column.

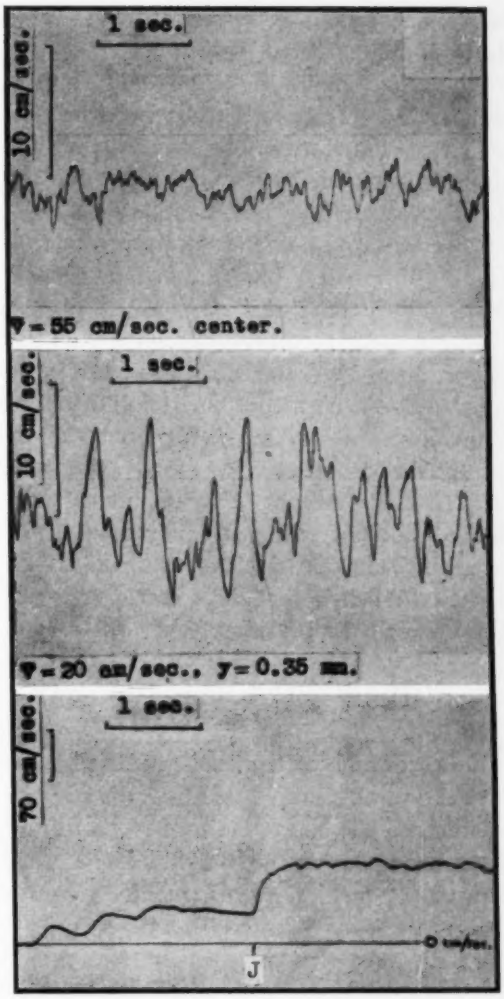


FIG. 8. (a) Turbulence at the center of a pipe. (b) Turbulence near the pipe wall. (c) Transition from laminar to turbulent flow as observed in the vicinity of the pipe wall.

of 5 percent, the deviations near the wall measure up to 30 percent. This example is particularly important, for it illustrates the possibility of using the electromagnetic method for systematic studies of turbulence in liquids. In cases where the turbulent velocity fluctuations constitute but a small percentage of the value of average flow, a reasonably large amplitude of turbulence can be obtained on the photographic record by increasing the gain of the amplifier to a point where the average deflection due to the main flow would be far beyond the limits of the scale and by restoring the fluorescent spot by means of the compensator to a position on the

fluorescent screen in which it could be easily photographed.

Figure 8c shows the change in time of the velocity regimen and the eventual abrupt velocity redistribution observed in the course of the establishment of flow following the opening of the valve. The record refers to velocities observed at a distance of 0.3 mm from the wall. As the motion sets in, friction is engendered in the boundary zone near the wall, the pattern in this layer first becoming laminar. This velocity redistribution explains the gradual diminution of velocity observed in the beginning of our record following each step in opening the valve. The sudden increase in velocity at $J$ signifies "transition," i.e., the advent of turbulent motion. The border velocities are greatly increased, due to the flattening out of the velocity profile, and the newly established turbulent state evidences the characteristic fluctuations.

## ELIMINATION OF THE EFFECT OF INDUCED CURRENTS

We have made so far the simplifying assumption that our instrument reading was strictly proportional to the e.m.f. induced in the liquid due to its motion across the magnetic field. Actually, however, the potential gradient which we measure is more precisely described by Eq. (2a):

$$\partial U/\partial y=(\mu/c)v_x H_z-\gamma i_y,$$

where $i_y$ is not a constant, but rather changes from point to point.

The distribution of the circulating currents (which, of course, varies according to the prevailing velocity distribution) is shown in Fig. 2b[3] for the case of laminar flow through a straight cylindrical pipe. While in aforementioned measurements inside of a pipe the effect of circulating currents was found to be negligible, we can readily see from this diagram that under circumstances the influence of such currents could become very confusing. Thus, for example, if a small obstacle were introduced into the pipe, the axial velocity immediately behind it would be zero; but the exploring electrodes would nevertheless pick up a potential difference in that location due to the voltage drop created by the circulating electrical currents. A situation of this kind arises, when one inserts into the pipe a nozzle as pictured in Fig. 9. The resulting flow

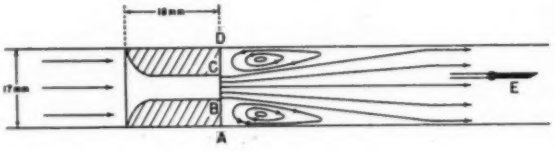


FIG. 9. Pattern of flow behind the nozzle.

form, as indicated schematically in the figure, features the "live jet" separated from the roller filled wake, formed back of the ring-shaped base $B$–$A$, $C$–$D$ surrounding the opening. At some distance from the nozzle, there is a region of back flow close to the pipe wall, but in the immediate vicinity of the nozzle the flow in the wake is in the radial direction with the axial velocity component obviously zero. Consequently, when taking a distribution of longitudinal velocities in the region between $C$–$D$ and $B$–$A$ immediately behind the insert, the instrument should record no deflections. Actually, however, when measurements are performed with electrodes typified by Fig. 4a, a strong negative deflection is obtained between $A$–$B$ and $C$–$D$, while the instrument reading for the region between $B$–$C$ shows the anticipated positive deflection (Fig. 10a). This negative deflection, which obviously cannot be due to a backward flow in this region, can be explained as follows: A potential gradient is induced in the direction of the diameter $BC$ of the moving water column. After leaving the nozzle (which is made of a nonconductive material) the water enters the wider glass pipe, and can be considered, from there on, as moving through electrolytic confines. Consequently intense electrical currents are set up in the water surrounding the moving water column, by the e.m.f. induced in the flowing liquid. The voltage drop created by these currents is opposite in direction to the e.m.f. induced in the moving liquid. This provides an explanation for the negative part of the curve in Fig. 10a, giving the false impression of backflow.

To obtain, for a specific case, a quantitative appraisal of the influence of these induced currents on the potential difference picked up by the probe, the exploring electrodes were inserted deep into the 8-mm nozzle, noting the instru-

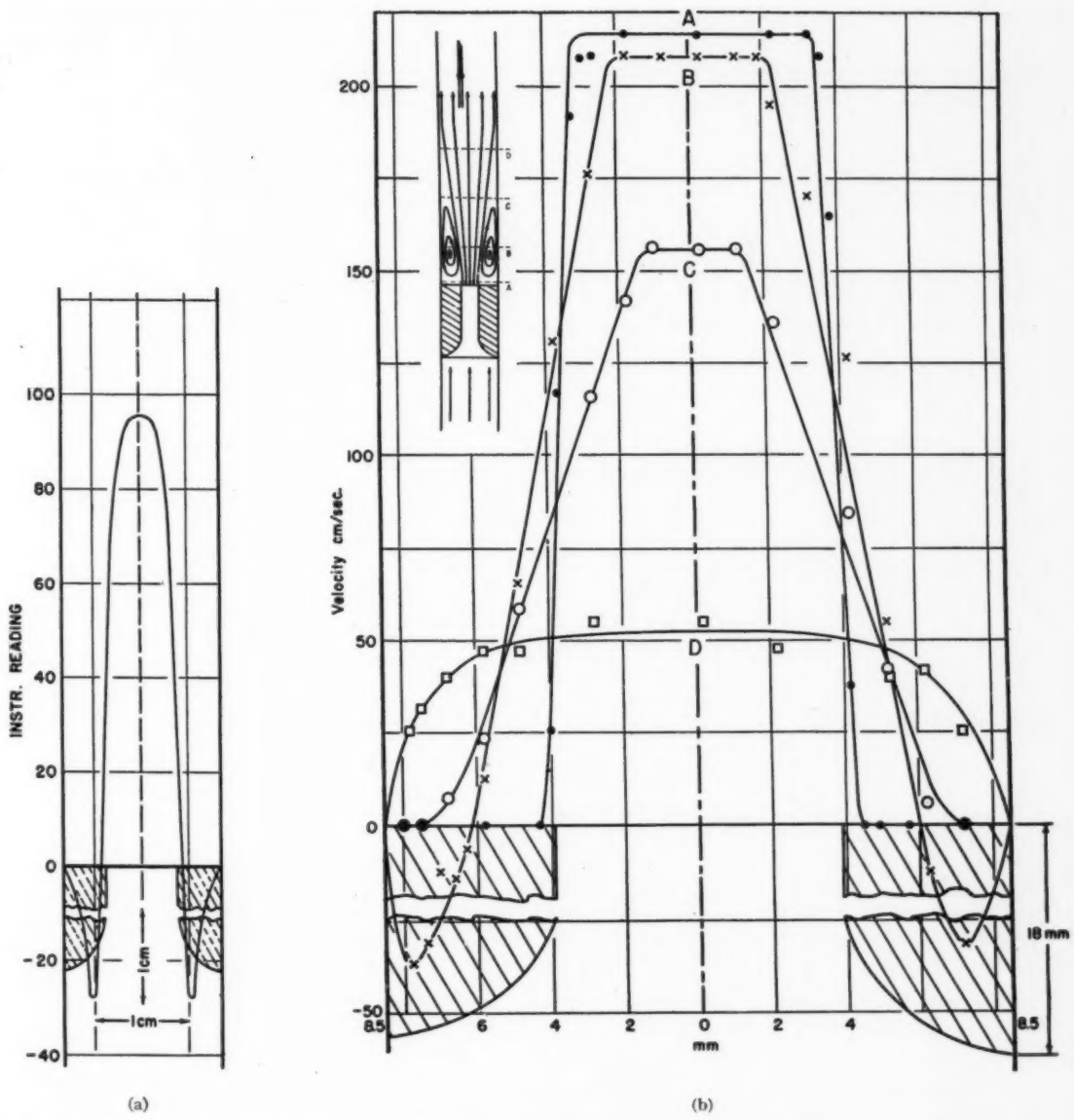


FIG. 10. (a) Effect of induced currents visualized in close proximity to the nozzle. (b) Distribution of velocities at different distances $x$ below the nozzle. $A$, $x=1$ mm; $B$, $x=20$ mm; $C$, $x=45$ mm; $D$, $x=70$ mm.

ment reading at a certain constant rate of flow. When, thereafter, the probe was moved in the axial direction to just outside the orifice, where the velocity could be anticipated to remain the same, the instrument reading showed a drop to 72 percent of its previous value. For smaller orifices the voltage drop is considerably larger; it is due to the electrical currents circulating through the environment of the moving water column. They are negligible while the water flows through the nozzle of non-conductive material, but they become substantial when the water flows through an electrolytically conductive environment.

In order to avoid the disturbance due to the circulating currents and to obtain a true picture of the velocity distribution behind the nozzle, an alternative type of electrode was devised (Fig. 4, b and c). Two thin aluminum foils ($2.5 \cdot 10^{-4}$ in. thick) or, preferably, sheets of mica of similar

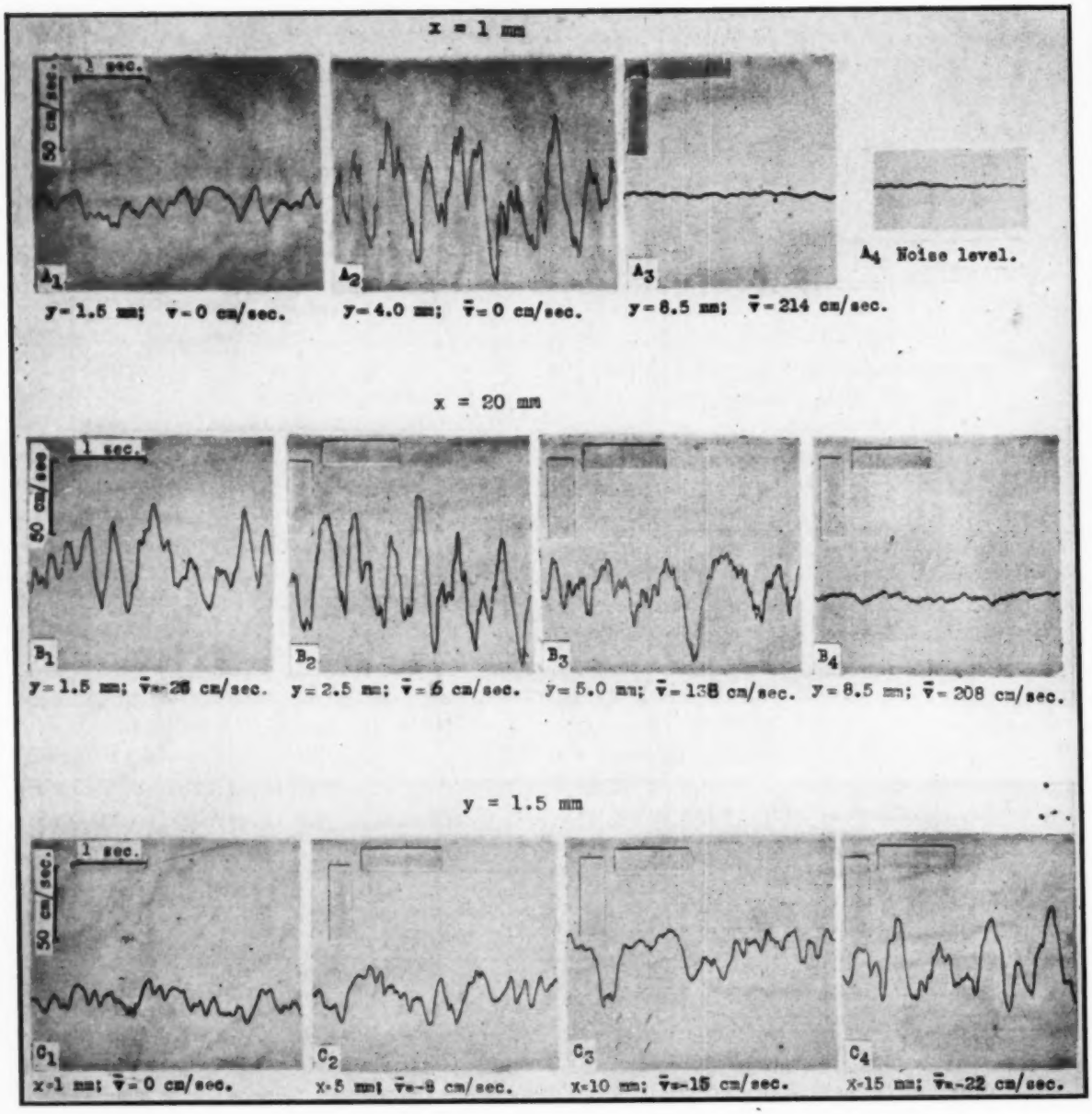


(a)

FIG. 11(a). Local turbulence recorded at points indicated in the pilot drawing.

thickness, designated in the figure by $F$, were coated with a thin layer of water resistant lacquer (for instance, "Zapon" lacquer) and were cemented on both sides of the exploring electrodes, so as to prevent the extraneous currents from passing through the interspace between the two bare graphite rings $C$ which were left uncoated by the lacquer while the rest of the wire was thoroughly insulated. As shown by measurements, the addition of these foils does not to any noticeable degree increase the hydrodynamic resistance of the electrodes. On the other hand, the measure of protection realized with such shielded electrodes in making the instrument readings independent of the circulating currents is convincingly demonstrated by placing

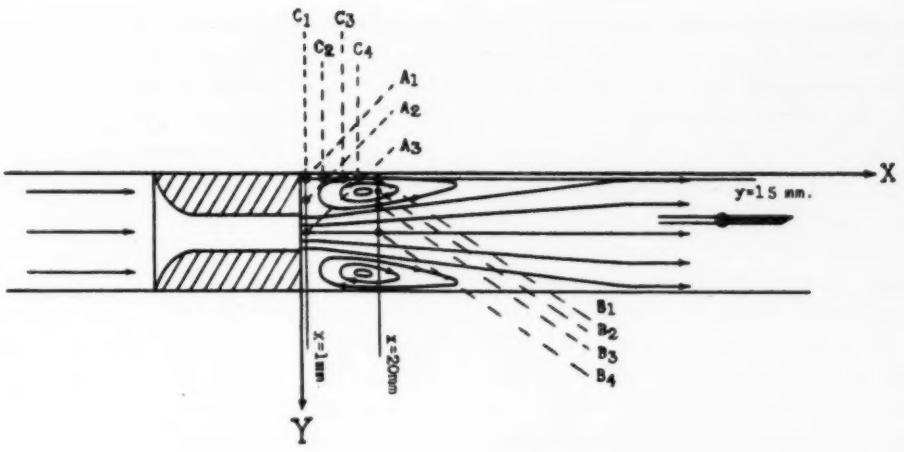


(b)

Fig. 11(b). $x$, distance from the nozzle; $y$, distance from the pipe wall; $\bar{v}$, time average of local velocity.

them inside and outside the barrel of a nozzle, and obtaining identical readings for a certain rate of flow, whereas, as stated before, widely different readings were obtained with unprotected electrodes.

Figure 10b shows a set of velocity distributions obtained with the shielded electrodes at different distances from the 7.8-mm nozzle. As seen, the velocity distribution 1 mm below the orifice, marked in the figure as $A$, exhibits a totally different appearance from Fig. 10a, registering no axial velocity in the annular space between $A$–$B$ and $C$–$D$, and indicates, as anticipated, a region of constant velocity across the jet between $C$ and $B$ (compare Fig. 9). The distribution at a distance $X=20$ mm from the orifice, marked $B$, shows a distinct region of backflow in the vicinity of the wall in accord with the schematic Fig. 9. At $X=45$ mm (curve $C$), the wake, and with it the possible region of backflow, are reduced to an extent, where the probe is unable to detect the negative velocity, while in traverse $D$, at $X=70$ mm from the nozzle, the velocity profile approaches the forms typical for the unobstructed pipe (Fig. 6).

Since the volume of water passing through the different cross sections of the conduit is the same, the volume of the bodies generated by rotating the curves of Fig. 10b about their central axis should be identical.* Indeed, the figures presented in Table II show that the volumes of the

TABLE II.

| | Distance from the nozzle | Volume in arbitrary units | Percent deviation from average |
|---|---|---|---|
| $A$ | 1 mm | 31.2 | 5 |
| $B$ | 20 mm | 29.3 | 1 |
| $C$ | 45 mm | 29.8 | 1 |
| $D$ | 70 mm | 27.9 | 6 |
| | | Average 29.6 | |

bodies of revolution so obtained agree within the limits of the experimental error. The anticipated error is particularly large in the cases of curves $A$ and $D$, due to the following reasons: The volume of revolution for curve $A$ is roughly equal to that of a cylinder of 4-mm radius. Since the possible error in determining its radius is about 0.1 mm—or 2.5 percent—the error in estimating the cross section will be about 5 percent. The error of 1.5 percent in determining the cylinder height will make the error in computing the volume about 6.5 percent. On the other hand, in taking measurements for the curve $D$, the deflections of the instrument amounted to about 1 cm in the region of maximum velocity. Due to intense turbulence the error in estimating the mean deflection was roughly $\frac{3}{4}$ mm or 7.5 percent.

Figure 11 presents records of the turbulent fluctuations in the axial direction, obtained with

* Volume generated by the negative branch of curve $B$ is to be counted as negative.

the shielded electrodes at various distances from the nozzle insert and at different locations relative to the pipe wall. The use of this type of probe for studies of turbulence permits a sharp localization of the region in which the velocity fluctuations are to be studied. In Fig. 11 the position of the respective points, at which the local turbulence was recorded, is indicated in the "pilot drawing." In particular, the set marked $A$ shows the turbulent fluctuations of the local velocity in the cross section 1 mm below the nozzle at the different distances $y$ from the pipe wall. (These records were obtained under the same circumstances as the velocity distributions of Fig. 10b.) The group marked $B$ exhibits similar records at a distance of 20 mm below the nozzle. In both cases turbulence practically disappears at the center of the pipe, as could be expected for the "potential core" of the jet. On the other hand, most intense manifestations in group $A$ are shown at $y=4$ mm, that is, in the separation region between the live vein and the wake. For the group $B$, the records $B_1$ and $B_2$ are characteristic of the intense agitation prevailing in the wake with the turbulent fluctuations exceeding the average velocity. Insert $C$ depicts, finally, turbulence in the region of the wake at a constant distance of $y=1.5$ mm from the pipe wall, but at different locations $x$ below the orifice. The absolute value of the velocity fluctuation is seen to increase as one recedes from the wall of the nozzle, while the relative intensity of turbulence, in ratio to the mean local velocity, declines.

Theoretically the method described should work with any fluid, since the induced potential gradient does not depend on the electrical properties of the material. In a dielectric moving through an alternating magnetic field, polarization currents would be induced. Owing to a high noise level at high values of the input impedance of the amplifying circuit, it is advisable to work with a good electrolytic conductor in preference to a dielectric. The present work was done with a 1 percent NaCl solution to create the most favorable conditions for the preliminary work.

## SELF-CONTAINED UNIT

The two types of electrodes, described in the preceding sections, were mainly presented for the purpose of illustrating the mode of application of the method. Actually, with the same general set-up a great variety of electrode arrangements is possible, some of which would permit to measure transverse turbulent components, perpendicular to the direction of main flow. The limiting feature of the set-up as described above is the requirement of a magnetic field generated by an extraneous magnet which naturally confines the application of the method mostly to model experiments in laboratory surroundings. Under all conditions the conduit must be small enough to fit into the gap of a reasonably large electromagnet.

In order to demonstrate the practicability of a "self-contained unit," avoiding the limitations imposed by the use of an external field, a small exploring probe containing a minute a.c. electromagnet next to its pick-up electrodes was built, with the iron core of the magnet consisting of a flat, approximately elliptical disk of 2.5 by 6 mm and about 1 mm in thickness. The iron core and the coil which is wound around its rim were thoroughly insulated by a coat of water resistant varnish. The tips of the pick-up electrodes were fixed at the extremities of the major axis. For effecting measurements, the self-contained unit is placed in the streaming with the faces of the disk parallel and the major axis perpendicular to the direction of the flow. By changing the orientation of the unit, one may determine the velocity components in any desired direction. Calibration experiments showed the deflections obtained with the self-contained unit to be a linear function of the velocity. The device proved to be reasonably sensitive and fully capable of measuring turbulent fluctuations. Thus, Fig. 12 shows records of turbulent velocity variations, obtained at different distances from an 8-mm nozzle, along the central axis of a jet entering the tank with an initial velocity of 340 cm/sec. The turbulence appears increasing in intensity and scale as one recedes from the nozzle.

## HISTORICAL NOTES

Although the above results represent, to our knowledge, the first attempt at a direct determination of instantaneous local velocities in moving liquids, we should like to mention a few references on the general subject of the utilization

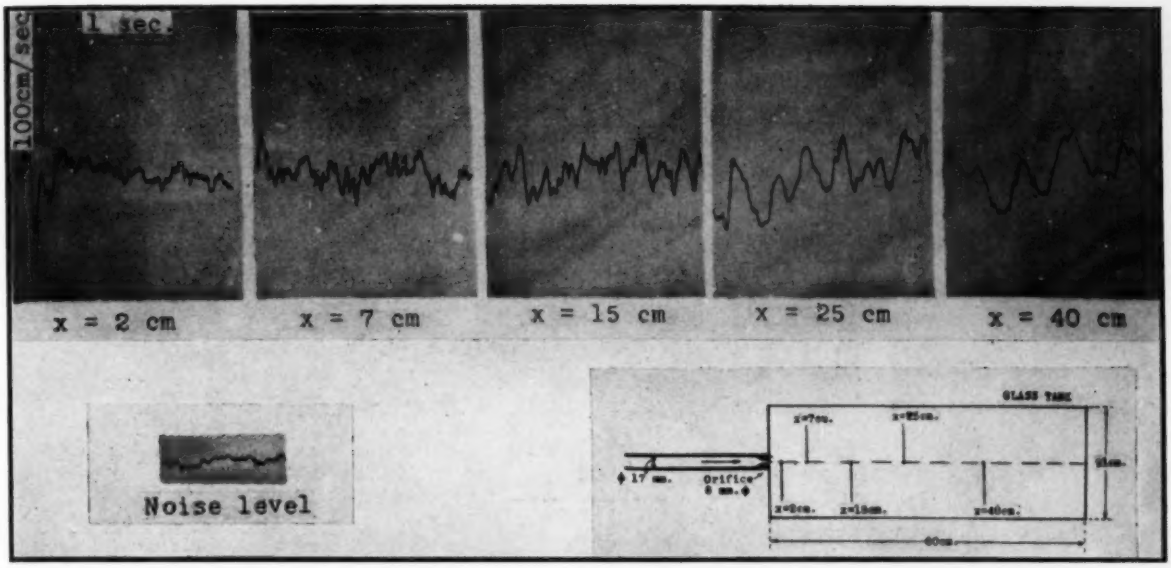


FIG. 12. Turbulence in a live jet entering a glass tank through a nozzle at different distances from the latter. The pilot drawing below indicates the points at which the local turbulence was recorded.

of electromagnetic induction for measurement of fluid flow which have reached our attention after the publication of our first communication on this subject.[5] In most of the cases referred to, the authors worked independently and unaware of each other's work, since the papers in question were published in out-of-the-way journals not widely read.

Faraday[6] himself seems to have been the first to consider the possibility of inducing an e.m.f. in a liquid moving through a magnetic field. He made experiments at the Waterloo Bridge in London in an attempt to detect an e.m.f. induced in the River Thames during the tides owing to the motion of large quantities of water across the earth's magnetic field. These experiments, mentioned by Faraday in a Bakerian lecture, were unsuccesful. Williams[7] considered the flow of liquids through a magnetic field and made calculations permitting him to evaluate the effect of induced currents. His experimental approach did not permit a direct observation of local velocities and of their variation in time. In 1932 Fabre,[8] in a letter to the French Academy of Sciences, suggested the use of electromagnetic induction for qualitative observations of velocity fluctuations in cut blood vessels ("un hémodromograph sans Palette"). This letter was not followed by any further publications. In 1936 Kolin[5] described the "electromagnetic flowmeter," a method for quantitative determination of the instantaneous values of the average velocity of the blood flow in intact blood vessels. This communication was followed by a series of publications in biological journals. In 1937 Wetterer[9,10] used an identical set up for the same purpose.

In 1937 and in the course of the following years, Kolin[4,11–13] introduced the use of an alternating magnetic field for the purpose of measuring average flow through pipes and blood vessels.

In 1940 Einhorn,[14] unaware of the work of the above-mentioned authors, essentially confirmed

[5] A. Kolin, Proc. Soc. Exper. Biol. and Med. **35**, 53–57 (1936).
[6] M. Faraday, Bakerian Lecture.
[7] E. J. Williams, Proc. Phys. Soc. London **42**, 466–78 (1930).
[8] P. Fabre, Comptes rendus **194**, 1097 (1932).
[9] E. Wetterer, Zeits. f. Biol. **98**, 26 (1937).
[10] E. Wetterer, Zeits. f. Biol. **99**, 158 (1938).
[11] A. Kolin, Am. J. Physiol. **122**, 788 (1938).
[12] A. Kolin, U. S. Patent No. 2,149,847 (1939).
[13] A. Kolin, Proc. Soc. Exper. Biol. and Med. 1941, **46**, 235–39 (1941).
[14] H. D. Einhorn, Roy. Soc. S. Africa **33**, 143–160 (1940).

their findings using an alternating magnetic field. In 1941 Thürlemann,[3] working with constant magnetic fields, verified the calculations and experimental findings of his predecessors in a careful study. Finally in 1943 electromagnetic induction was utilized by this author[1] for a direct determination of velocity distribution and a study of local turbulence in liquid flow.


### ACKNOWLEDGMENTS

This work was carried out under the sponsorship of the Civil Engineering Department of Columbia University, and its successful completion is in a large measure due to the vision and initiative of Professor B. A. Bakhmeteff, Director of the Fluid Mechanics Laboratory. The author takes great pleasure in thanking Professor Bakhmeteff for innumerable suggestions, valuable criticism, and guiding advice, which have proved invaluable throughout the course of this work. The author is equally indebted to Dean J. K. Finch for his active interest in this work and his never-failing effective support. Thanks are also due to the Research Corporation for a generous grant of funds for the purchase of instruments.


---

## Twinning in Zinc Oxide


M. L. FULLER

*Research Division, Technical Department, The New Jersey Zinc Company, Palmerton, Pennsylvania*



(Received November 3, 1943)



A crystallographic analysis of a characteristic shape of particle found in zinc oxide produced by burning zinc vapor has been made with the aid of the electron microscope. This particle consists of four needle-shaped crystals united at a common juncture. The spatial angles among the four crystals were determined from stereoscopic micrographs with the use of the stereographic projection. The crystals were found to be united by twinning on planes of the form (112).


### INTRODUCTION

TWINNING is a common crystallographic phenomenon in which two or more crystals are united in some symmetrical manner characteristic of the particular substance. Most determinations of twinning relationships have been made on crystals of macroscopic size where the spatial arrangement can be determined by the conventional methods of the crystallographer. The present paper is an account of a determination of the twinning relationship in crystals of microscopic dimensions, pigment zinc oxide. Stereoscopic electron microscopy was employed to make the measurements and the method described in the paper is applicable to other problems in stereoscopic electron microscopy.

The twinned form commonly seen in pigment zinc oxide consists of four acicular crystals united at a common juncture. A pair of stereoscopic electron micrographs of particles of this shape is shown in Fig. 1. In manufacturing parlance, the

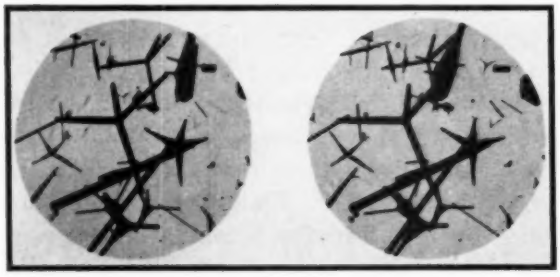

FIG. 1. Stereoscopic electron micrographs of fourling zinc oxide 3500×.

particles are known as fourlings. The paper will show that the arrangement of the four legs of the fourling is such that the planes formed by each of two pairs of legs are perpendicular to each other, the legs within a pair making angles of 97.7° to each other, the other four angles between legs being 115.7°.

## ORIENTATION OF THE CRYSTAL AXES IN EACH OF THE FOUR CRYSTALS

When single-needle acicular zinc oxide is incorporated in a paint and the paint is applied by brushing in one direction it has been found by x-ray diffraction that the zinc oxide crystals are oriented so that the hexagonal or *C* axis of the crystal is parallel to the brushing direction. Similarly, when single-needle acicular zinc oxide is used in the pigmentation of rubber and the rubber is stretched, the *C* axis is oriented parallel to the stretching direction. It has also been shown (using the light microscope) that the acicular particles orient themselves with their needle axes parallel to the direction of flow. From these experiments it is concluded that the crystallographic *C* axis and the long axis of the needle coincide.

The foregoing experiments were repeated with fourling type particles. Fourlings can be broken down into single needles by mulling on a glass plate with a glass muller. This can be established by electron microscope examination of a fourling type zinc oxide before and after mulling. X-ray examination of brushed paint films in which the pigment consists of broken fourlings reveals the same orientation of the zinc oxide crystals that was found for originally single-needle type particles. The individual legs of the fourling, therefore, are crystals in which the *C* axis is coincident with the needle axis.

## METHOD OF DETERMINING THE SPATIAL ARRANGEMENT OF THE FOURLING

The spatial arrangement of the fourling was determined from stereoscopic electron micrographs made with an RCA type B microscope. The specimens were prepared by allowing zinc oxide to deposit on thin Formvar membranes directly from the fume of a zinc oxide furnace. The mounts thus prepared were introduced into the electron microscope so that at no time was the mount subjected to any mechanical force.

The stereoscopic device of the RCA microscope is arranged so that two micrographs may be taken of the same field with two different angles of the specimen mount to the electron optical axis. The difference in angle is 8°. The effect of this change of angle of the specimen to the electron rays is to produce differences in the directions of the projected images of the four legs of the fourling between the two micrographs. This is illustrated in Fig. 1, which is one of the pairs of stereoscopic micrographs used in this investigation.

The first step in the analysis is to determine the direction of the stereoscopic shift. This cannot be determined from geometrical optics because of the indeterminate image rotation in an electron microscope. Enlarged prints (8×10″ or 4×) of the original plates are made. These prints are mounted on a drawing board with a single thumb tack for each. The tacks are mounted through corresponding points on the two prints so that these two points are in line with the blade of the T-square. The points selected are two easily recognizable points on the image of the membrane upon which the zinc oxide particles are mounted. These membranes usually have holes or other imperfections which can be recognized. The prints are then adjusted by rotation about the thumb tacks as axes until the prints are so positioned that a line joining any point on the one print to the corresponding point on the other print is parallel to the blade of the T-square. This direction is then marked on the prints, and will hereinafter be designated as the stereoscopic shift. The direction on the print normal to the stereoscopic shift is the axis of rotation of the specimen through the 8°. In mounting prints for viewing in a stereoscope the stereoscopic shift is made parallel to the interpupillary line of the observer.

The second step is to measure the angles between the legs of the fourling and the stereoscopic shift on the two micrographs. This is done on the enlarged prints with a protractor.

Finally, the positions of the four legs in space are derived from the positions of the projected images by the graphical methods of the crystallographer's stereographic projection.* To facilitate this graphical operation, a $15\frac{5}{8}$″ diameter stereographic net is used. The net is a stereographic projection of a sphere showing the great circles (longitudes) and the small circles (latitudes) for every degree.

Tracing paper is mounted on the net and the projected images of the fourlings are drawn. This

* An excellent description of the method of the stereographic projection may be found in a paper by C. S. Barrett, Trans. A.I.M.E. **124**, 29–58 (1937).

is illustrated in Fig. 2. The inset shows a repro-

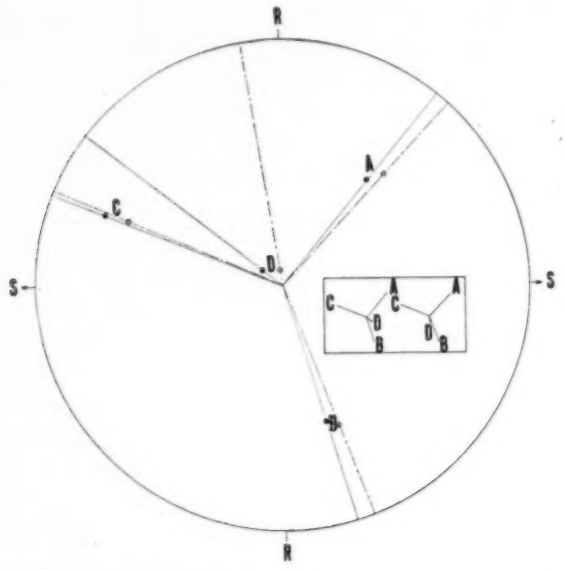


FIG. 2. Method of evaluating stereoscopic micrograph.

duction of the two stereoscopic images of a fourling. The equator of the projection is selected as the stereoscopic shift *SS*. The radial lines on the plot are the directions of the projected images of the legs of the fourling.† Solid lines correspond to the left-hand image, dot-dash lines, to the right-hand image. *The projected image direction on the stereographic plot is the locus of all possible directions in space, stereographically projected, which could have given rise to the micrographic image obtained. The location of the two needle directions on each pair of loci is found by the fact that they must be separated by 8° rotation about the normal to the stereoscopic shift as axis; this rotation axis on the plot is the axis RR.* The points of 8° separation are readily found with the small circles of the net. The circled points are the stereographic projections of the four legs of the fourling. The solid circles correspond to the left-hand image and the open circles to the right-hand image. The two sets are equivalent and either may be used to determine inter-needle angles.

The angles between the legs of the fourling may be determined by rotation of the plot on the stereographic net until the two points in question fall on the same great circle. The separation between the two may then be read directly from the small circles of the net. Thus each of the six angles *AB*,* *AC*, *AD*, *BC*, *BD*, and *CD* may be determined.**

The results of the inter-needle angle measurements are presented in Table I. Eight different

TABLE I. Results of inter-needle angle measurements.

| Fourling No. | Stereoscopic pair | Inter-needle angles—degrees | | | | | |
|---|---|---|---|---|---|---|---|
| 1 | *A* | 116.8 | 117.0 | 100.9 | | | |
| 2 | *A* | 121.2 | 116.1 | 113.2 | 110.5 | 98.0 | 95.4 |
| 3 | *A* | 117.9 | 114.8 | 95.7 | | | |
| 4 | *A* | 98.5 | | | | | |
| 5 | *B* | 99.5 | | | | | |
| 6 | *B* | 117.0 | 114.5 | 109.5 | 109.5 | 101.0 | 94.0 |
| 7 | *C* *D* | 120.7 | 117.5 | 115.0 | 114.0 | 97.8 | 95.5 |
| 8 | *C* *D* | 120.0 | 115.5 | 115.0 | 111.0 | 98.0 | 97.0 |

fourlings were measured on four different pairs of stereoscopic micrographs, yielding measurements of 32 inter-needle angles. Fourlings Nos. 7 and 8 were photographed on two pairs of micrographs, the two pairs differing from one another by a rotation of 45° about an axis normal to the plane of the specimen mount. In this manner accurate measurements were possible on all six angles. Six angles each were also measured on fourlings Nos. 2 and 6 but the validity of some of

† Note: The convention is adopted that if, when the micrographs are viewed stereoscopically, a needle appears to point above the horizontal, its radial line on the plot is drawn in the same sense as it appears on the micrograph. If the needle appears to point below the horizontal, the radial line on the plot is drawn in the opposite sense.

* The inter-needle angles in this paper are designated as *AB*, *AC*, etc., meaning the angles between leg *A* and leg *B*, leg *A* and leg *C*, etc.

** Note: Some practical difficulties preclude accurate determinations in some instances. If the needle is nearly parallel to the plane of the specimen mount or the projected image nearly parallel to the stereoscopic shift, little or no change in the direction of the projected image will be observed. If no change occurs, the spatial position of the leg cannot be determined. If only a small change occurs, particularly for directions near the stereoscopic shift, the spatial directions cannot be located accurately with the stereographic net and small errors in the protractor measurements on the micrograph have a seriously large effect. The net effect of this is that in general all six of the inter-needle angles on any one fourling cannot be determined from one pair of micrographs. If three legs can be located only three of the six angles are determinable; if two legs, one of the six angles is determinable. This difficulty was overcome in two instances by the following device. After taking one pair of micrographs, the specimen was rotated 45° about an axis perpendicular to the plane of the specimen and a second pair of micrographs was made. This made possible a determination of all six angles using the two pairs of micrographs.

the angles is in question because, taken at their face value, the angles are related to one another so that the symmetrical arrangement found for fourlings Nos. 7 and 8 (described in detail below) is not obtained. It is not possible to weight accurately the value of each angle. The angles fall into two groups, the one with an arithmetic mean of 97.6° and the other with an arithmetic mean of 115.3°. These values are tabulated in Table II in numerical order.

TABLE II.

| Small angle corresponding to two of the six angles | Large angle corresponding to four of the six angles |
|---|---|
| 94.0° | 109.5° |
| 95.4 | 109.5 |
| 95.5 | 110.5 |
| 95.7 | 111.0 |
| 97.0 | 113.2 |
| 97.8 | 114.0 |
| 98.0 | 114.5 |
| 98.0 | 114.8 |
| 98.5 | 115.0 |
| 99.5 | 115.0 |
| 100.9 | 115.0 |
| 101.0 | 115.5 |
| | 116.1 |
| | 116.8 |
| | 117.0 |
| | 117.0 |
| | 117.5 |
| | 117.9 |
| | 120.0 |
| | 120.7 |
| | 121.2 |

The values were plotted on arithmetic probability cross section paper in order to find the most probably correct value. The most probably correct values were found to be 97.7° and 115.7°.

There is a considerable spread in the measured values. Because they appear to fall into two groups it was assumed that there are two angular values and that variations from the mean were due to the combinations of measurement of the images on the micrograph and use of the method of the stereographic net. Of these two errors, the latter is quite variable and could well account for the spread of the measurements. In the succeeding section of the paper justification is advanced for the assumption that there are only two angular values.

## SPATIAL ARRANGEMENT OF THE FOURLING

A drawing of the fourling is shown in Fig. 3 in

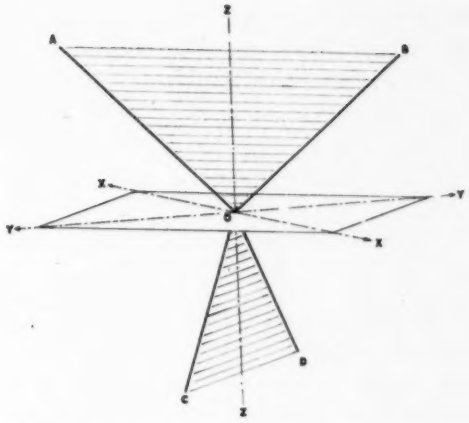


FIG. 3. Fourling of zinc oxide. *AO*, *BO*, *CO*, and *DO* are the four legs of the fourling. *XX* and *YY* are the twin axes.

clinographic projection. A stereographic projection of the fourling is shown in Fig. 4.

The features of this arrangement are as follows:

1. Corresponding legs of the fourling are labeled *A*, *B*, *C*, and *D* in the drawing and in the stereographic projection.

2. Angle *AB* = angle *CD* = 97.7°.

3. Angle *AC* = angle *AD* = angle *BC* = angle *BD* = 115.7°.

4. The plane formed by legs *A* and *B* is perpendicular to that of legs *C* and *D*.

The symmetry of this arrangement lends credence to the correctness of the measured angles. Assuming that angles *AB* and *CD* are equal and that the planes of *AB* and *CD* are mutually perpendicular, angles *AC*, *AD*, *BC*, and

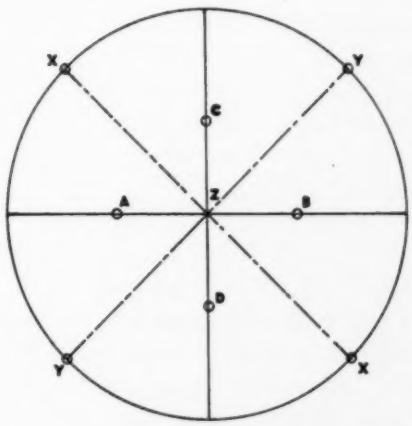


FIG. 4. Stereographic projection of fourling zinc oxide. *A*, *B*, *C*, and *D* are directions of the four legs. *XX* and *YY* are twin axes. Plane of projection is plane *XYXY* of Fig. 3.

*BD* are necessarily equal. If the two equal angles are 97.7° then the other four angles should be 116.0°. If the four equal angles are equal to 115.7° the other two angles should be 98.0°. The agreement of measured angles 97.7° and 115.7° with this symmetry is, therefore, excellent.

### TWINNING RELATIONSHIP

Twinning in crystals is a phenomenon, shown by a number of substances, in which two or more crystals are joined together as one unit in some definite fashion characteristic of the material. One twin is united to another symmetrically about a plane, the twin plane, which is a plane of the crystal lattice, usually of low Miller indices and/or about an axis which is an atom row in the lattice, usually one of the principal atom rows. The one twin may be derived from the other by a rotation of 180° in the twin plane or 180° about the twin axis or both.

An intensive search for a twinning relationship to satisfy the spatial arrangement found was made. Two possible twin axes were found (referring to Figs. 3 and 4) in the plane *XYXY*. This plane is perpendicular to the planes of *AB* and *CD*. The twin axes are *XX* and *YY*, at 90° to each other and at 45° to planes *AB* and *CD*. A rotation of 180° around *XX* will cause leg *D* to develop from leg *A* and leg *B* to develop from leg *C*. Rotation of 180° around *YY* will cause leg *C* to develop from leg *A* and leg *B* to develop from leg *D*. These twin axes are normal to crystal planes of the form (112) in the zinc oxide crystals. In zinc oxide with axial ratio 1.602 the (112) plane makes an angle of 58.03° with the basal plane or 31.97° with the principal or *C* axis. Twinning on (112) would thus give rise to an inter-needle angle of 116.06° in close agreement with the angle found of 115.7°.

It is to be noted that there is a fallacy in the hypothesis of (112) twinning which can only be accounted for by a small distortion in the structure at the juncture of the four legs. (This thought will be developed further in the next section of the paper.) The existence of the fallacy is described as follows. Rotation about twin axis *XX* causes leg *A* to develop into leg *D*; rotation about twin axis *YY* causes leg *A* to develop into leg *C*. The two twin planes involved are necessarily at 90° to each other, from the symmetry of Figs. 3 and 4. These two twin planes are common to leg *A*, however, and should therefore make an angle with each other consistent with the crystal structure of zinc oxide. The angle between these two planes of the form (112) in zinc oxide is 94°—not 90°.

It is of interest to note additional features of the symmetry of the fourling. By successive rotations of 90° about the axis *ZZ* (Fig. 3) each of the legs of the fourling may be reproduced successively from any one leg. For instance, rotations of 90, 180, and 270° cause leg *A* to develop successively into legs *C*, *B*, and *D*, respectively. The rotation axis *ZZ*, however, is not an important lattice direction in any of the legs, and the plane *XYXY* to which *ZZ* is perpendicular is not an important lattice plane in any of the legs. Another feature is the shape of the tetrahedron of which the normals to the four faces are the spatial directions of the four legs of the fourling. This tetrahedron is one having four equivalent isosceles triangles as faces. The length of the equal sides of each triangle is to the length of the third side as 0.91 is to 1.00.

Before the stereoscopic measurements had been made, it was expected that the fourling would be found to have the arrangement of the post and legs of a tripod music stand. The post would be the parent crystal to which the three legs would be related by twinning. Supposing the twinning to be of the (112) type then the three equal angles between the post and the legs would be 116°. The three equal angles between the legs would be 102°. The stereoscopic measurements, however, show that four of the angles are 116° and two are 98°.

### FORMATION OF THE FOURLING

The problem of why zinc oxide may form a fourling is not only one of crystal symmetry, but is also one of atomic arrangement. Zinc oxide is commonly thought of in terms of its hexagonal close-packed crystal symmetry. The fundamental thing about the zinc oxide structure is not its hexagonal crystal class, however, but more important is its atomic arrangement. Figure 5 is a drawing in clinographic projection of the atomic arrangement in the fundamental unit of zinc

oxide. Each atom of one kind is surrounded by a tetrahedron at the corners of which are atoms of the other kind. In a perfect crystal of zinc oxide of axial ratio 1.602, this tetrahedron is a triangular pyramid having an equilateral triangle *ABC* as base and three equivalent isosceles triangles *ABD*, *BCD*, and *ACD* as pyramidal faces. The ratio of the equal sides of the isosceles triangles to the side of the base triangle is as 0.989 is to 1.000.

The triangle at the base of the pyramid is the fundamental atomic grouping on the basal plane of the zinc oxide crystal. The triangles on the pyramid faces are so nearly equivalent to the base triangle that it seems entirely reasonable that a nucleus of a zinc oxide crystal might, under special conditions, elect to develop each of the sides of the tetrahedron as basal planes, thus producing a fourling. It is a fact of nature that regularly recurring forms of composite crystals obey the twinning law by having a twin axis or twin plane or both.

If the development of the fourling had taken place by the growth of needles perpendicular to the faces of a regular tetrahedron, all six inter-needle angles would be 109.5°. If needles developed normally to the faces of the triangular pyramid illustrated in Fig. 5, three of the angles would be a fraction of a degree less than 109.5° and three would be a fraction of a degree more than 109.5°. One or the other of these two arrangements is what might be expected from the standpoint of crystal growth alone. An examination of the crystal structure of zinc oxide, however, shows that there are no probable twinning mechanisms that would give rise to inter-needle angles close to 109.5°.

It appears, therefore, that the growth of the fourling took place with as high a tetrahedral symmetry as would be compatible with a twinning relationship among the four crystals. As pointed out in the foregoing section, however, a distortion must exist at the juncture of the legs of the fourling. Each leg is related to two other legs by (112) twinning. Each leg has two twinning planes. These twinning planes are 90° apart but in a perfect single crystal of zinc oxide the angle is 94°. This means that at the juncture and at the base of each leg there must be lattice distortion totaling 4° between the two twinning planes.

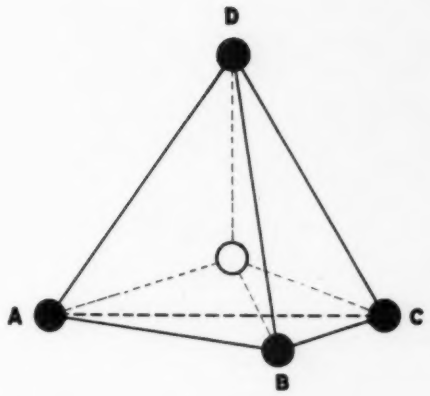


FIG. 5. Fundamental tetrahedral atomic grouping in zinc oxide.

Published information on twinning that has been studied has not reported a case of twinning in which a lattice distortion must be assumed. On the other hand, a case in which more than three differently oriented twins are united at one juncture has not been noted. Multiple twinning has been described but this has been a successive or chain type of twinning in which more than two crystals are connected but no more than two meet at one juncture. The existence of four crystals at one juncture imposes difficult requirements for undistorted conformity of the crystal lattices with one another.

The conclusion that the twinning plane is of the form (112) becomes more reasonable when it is noted that this is the plane of highest atomic population that could possibly serve as the twinning plane of zinc oxide. The relative atomic populations per unit area of the four most densely populated planes are given in Table III. Rotation of 180° on (110), (100), or (001) would give rise to

TABLE III.

| Plane *hkl* | Relative atomic population per unit area | Kind of atoms |
|---|---|---|
| 110 (prism) | 1.000 | Equal proportions zinc and oxygen |
| 100 (prism) | 0.866 | Equal proportions zinc and oxygen |
| 001 (basal) | 0.800 | All zinc or all oxygen |
| 112 (pyramid) | 0.425 | All zinc or all oxygen |

a crystal with crystal axes identical with the original and could not, therefore, possibly account for the fourling type of composite crystal. The plane (112) is the most important and most densely populated plane that could possibly act as the twinning plane.


### SUMMARY

Twinning has been observed in crystals of pigment zinc oxide. With the aid of stereoscopic electron microscopy and the graphical method of the crystallographer's stereographic projection, the spatial arrangement of the components of the twinned crystal has been determined. The arrangement found is explained on the basis of twinning on the (112) plane of the crystal lattice.



### ACKNOWLEDGMENT

The writer appreciates the assistance of Mr. H. M. Cyr and Dr. C. W. Siller in preparing the zinc oxide, and of Dr. D. G. Brubaker and Mr. R. W. Berger in the electron microscopy.


---

# The Impedance of Short, Long, and Capacitively Loaded Antennas with a Critical Discussion of the Antenna Problem


RONOLD KING AND CHARLES W. HARRISON, JR.

*Cruft Laboratory and the Research Laboratory of Physics, Harvard University, Cambridge, Massachusetts*



(Received November 8, 1943)



In Part I curves computed from Hallén's formula for the self-impedance of a center-driven antenna of half-length $h$ and radius $a$ are given for $\Omega=2\ln(2h/a)=7$, 10, 20, 30 for values of $h$ from zero to two wave-lengths. A simple formula for the impedance of short antennas is obtained; the reactance is shown to agree with that computed from the static capacitance between the two halves of the antenna. The effect of a capacitive reactance connected across the input terminals of the antenna is investigated. It is shown that the resistance at anti-resonance is reduced, the capacitive lobes of the curve for reactance relatively increased, the inductive lobes relatively very much decreased, and curves for both resistance and reactance shifted to shorter lengths. In Part II the differences between various methods used by different investigators to compute the impedance of an antenna are examined critically. It is concluded that Hallén's formula probably is a better approximation for an antenna consisting of two sufficiently thin ellipsoids each of semi-minor axis **a** placed end to end than for cylinders, but that cylindrical antennas driven in various ways can be approximated by using an effective value of $h/a$ and a suitably chosen capacitance across the input terminals.


THIS paper consists of two parts. Of these the first extends and supplements the data computed from Hallén's formula[1,2] for the self-impedance of a symmetrical, center-driven antenna and represented graphically in an earlier paper.[3] The second part is a critical discussion of formulas for the self-impedance of antennas obtained in different ways by a number of investigators including Hallén.

## PART I

### Impedance Data

Hallén's formula for the impedance of an isolated, symmetrical, center-driven antenna of half-length $h$ and radius $a$ is

$$Z_0=-j60\Omega\left\{\frac{\cos H+\alpha_1/\Omega+\alpha_2/\Omega^2+\cdots}{\sin H+\beta_1/\Omega+\beta_2/\Omega^2+\cdots}\right\}. \quad (1)$$

The following symbols are used:

$$H=\beta h=2\pi h/\lambda;\quad \Omega=2\ln(2h/a). \quad (2)$$

$\Omega$ is shown in Fig. 1 as a function of $h/a$.

$$\alpha_1=\alpha_1^{\mathrm{I}}+j\alpha_1^{\mathrm{II}}+jhr_a z^i/30, \quad (3)$$

$$\beta_1=\beta_1^{\mathrm{I}}+j\beta_1^{\mathrm{II}}+jhr_\beta z^i/30. \quad (4)$$

The real functions $\alpha_1^{\mathrm{I}}$, $\alpha_1^{\mathrm{II}}$, $\beta_1^{\mathrm{I}}$, and $\beta_1^{\mathrm{II}}$ are given in Figs. 2a, b for a range of $H$ extending to 14.

[1] E. Hallén, Nova Acta Uppsala [4] **11**, 1 (1938).
[2] R. King and C. W. Harrison, Jr., Proc. I. R. E. **31** (October, 1943).
[3] R. King and F. G. Blake, Jr., Proc. I. R. E. **30**, 335 (1942).

Their analytical form is

$$\alpha_1^{I}=(1/2)[\cos H(\text{Cin } 4H-2\text{ Cin } 2H) -\sin H\text{ Si } 4H], \quad (5)$$

$$\alpha_1^{II}=(1/2)[\cos H(\text{Si } 4H-2\text{ Si } 2H) +\sin H\text{ Cin } 4H], \quad (6)$$

$$\beta_1^{I}=(1/2)[\cos H(4\text{ Si } 2H-\text{Si } 4H) +\sin H(2\text{ Cin } 2H-\text{Cin } 4H+4\ln 2)], \quad (7)$$

$$\beta_1^{II}=(1/2)[\cos H(\text{Cin } 4H-4\text{ Cin } 2H) +\sin H(2\text{ Si } 2H-\text{Si } 4H)], \quad (8)$$

where

$$\text{Si } x=\int_0^x \sin u/u\,du=x-\frac{1}{3}\frac{x^3}{3!}+\frac{1}{5}\frac{x^5}{5!}-\cdots, \quad (9)$$

$$\text{Ci } x=-\int_x^\infty \cos u/u\,du =0.5772+\tfrac{1}{4}\ln x^4-\text{Cin } x, \quad (10)$$

$$\text{Cin } x=\int_0^x (1-\cos u)/u\,du =\frac{1}{2}\frac{x^2}{2!}-\frac{1}{4}\frac{x^4}{4!}+\cdots. \quad (11)$$

The real functions $r_\alpha$ and $r_\beta$ are

$$r_\alpha=(1/2)\sin H-\cos H(1-\cos H)/H, \quad (12)$$

$$r_\beta=(\sin 2H-\sin H)/2H-(1/2)\cos H. \quad (13)$$

The internal impedance $z^i=r^i+jx^i$ of a conductor of conductivity $\sigma$(1/ohm-m), relative permeability $\mu$, and radius $a(m)$ is

$$z^i(\text{ohms/m})=\frac{(1+j)}{2\pi a}\left(\frac{\omega\mu\mu_0}{2\sigma}\right)^{\frac{1}{2}}; \quad (14)$$

$$\mu_0=4\pi\times10^{-7}\text{ henry/m}.$$

For copper conductors the terms in $z^i$ contribute a negligible amount to the functions $\alpha_1$ and $\beta_1$. They have been neglected in computing the curves shown in this paper.

The complex functions $\alpha_2$, $\beta_2$, etc., cannot be expressed in terms of known functions. They are given in complete form by Hallén[1] and can be evaluated by graphical or numerical methods in specific cases. In calculating from (1) terms involving higher powers of $1/\Omega$ than the first have been neglected. It is assumed that this is equivalent to requiring

$$(\Omega^2)^{-1}\ll 1. \quad (15)$$

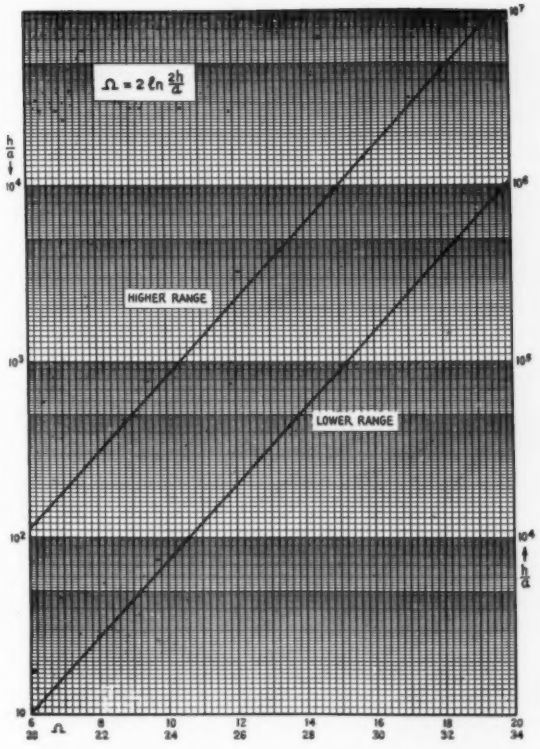


FIG. 1. The parameter $\Omega=2\ln(2h/a)$ as a function of $h/a$.

In Fig. 3 computed values of the resistance $R_0$ in $Z_0=R_0+jX_0$ are plotted on a semi-logarithmic scale as a function of $H$ with $\Omega$ as parameter. Figure 4 shows the corresponding values of $X_0$. Values of $X_0$ near resonance ($H$ near $\pi/2$), and anti-resonance ($H$ near $\pi$) which cannot be shown in a logarithmic scale, are plotted in Figs. 5 and 6. In Figs. 7 and 8, $R_0$ and $X_0$ from Figs. 3 and 4, respectively, are plotted as functions of $\Omega$ with $H$ as parameter.

The first resonant half-length of an infinitely thin antenna occurs with $H=\pi/2$. For antennas of non-vanishing radius resonance occurs for values of $H$ less than $\pi/2$. Let these be denoted by $H_R$. The difference $\pi/2-H_R$ is plotted in solid line in Fig. 9 as a function of $\Omega$. The first resonant radius of a conducting sphere[4] is

$$a=\lambda/7.3. \quad (16)$$

If it is assumed that a sphere corresponds to an antenna with $h=a$, and $\Omega=2\ln 2=1.386$, then

[4] J. A. Shatton, *Electromagnetic Theory* (McGraw-Hill Book Company, New York, 1941), p. 558.

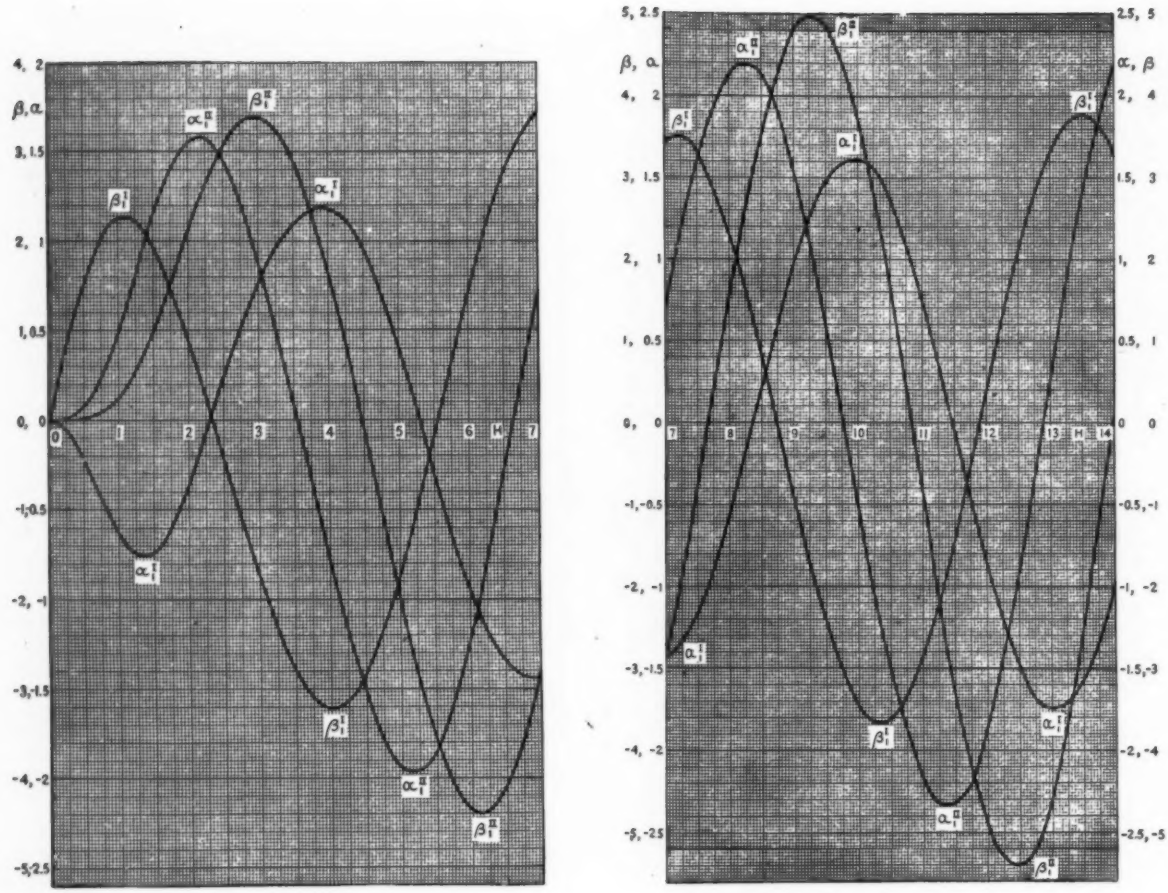

a b

FIG. 2a, b. The parameters $\alpha_1^{I}$, $\alpha_1^{II}$, $\beta_1^{II}$, $\beta_1^{II}$ as a function of $H=2\pi h/\lambda$.

$H_R=2\pi h_R/\lambda=0.86$ and $\pi/2-H_R=0.71$. This point is plotted in Fig. 9 and the curve computed from Hallén's formula is extrapolated to it in broken line. The resistance $R_0$ for the resonant lengths obtained from Fig. 9 is plotted in Fig. 10 as a function of $\Omega$. An approximate value of radiation resistance computed for a sphere[5] is also shown and the curve is extrapolated to it.

### The Short Antenna

Hallén's formula (1) may be simplified for short antennas which permit writing

$$H^2 \ll 1. \tag{17}$$

Subject to (17) the trigonometric and integral functions in (5)–(8) may be expanded in series and only the leading terms retained. In this way

$$\alpha_1^{I} \doteq -H^2; \qquad \alpha_1^{II} \doteq 2H^3/3; \tag{18a}$$

$$\beta_1^{I} \doteq 2H(1+\ln 2)=3.386H; \quad \beta_1^{II} \doteq H^4/3; \tag{18b}$$

$$Z_0=-j60\Omega\left[\frac{1+j2H^3/3\Omega}{H\left(1+\dfrac{3.386}{\Omega}\right)+jH^4/3\Omega}\right]. \tag{19}$$

Neglecting terms in $1/\Omega^2$ and retaining only the leading terms in $H$ according to (17), (19) gives

$$R_0 \doteq 20H^2, \tag{20}$$

$$X_0 \doteq -\frac{60\Omega}{H\left(1+\dfrac{3.386}{\Omega}\right)}. \tag{21}$$

[5] E. B. Moullin, J. Inst. Elec. Eng. Part III, **88**, 50 (1941). The radiation resistance of a cylinder is also computed, but since an axially sinusoidal current is assumed the result is almost meaningless for thick cylinders.

Since (20) does not contain $\Omega$, the resistance $R_0$ for antennas which are short and not too thick is independent of thickness. It is equal to the resistance of an infinitely thin antenna as computed more conventionally by the Poynting vector method. It is plotted in Fig. 11.

The static capacitance between two cylinders of radius $a$ placed end to end and separated a negligible distance in air compared with their individual lengths $h$ is[6]

$$C_s=\frac{2\pi\epsilon_0 h}{2\ln\frac{2h}{a}-\ln 12}=\frac{2\pi\epsilon_0 h}{\Omega\left(1-\frac{2.485}{\Omega}\right)}, \quad (22)$$

where $\epsilon_0=8.859\times10^{-12}$ farad/m. It is well to note that (22) (as all other capacitances calculated for static conditions) is of physical significance only if the condition of uniform distribution of charge which is assumed in deriving (22) obtains. This is true to a good approximation if (17) is satisfied. The reactance corresponding to

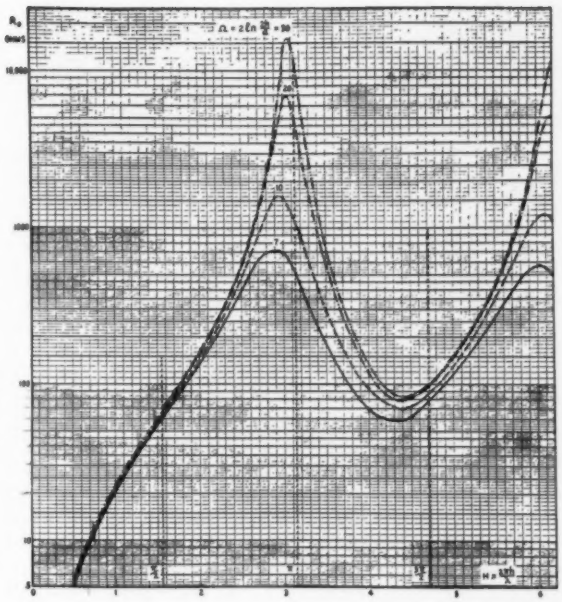

FIG. 3. Input resistance $R_0$ of center-driven antenna as a function of $H=2\pi h/\lambda$ for $\Omega=7$, 10, 20, 30.

[6] K. Küpfmüller, *Einführung in die theoretische Elektrotecknik* (Julius Springer, Berlin, 1932), p. 66.

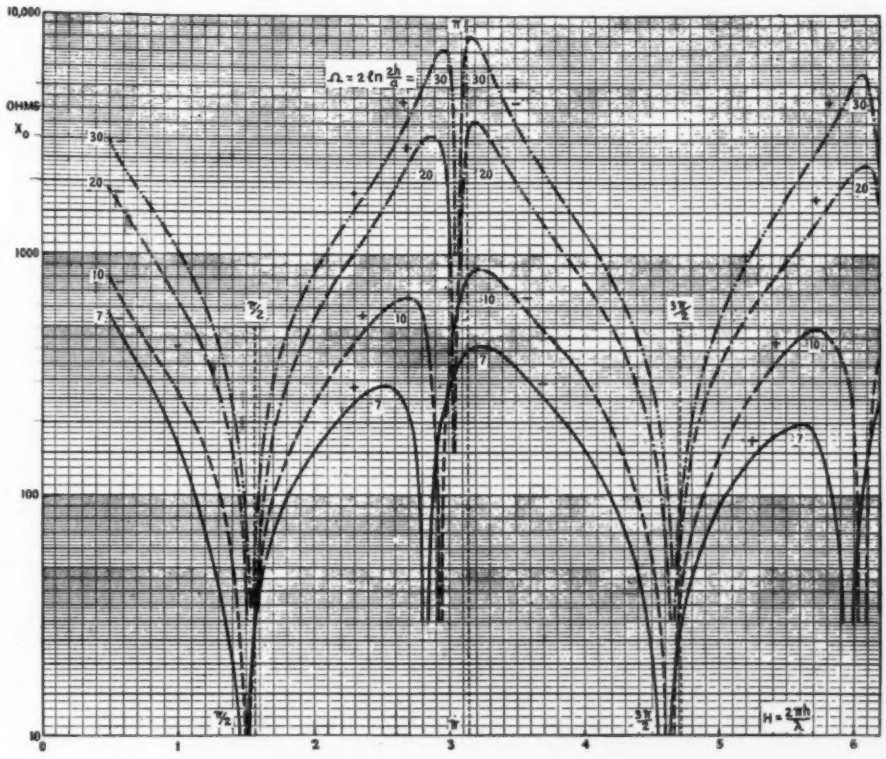

FIG. 4. Input reactance $X_0$ corresponding to $R_0$ in Fig. 3.

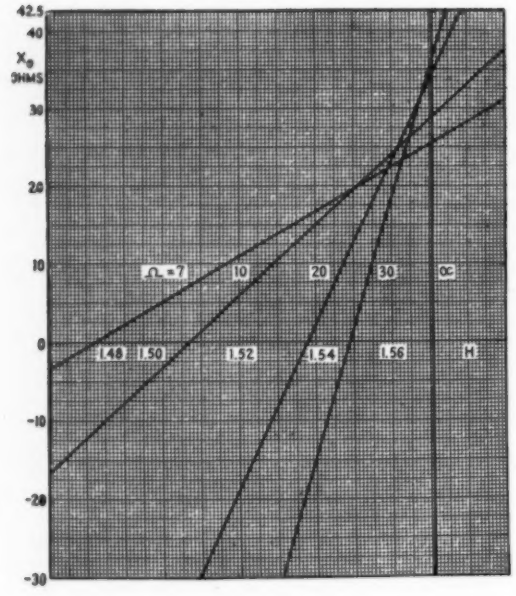


FIG. 5. Input reactance $X_0$ near first resonance.

(22) is

$$X_e = -\frac{1}{\omega C_e} = -\frac{60\Omega}{H}\left(1-\frac{2.485}{\Omega}\right). \qquad (23)$$

The "static" formula (23) differs by a negligible amount from (21) for the range (17) when both are good approximations. They are exactly equal when $\Omega=\infty$ or $\Omega=9.35$. The value of $X_0$ as computed from (1) is plotted in Fig. 12 together with points calculated from (21) and (23). It is clear that (21) and (23) are good approximations of (1) if (15) is satisfied and (17) is understood to mean

$$H \leqq 0.5 \qquad (24a)$$

or, approximately,

$$h/\lambda \leqq 0.08. \qquad (24b)$$

### The Long Antenna

Since (1) involves no restriction on the length of the antenna, it may be used to compute the impedance of long antennas as well as of short ones. In Figs. 13–16 the resistance and reactance for four different ratios $h/a$ are plotted for antenna half-lengths exceeding two full wavelengths so that four anti-resonances are represented. The maximum values of resistance and the extreme values of reactance are given in Fig. 17 as functions of $\Omega=2\ln(2h/a)$ for all four anti-resonances, numbered 1–4. It is interesting to note that the minimum (capacitive) reactance decreases more slowly than the maximum (inductive) reactance as the antenna is made relatively thicker. This effect is more pronounced the longer the antenna. The relative increase in the size of the capacitive lobes as compared with the inductive lobes of the reactance curves for thicker and longer antennas is seen in Figs. 13–16.

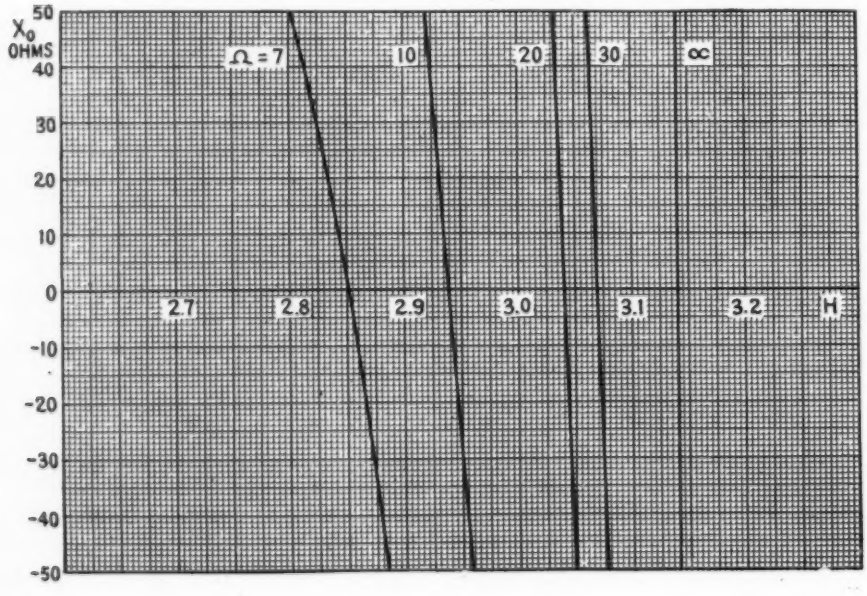


FIG. 6. Input reactance $X_0$ near first anti-resonance.

### Capacitive Loading at the Input Terminals

In practical methods of driving antennas a capacitive reactance across the terminals is often difficult to avoid, so that a study of its effect is important. The equivalent resistance $R_0'$ and reactance $X_0'$ of an impedance $Z_0=R_0+jX_0$ in parallel with a capacitive reactance $(-1/\omega C)$ are

$$R_0'=\frac{R_0}{1-2\omega CX_0+\omega^2C^2(R_0^2+X_0^2)}, \quad (25)$$

$$X_0'=\frac{X_0-C(R_0^2+X_0^2)}{1-2\omega CX_0+\omega^2C^2(R_0^2+X_0^2)}. \quad (26)$$

If the ratio $h/a$ of an antenna is constant and the frequency is varied, it is convenient to express $C$ as a fraction of the static capacitance $C_s$ between the two halves of the antenna as defined in (22). A parallel capacitance $C$ across the input terminals can be written in the form

$$C=k'C_s=kh \quad (27)$$

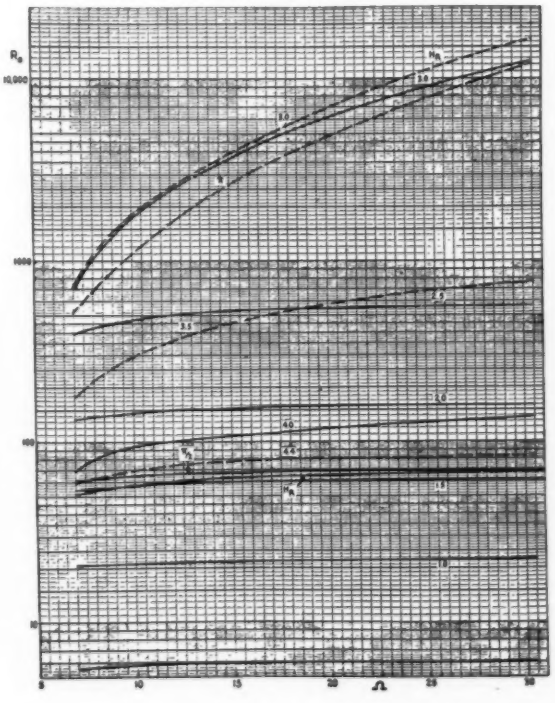

FIG. 7. Input resistance $R_0$ of center-driven antenna as a function of $\Omega=2\ln(2h/a)$ for several values of $H=2\pi h/\lambda$. The curves marked $H_R$ apply to antennas which are kept adjusted to resonance (lower curve) or anti-resonance (upper curve) as $\Omega$ is varied.

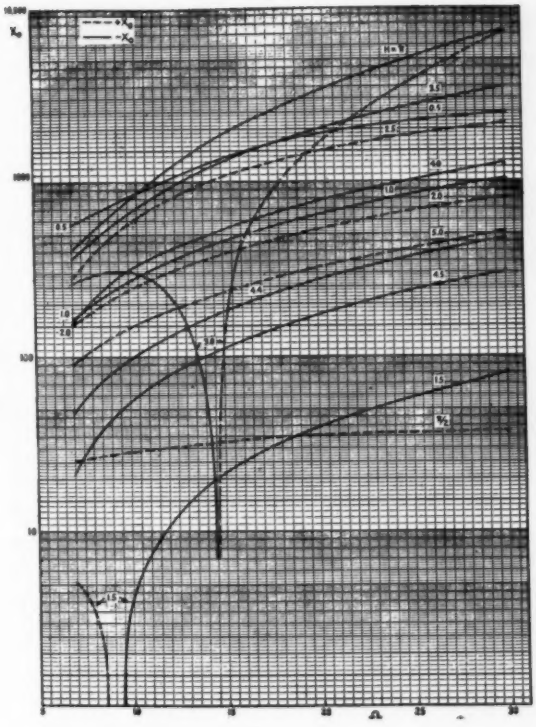

FIG. 8. Input reactance $X_0$ corresponding to $R_0$ in Fig. 5.

with $k'$ a constant and

$$k=\frac{2\pi\epsilon_0k'}{\Omega\left(1-\frac{2.48}{\Omega}\right)}. \quad (28)$$

For any given values of $h$ and $h/a$, $k$ is constant.

The resistance and reactance of an antenna with fixed but arbitrary half-length $h$(meters), with $\Omega=2\ln(2h/a)=10$, and with a fixed capacitance $C=1.035h$ $\mu\mu$f across its input terminals are shown in Fig. 18 as $f=\omega/2\pi$ and hence $H=\omega h/c(c=3\times10^8$ m/sec.) are varied. Figure 19 is like Fig. 18 but with $C$ doubled. Comparison of Figs. 15, 18, 19 which apply to the same antenna with $C=0$, $1.035h$ $\mu\mu$f, $2.07h$ $\mu\mu$f shows that a capacitance across the terminals of an antenna reduces the maximum values of resistance at anti-resonance; decreases the resonant and anti-resonant lengths at which $X_0'=0$; enlarges the capacitive lobes of the reactance curve and decreases the inductive lobes so that with moderately long antennas the reactance may even become entirely capacitive. Depending on

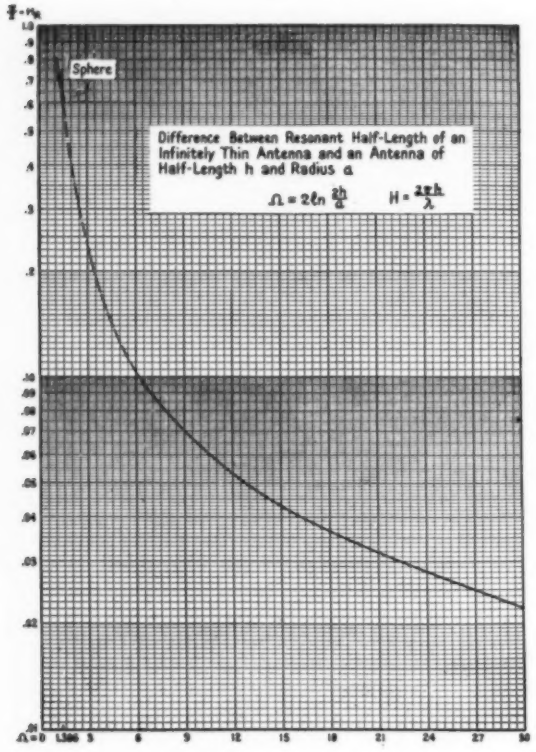
Sphere
Difference Between Resonant Half-Length of an Infinitely Thin Antenna and an Antenna of Half-Length h and Radius a
Ω = 2ℓn 2h/a
H = 2πh/λ

FIG. 9. Difference between resonant angular half-length $\pi/2$ of an infinitely thin antenna and an antenna of angular half-length $H_R$ and radius $a$. $\Omega=2\ln(2h/a)$; $H=2\pi h/\lambda$.

the size of the capacitance connected across the terminals these effects may be small, or they may be very large.

## PART II

A meaningful comparison of theoretical results with experimental measurements involves much more than a mere plotting of experimental points along a theoretically derived curve. Two questions must always be studied with care: What has been calculated? What has been measured? Theory often solves a different problem from that originally formulated, and this fact is at times well concealed in both the symbolism and the accompanying text. Experimental arrangements frequently differ considerably from the ideal they are assumed to represent, sometimes because the effect of the measuring instruments is significant. This is especially true in the field of antennas where both theory and experiment are faced with great difficulties.

### Antenna Theory

The distribution of current in an antenna and the determination from it of the impedance between two specified terminals is a boundary value problem in general electrodynamics. There are many ways by which analysis may proceed, but according to the uniqueness theorm[7] there is only one electromagnetically correct solution for each antenna as defined in terms of a definite set of boundary conditions. Conversely, a solution once obtained can apply to only one set of boundary conditions. Since the several available theoretical formulas for the impedance of a cylindrical antenna differ, one must conclude either that they are not all electromagnetically correct, or that they do not actually apply to the antenna in question. It is instructive to examine them in turn.

#### *Method 1*

Siegel and Labus[8] and later Wells[9,10] have obtained formulas for the input impedance of a *section of two-wire transmission line* of length $h$, with an open end, and with an attenuation constant so adjusted that the energy dissipated in heating the conductors of the line is equal to the energy radiated from a perfectly conducting center-driven antenna of half-length $h$ and vanishingly small radius, as determined by integrating the normal component of the Poynting vector over a surface enclosing the antenna. Since such a transmission line is electromagnetically possible, the formula is physically meaningful and actually the correct solution for the section of line. According to the theorem of uniqueness the same formula cannot be correct for a center-driven antenna of half-length $h$ because the boundary conditions for antenna and line are entirely different. However, even though not the correct solution for the antenna, the transmission-line formula with properly chosen attenuation constant may approximate the impedance of the antenna over a limited range. By further adjustments the degree of approximation may be in-

[7] A. Rubinowicz, Physik. Zeits. **27**, 707 (1926).
[8] E. Siegel and J. Labus, Hoch:tech. u. Elek:akus. **43**, 166 (1934).
[9] N. Wells, J. Inst. Elec. Eng. Part III, **89**, 76 (1941).
[10] N. Wells, J. Inst. Elec. Eng. Part III, **90**, 24 (1941).

creased[11] and the formula may be of *practical value as an engineering formula for antennas* within a specified range. It has no *physical significance* in antenna theory because, after all, a transmission line made of resistance wire is not an antenna. If the attempt is made, nevertheless, to attach physical significance *in antenna theory* to a formula that is correct for a transmission line, the inevitable result is an electromagnetic monstrosity. An example is an explanation of the formula of Siegel and Labus in terms of a non-radiating antenna with a series resistance that dissipates in heat the energy that would be radiated by the antenna if it did radiate, if it carried a sinusoidal current, and if it obeyed transmission-line theory. Such an "antenna" is not only fictitious, it is electromagnetically impossible and physically meaningless. The results of Siegel and Labus and of Wells do not approximate an antenna by a transmission line in a physical sense. They show that a suitably designed transmission line may have an input impedance, but not necessarily any other quality, that resembles that of an antenna. The approximation is a mathematical one in terms of formulas, not a physical one in terms of structure or theory.

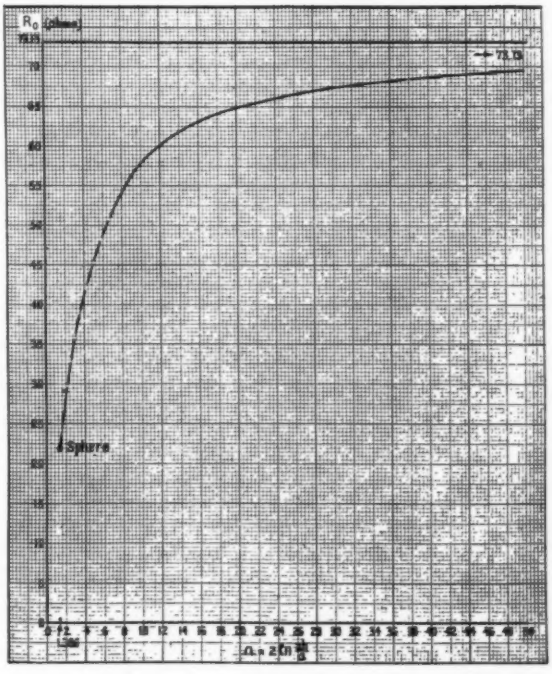


FIG. 10. Radiation resistance of a resonant antenna (solid line) extrapolated (broken line) to an approximate radiation resistance for a sphere.

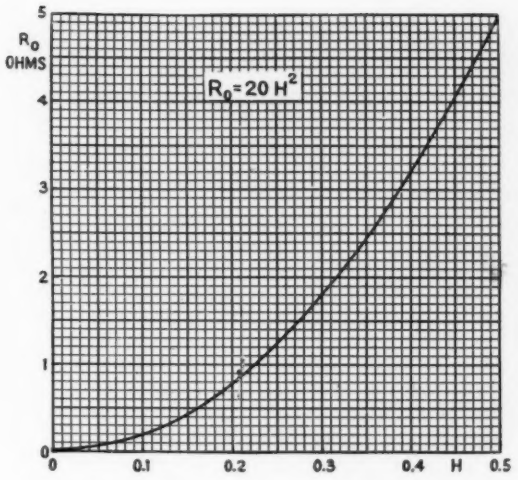


FIG. 11. Resistance of short antenna as a function of $H=2\pi h/\lambda$.

*Method 2*

Schelkunoff[12] has devised a formula that is both more flexible and more intricate than that of Siegel and Labus or of Wells. Specifically it gives the input impedance of a *terminated* section of transmission line with both characteristic impedance and output impedance so adjusted that the input impedance of a symmetrical, center-driven antenna of a variety of shapes may be approximated. The characteristic impedance of the "equivalent" line is defined by $(l/c)^{\frac{1}{2}}$ in terms of a capacitance $c$ per unit length equal to the static capacitance per unit length between the halves of the antenna, and an inductance per unit length defined by $l=1/cv^2$ with $v=3\times10^8/(\mu\epsilon)^{\frac{1}{2}}$ meters/sec. If the shape of the antenna is such that $c$ and $l$ are not independent of the distance from the center of the antenna the *average* value of $(l/c)^{\frac{1}{2}}$ over the half-length is used. The output impedance is defined in such a way that (a) the energy dissipated as heat in its resistive part is equal to the power radiated from the antenna, (b) the distribution of current along the "equivalent" line is such that its input value *approxi-*

[11] S. A. Schelkunoff, J. App. Phys. **15**, 54 (1944).

[12] S. A. Schelkunoff, Proc. I. R. E. **29**, 493 (1941).

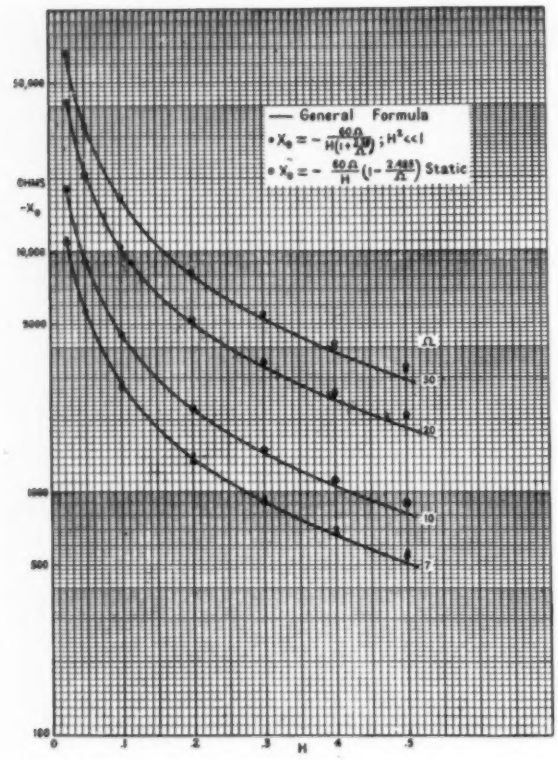


FIG. 12. Reactance of short antenna computed from Hallén's formula (1) (solid line). Points represented by black dots are computed from the approximate formula (21), circles from (23) using the static capacitance.

*mates* the input value of the current in the actual distribution in the antenna. The distribution in the antenna is one for which the components of the electric field tangent to the surface of the perfectly conducting antenna must vanish. The evaluation of the "radiation" output impedance to satisfy these conditions is based on an expansion of the electromagnetic field in a series of characteristic wave functions adjusted to the shape of the antenna, except that its end surfaces are neglected. The field is matched at an arbitrarily introduced sphere of diameter equal to the length of the antenna. This method for evaluating the output impedances is intricate but powerful, so that good approximations should be possible.

Since the input impedance in the words of Schelkunoff[12] is "obtained from the usual transmission line equations" it must be concluded that it gives strictly and accurately the impedance of a section of transmission line with specified characteristic impedance and load as stated above. If the uniqueness theorem is applicable, it cannot also be the input impedance of an antenna which has quite different boundary conditions from the line. On the other hand it may approximate this very closely over a considerable range because three adjustable parameters are provided, *viz.*, the characteristic impedance of the line, and its output resistance and reactance.

From the physical point of view it seems unfortunate that a section of transmission line, even though skillfully adjusted to approximate the impedance of an antenna, should be *identified* with that antenna. Line and antenna are fundamentally different from the electromagnetic point of view, and the mere fact that they have approximately the same input impedance over a limited range does not make them identical or even equivalent in any general sense. Thus, the antenna has no output terminals; its input impedance does not become equal to the characteristic impedance of the "equivalent" line as the length of the antenna is increased without limit; it is not possible to load the antenna so that its input impedance becomes equal to the characteristic impedance of the line. Furthermore, the voltage difference used in transmission-line theory is a true scalar potential difference independent of a path of integration, and it can be measured on a voltmeter; whereas the "voltage difference" used for antennas is not a scalar potential difference at all, can be evaluated only by integrating along a definite contour, and is experimentally meaningless. The characteristic impedance of the "equivalent" line is physically meaningful for the antenna only subject to (17) when the antenna is sufficiently short that charge is distributed uniformly along it, and a scalar potential difference may be used *both* in defining capacitance and voltage difference. It would seem that output impedances, characteristic impedances, and potential differences (except at the input terminals) are as foreign to the theory of antennas as is radiation to the conventional theory of lines. Surely, from the general point of view of electromagnetism, a two-wire line is a special form of antenna in which equal and opposite currents close together provide a cancellation of effects. On the other hand it is difficult to see how an antenna is in any physical sense a special form of two-wire line.

*Method 3*

Bohm (in an analysis outline by Wells[9,10]) has analyzed the symmetrical center-driven antenna by calculating the tangential field which would exist at the surface of the antenna if a current $i_0$ were distributed sinusoidally, and then determines an additional current $i_w$ necessary to reduce this field to zero as a first step in a method of successive approximations of which only the first term is derived. The *resultant current is required to satisfy the conventional transmission-line equations* in which the potential difference is assumed to be modified just as though the antenna current flowed on a transmission line. In carrying out the solution it is assumed that only that component of $i_w$ which is in phase-quadrature with $i_0$ is significant, and curves for the input impedance are computed neglecting the component of $i_w$ in phase with $i_0$. The fact that with this approximation Bohm's formula leads directly to the classical formula of Van der Pol[13] for the radiation resistance of an *infinitely thin* antenna, suggests that the approximation neglecting the component of $i_w$ in phase with $i_0$ may not be justified for antennas of non-vanishing radius. The impedance curves rise to the same high values as those of Wells[10] calculated from the formula of Method I in which radiation was actually calculated for an infinitely thin antenna. If the neglected terms were included, Bohm's analysis should give a better approximation for antennas with non-vanishing radius, although higher order terms might also be required. In describing Bohm's method Wells does not specify how the values of $l$ and $c$ used in defining the characteristic impedance of the "equivalent" line are defined. A possible method differing somewhat from Schelkunoff's is to use (22) in the form

$$c=\frac{C_e}{h}=\frac{2\pi\epsilon_0}{\Omega\left(1-\dfrac{2.485}{\Omega}\right)} \tag{29}$$

and

$$l=\frac{1}{cv^2}=\frac{\mu_0\Omega\left(1-\dfrac{2.485}{\Omega}\right)}{2\pi}, \tag{30}$$

[13] B. Van der Pol, Proc. Phys. Soc. **29**, 269 (1917)

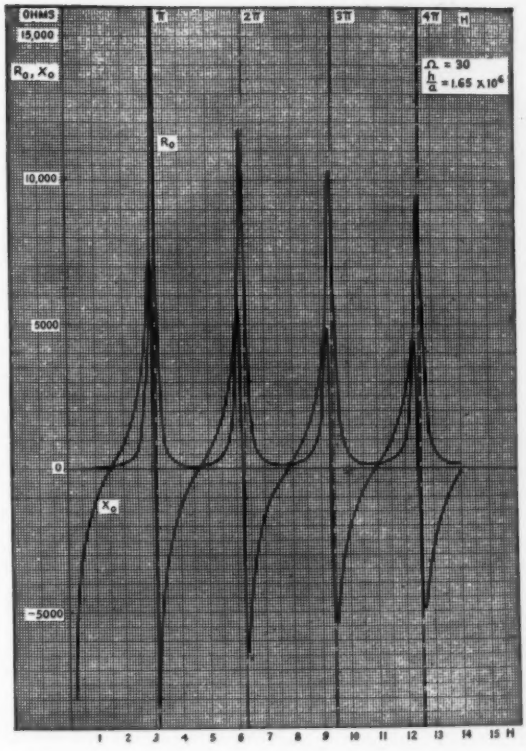


FIG. 13. Resistance and reactance of extremely thin antenna, $h/a=1.65\times10^6$.

so that

$$R_c=\left(\frac{l}{c}\right)^{\frac{1}{2}}=\frac{1}{2\pi}\left(\frac{\mu_0}{\epsilon_0}\right)^{\frac{1}{2}}\Omega\left(1-\frac{2.485}{\Omega}\right)$$

$$=60\Omega\left(1-\frac{2.485}{\Omega}\right). \tag{31}$$

For $\Omega$ sufficiently large, one can write

$$R_c=60\Omega. \tag{32}$$

Formulas (29) and (31) have physical significance only for an antenna that satisfies (17) so that the distribution of charge is essentially uniform. Either (31), (32), or any other value of $R_c$ may be used in a transmission line formula, preference being given to the one which yields an impedance formula that best approximates the antenna in question.

*Method 4*

L. V. King[14] has derived a formula for the input impedance of a base-driven perfectly conducting

[14] L. V. King, Phil. Trans. Roy. Soc. London **A236**, 381 (1937).

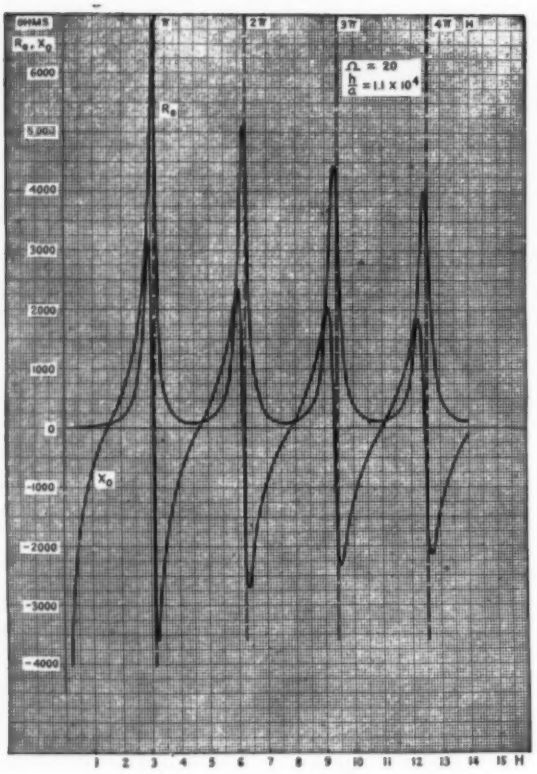


FIG. 14. Resistance and reactance of very thin antenna, $h/a = 1.1 \times 10^4$.

cylindrical antenna of length $h$ erected vertically over a perfectly conducting plane. From the theorem of images the impedance so determined is one-half of that for an isolated center-driven antenna. King's method resembles Bohm's in that the additional electric field, which is required to reduce to zero the tangential field due to an assumed *sinusoidally* distributed current, is obtained. Unlike Bohm's method the resultant current is not required to obey the transmission-line equations. King obtains an integral equation in the electric field which he solves approximately in terms of the parameter $\ln(2h/a) = \Omega/2$. The formula derived for the input impedance is made to depend upon the assumption that for antennas for which $0 < 2\pi h/\lambda < 4$ it is legitimate to replace the electric field along the mid-plane due to the actual current by the field due to a sinusoidal current, i.e., due to an infinitely thin antenna. The effect of this assumption appears to be similar to that in Bohm's analysis where the component of added current $i_w$ in phase with the sinusoidal current $i_0$ is neglected. In both analyses part of the effect of the thickness of the antenna on the impedance is disregarded in this way. It may be because of this that the computed impedances are so much higher than those obtained from Hallén's formula. Unlike methods 1–3, L. V. King does not introduce line theory at all. However, since King's formula even if corrected to take complete account of thickness would remain approximate for mathematical reasons, it might still be less accurate than a transmission-line formula for lengths for which the latter is a good approximation unless higher order terms were used.

### *Method 5*

In deriving (1) Hallén[1] obtains an integral equation for the current in a rotationally symmetrical antenna and solves this for the current by a method of successive approximations using the parameter $\Omega = 2 \ln(2h/a)$. The integral equation involves only the axial variable, and approximations are made or implied in the representation both at the driving point and at the ends of the center-driven antenna when this is assumed to be a cylinder a degree of vagueness exists as pointed out by Schelkunoff.[11] (A similar uncertainty apparently exists in Schelkunoff's evaluation of the "radiation" output impedance for the "equivalent" line in terms of a conical antenna since no account is taken of the base surfaces of the cones. When application is made to the cylinder neither the driving point nor the end faces are clearly defined or taken into account. But since the entire calculation serves to define an output impedance in an "equivalent" line and not directly the input impedance of an antenna this uncertainty does not appear in the formula for the impedance of the "equivalent" line but is involved in the degree of approximation achieved.) Since Hallén's analysis seeks to solve a boundary-value problem rather than construct an "equivalent" transmission line, it has a physical meaning in terms of the physical structure actually represented. According to the uniqueness theorem it is the solution of a particular set of boundary conditions *for an antenna*, just as Schelkunoff's or Siegel and Labus' formula is the correct electromagnetic solution for a specified transmission line. Analyses involving cylinders lead to mathematical discontinuities

and the approximations made in Hallén's analysis at the driving point and at the ends of the antenna evidently serve to avoid these and permit a mathematical solution with no infinities. It is reasonable to suppose, therefore, that the solution for the current appearing in Hallén's solution is more nearly correct for a shape with rounded ends than for the sharp-edged cylinder with its flat ends. This could be determined by calculating the electric field due to the distribution of current[1,2] given by Hallén's formula, if necessary including terms of order higher than $1/\Omega$, and from this determining the shape of a contour perpendicular to the field. Since such a determination has not been carried out, and in view of the fact that (21) for the reactance of a short antenna differs only slightly from (23) for the same reactance obtained from the static capacitance, the shape of the antenna may be obtained at least approximately by noting what shape is implied by (22) for the static capacitance. Study of the approximations involved in the derivation of (22) discloses that in specifying the potential difference between the two halves of the antenna *each* cylinder is actually replaced by an ellipsoid of revolution with semi-minor axis $a$. The cylinders and the ellipsoids (solid line) are shown in Fig. 20. It seems reasonable to suppose, therefore, that Hallén's formula applies more nearly to two ellipsoids placed end-to-end and driven by a point generator between them rather than to two cylinders. Such a conclusion is reasonable from the electromathematical point of view. Furthermore, the lack of agreement with Schelkunoff's results[11,12] is explained in a way which appears to be consistent with the modification of Hallén's formula for cylinders suggested by Miss Gray.[15] An ellipsoid of semi-minor axis **a** has a mean radius considerably smaller than **a**, so that it should have impedance characteristics resembling those of a cylinder of radius smaller than **a**. Or, inversely, a cylinder of radius **a** has impedance characteristics resembling those of an ellipsoid with semi-minor axis considerably greater than **a**, such as the ellipsoid in broken line in Fig. 20.

A cylinder differs from an ellipsoid not only in having a constant radius but also in having flat end-surfaces. If the driven ends of the two

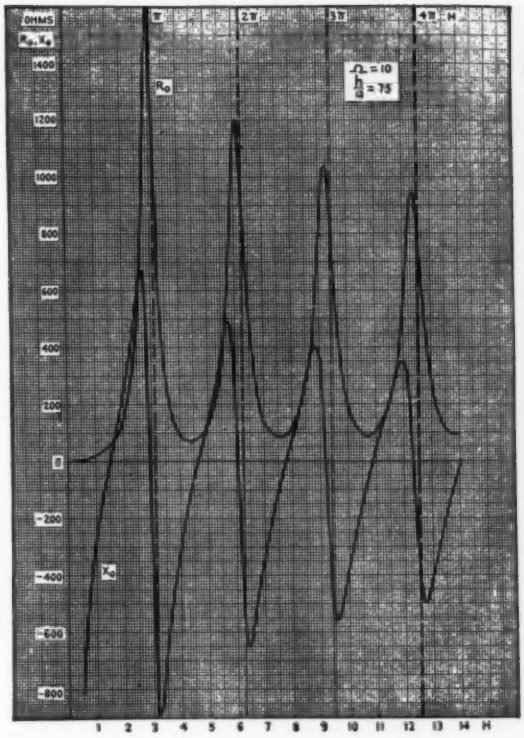


FIG. 15. Resistance and reactance of thin antenna, $h/a=75$.

halves of antenna are close together the parallel surfaces of the cylinders are roughly equivalent to an added capacitance across the driving terminals of the ellipsoids. It has been shown in Figs. 18, 19 that the effect of such a capacitance is to decrease the input resistance, shift the curve of reactance toward capacitive values, and move the curves for both resistance and reactance toward smaller values of $H=2\pi h/\lambda$. By an appropriate choice of the radius, or probably more correctly of the semi-minor axis **a** in Hallén's formula, and the addition of a suitable capacitance across the input terminals, the impedance of a cylindrical antenna with small separation at the input terminals can be represented approximately. By proper choice of the terminal capacitance the impedance at the terminals of antennas driven in various ways can be approximated.

### *Method 6*

Page and Adams[16] have determined the forced oscillations of a prolate spheroid in an electric

[15] M. C. Gray, J. App. Phys. **15**, 61 (1944).

[16] L. Page and N. I. Adams, Phys. Rev. **53**, 819 (1938).

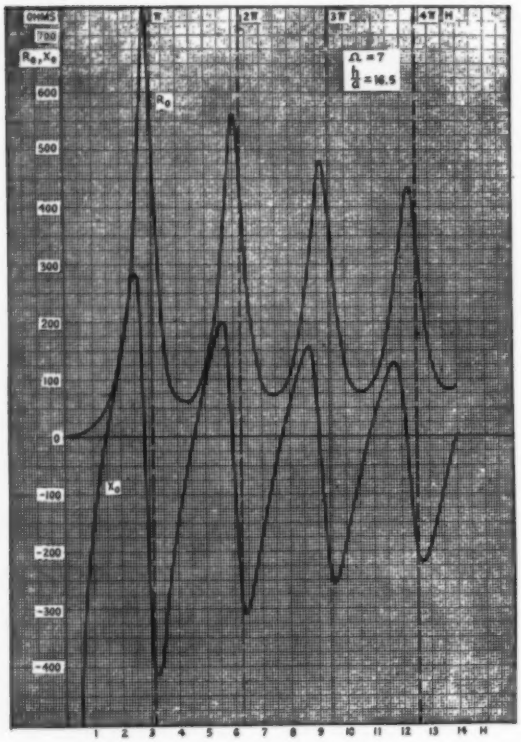


FIG. 16. Resistance and reactance of moderately thick antenna, $h/a = 16.5$.

field parallel to the axis. The solution is of interest in the study of a receiving antenna, but the problem solved is not that of a center-driven antenna.

*Method 7*

Stratton and Chu[17] have analyzed forced oscillations in a prolate spheroid driven by an axially directed external field applied symmetrically over the surface of a narrow segment of the spheroid at its center. A critical discussion is given by Schelkunoff.[11]

### Antenna Theory and Experiment

The experimental determination of the impedance of antennas for comparison with theoretical values is not a simple problem and it will not be considered here. A careful study of transmission-line methods for measuring the impedance of antennas has been begun at this laboratory both from theoretical and experimental points of view. In due course a report will be made. Aspects of the transmission-line problem are considered in general terms in a recent paper.[18] Until reasonably accurate and extensive experimental data together with an analysis of what is actually measured are available, a systematic comparison of theoretical and experimental results is not possible. In any event great care must be exercised in interpreting theoretical curves and experimental data and drawing conclusions either from agreement or disagreement. Lack of agreement between experimental observations and results computed from Hallén's formula neglecting terms of order higher than $1/\Omega$ may be due to one or more of the following reasons. 1. Measurements may have been made under conditions which do not approximate those implied in the theory. For example, if experimentally determined curves resemble Fig. 18 more than Fig. 15, it may be concluded that the terminals of the antenna involve an effective shunt capacitance in one form or another as compared with the rounded ends assumed in the calculation. 2. The antenna may be sufficiently thick so that higher order terms

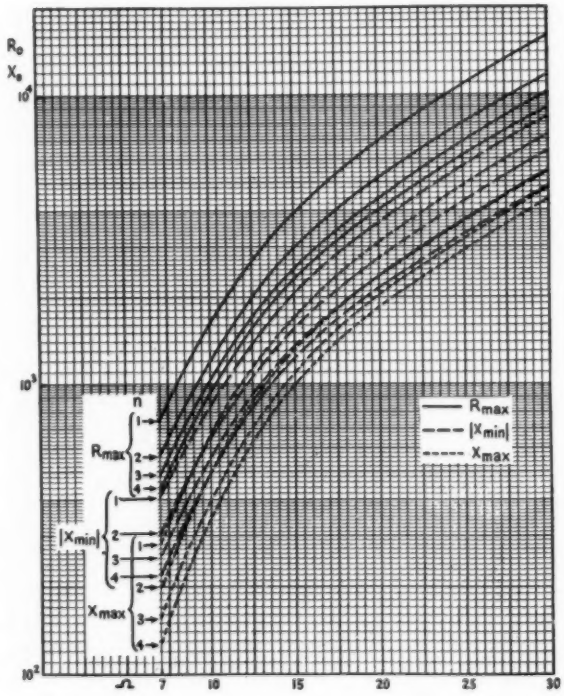


FIG. 17. Maximum value of $R_0$ (solid line), magnitude of minimum (long dashes), and maximum (short dashes) values of $X_0$ as functions of $\Omega = 2 \ln 2h/a$ for values near four anti-resonant lengths numbered 1, 2, 3, 4.

[17] J. A. Stratton and L. J. Chu, J. App. Phys. **12**, 230 (1941).

[18] R. King, J. App. Phys. **14**, 577 (1943).

than those in $1/\Omega$ should be retained in the theoretical formula (1). This is especially true near anti-resonance where the term in $1/\Omega$ in the denominator of (1) is the leading term. Until the magnitudes of the factors in the $1/\Omega^2$ terms are known, no limiting value can be assigned to the ratio $h/a$ below which (1) is adequate without terms in $1/\Omega^2$. It is quite possible that near anti-resonance errors of 20 percent or more are made in the impedance of even moderately thick antennas if terms in $1/\Omega^2$ are neglected.[19] It follows

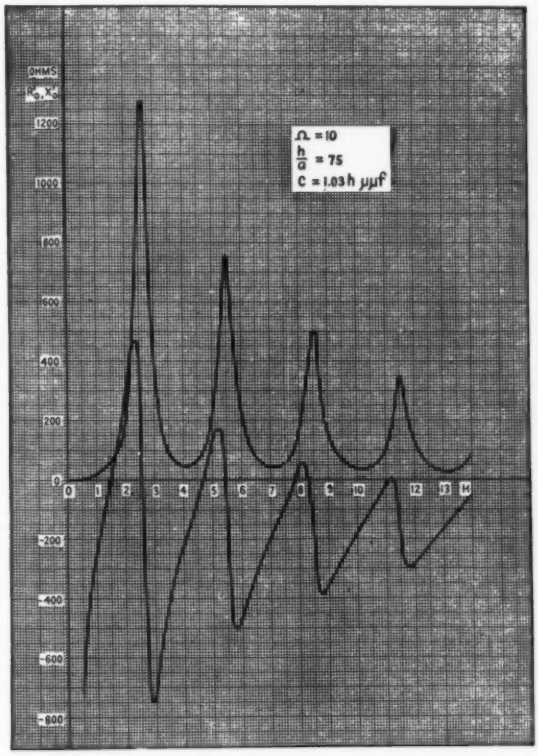


FIG. 18. The input resistance $R_0'$ and reactance $X_0'$ of the antenna of Fig. 15 with a capacitance $C=1.035h$ $\mu\mu$f across the terminals of the antenna if this is fixed in length at $h$ (meters) and the frequency is varied.

[19] E. Glas in a dissertation entitled "On radiation problems concerning vertical antennas" (Royal Administration of Swedish Telegraphs, Stockholm, 1943) writes on p. 29: "It should be noted that Bouwkamp [Physica 9, 609 (1942)] has given expressions of the second-order terms in Hallén's results; Bouwkamp's values make it probable that the successive swings, as the order is raised, are great, if $\Omega$ has a relatively small value, e.g., $\Omega=10$. As the question of convergence is still unsettled, this fact may signify that the descending series in $\Omega$, constituting the solution, is semi-convergent with swings making its strict application to relatively thick conductors difficult. It is for instance quite possible that in such a case the first approximation approaches nearer to the limiting value than does the second one." Unfortunately Bouwkamp's paper has not been available to the writers.

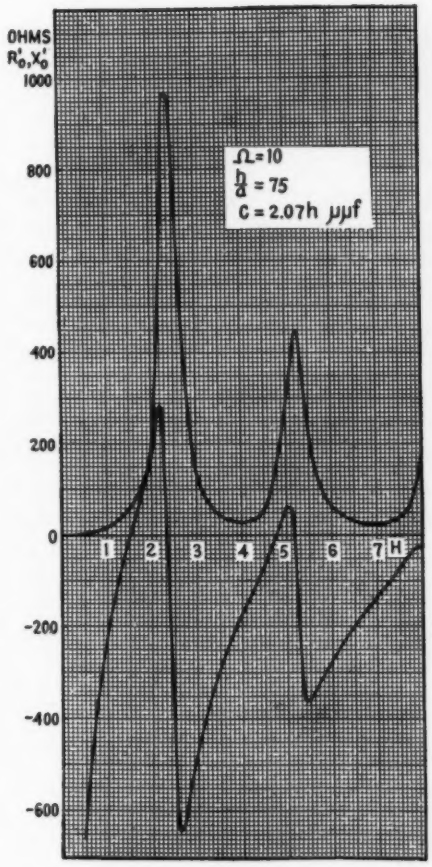


FIG. 19. Same as Fig. 18 with $C=2.07h$ $\mu\mu$f.

that impedance curves computed from (1) neglecting these terms may be quantitatively inaccurate near anti-resonance. 3. Experimental measurements may not be accurate. For example, if a transmission-line method depending on the measurement of the standing-wave ratio is used, large errors are difficult to avoid or even to estimate because of the effect of the standing-wave detector.[18]

The calculation of the impedance of an antenna is a part of the larger problem of determining the distribution of current. The analyses of L. V. King[14] and of Hallén[1,2] lead to approximate expressions for the current in an antenna. They appear to be in good qualitative agreement but differ quantitatively just as do the impedances. The assumption made by L. V. King, that the electric field along the mid-plane for antennas of non-vanishing thickness is the same as that for infinitely thin antennas, is in effect equivalent to assuming the radiation re-

sistance referred to maximum current amplitude, *viz.*,

$$R_m^e = \frac{P_0}{|I|^2_{\max}},$$

to be independent of the ratio $h/a$. $P_0$ is the input power. Hallén's analysis, on the other hand, makes no such assumption and $R_m^e$, as computed neglecting terms in $1/\Omega^2$, varies with the ratio $h/a$ as shown in Fig. 21, reference 2. As pointed out by Schelkunoff this variation appears to be very much larger than justified by the corresponding change in current distribution, in distant electric field, and in radiated power as computed by integrating the normal component of the Poynting vector over a great sphere. This is true especially for thicker antennas. On the other hand, there is experimental evidence[19] indicating that radiated power determined by Poynting vector methods using *measured* values of the electric field may be considerably greater than the power *measured* at the terminals. The difficulties underlying this paradoxical situation have not been fathomed. They obviously require investigation.

The analyses of Siegel and Labus,[8] Wells,[9] and Bohm[9] all permit the calculation only of the current distribution along an "equivalent" uniform transmission line. "In order to find the current distribution in non-uniform antennas" from Schelkunoff's analysis and quoting from his paper,[12] p. 512, "we should calculate the principal current distribution from Carson's equations [for non-uniform transmission lines], assuming the transmission line is terminated by the output radiation resistance as given in this paper." The transmission lines of Siegel and Labus, Wells, and Bohm are so constructed that if the transmission line currents are assumed to exist in the antenna to be represented, $R_m^e$ is independent of the ratio $h/a$. The curves reproduced by Wells[9] from Bohm's analysis differ considerably in shape from those of L. V. King and Hallén. The non-uniform transmission line of Schelkunoff is not adjusted to have $R_m^e$ independent of $h/a$ and it is not to be expected that $R_m^e$ for an antenna assumed to carry the current computed for the line will be independent of $h/a$. Schelkunoff shows,[12] p. 505, that the ratio $I_{\max}/I_0$ computed from his analysis for a conical antenna is in

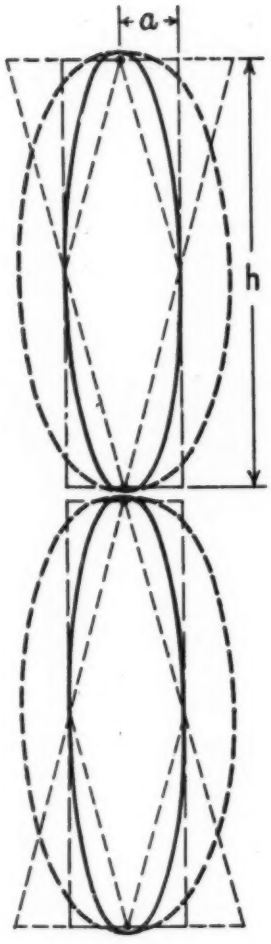


FIG. 20. Cross section of several shapes for center-driven antennas. The thickness is very much exaggerated. The ellipsoids (in solid line) have a semi-minor axis equal to the radius of the cylinder; the ellipsoid in broken line should have more nearly the impedance characteristics of the cylinder than those in solid line.

surprisingly good agreement with the same ratio measured experimentally by Pedersen on a cylindrical antenna with the same "average characteristic impedance." Accordingly it seems reasonable to assume that the distribution of current for a conical antenna, Fig. 18,[12] approximates that along a cylindrical antenna. Using Fig. 23[12] to obtain the input resistance $R_0$, the value of

$$R_m^e = \left(\frac{I_0}{|I_{\max}|}\right)^2 R_0$$

turns out to be considerably lower even than that obtained from Hallén's formula neglecting terms in $1/\Omega^2$ and higher powers. On the other hand if $R_0$ is determined from Fig. 13[12] for conical antennas a larger value of $R_m^e$ is obtained. A more exact check of Schelkunoff's formula for current in a cylindrical antenna must await the publication of distribution curves for current and of values of $R_m^2$.

Judged on the basis of the limited available experimental data,[11,12] and without investigating either the accuracy or what was actually measured, Schelkunoff's formula seems to be the best approximation for the impedance of cylindrical antennas that are not too long, although Hallén's formula (without terms in $1/\Omega^2$) may serve equally well if modified either as suggested by Miss Gray,[15] or by using an effective value of $\mathbf{a}$ or $\Omega$ with or without an added input capacitance. Glas[19] suggests an average value, $\Omega_{Av}=\Omega-2$. The factor 60 $\Omega_{Av}$ is Schelkunoff's average characteristic impedance, $K_a=120[\ln(2h/a)-1]$. Effective values of $\mathbf{a}$ and $\Omega$ which make (1) a better approximation of the available experimental data for cylinders of radius $\mathbf{a}'$ are $a=3.5a'$, $\Omega=2\ln(2h/a')-2.5$. If this value is used, the experimental data[11,12] for $R_{0\,max}$ is more closely approximated by Hallén's formula than by Schelkunoff's. A smaller effective radius with an appropriately adjusted added input capacitance may serve as well. It is, however, not the purpose of this paper to make exaggerated claims about the accuracy of Hallén's or any other formula, since all are at best approximations, and sufficient experimental data are not available nor the conditions under which measurements were made sufficiently clear to justify positive conclusions. It is to be noted that the formulas of Bohm, L. V. King, and Schelkunoff as well as of Hallén neglect higher order terms which all appear to be of the same order of magnitude. This was pointed out by Schelkunoff in so far as his own and L. V. King's formulas are concerned.[12]

The significance of Hallén's analysis actually far transcends the problem of determining the self-impedance of an antenna. It represents an application of the powerful and electromagnetically correct vector-potential method[20] for analyzing a wide variety of antenna problems involving sufficiently thin conductors which cannot be approximated by transmission-line formulas.[21]

The writers are indebted to Dr. S. A. Schelkunoff of the Bell Telephone Laboratories for criticism of the manuscript and for prepublication copies of his paper[11] and that of Miss Marion C. Gray.[15]

---

[20] See, for example, S. A. Schelkunoff, *Electromagnetic Waves* (D. Van Nostrand Co., New York, 1943), pp. 140, 142 ff.

[21] For example, R. King and C. W. Harrison, Jr., "Mutual- and self-impedance of coupled antennas," submitted to the *Journal of Applied Physics*.

# Terminal Functions for Antennas

D. D. King and Ronold King
*Cruft Laboratory and the Research Laboratory of Physics, Harvard University, Cambridge, Massachusetts*
(Received October 20, 1943)

Recently calculated values of the input impedance of cylindrical antennas are expressed in a form adapted to transmission-line equations. Curves are plotted to show the effect of various antenna and line parameters on a circuit consisting of a line with an antenna as load, and application is made to the transfer of power from the line to the antenna.

## INTRODUCTION

THE mathematical form of a new theoretical or experimental result is often determined by the methods used to obtain it, or perhaps by some long-standing convention. A suitable transformation may facilitate the physical interpretation and engineering application of the original expression. In this paper certain results of antenna analysis will be considered in a form adapted to transmission-line circuits. One of the most complete and satisfactory solutions of the problem of the cylindrical antenna in space is due to Hallén.[1] Tables of the input self-impedance of a symmetrical center-driven antenna, based on this solution, are available[2] and form the basis for the calculations carried out for this paper.

Supposing that one is furnished with the data necessary for treating the antenna as a circuit element, what is the most convenient form for expressing this information? The input resistance and reactance $R_s$ and $X_s$ have certain disadvantages due to the fact that antennas are almost invariably associated with some form of line used to drive them. Transmission-line theory is conveniently couched in terms of a propagation constant $\beta$, an attenuation constant $\alpha$, and a characteristic impedance $Z_c$. In conventional formulation the over-all attenuation and phase shift due to the line itself is not readily combined with the same effects due to a terminating impedance. The theory has been extended,[3,4] however, to make this possible. Accordingly, the impedance of an antenna serving as a terminal impedance may be put into the form set forth previously,[3,4] in which the attenuation $\rho$ and phase shift $\Phi$ due to the antenna may be added directly to $\alpha s$ and $\beta s$ for the line of length $s$. Considerable information on the behavior of an antenna as a circuit element may be obtained from the curves of the terminal functions $\rho$ and $\Phi$.

## FORMULAE

Consider the case of an antenna with input self-impedance $Z_s = R_s + jX_s$ terminating a transmission line of length $s$ with characteristic im-

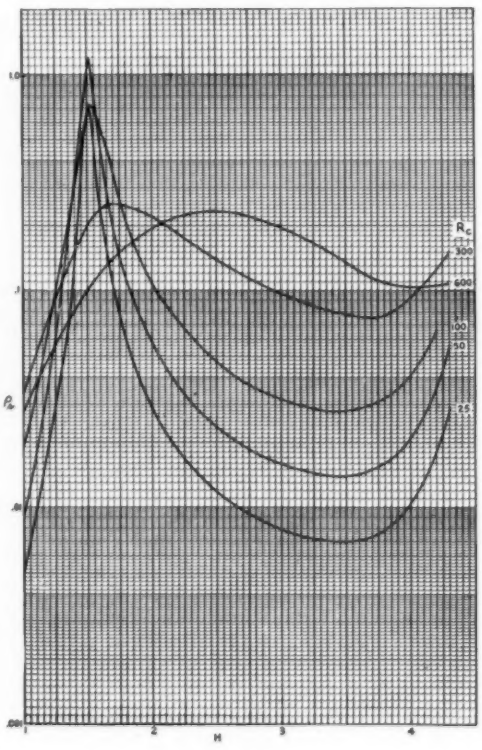

FIG. 1a.

[1] E. Hallén, Nova Acta Uppsala [4] **11**, No. 4, 1–44 (November, 1938).
[2] R. King and F. G. Blake, Jr., Proc. I. R. E. **30**, 335–349 (July, 1942).
[3] R. King, Proc. I. R. E. **29**, No. 12 (December, 1941).
[4] R. King, J. App. Phys. **14**, 577 (1943).

pedance $Z_c=R_c(1-j\phi)$ and complex propagation constant $K=\alpha+j\beta$. Terminal functions for the antenna are defined as follows:

$$\rho_s=\tfrac{1}{2}\tanh^{-1}\left[\frac{2R_c(R_s-\phi X_s)}{R_s^2+X_s^2+R_c^2(1+\phi^2)}\right], \quad (1)$$

$$\Phi_s=\tfrac{1}{2}\tan^{-1}\left[\frac{-R_c(X_s+\phi R_s)}{R_s^2+X_s^2-R_c^2(1+\phi^2)}\right]. \quad (2)$$

Assuming that $\phi^2\ll 1$ and after dividing by $R_c$ one obtains the approximate forms:

$$\rho_s=\tfrac{1}{2}\tanh^{-1}\left[\frac{2\left(\frac{R_s}{R_c}-\phi\frac{X_s}{R_c}\right)}{\left(\frac{R_s}{R_c}\right)^2+\left(\frac{X_s}{R_c}\right)^2+1}\right], \quad (3)$$

$$\Phi_s=\tfrac{1}{2}\tan^{-1}\left[\frac{-\left(\frac{X_s}{R_c}+\phi\frac{R_s}{R_c}\right)}{\left(\frac{R_s}{R_c}\right)^2+\left(\frac{X_s}{R_c}\right)^2-1}\right]. \quad (4)$$

The advantage of this form of representation is that the effect of the terminal impedance as expressed by the terminal functions now appears directly in the arguments of the conventional hyperbolic, trigonometric, and exponential functions which characterize the line equations. Thus, for the input impedance of the line one has:

$$Z_{\text{in}}=Z_c\coth\left[(\alpha s+\rho_s)+j(\beta s+\Phi_s)\right]. \quad (5)$$

From formula (49b) of reference 3 the current at a distance $z$ from the input end of a line of length $s$, driven by a generator of impedance $Z_0$, and loaded with an impedance $Z_s$ is:

$$|I_z|=\left|\frac{V_0^e}{Z_c}\right|\left\{\frac{[\sinh^2\rho_0+\sin^2\Phi_0][\sinh^2(\alpha w+\rho_s)+\sin^2(\beta w+\Phi_s)]}{\sinh^2(\alpha s+\rho_0+\rho_s)+\sin^2(\beta s+\Phi_0+\Phi_s)}\right\}^{\frac{1}{2}}. \quad (6)$$

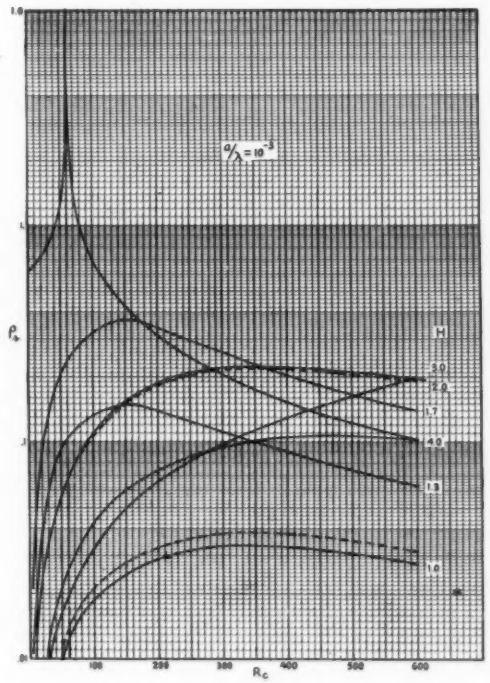


FIG. 1b

Here $V_0^e$ is the applied voltage of the generator at $z=0$; $\rho_0$ and $\Phi_0$ are the terminal functions of the generator; $\rho_s$ and $\Phi_s$ the terminal functions of the load at $z=s$; $w=s-z$ is the distance from the output end to the point $z$ where $|I_z|$ is measured.

The magnitude of $\rho_s$ measures the attenuation due to the load as compared with the over-all attenuation $\alpha s$ of the line and the attenuation $\rho_0$ of the generator. The larger $\rho_s$ as compared with $(\alpha s+\rho_0)$, the greater the fraction of power consumed in the load. If $\rho_s$ is the terminal function of an antenna, the greatest power is radiated for given values of $\alpha s$ and $\rho_0$ when $\rho_s$ is a maximum. By means of a suitable matching network the line can always be terminated in its characteristic impedance so that

$$Z_s=Z_c; \quad R_s=R_c; \quad X_s=-\varphi R_c, \quad (7)$$

then one has

$$\rho_s=\infty. \quad (8)$$

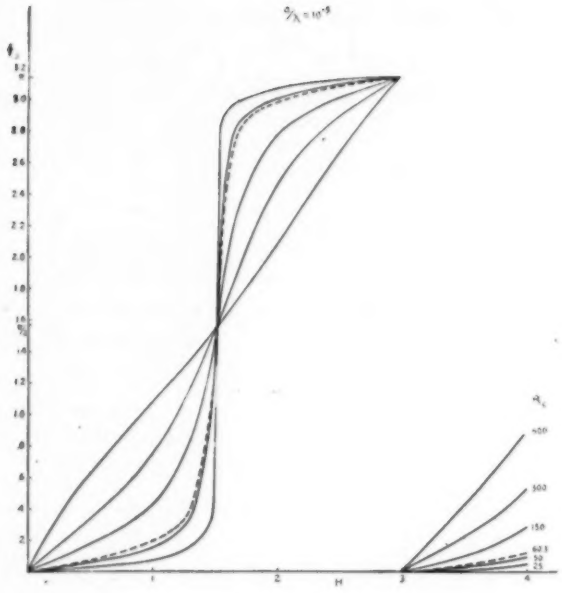

FIG. 2a.

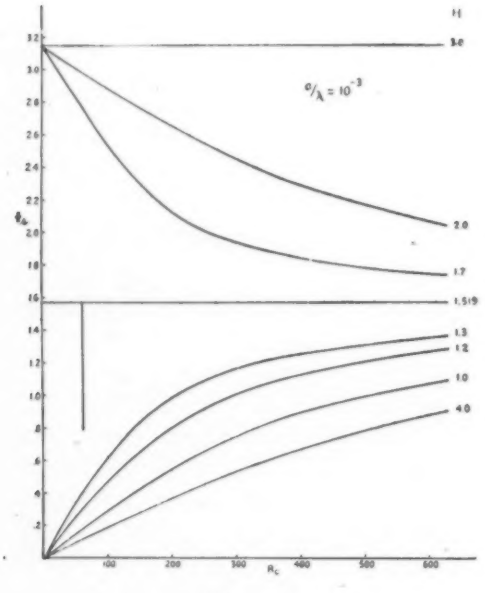

FIG. 2b.

In this case (5) gives:

$$Z_{in}=Z_e \tag{9}$$

and (6) reduces to:

$$|I_z|=\left|\frac{V_0^e}{Z_e}\right|(\sinh^2\rho_0+\sin^2\Phi_0)e^{-2\alpha w}. \tag{10}$$

If a resonant line is required the optimum length and radius of an antenna for a given line may be determined from the value of $\rho_s$ for the antenna. The corresponding tuning adjustment depends on the value of $\Phi_s$ for the antenna. These values will be given below.

## DISCUSSION OF CURVES

In plotting the curves of $\rho_s$ and $\Phi_s$ for a cylindrical center-driven antenna one is confronted with a number of independent variables from which to choose parameters. For the antenna there are the two quantities

$$H=2\pi h/\lambda, \quad a/\lambda,$$

where $\lambda$ is the wave-length, $a$ the radius of the antenna, and $2h$ its length; for the line one has $R_c$ and $\phi$. For the moment let it be assumed that $\varphi$ is negligible, which means $\phi \leq 10^{-4}$. $\rho_s$ and $\Phi_s$ are taken as dependent variables throughout.

First, consider the curves in $\rho_s$ of Fig. 1. An antenna of thickness $a/\lambda=10^{-3}$ is resonant at $H_r=1.519$ and anti-resonant at $H=2.997$. With the antenna adjusted to resonance $\rho_s$ can be made to increase without limit by setting $R_c$ equal to the resonant resistance of the antenna (here 60.3 ohms). However, the point of maximum $\rho_s$ for values of $R_c$ different from this does not occur at antenna resonance. In general,

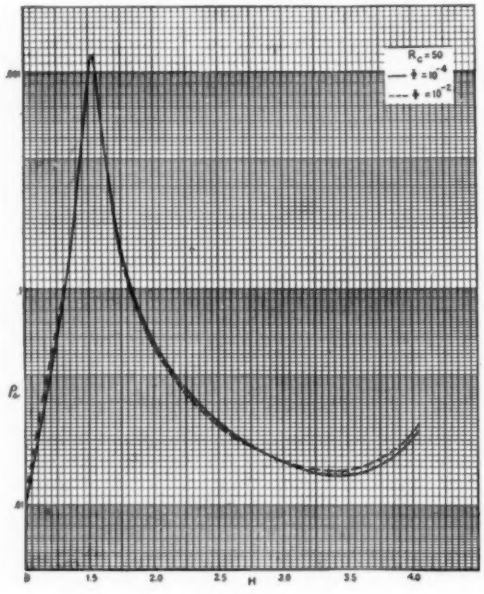

FIG. 3.

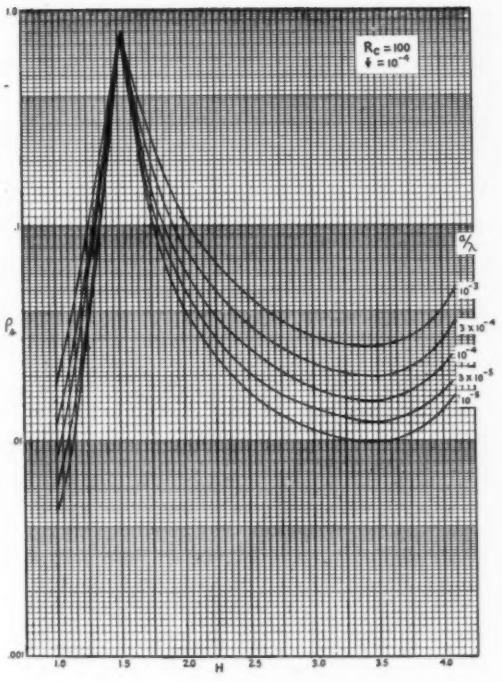


FIG. 4a.

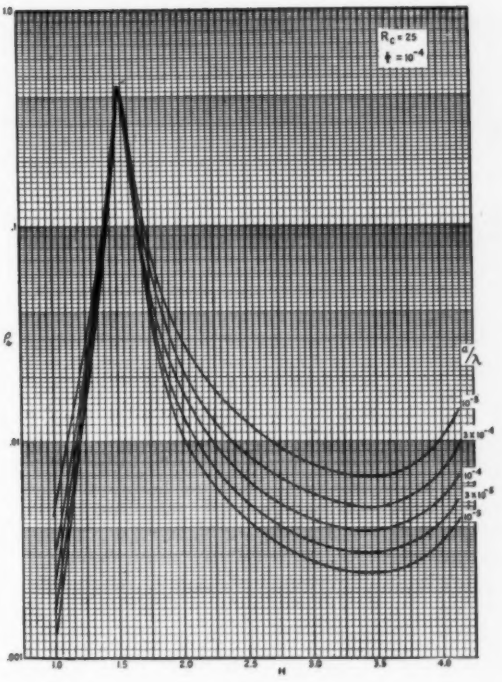


FIG. 4b.

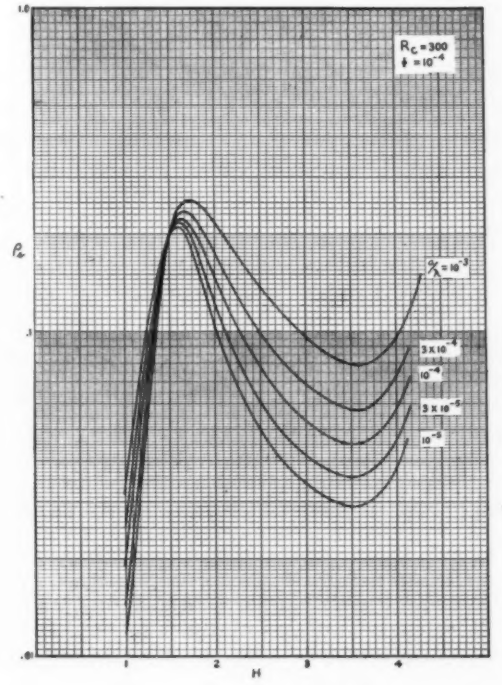


FIG 4c.

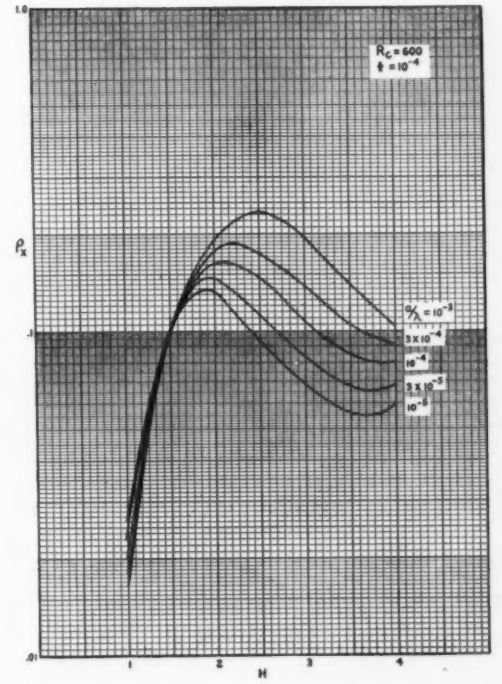


FIG. 4d.

the maximum $\rho_s$ is obtained at $H < H_r$ for $R_c < R_r$ and at $H > H_r$ for $R_c > R_r$, where the subscript $r$ stands for "resonant." This shift is considerable for the higher values of $R_c$ commonly found on parallel lines. As is to be expected, the peaks become less pronounced as the resistance $R_c$ of

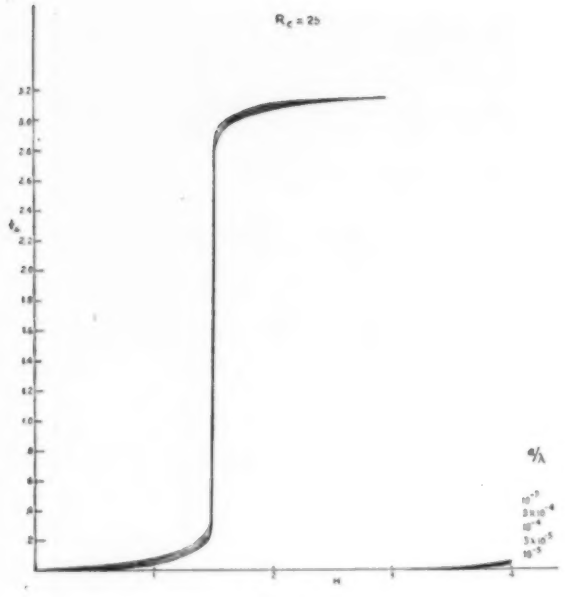

FIG. 5a.

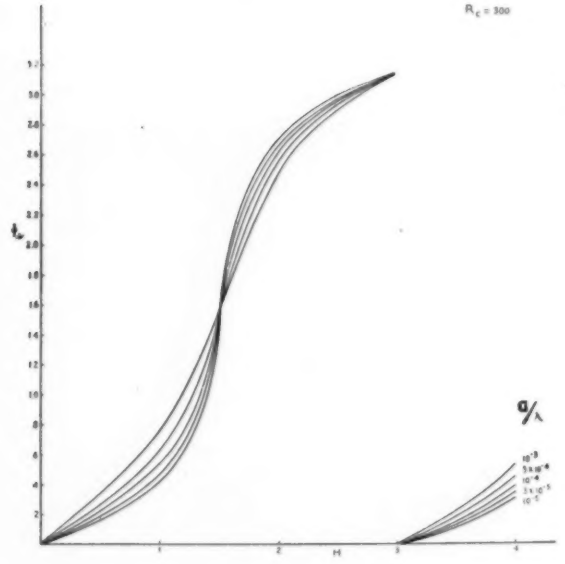

FIG. 5b.

the line is increased. The cycle repeats $n$ times for $H=n\pi h/\lambda$ with declining amplitude.

The curves of Fig. 2 in $\Phi_s$ also have a period of $\pi$ radians and a singularity at the resonant point when $R_c=R_r$ of the antenna. At $H=H_r$ the phase shift is $\pi/4$ radians for $R_c=R_r$ and $\pi/2$ for all other values of $R_c$. The transition between these two values is very abrupt and is caused by the fact that $\phi$, although small, has a finite value. The magnitude of $\phi$ has no influence on the

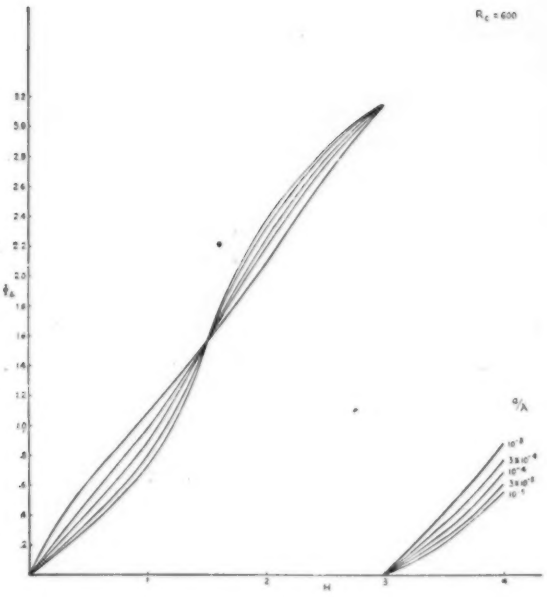

FIG. 5c.

location of the singular point at $H=H_r$, $R_c=R_r$, for either $\rho_s$ or $\Phi_s$. However, for other values of $R_c$ the effect of $\phi$ may be appreciable since the restriction $\rho\leq 10^{-4}$ imposed above is ordinarily not satisfied. An inspection of the expressions for $\rho_s$ and $\Phi_s$ in the interval $R_s > |X_s|$. The dotted portions of Figs. 2a and 3 show the magnitude of the error introduced by neglecting $\phi$. For three-place accuracy it follows that the reactive term $-j\phi R_c$ of the line cannot always be discarded. (In the figures $\Phi$ is written for $\phi$.)

The curves of Figs. 4 and 5 show the behavior of the terminal functions when the relative thickness of the antenna is varied. It is apparent that the ratio $a/\lambda$ has much the same influence as $R_c$. This is to be expected since increasing $a/\lambda$ reduces the sharpness of resonance of the antenna and therefore broadens the resonance peaks.

## APPLICATION TO THE TRANSFER OF POWER

The question of power transfer is of particular interest and at the same time easily treated by means of the terminal functions.[4] Consider a line of length $s$ coupled to a generator with terminal functions $\rho_0$ and $\Phi_0$, and to an antenna with terminal functions $\rho_s$ and $\Phi_s$. (Equations (1) and (2) or (3) and (4) are used to calculate $\rho_0\rho_s\Phi_0\Phi_s$.) Now,

$P_0=|I_0|^2R_{\text{in }0}$ is the input power; (11)

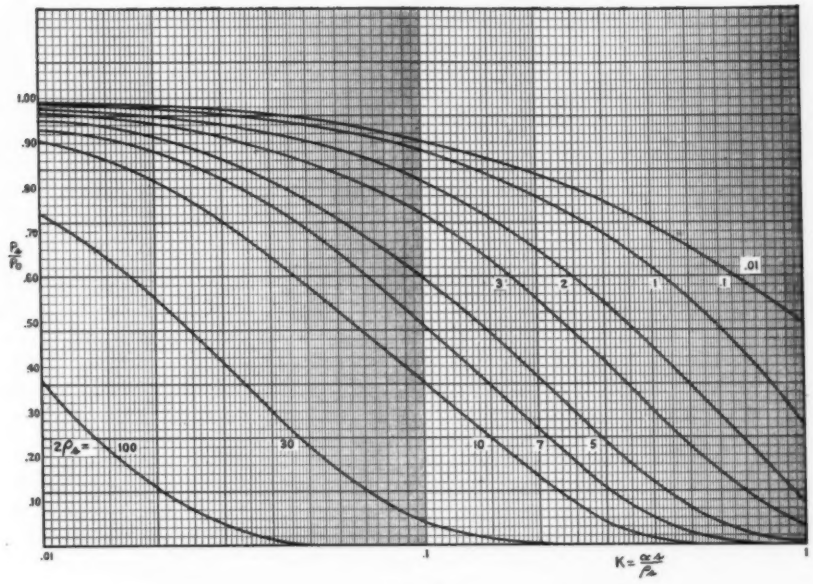


FIG. 6a.

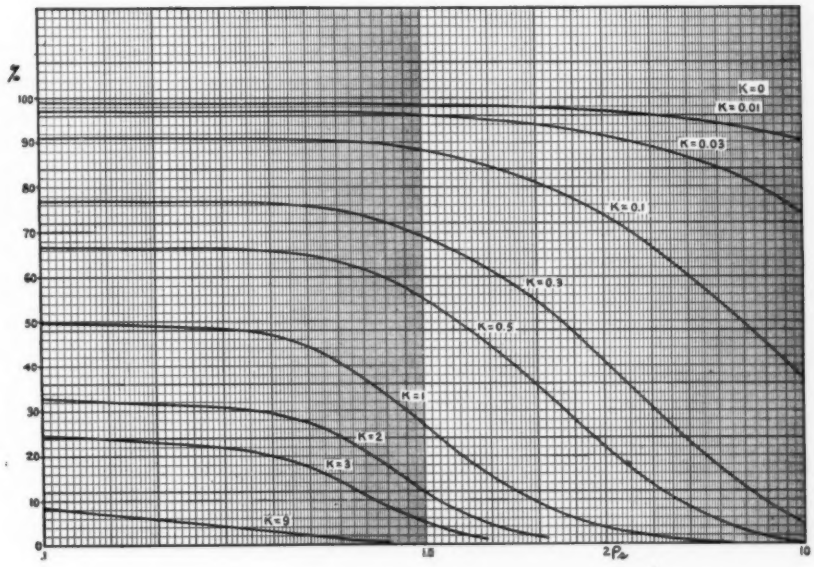


FIG. 6b.

$P_s=|I_s|^2R_s$ is the output power delivered to the antenna at $s$. (12)

The general expression for the current along a line is given by (6). From this one obtains the input and output currents. They are:

$$|I_0|=\left|\frac{V_0^e}{Z_c}\right|\left\{\frac{[\sinh^2(\alpha s+\rho_s)+\sin^2(\beta s+\Phi_s)][\sinh^2\rho_0+\sin^2\Phi_0]}{\sinh^2(\alpha s+\rho_0+\rho_s)+\sin^2(\beta s+\Phi_0+\Phi_s)}\right\}^{\frac{1}{2}}, \tag{13}$$

$$|I_s|=\left|\frac{V_0^e}{Z_c}\right|\left\{\frac{[\sinh^2\rho_0+\sin^2\Phi_0][\sinh^2\rho_s+\sin^2\Phi_s]}{\sinh^2(\alpha s+\rho_0+\rho_s)+\sin^2(\beta s+\Phi_0+\Phi_s)}\right\}^{\frac{1}{2}}. \tag{14}$$

The real part of (5) is

$$R_{\text{in }0}=R_c\left\{\frac{\sinh 2(\alpha s+\rho_s)-\varphi\sin 2(\beta s+\Phi_s)}{\cosh 2(\alpha s+\rho_s)-\cos 2(\beta s+\Phi_s)}\right\}$$
$$=\frac{R_c}{2}\left\{\frac{\sinh 2(\alpha s+\rho_s)-\varphi\sin 2(\beta s+\Phi_s)}{\sinh^2(\alpha s+\rho_s)+\sin^2(\beta s+\Phi_s)}\right\}. \tag{15}$$

Upon substituting (13), (14), and (15) in (11) and (12) one obtains a relatively simple expression for the ratio of output to input power. It is:

$$\frac{P_s}{P_0}=\frac{2R_s}{R_c}\left\{\frac{\sinh^2\rho_s+\sin^2\Phi_s}{\sinh 2(\alpha s+\rho_s)-\phi\sin 2(\beta s+\Phi_s)}\right\}$$
$$2=\frac{R_s}{R_c}\left\{\frac{\cosh 2\rho_s-\cos 2\Phi_s}{\sinh 2(\alpha s+\rho_s)-\phi\sin 2(\beta s+\Phi_s)}\right\}. \tag{16}$$

Formula (16) may be rearranged by noting that the ratio $P_s/P_0$ must reduce to unity when $s=0$. In this case

$$1=\frac{R_s}{R_c}\left\{\frac{\cosh 2\rho_s-\cos 2\Phi_s}{\sinh 2\rho_s-\phi\sin 2\Phi_s}\right\}. \tag{17}$$

Upon dividing (16) by (17) one has the following perfectly general formula:

$$\frac{P_s}{P_0}=\frac{\sinh 2\rho_s-\phi\sin 2\Phi_s}{\sinh 2(\alpha s+\rho_s)-\phi\sin 2(\beta s+\Phi_s)}. \tag{18}$$

Multiplying (18) by 100 gives the efficiency of transmission directly. In all practically important cases involving a power absorbing load, $\rho_s$ is necessarily sufficiently large so that the small terms in $\phi$ are negligible. In such cases one obtains the following extremely simple and very general form of the power ratio:

$$\frac{P_s}{P_0}=\frac{\sinh 2\rho_s}{\sinh 2(\alpha s+\rho_s)}, \tag{19a}$$

$$\frac{P_s}{P_0}=\frac{\sinh 2\rho_s}{\sinh 2\rho_s(1+K_s)}. \tag{19b}$$

Here $K_s=\alpha s/\rho_s$. Using formulas (1) or (3) for computing $\rho_s$ or the curves of $\rho_s$ given above for an antenna, the ratio of the output to the input power, $P_s/P_0$ is readily evaluated for lines of any length or conditions of resonance or non-resonance. Curves of $P_s/P_0$ as functions of $2\rho_s$ with $K_s$ as a parameter and as functions of $K_s$ with $2\rho_s$ as a parameter are shown in Fig. 6. In the case of a non-resonant line defined by

$$Z_s=Z_c;\quad \rho_s=\infty, \tag{20}$$

formula (19) reduces to the familiar form

$$P_s/P_0=e^{-2\alpha s}. \tag{21}$$

The ratio of the power lost in the line $P_L$ to the power supplied $P_0$ is given in general by

$$P_L/P_0=1-(P_s/P_0). \tag{22}$$

By comparing the magnitude of this ratio for a resonant and non-resonant line in any particular case it is a simple matter to determine whether a matching section is required or not.

# Bonding and Structural Variations of Commercial Electroplatings 2–55 $\times 10^{-6}$ Inch Thick

GEORGE L. CLARK, GEORGE PISH, AND LEONARD E. WEEG
*Noyes Chemical Laboratory, University of Illinois, Urbana, Illinois, and Research Laboratory, American Nickeloid Company, Peru, Illinois*
(Received November 19, 1943)

## INTRODUCTION

THE deposition of metal platings which afford satisfactory protection against corrosion of a wide variety of fabricated metal products is a problem of great practical importance, accentuated by present war demands. There is a fundamental and theoretical significance to the problem of producing a satisfactory plating which involves a knowledge of the bonding between a coating, particularly the very first layers of atoms, and the underlying substrate metal. In this bond there resides the ability of the plated film to adhere even to a dissimilar metal under disruptive conditions. A number of studies[1] have been made by x-ray and electron diffraction of the structure of the whole film of metal produced by electrodeposition and then peeled off. In a few cases beams have been reflected from surfaces to produce diffraction patterns which integrate the structure through a considerable thickness and thus fail to show the true *interfacial* structure. The present study was undertaken for the purpose of (1) developing a convenient x-ray diffraction technique for evaluation of commercial platings directly on the base metals and over a series of thicknesses from the first invisible thinnest layer ($2\times10^{-6}$) stepwise to films about 30 times this thickness; (2) correlating these results especially for the thinnest interfacial layers with electron diffraction patterns which hitherto have been considered the only possible source of information on these very thin films; (3) and also correlating with measurements of optical reflectances on the Hardy recording spectrophotometer. Such a study would be expected to show not only the true interfacial or interpenetrating crystalline structure and texture, but also variations as the film increases in thickness so that the last atoms deposited are farther and farther removed from the atomic forces of the base metal.

## EXPERIMENTAL

### (a) Preparation of Samples

Samples used in this study were prepared using commercial plating methods and equipment. The substrate metals chosen for the experiments were 1.5 inches wide, 8 inches long, and 0.010 inch thick. After cleaning the surface of the substrate material electrolytically in an alkaline bath, the sheet was submerged in the plating bath containing the proper solution. After electrical contact was made, the sheet was plated for a specified period. Then the sheet was raised one inch out of the solution and plating continued on the submerged portion for another increment of time. The current was adjusted at each step to maintain a constant current density on the area being plated. Each time the plate was lifted from the solution the exposed portion was sprayed with water in order to remove the electrolyte which would redissolve the plating. The process of stepwise plating was repeated until a graded series of eight platings of varying thicknesses was obtained on each sample sheet. The time of plating for each step for all the samples was constant and of course determined the thickness. For example, most of the samples had a final plating thickness, as determined by microscopic measurement at a magnification of 800× checked by weights, for step 8 of $55\times10^{-6}$ (0.000055) inch. Thicknesses of lower steps are also constant and approximately proportional to the plating time as follows:

| Step | 1 | 2 | 3 | 4 | 5 | 6 | 7 | 8 |
|---|---|---|---|---|---|---|---|---|
| Time (sec.) | 10 | 20 | 35 | 55 | 80 | 120 | 180 | 260 |
| Approx. thickness (in.) | 2.1 | 4.2 | 7.4 | 11.55 | 16.9 | 25.3 | 38.0 | $55.0\times10^{-6}$ |

In Table I are given descriptions of the substrate materials and platings for all samples investigated.

[1] For the most recent summary, see Barrett, *Structure of Metals* (McGraw-Hill Book Company, New York, 1943), p. 437.

After the samples were plated, they were first sheared around the edges to remove the plated portion excessively thickened due to the sharp edge effect which allowed the plating to build up more rapidly. Finally the sheet was sheared into strips approximately one inch by eight inches. These were individually wrapped in several thicknesses of heavy paper and finally sealed in Cellophane to protect the surface from air oxidation until needed for the experiments. When it was found necessary to store the samples for any length of time, they were placed in vacuum.

When a sample was ready to be investigated, the sheared edges of the sample sheet were honed to remove the cold work produced by the shearing process. Each plated step was then cut off giving samples of about one inch square—a convenient size for the equipment used.

### (b) X-Ray Diffraction Method

In order to be sure that the patterns from each series of graded stepwise samples gave patterns which did not vary in sample-film distance and angular tilt, it was desirable to construct a sample holder and collimating system suitable for this work. After several experimental arrangements were tried, the combination sample holder and collimating system indicated in Fig. 1 was finally considered most satisfactory for the experiments. The entire apparatus was made of brass with the exception of the sample hold-down clip which is spring bronze. The sample platen could be tilted

TABLE I.

| Series | Base metal | Cleaning procedure | Flash coat | Plating solution | Deposited metal | Interface structure |
|---|---|---|---|---|---|---|
| *A* | Steel | *A*[1] | Cu | Copper cyanide | Cu | Base metal: Fe pattern; random orientation<br>Cu flash: Cu pattern; random orientation<br>Platings 1–8: Cu pattern; random orientation |
| *B* | Steel | *C*[2] | None | Copper cyanide | Cu | Base metal: Fe pattern; random orientation<br>Platings 1–8: Cu pattern; random orientation |
| *C* | Zinc | *A* | Cu | Copper cyanide | Cu | Base metal: Zn pattern; random orientation<br>Cu flash: Cu pattern; random orientation<br>Platings 1–8: Cu pattern; random orientation |
| *D* | Tinplate | *A* | Cu | Copper cyanide | Cu | Base metal: Sn, Fe patterns; random orientation<br>Cu flash: Cu pattern; line shift indicating solid solution; random orientation<br>Platings 1–8: Cu pattern; random orientation |
| *E* | Copper-plated steel | *C* | None | Nickel sulfate | Ni | Base metal: Cu, Fe pattern; random orientation<br>Platings 1–8: Ni pattern; random orientation |
| *F* | Copper | *C* | None | Nickel sulfate | Ni | Base metal: Cu pattern; random orientation<br>Platings 1–8: Ni pattern; random orientation |
| *G* | Brass soft temper | *A* | Cu | Nickel sulfate | Ni | Base metal: $\alpha$-brass pattern; random orientation<br>Cu flash: Cu pattern, random orientation<br>Platings 1–8: Ni pattern; random orientation |
| *H* | Brass half-hard temper | *A* | Cu | Nickel sulfate | Ni | Base metal: $\alpha$-brass pattern; nearly random orientation<br>Cu flash: Cu pattern; random orientation<br>Plating 1: No Ni—same as Cu flash<br>Platings 2–8: Ni pattern; random orientation |
| *I* | Tinplate | *A* | Cu | Nickel sulfate | Ni | Base metal: Sn, Fe pattern; random orientation<br>Cu flash: Cu pattern; line shift indicating solid solution; random orientation<br>Platings 1–8: Ni pattern; random orientation |

TABLE I.—*Continued.*

| Series | Base metal | Cleaning procedure | Flash coat | Plating solution | Deposited metal | Interface structure |
|---|---|---|---|---|---|---|
| *J* | Zinc | *A* | Cu | Nickel sulfate | Ni | Base metal: Zn pattern; random orientation<br>Cu flash: Cu pattern; random orientation<br>Platings 1–8; Ni pattern; random orientation |
| *Q* | Cold-rolled steel | *C* | None | Zinc cyanide | Zn | Base metal: Fe, oriented [111] direction<br>Plating 1: No Zn; same as substrate steel<br>Plating 2: Zn oriented [111] or [110] direction<br>Platings 3–8: Zn, random orientation |
| *R* | Cold-rolled copper | *C* | None | Zinc cyanide | Zn | Base metal: Cu, oriented [110]<br>Platings 1–2: No Zn, same as substrate<br>Plating 3: Zn, oriented [110]<br>Platings 4–8: Zn, random orientation |
| *S* | Cold-rolled brass | *C* | None | Zinc sulfate | Zn | Base metal: α-brass, oriented [110]<br>Plating 1: Zn, oriented [110]<br>Platings 2–8: Zn, random orientation |
| *V* | Cold-rolled steel | *C* | None | Copper cyanide | Cu | Base metal: Fe, oriented [111]<br>Plating 1: Cu, oriented Cu [111] or [110]<br>Platings 2–8: Cu, random orientation |
| *W* | Cold-rolled brass | *C* | None | Copper cyanide | Cu | Base metal: α-brass, oriented [110]<br>Plating 1: No Cu; same as substrate<br>Plating 2: Cu, oriented [110]<br>Platings 3–8: Cu, random orientation |
| *X* | Cold-rolled copper | *C* | None | Nickel sulfate | Ni | Base metal: Cu, oriented [110]<br>Plating 1: No Ni; same as substrate<br>Plating 2: Ni, oriented [110] or [111]<br>Platings 3–8: Ni, random orientation |
| *Y* | Cold-rolled brass | *C* | None | Nickel sulfate | Ni | Base metal: α-brass, oriented [110]<br>Plating 1: Ni, oriented [110] or [111]<br>Platings 2–8: Ni, random orientation |

[1] Cleaning procedure *A* consisted of cathodic cleaning in combination with a commercial cleaner and a copper strike solution (copper cyanide). This was followed by rinsing in water before stepwise plating.
[2] Cleaning procedure *C* was similar to that of *A* with the exception that the copper strike solution was omitted.

and then permanently fixed into position. The defining front pinhole was 0.025-inch diameter and the back pinhole 0.040-inch diameter.

For the experiments carried out, the reflection method was employed as shown schematically in Fig. 1. The angle of tilt ($\beta$-angle) finally decided upon was 50°. Each sample was set in the apparatus so that most of the x-ray beam struck its surface with only a small portion grazing over the honed edge. After the first sample of a series was adjusted upon the sample platen and the sample film-distance adjusted to 1.50 cm, the entire set-up (flat film cassette holder and apparatus) was firmly clamped to the top of the x-ray table. With the aid of a vernier micrometer the height of the upper honed edge of the sample was measured. Then each succeeding sample of the series was set to this height on the platen. As a consequence one diffraction pattern may be compared directly with any other of the series since the experimental conditions are constant for any particular series.

All patterns were obtained using radiation from a Machlett cobalt target x-ray tube from which the $\beta$-radiation was filtered out using a ferric oxide filter. The tube was operated at 38 kv, 10 ma with an exposure time of one hour for each pattern.

### (c) Electron Diffraction Method

Purely for confirmatory observation of the first 1 or 2, or thinnest, films, the samples used in the x-ray method were subjected to electron diffraction analysis at grazing incidence. The apparatus used was described fully elsewhere by Clark and Wolthuis.[2] For each sample an exposure

[2] G. L. Clark and E. Wolthuis, J. App. Phys. **8**, 630 (1937).

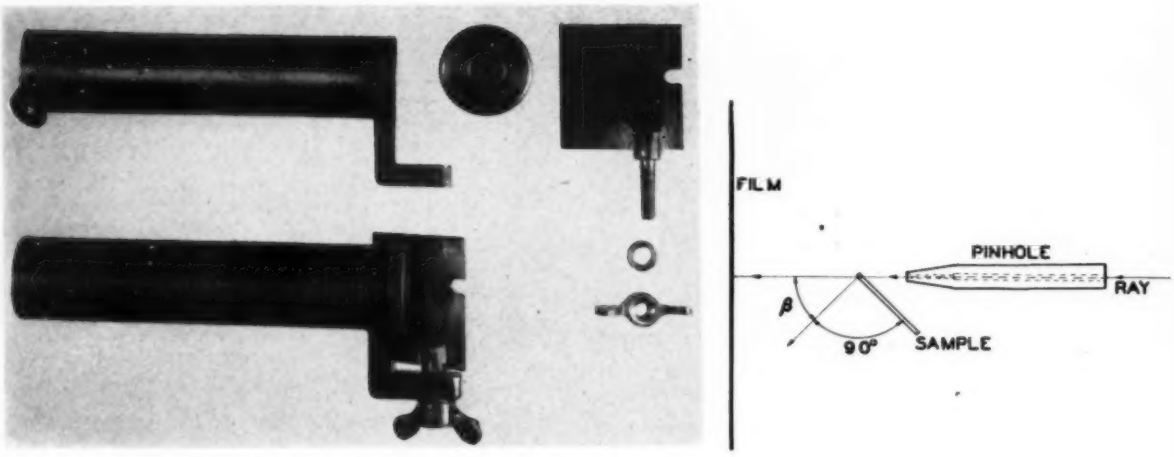


FIG. 1. Combination sample holder for oblique angle of incidence and collimation system for x-ray beam.

of a few seconds at 35 kv and 10 ma was required. The sample holder for the electron diffraction apparatus was fixed for the first specimen of each series only. Then the succeeding members of the same series were obtained by slipping each sample into the holder after removing the preceding one.

### (d) Optical Reflection Measurements

Because of the high reflecting power of many of the electrodeposited film samples, it was decided to measure quantitatively the reflectances both as functions of wave-length of visible light and of plating time on substrates. No record of such measurements on samples of this type could be found in the literature. Conceivably these measurements could throw additional light on the nature of any interface. The apparatus employed for this purpose was the Hardy-General Electric Recording Spectrophotometer. To study the character of the surfaces critically the equipment was adjusted so that the sensitivity of the instrument was accurate to 0.4 percent. Standard magnesium oxide with a reflectance of 98 percent was used throughout this work.

## DISCUSSION

It is obvious that the structure of the very first layer deposited on a base metal is of greatest significance in disclosing the type of bond between coating and substrate. It was clearly demonstrated that a layer deposited in 10 seconds with a thickness of about $2.1\times10^{-6}$ in. ($5.36\times10^{-6}$ cm, or something over a hundred unit cells of crystalline face-centered cubic copper or nickel) is quite adequate for detection not only by electron diffraction but also by the x-ray diffraction technique described in this paper. Thus, when the deposited metal of this minimum thickness produces its own characteristic diffraction interferences on the pattern, in addition to the base metal interferences which appear since the x-ray beam penetrates through to it, this can mean only that the film atoms neither enter the substrate lattice to form a solid solution or intermetallic compound, nor in their own layer simulate exactly the lattice type and spacing of the substrate metal (so-called pseudobasal isomorphism); but that the first deposited atoms assume at once the characteristic lattice structure of the metal in massive form. The bonding, may, therefore, be termed mechanical by clinging to the faults and irregularities which have been demonstrated for even the most highly polished and plane surfaces of metal sheets. On the other hand, if the interferences for this film do not appear, then it is logical to conclude that either solid solution has occurred by penetration of deposited atoms into the substrate lattice, in which case some shift in lines indicative of lattice parameter change would be expected and could be measured; or the deposited atoms have built a layer in which the underlying base metal structure is exactly copied, even though the lattice type and spacing may be entirely foreign to the

normal positions taken by these atoms on crystallization. This would indicate the powerful forces exerted at this interface which could force atoms under a condition of high strain into an abnormal configuration. It could not be expected that this pseudobasal isomorphism would persist through more than a very few layers, for with increasing thickness the normal lattice forces would prevail over the substrate surface forces. So it is of interest to discover at what step in the plating process the normal characteristic structure of the metal being electrodeposited will first come into evidence.

An examination of Table I shows that even the copper flash coating and all 8 plating steps give evidence of copper superposed with apparently purely mechanical bonding on steel and zinc (*A*, *B*, *C*) but there is evidence of some solid solution of copper in the tin layer of tinplate base (*D*); nickel appears from the beginning in copper-plated steel, copper, brass, tinplate, and zinc (*E*, *F*, *G*, *I*, *J*), but simulates in the first layer the structure of the copper flash on brass (*H*); zinc takes the structure of the base steel in plating 1 (*Q*), and of cold-rolled copper through two platings (*R*), the only such case, but appears in the first layer on brass (in which copper is already alloyed with zinc); copper appears in the first layer on cold-rolled steel (*V*), but only in the second plating on cold-rolled brass (*W*), thus duplicating the interplanar spacing of the brass in the absence of zinc; nickel simulates cold-

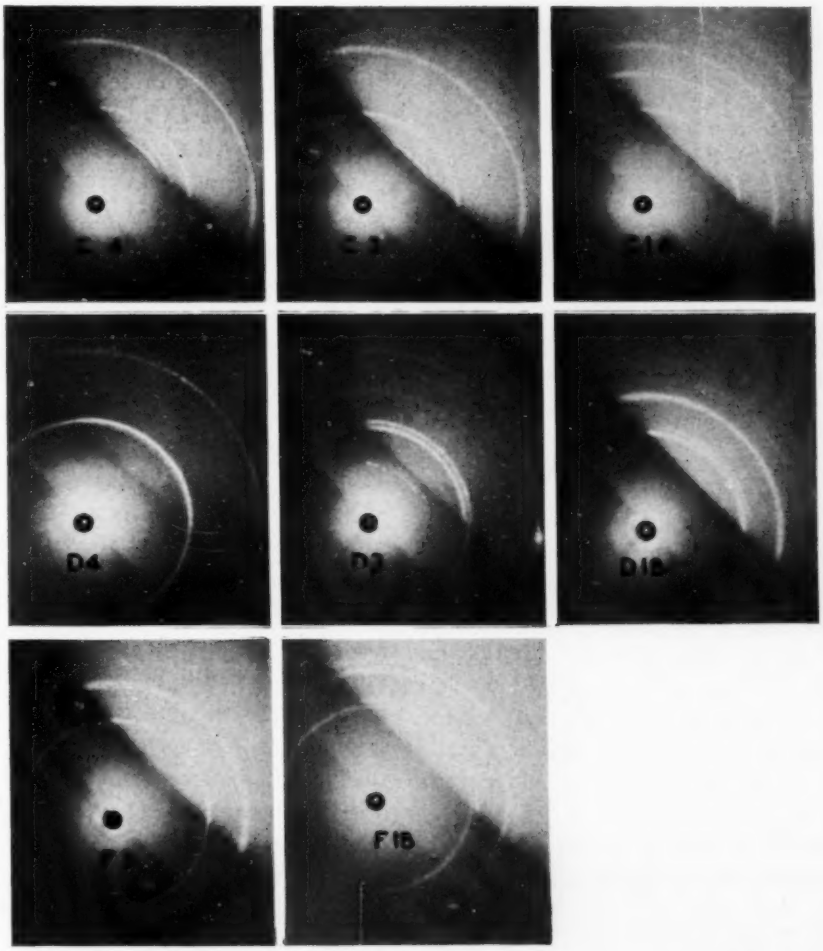


FIG. 2. Typical x-ray diffraction patterns of plated layers on base metals with random orientation: *C*4, zinc base metal; *C*3, with copper flash coat; *C*18, with copper plating. *D*4, tinplate base; *D*3, with copper flash coat; *D*18, with copper plating. *F*3, copper base; *F*18, with nickel plating.

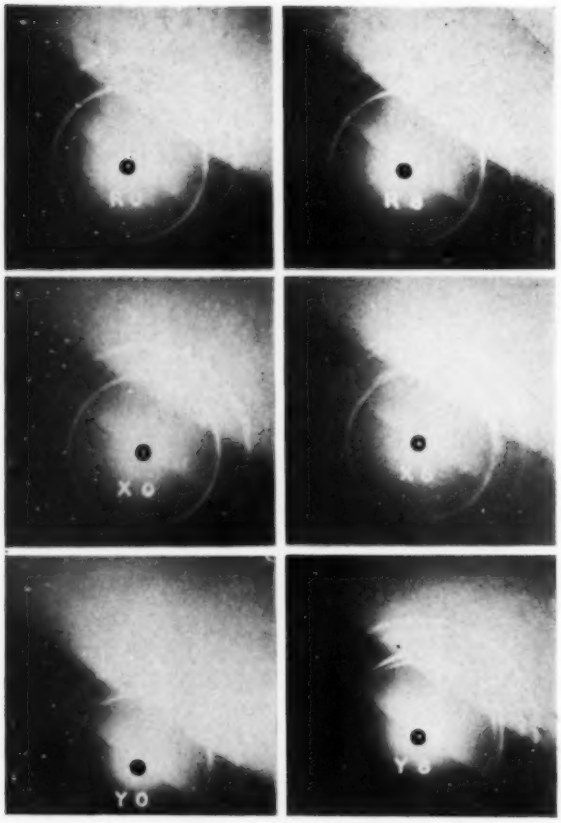


FIG. 3. Typical x-ray diffraction patterns of base metals with preferred orientation (0) and deposit thereon (8): *R*, cold-rolled copper base, zinc plated; *X*, cold-rolled copper base, nickel plated; *Y*, cold-rolled brass base, nickel plated.

rolled copper in the first layer (*X*), but appears for plating 1 on cold-rolled brass (*Y*). In all cases of non-appearance of characteristic structure in the first layer except for films on a tinplate base, precision measurements have disclosed no evidence of solid solution in the base metal from line shifts. That a discrete film exists is evident from visual inspection and especially from the optical reflectance measurements as described in a later section. Thus pseudobasal isomorphism is indicated both by x-ray and electron diffraction analysis.

In addition to the variations in actual crystalline structure as affected or not by the substrate lattice, another variable, namely, texture, as affected or not by whether the base metal sheet has a random orientation of grains (as produced by recrystallization or annealing), or a preferred orientation or fiber structure such as introduced by cold rolling, can be followed by the diffraction patterns of the stepped samples.

The first samples to be studied were platings upon annealed substrate metals without preferred orientation from cold rolling, or nearly so. Some of the samples were given a very light copper flash before plating. This was done to see if this coating would change the effect of the base metals upon the deposited coatings. Examples of both cases are shown in Table I (series *A*–*J*). The typical illustrations in Fig. 2 show the results on x-ray patterns of the base metals (zinc *C*4, tinplate *D*4, copper *F*3), the copper flash coating on the base metal (zinc *C*3, tinplate *D*3), and the deposit (copper on zinc *C*18, copper on tinplate *D*18, nickel on copper *F*18).

Results from the x-ray patterns indicated only random orientation of the plating in the first step on the base metal. In the following stepwise deposits only the intensities of the interferences became stronger. The copper flash coatings in the other samples were without preferred orientation also, and the stepwise deposits behaved in exactly the same manner. Thus plating crystals grow out in random fashion on a random array of substrate crystals under the usual commercial conditions of deposition employed.

After repeating the work with highly oriented substrate metals (Table I, series *R*–*Y*), different results were observed. The x-ray patterns in Fig. 3 show patterns of the samples before plating (0) and after a deposit was applied (8). When the plating first appeared, it was found always to be oriented. In general the direction of orientation is identical with that of the base metal, and thus simulates the texture. In some samples two possible directions of orientation are indicated in Table I since the data on positions of interference maxima were insufficient to fix the orientation with certainty. The coating following the oriented layer was found to be without orientation again and remained as such to the final deposited coating. So, just as in the case of the lattice structure and spacings, the influence of the base metal in orientation is lost after a critical thickness of the coating is exceeded.

The oriented samples with a flash coating were found to be without orientation in this coating, and therefore no further work was carried out

since the subsequent platings behave in the same manner as the samples on randomly oriented base metals.

The results obtained by electron diffraction were found to be in exact agreement with those obtained by x-rays.

Traces of percent reflectance ($\rho$) *versus* wave-length were taken of many of the stepwise plated series using the Hardy-General Electric Recording Spectrophotometer. A typical trace of this kind for a complete series ($S$) is illustrated in Fig. 4. The zero curve corresponds to the unplated base metal of brass and curves 1, 2, 3, $\cdots$ correspond to zinc deposits 1, 2, 3, $\cdots$.

Each family of the above curves may be plotted as reciprocal percent reflectance ($1/\rho$) *versus* plating time in seconds for the complete series at some definite wave-length. A family of curves of this kind for series $S$ is shown in Fig. 5A. Curves 1, 2, 3, and 4 were plotted for 7000A, 6000A, 5000A, and 4000A, respectively. In this series of zinc deposits upon cold-rolled brass it may be observed that the substrate metal exerts a profound influence upon the plating especially in the initial stages of the deposition process while in the heavier deposits this effect is not very great. As the deposit on the sample increases in thickness, the quality of the surface changes also. In some specimens the heavier deposits became brighter and smoother than the initial deposited layers as in the case of deposited nickel or copper. The opposite also occurs depending upon the nature of the base metal and conditions of plating solution. Various

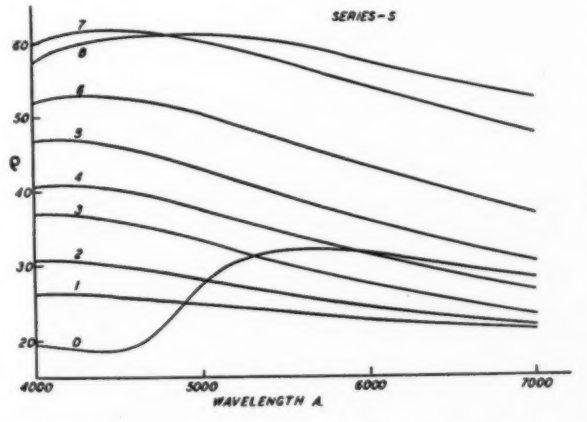


FIG. 4. Reflectance values ($\rho$) as they vary with wave-length for cold-rolled brass with zinc plating.

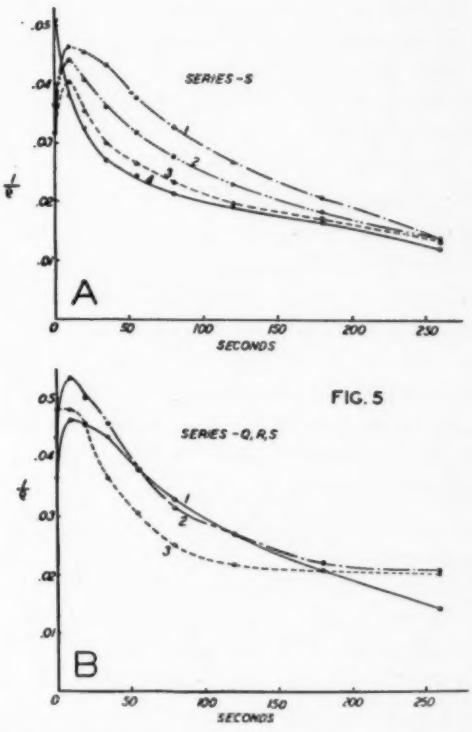


FIG. 5

FIG. 5. A. Reciprocal reflectance plotted against time of plating for zinc on cold-rolled brass: 1, at 7000A; 2, at 6000A; 3, at 5000A; 4, at 4000A. B. Reciprocal reflectance at 7000A plotted against time of plating for zinc deposits on (1) brass, (2) copper, (3) steel.

other samples plotted in the above manner showed the same behavior.

In order to see what effect similar platings had upon different materials, various graphs were plotted using the same coordinates as above. In Fig. 5B are shown the results of zinc deposits upon brass, copper, and steel for 7000A and are represented by curves 1, 2, and 3, respectively (sample series $Q$, $R$, and $S$ of Table I). Here again the deposit is strongly affected by the base metal during the first stages of the deposition process and less in the heavier deposits. These curves indicate remarkably well the same phenomena of structure and texture as interpreted from the x-ray and electron diffraction patterns.

## SUMMARY AND CONCLUSIONS

1. A method of studying the interfacial structure and bonding of electrodeposited metals exactly as produced commercially by the use of a stepwise plating process and without stripping platings from the base metals was devised. By

this method it was possible to show not only the true interfacial structure but also variations as the film increases in thickness and becomes farther and farther removed from the effects of the base metal.

2. In order to make it possible to obtain x-ray patterns which would not vary in sample-film distance and the angle at which the sample is tilted for the surface reflection studies, a special collimating system containing an adjustable sample holder was constructed. Using this apparatus the angle of tilt could be permanently fixed at any desired position. The sample-film distance was measured once and then the entire assembly clamped into position. With this arrangement patterns obtained could be compared accurately for any series of electroplated substances.

3. X-ray and electron diffraction patterns (the latter purely for confirmatory purposes) were obtained of various substrate materials (with both random and preferred orientation) upon which were stepwise deposited platings of different metals. In some systems the characteristic structure of the deposited metal is observed in the first plating only 0.000002 in. thick; in others the deposited metal simulates the lattice and interplanar spacings of the base metal through steps 1 and sometimes 2, before subsequently assuming normal structure. It was found that under the conditions of deposition employed, deposited platings upon base material with random orientation follow the random structure throughout the entire thickness. On the other hand, coatings deposited on fibered base metals were also fibered in the initial plating. Subsequent to the initial plating additional steps no longer show the orientation.

4. An attempt was made to correlate results obtained by x-ray diffraction with those of optical reflectance measurements. Various traces were made of the samples using a recording spectrophotometer. These were replotted into simpler form and show that the substrate metal affects the deposited metal very markedly in the initial stages of the deposition process. This effect then diminishes in characteristic fashion as the thickness of the film increased.

5. Three types of bonding of electroplates on substrate metals have been demonstrated in the various combinations studied:

a. Mechanical, in which the deposited metal forms its own characteristic lattice from the beginning and clings to the faults and irregularities of the base metal surface which may appear at only high microscopic magnifications or in electron micrographs; the first atoms undoubtedly come within range of strong fields of force of the base metal atoms in these minute faults which increase the effective total surface of the interface.

b. Solid solutions, in which the first deposited atoms enter the lattice of the substrate metal, the resulting solid solution forming a transition layer between normal base metal and normal electroplated metal, which appears as a separate phase beyond a limiting thickness.

c. Pseudobasal isomorphism, in which through a few transitional atomic layers the deposited metal forms a crystalline arrangement which similates and extends the type and dimensions of the base metal, though this may be entirely foreign to the depositing metal, until in thickening films it reverts to its normal structure.

Under best conditions bonds of great strength of all three types are possible and commonly observed in commercial practice.

Further work is now in progress on films deposited in steps of (1) 1-second interval up to 10 seconds plating time (this being the minimum in the work here reported); (2) electron microscope examinations of interfaces and transition zones by a new technique; (3) study of structures after samples are subjected to repeated stresses and fatigue in order to evaluate bonding strengths by degree of resistance to rupture or change.

# Letter to the Editor

## Mounting of Pigments for Electron Microscopy

M. L. Fuller, D. G. Brubaker, and R. W. Berger
*Research Division, Technical Department, The New Jersey Zinc Company, Palmerton, Pennsylvania*
December 3, 1943

A TECHNIQUE for the preparation of pigment mounts for the electron microscope has been devised and is described in this note because it may be of interest to other laboratories using the electron microscope.

Two principal requirements of a mount are that the supporting membrane be very thin and that the dispersion of the pigment particles be such that the individual particles are clearly separated. A good dispersion is particularly important where particle size measurements are to be made.

The technique described below has been found successful with a wide variety of zinc oxide pigments and has been successful also with leaded zinc oxide, titanium dioxide, zinc sulfide, and lithopone.

Step 1. Approximately 0.01 gram of the pigment is mulled on a glass plate with a glass muller using 3 drops of a 1 percent by volume solution of poppy-seed oil in amyl acetate. The mulling is continued until the paste is nearly dry.

Step 2. To the paste are added 3 drops of a 2 percent by weight solution of nitrocellulose in amyl acetate. This is mulled until the solvent has evaporated.

Step 3. About 8 drops of a 2 percent by weight solution of nitrocellulose in isopropyl acetate are added and mulled for a few seconds (long enough to put the pigment in suspension), and 1 drop of this is allowed to spread on the surface of a saturated solution of sodium chloride in water. A portion of the resulting thin film is removed on a glass slide, refloated on water to wash away the sodium chloride, and then attached to the standard 200-mesh screen disk.

The poppy-seed oil generally contributes to good dispersion. With the larger particle size zinc oxide pigments, however, it is better to carry out Step 1 with amyl acetate alone. Glyceryl oleate has also been found to aid in getting good dispersions.

Step 2 is essential to accomplish a thorough dispersion. It must be recognized, however, that the vigorous mulling treatment of this step may fracture or break down some shapes and sizes of particles.

The preparation of the final suspension in a nitrocellulose solution in isopropyl acetate is the most important single step in the procedure. Pigment mounts using this solvent are far superior to those made with the more commonly used solvent, amyl acetate. Pigment suspensions in amyl acetate solutions appear to be well dispersed, but as soon as the suspension is cast on water, the pigment usually flocculates badly. The merit of using sodium chloride solution instead of water in the casting tray is not definitely understood but may be associated with the lower solubility of isopropyl acetate in brine as compared to water.

Since the particular grade of chemical used in a laboratory method of this type so often is an essential, although unexplained, requirement for the success of the technique, the particular chemicals used are listed below:

Poppy-seed Oil.....Eimer & Amend,
Amyl acetate.....Technical grade, Sharpless Chemicals Company,
Nitrocellulose.....Mallinckrodt Parlodion,
Isopropyl acetate...U. S. Industrial Chemicals Company.

# Recent Applications of Physics

Prepared by CLARK GOODMAN, Associate Editor

Material to be included in this section should be submitted to Dr. Clark Goodman, Massachusetts Institute of Technology, Cambridge 39, Massachusetts.

**Bending Copper Tubing** The Cerro de Pasco Copper Company has developed a modification of Wood's metal which enables thousands of feet of copper tubing used in airplanes to be bent to exact shapes without danger of breaking or collapsing at the bends. This alloy, known as "Cerrobend," has a melting point of only 70°C. The tube is filled with the molten alloy which, upon solidification, expands and fills all the small imperfections in the tubing. When the bending operation is completed, the metal is easily removed by immersing the tube in hot water.

**Machine Gun Trainer** A training device has been developed by Polaroid Corporation which uses 3-dimensional sound movies and optical bullets—instead of real ones—to give our machine gunners the experience of fighting off attack by enemy planes. The danger of enemy bullets and bombs is the only element of battle lacking as the gunner actually sees and hears planes come roaring across the sky or directly at him. The training device not only enables the gunner to follow his machine gun tracer bullets but also registers his hits precisely. The gunner wears goggles fitted with polarizing lenses through which he sees stereoscopic images of his target in exactly the proper perspective.

**Phantom Target** Another Polaroid development that has proved of value in combat practice of a different type is the Offset Wedge. Two ships steaming along beside each other can serve as mutual targets without the slightest danger. The gun crews and fire-control officers sight through this vest-pocket-size instrument. Instead of sighting the other vessel nearby, they see an image of the ship which appears to be miles away and displaced laterally from where the wedge is pointed. Using this phantom ship as a target, practice can take place under conditions that look the same as those of actual battle.

**Physics Promotes Penicillin Production** A high vacuum diffusion technique, developed by the National Research Corporation of Boston and adapted to the drying of penicillin, is believed to solve the problem of processing the active germ-killing organism once it is extracted on the large scale planned. The process is being made available royalty-free for the production of penicillin in government-sponsored plants during the war emergency. On the basis of preliminary tests, the Chemicals Division of the War Production Board believes that the 20- to 40-hour cycle now considered necessary for processing penicillin in the last stage can be reduced through this high vacuum diffusion method to six hours, and the cost of dehydration cut to one-sixth of any conventional method.

Army and Navy experts expediting the production of penicillin are convinced that a single installation of this novel dehydrator can handle ten billion units of this life-saving drug a week, far surpassing the output by methods now in use. Such an installation would make available 1300 doses of penicillin a day, when used to treat certain types of pneumonia. Since penicillin in solution form, after extraction from the mold, is an unstable product, dehydration is necessary. Even minute amounts of moisture are harmful. Proper desiccation and packaging are highly important parts of the whole process, and have proved costly and troublesome to firms making penicillin. The use of heat to accomplish this is out of the question, so the dehydration is achieved through vacuum. Extracting the last 2 percent of water vapor ordinarily has taken as much time as and is more difficult than driving off all the rest of the original content. In the new process the penicillin is dehydrated in a frozen state, the moisture being removed without liquefaction. Because of the enormous expansion of gases under the vacuum employed ($10^{-4}$ atmosphere), a pumping system of tremendous capacity is required. The water vapor is continuously frozen out and removed from the system in the form of ice by means of a rotary condenser which passes through a vacuum seal.

**Commercial Mass Spectrometers** Consolidated Engineering Corporation and Westinghouse Electric International Company have recently announced, almost simultaneously, commercial mass spectrometers for rapid analysis of complex mixtures of organic gases. Brief mention of the application of the mass spectrometer in synthetic rubber production was made in an earlier edition of this section. This instrument is also proving of value in controlling the production of aviation gasoline and other vital war materials.

Thomson's initial researches on the parabolic method and the extensive subsequent developments by Dempster, Bainbridge, Bleakney, and Nier, to mention only a few of the numerous workers, have been devoted largely to the study of isotopic masses and abundances. The recent commercial applications of the mass spectrometer are based on the same fundamental principle of sorting charged particles with a magnetic field. However, the ions are not individual atoms but are molecular fragments split from the gaseous molecules by an electron beam. For any given gas the particular fragments formed depend for the most part upon the number and type of atoms in the molecule. The relative abundance of the different fragments varies with the structure of the molecule and dictates the intensity of the beam current for each mass number in the "cracking-pattern" spectrum obtained.

Even a pure, light hydrocarbon has a large number of peaks in its intensity spectrum, almost every permutation of C and H below the original molecular composition being represented. The spectrum rapidly increases in complexity with the number of components in the gaseous mixture.

# "WRATTEN LIGHT FILTERS"

## A Book of Data on Wratten Filters

THERE are more than 100 filters in the series of Wratten light filters. They are designed for use in general monochrome and color still photography, cinematography, and special scientific fields—including astronomy, photometry, and spectroscopy.

Each Wratten Filter is made to meet a rigid standard, and is supplied in the form most convenient for its application.

The purpose of the book, *Wratten Light Filters*, is to facilitate selection of filters by providing complete spectrophotometric data concerning them.

The 88-page Sixteenth Edition of this publication gives transmission curves and tables for all filters, as well as notes on the use of filters for special purposes. It is available at dealers in photographic supplies.

**EASTMAN KODAK COMPANY**

***Research Laboratories*** **Rochester, N. Y.**

# A High-speed Semi-fractionating Diffusion Pump

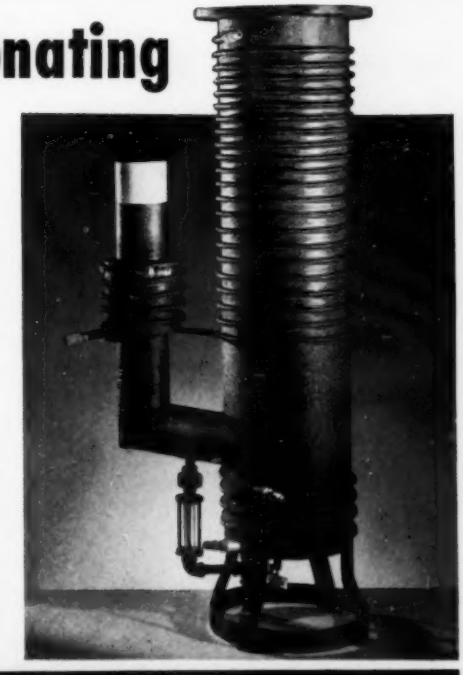

THE new Distillation Products *Metal Diffusion Pump, Type MC-500,* makes available for commercial and laboratory use an unbreakable high-speed unit adapted to large kinetic vacuum systems. It is particularly useful in the mass production of coated optical parts such as large front-surface mirrors, or in the deposition of metals on plastic sheets and films. Note particularly the speed and ultimate vacuum listed in the following *MC-500* specifications:

| | |
|---|---|
| **Speed** | **700 l/s. at $10^{-4}$ mm.** |
| **Ultimate Vacuum** | **$5 \times 10^{-6}$ mm.** |
| **Maximum Forepressure** | **.2 mm.** |
| **Heater Input** | **500 watts** |
| **Pumping Fluid** | **Octoil** |
| **Height** | **30 in.** |
| **Diameter** | **6 in.** |

Write "High-Vacuum Headquarters" today for complete information on this pump, as well as on the many other models which are available.

DP INC. HIGH-VACUUM HEADQUARTERS

**DISTILLATION PRODUCTS, INC.**

Jointly owned by EASTMAN KODAK COMPANY and GENERAL MILLS, INC.

ROCHESTER, N. Y.

In order to complete the analysis of a mixture from its composite spectrum, it is necessary to calibrate the instrument with pure gases. Calculations are facilitated by simultaneously recording the spectrum at a number of sensitivities.

In addition to the small quantity of sample required—less than 1 cc under standard conditions is usually sufficient—the mass spectrometer is much more rapid than conventional methods of analysis and can often handle mixtures of up to 15 or more components.

**High Frequency Heating** In a recent summary of industrial electronics Mr. Carl J. Madsen, Engineer of the Westinghouse Electric and Manufacturing Company, reviewed the developments in electronics under nine classifications. Of particular interest to physicists are his observations on high frequency heating. Some of the present applications are the bonding of plywood and the heating and curing of plastic materials. Dielectric heating is of value for thick sections of plywood, thermoplastic or thermosetting materials. Whereas hours were required with steam or other sources of heat, present methods take only three to five minutes. In addition to speed, the electronic method is more thorough and gives a more uniform heating.

Induction heating is being used extensively in metal working. Faster and more uniform heat treating, annealing, brazing, welding, soldering, and tempering are made possible. In some processes, the time required has been reduced from two minutes to five seconds. It is possible, by proper choice of frequency and equipment, to case-harden gears and shafts. Although it was only a year ago that the initial experiments were made on the conservation of tin in making tinplate, high frequency power in a single plant of this type now equals the entire power of all our conventional broadcasting stations. Total installations for tinplating will soon exceed 2½ times this figure. Mr. Madsen predicts that after the war hundreds of new applications of importance to the steel, aluminum, tool, and general manufacturing industries will be found.

**Most Mighty Motor** One of the most powerful electric motors in the world, 7000 horsepower at 25 r.p.m. and capable of exerting a torque of 4 million pound-feet, has just been built by General Electric and shipped from Schenectady to the Utah steel mill of the Geneva Steel Company. It will operate the reversing rougher of a 132-inch, semicontinuous plate mill which will turn out slabs one-fourth to three-fourths of an inch thick and 200 feet long for shipyards and other war industries. Some idea of the size and construction of the motor can be obtained from the photograph. The motor has an over-all length of 44 feet, an outside diameter of 16 feet, and weighs nearly a million pounds; when installed, it will stand 13 feet above the floor level. An unusual feature is the absence of the continuous shaft found in most large motors. Instead, two 3500-horsepower rotors are built up on hollow cylindrical bodies, coupled together at the center and provided with flanges at the ends. To these flanges are securely bolted shafts of sufficient size to support the rotor in its bearings and transmit the driving power. This arrangement saves time in erection; also, since this "hollow shaft" construction is more rigid than a solid shaft, the whole rotor structure is much lighter for the same strength, resulting in an important saving in weight of steel required. The motor will be powered by a 7000-kilowatt, six-unit flywheel motor-generator set already installed.

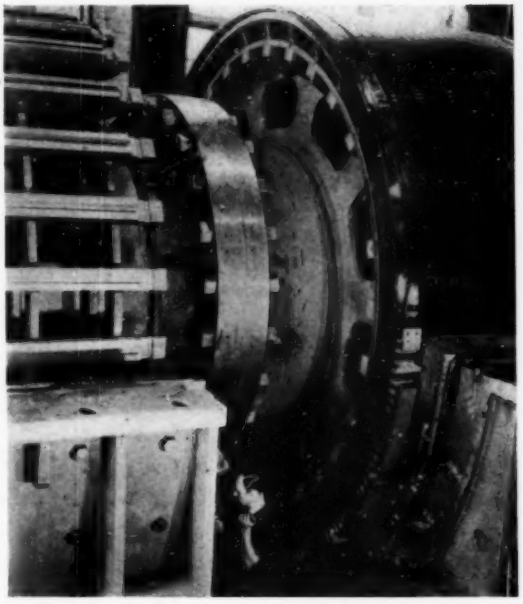

General Electric motor showing armature spider at left and wound armature at right.
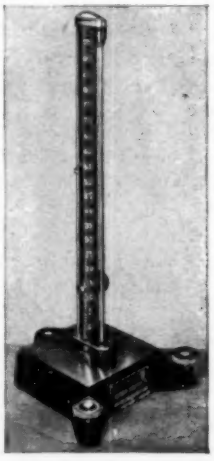
**The Resiliometer** The Resiliometer, now manufactured by the Precision Scientific Company, 1750 North Springfield Avenue, Chicago 47, Illinois, measures the resiliency of rubber and extensible plastic compounds by indicating the rebound of a weighted plunger dropped from a predetermined height. It has been found useful in the development of rubber and plastic compounds, for measuring rate and state of cure, for matching competitive compounds, for factory control tests on cured samples of mixed batches, for factory control on uncured samples of mixed batches, for factory control on uncured samples of materbatches, for controlling the quality of the finished product without destroying the product, for comparing heat build-up of various compounds, and for measuring plasticity of uncured compounds and masticated rubber.